Bioelectrochemistry
Principles and
Practice

Volume 6

Bioelectrochemistry of Membranes

Edited by
D. Walz
J. Teissié
G. Milazzo†

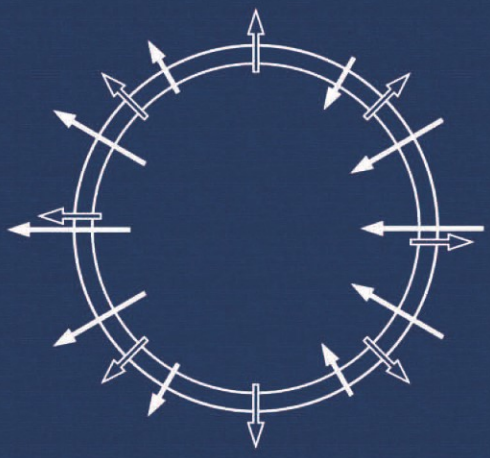

Springer Basel AG

Bioelectrochemistry: Principles and Practice

Volume 6

Bioelectrochemistry of Membranes

Edited by
D. Walz
J. Teissié
G. Milazzo†

Springer Basel AG

Editors:

Dieter Walz
Biozentrum der Universität Basel
Klingelbergstrasse 70
4056 Basel
Switzerland
(retired)

present address:
Lerchenstrasse 21
4059 Basel
Switzerland

Justin Teissié
IPBS-CNRS (UMR 5089)
205 route de Narbonne
31077 Toulouse Cedex
France

Giulio Milazzo†
Formerly Professor
IstitutoSuperiore di Sanità
Rome
Italy

A CIP catalogue record for this book is available from the
Library of Congress, Washington, D.C., USA

Bibliographic information published by Die Deutsche Bibliothek
Die Deutsche Bibliothek lists this publication in the Deutsche Nationalbibliografie;
detailed bibliographic data is available in the internet at http://dnb.ddb.de

ISBN 978-3-0348-9597-2 ISBN 978-3-0348-7853-1 (eBook)
DOI 10.1007/978-3-0348-7853-1

Originally published by 2000 Birkhäuser Verlag in 2004
Softcover reprint of the hardcover 1st edition 2004
Printed on acid-free paper produced from chlorine-free pulp. TCF ∞
Cover design: Markus Etterich, Basel
Cover illustration: see page 213
ISBN 978-3-0348-9597-2
9 8 7 6 5 4 3 2 1

www.birkhasuer-science.com

GIULIO MILAZZO (1912–1993)

Giulio Milazzo, the father of Bioelectrochemistry, died on January 6, 1993 in Rome. He often pointed out that the roots of the subject go back two hundred years to Galvani and Volta, and that he had only resurrected the science. But the Bioelectrochemistry he started was certainly different from the Natural Philosophy of the past, and in many ways quite different from parallel modern developments.

At a time when science is becoming more narrowly focused and scientists more specialized, Giulio Milazzo catalyzed the formation of an interdisciplinary grouping that was broad in scope and inclusive in its organization. He envisaged Bioelectrochemistry as a discipline including all aspects of the overlap of biology and electrochemistry. He believed that science is international and that one should use all scientific means possible to foster cooperation across national barriers. His ideas catalyzed the founding of the *Bioelectrochemical Society* which to this day attempts to follow the high standards set by him.

Giulio Milazzo was convinced that communication between scientists from various fields would be greatly facilitated if a comprehensive textbook written in a common language existed. He therefore initiated the preparation of what he called a *Treatise on Bioelectrochemistry*, but his untimely death prevented him from finishing this enormous task. The Bioelectrochemical Society, under whose auspices the work had been commenced, considers it both an honor and a duty to pursue the project to completion. But with the guiding spirit no longer with us, the project of a comprehensive textbook seemed too ambitious, and the Treatise was therefore converted to the present Series of Texts. May it nevertheless not only serve the purpose envisaged by Giulio Milazzo, but also be a living memory to a great scientist and a dear friend.

Martin Blank *Roy Caplan* *Dieter Walz*

Contents

Contributors

Alfred Blume, Martin-Luther-Universität Halle-Wittenberg, Department of Chemistry, Institute of Physical Chemistry, Muehlpforte 1, 06108 Halle/Saale, Germany; e-mail: blume@chemie.uni-halle.de

Yuri A. Chizmadzhev, Frumkin Institute of Electrochemistry, Russian Academy of Sciences, Moscow, Russia; e-mail: chiz@bioel.glas.apc.org

Paul O'Shea, Cell Biophysics Group, School of Biomedical Sciences, University of Nottingham, Nottingham NG7 2UH, United Kingdom; e-mail: Paul.Oshea@nottingham.ac.uk

Justin Teissié, Institut de Pharmacologie et de Biologie structurale du CNRS, UMR 5089, 205 Route de Narbonne, 31077 Toulouse cédex, France; e-mail: justin@ipbs.fr

Tian Yow Tsong, Department of Biochemistry, Molecular Biology and Biophysics, University of Minnesota College of Biological Sciences, St. Paul, Minnesota 55108, USA; e-mail: tsong@biosci.cbs.umn.edu

Dieter Walz, Biozentrum der Universität Basel, Klingelbergstrasse 70, 4056 Basel, Switzerland (retired); present address: Lerchenstrasse 21, 4059 Basel, Switzerland; e-mail: dieter.walz@magnet.ch

Introduction

Membranes, the topic of volume 6 of this Series, play a key role in biology. Their selective permeability to different molecular species provides the basis for the important compartmentalization of biological systems. In addition and equally important, they behave as electrical insulators and very frequently carry charges on their surfaces. This, together with the selective permeability for charged species, gives rise to complex electrical phenomena, which are involved in divers properties and functions of biological systems. Therefore some membrane-associated phenomena were already treated in previous volumes of this Series, such as double layer phenomena and interaction between membranes in volume 1, signal transduction, dielectric properties and dielectrophoresis of biological cells in volume 2, or generation of transmembrane potential differences and their role in bioenergetics in volume 4.

This volume then is devoted to the bioelectrochemistry of the membrane proper. After a survey of relevant physical principles in Chapter 1, origin and properties of the different membrane potentials are discussed in Chapter 2. Lipids, one of the major constituents of membranes, do not just form a scaffold but also substantially contribute to their electrical properties. Hence a comprehensive treatise on lipids is given in Chapter 3. That the electric field within the membrane associated with a transmembrane potential difference can affect the performance of a charged membrane-bound enzyme is shown in Chapter 4. The perturbation of electrochemical properties by an externally applied electric field leading to a transient permeabilization of membranes is now routinely exploited in clinical and biotechnological applications to cells and tissues. Mechanisms that can explain this phenomenon in pure lipid membranes are discussed in Chapter 5, while the current knowledge about the processes occurring in biological membranes is presented in Chapter 6.

Undoubtedly the electrochemistry of membranes is highly relevant to life sciences, yet the flow of information between these two research areas seems to be still limited. One reason for this gap may be the different nomenclatures used, but also some difficulties biologists may have in understanding concepts in electrochemistry, and vice versa. We hope this volume will help to bridge the gap, to the benefit of both biologists and electrochemists.

Dieter Walz
Justin Teissié

Bioelectrochemistry of Membranes
ed. by D. Walz, J. Teissié and G. Milazzo†

CHAPTER 1
Single membrane in electric field

Yuri A. Chizmadzhev
Frumkin Institute of Electrochemistry, Russian Academy of Sciences, Moscow, Russia

1. Introduction

Biological membranes play an important role in the vital activity of a cell. It is these membranes that make it possible to maintain non-equilibrium concentrations of substances in the cytoplasm. The free energy stored in the form of ionic gradients and transmembrane potential differences is used for transmitting information, for electrosynthesis, for performing mechanical work, for reception etc. All of these varied capabilities of biomembranes are essentially based on their excellent barrier properties, combined with their ability to realize selective transport. The latter can be controlled by an electric field. If a membrane loses its barrier function, nothing will prevent the system from a transition to an equilibrium state, but for a cell, equilibrium means death. Therefore the problem of biomembrane stability is of paramount importance. An electric field holds a unique position among the various factors diminishing the membrane stability. The point is that, under normal physiological conditions, in the majority of cells there exists a transmembrane potential difference of several tens of

millivolts. This means that the electric field in the membranes amounts to about 10^5 V/cm, i.e. it is close to the critical field which causes, for example, dielectric breakdown of liquid hydrocarbons. With a further increase in the electric field the biomembranes undergo changes that lead to a considerable (by 5–7 orders of magnitude) increase in their conductance.

Cells in electrolyte solutions actively interact with external electric fields. This interaction is primarily determined by the occurrence of a fixed surface charge on the cell membranes, by mobile ions which form the diffuse plates of the electric double layers, by the conducting and dielectric properties of solutions and the membrane proper, by the viscosity of the solutions and by the mechanical characteristics of the cells. A constant external field induces electrophoresis of the cells. An alternating inhomogeneous field causes dielectrophoresis and a mutual attraction of the cells due to the induced dipoles. In fields of higher intensity, membranes are subjected to deformations and structural rearrangements on a micro- and macroscale, which results in a sharp increase in permeability. All these phenomena can only be understood based upon a deep insight into the interaction of membranes with electric fields. This chapter therefore summarizes the essentials of electrostatics with special emphasis on interfaces and membrane phenomena.

2. Elements of the theory of electrified interfaces

2.1. Membrane potentials

In electrochemistry, it is common practice to distinguish between ideally polarized interfaces impermeable for any charged particles and non-polarized interfaces permeable for any charges. In the former case the equilibrium is of a purely electrostatic character, in the latter of a thermodynamic one. If a membrane carrying a fixed surface charge is impermeable for ions, an electrostatic equilibrium is established between its surfaces and the solutions. If, on the other hand, the membrane is permeable only to ions of one type, the system features a transmembrane potential difference determined by the condition of thermodynamic equilibrium for the permeant ion. When the membrane carries a fixed surface charge, the surface potential is determined by electrostatics. Thus, various types of equilibria which determine different components of the potential can be realized at the membrane. In a more general case of the interfaces permeable for a set of ion types, the distribution (or Gibbs-Donnan) potentials are realized. In any of these cases, a condition of thermodynamic equilibrium relative to a given permeant ion is the equality

of electrochemical potentials of respective ions in solutions on both sides of the membrane.

2.2. Electrochemical potential

The electrochemical potentials $\tilde{\mu}_i$ are of fundamental importance for the description of a broad range of membrane phenomena. The physical sense of the value of $\tilde{\mu}_i$ can be made clear by means of the following imaginary experiment (see Ref. 1 for details). Consider a body B containing, among others, particles of type i with a charge $Q = Z_i e$, where Z_i is the charge number and e the elementary charge (Fig. 1). Divide B mentally into the volume part V and the surface part S. Then the work for the transfer of charge Q from B to infinity, equal by definition to the electrochemical potential of particle i in phase B, can be calculated as the sum of the work for the transfer from V (equal to μ_i) and from S (equal to $Q\phi$),

$$\tilde{\mu}_i = \mu_i + Z_i e\phi \tag{1}$$

Here μ_i is the chemical potential of particle i in phase V, and ϕ is the internal (or Galvani) potential of a respective phase. Thus, μ_i represents the work against the chemical forces, and $Z_i e\phi$ the work against the electrical forces of interaction with the surface charges and dipoles:

$$\phi = \chi + \psi \tag{2}$$

Here χ is the dipole (or surface electric) potential and $Z_i e\chi$ is the work of the charge transfer across the surface layer, ψ is the external (or Volta) potential and $Z_i e\psi$ is the work of charge transfer from the surface to infinity, performed against the forces of interaction with the surface charges. It is convenient to rewrite Eqn. 1 in the form

$$\tilde{\mu}_i = \mu_i + Z_i e\chi + Z_i e\psi = \alpha_i + Z_i e\psi \tag{3}$$

where α_i is called the work function; α_i and ψ can be measured by thermodynamic methods. The internal potential ϕ is not thermodynamically measurable, only its changes with time or space can be determined. For sufficiently diluted solutions we have

$$\mu_i = \mu_i^o + kT \ln (c_i / c^o) \tag{4}$$

where μ_i^o is the standard chemical potential, k the Boltzmann constant, T the absolute temperature, c_i the concentration of particles i,

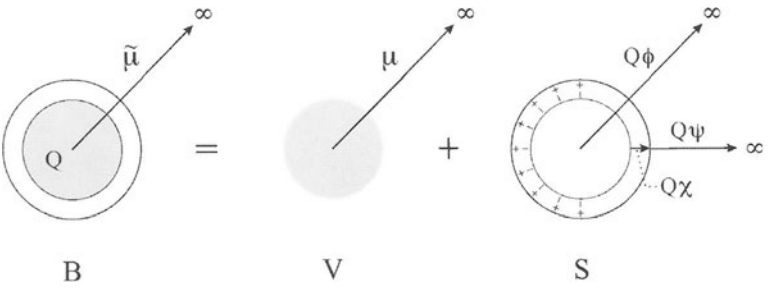

Fig. 1. Meaning of $\tilde{\mu}$. $Q = Z_i e$ is the charge of particles of type i, for further explanations see text.

and c^o a standard concentration (usually 1 M). In cell biology, we deal with internal (or Galvani) potentials ϕ whose changes are measured by some method. The external (or Volta) potential ψ can be measured in studies of the monolayers of bioactive molecules at the water-air interface usually employing the method of vibrating electrode or ionization of the inter-electrode space [1].

The equality of electrochemical potentials of particles in the subsystems freely exchanging these particles, which is a condition of equilibrium, ensues from the general principle of minimum work. This is evident from the imaginary experiment illustrated in Fig. 1. The use of this condition together with Eqns. 1 and 4 for a membrane permeable to the ions of only one type leads to the expression for the transmembrane potential difference $\Delta\phi_m$, which is known as the Nernst potential,

$$\Delta\phi_m = kT/(Z_i e)\, \ln(c_{i,1}/c_{i,2}) \tag{5}$$

Here $c_{i,1}$ and $c_{i,2}$ are the concentrations of permeant ions on both sides of the membrane, and $\mu^o_{i,1} = \mu^o_{i,2}$ is assumed.

The cell systems are exclusively at a non-equilibrium state so that the real transmembrane potential differences are virtually never described by the equilibrium formulae. The stationary transmembrane potential difference in this case is calculated from the condition that the current densities $Z_i e\, j_i$ associated with all permeable ionic species sum up to zero. The flow densities (or fluxes) j_i through the membrane are determined by the Nernst-Planck equation

$$dc_i/dx + Z_i c_i\, e/(kT)\, d\phi/dx = -j_i/(u_i kT) \tag{6}$$

with u_i denoting the mobility of the particles. Equation 6 is readily obtained from Eqns. 1 and 4 on the assumption that j_i is proportional

to the negative gradient of the electrochemical potential $\tilde{\mu}_i$. In the constant field approximation (e.g. Goldman equation) $d\phi/dx$, equal to minus the electric field intensity, is taken to be constant within the membrane.

2.3. Electrostatics of membranes

2.3.1. Elements of electrostatics: The basis of the theory of electrostatic fields is Coulomb's law. From this law it follows that the electric field **E** of a point charge Q at a distance r from this charge is

$$\mathbf{E} = Q\,\mathbf{r}/(4\pi\varepsilon_0 r^3) \tag{7}$$

where **r** is the radius vector drawn from the charge Q to the point under consideration and ε_0 is the absolute permittivity. For an electrostatic field in vacuum, the Gauss theorem is valid, i.e. the flow of the electric field vector **E** through an arbitrary closed surface equals the value of the charge inside this surface divided by ε_0. The Gauss theorem has some consequences. Thus, the jump of the normal component of the vector **E** on a charged surface with surface charge density σ is

$$E_{2,n} - E_{1,n} = \sigma/\varepsilon_0 \tag{8}$$

The field of a uniformly charged infinite surface is perpendicular to it but has opposite directions on different sides of the plane. The field vector is directed from the plane if its charge is positive or to the plane if it is negative. In the case of electrostatic equilibrium the field within a conductor vanishes and

$$E_n = \sigma/\varepsilon_0 \tag{9}$$

The electrostatic field is a potential field, hence the tangent component of **E** at the surface of a conductor is zero, i.e. the vector of the field is normal to the surface. It can be shown that the vectorial electric field **E** and the scalar electrical potential ϕ are related by

$$\mathbf{E} = -\nabla\phi \tag{10}$$

where ∇ denotes the gradient operator, which is equal to d/dx in the one dimensional case. Hence the potential difference $d\phi$ between two infinitely close points at a distance dl is equal to E dl.

A significant role in membrane electrostatics is played by the capacitance C of a capacitor, defined as

$$C = Q / \Delta\phi \tag{11}$$

where Q is the charge on the plates and $\Delta\phi$ the potential difference between them. The capacitance of a plane capacitor is

$$C = \varepsilon_0 A/d \tag{12}$$

where A denotes the area of the plates and d is the distance between them.

The charges are the source of an electric field, which is mathematically expressed by the Poisson equation

$$\nabla^2\phi = -\rho/\varepsilon_0 \tag{13}$$

Here ∇^2 denotes the Laplace operator, which is equal to d^2/dx^2 in the one-dimensional case, and ρ is the volume density of charges. In a region of the space where $\rho = 0$, the Laplace equation

$$\nabla^2\phi = 0 \tag{14}$$

is satisfied. The energy of interaction U between two charges Q_1 and Q_2 arises from the force exerted by the electric field of charge Q_1 on charge Q_2 (or *vice versa*) and can be expressed in the symmetric form

$$U = (Q_1 \phi_2 + Q_2 \phi_1)/2 \tag{15}$$

where ϕ_1 is the electric potential of charge Q_2 in the point where Q_1 is located, and *vice versa*. Using Eqn. 15 for a plane capacitor of capacitance C we obtain by means of $Q_2 = -Q_1 = Q$ and Eqn. 11

$$U = Q(\phi_2 - \phi_1)/2 = Q\,\Delta\phi/2 = C\,\Delta\phi^2/2 \tag{16}$$

The change of U due to a change in capacitance by δC at a constant $\Delta\phi$, maintained by an external source, is

$$\delta U = \Delta\phi^2\,\delta C/2 \tag{17}$$

In order to maintain $\Delta\phi$ the source has to perform the work

$$\delta W = -\Delta\phi_2\,\delta C \tag{18}$$

so that the energy change for the entire system is

$$\delta U_{tot} = \delta U + \delta W = -\Delta\phi^2\,\delta C/2 \tag{19}$$

In general the energy of an electric field is given by

$$U = (\varepsilon_0 /2) \int E^2 \, dV \tag{20}$$

where E is the field intensity in a given point in space, and dV denotes an infinitesimally small volume element, i.e. dxdydz.

2.3.2. Electrostatics of dielectrics: A dielectric is characterized by an electric dipole moment per volume unit called dielectric polarization **P**. For example, in the case of an aqueous solution, the main contribution to **P** comes from the orientation of the permanent dipole moments of water in the electric field. In a dielectric, two types of charges are distinguished; free ones, which can move under the action of the field, and bound ones. It can be shown that the electric field in a dielectric coincides with the field which would exist without the dielectric but with bound charges being present besides the free ones. The volume density of the bound charges ρ_b is determined by

$$\rho_b = - \text{ div } \mathbf{P} \tag{21}$$

Then the potential in the dielectric satisfies the equation

$$\nabla^2 \phi = -(\rho + \rho_b)/\varepsilon_0 \tag{22}$$

and

$$\text{div } (\mathbf{E} + \mathbf{P}/\varepsilon_0) = \rho/\varepsilon_0 \tag{23}$$

Since the dielectric polarization is caused by the electric field the two quantities can be related

$$\mathbf{P} = \alpha \, \varepsilon_0 \, \mathbf{E} \tag{24}$$

where α is called the polarizability of the dielectric.

In a dielectric it is more convenient to use the induction **D** instead of the electric field **E** defined as

$$\mathbf{D} = \varepsilon_0 \, \mathbf{E} + \mathbf{P} = \varepsilon_0 \, (1 + \alpha) \mathbf{E} = \varepsilon_0 \, \varepsilon_r \, \mathbf{E} = \varepsilon \, \mathbf{E} \tag{25}$$

The quantity ε is called the permittivity, while ε_r is known as relative permittivity or dielectric constant; the absolute permittivity ε_0 can then be interpreted as the permittivity in vacuum with $\varepsilon_r = 1$. The physical meaning of $\varepsilon_r = 1 + \alpha$ is obvious. For example, the orientation of the water dipoles in an outer electric field partially compensates

that field. As a result the field in the dielectric is smaller, and ε_r then indicates the ability of the dielectric medium to screen the outer field due to its polarizability α. In terms of the induction **D** Eqn. 23 adopts the simple form

$$\text{div } \mathbf{D} = \rho \tag{26}$$

At the charged interface of two media with different permittivities ε_1 and ε_2 we have

$$D_{2,n} - D_{1,n} = \varepsilon_2 E_{2,n} - \varepsilon_1 E_{1,n} = \sigma \tag{27}$$

where n indicates the normal components of **D** and **E**, while σ is the surface charge density. In the case of a dielectric with permittivity ε, Eqns. 7, 12, and 20 become

$$\mathbf{E} = Q\,\mathbf{r}/(4\pi\varepsilon r^3) \tag{28}$$

for Coulomb's law,

$$C = \varepsilon A/d \tag{29}$$

for the capacitance of a plane capacitor, and

$$U = (\varepsilon/2)\int E^2\,dV = {}^1/_2 \int D\,E\,dV \tag{30}$$

for the energy of the field.

2.3.3. Surface potentials: In a plane capacitor with a homogeneous liquid dielectric the electric field is constant. Hence the potential profile is linear (see Fig. 2), and the potential difference between the plates is related to the surface charge density σ on the plates by

$$\Delta\phi = \sigma\, d/\varepsilon \tag{31}$$

If a constant $\Delta\phi$ is imposed by means of an external voltage source, and the electrolyte $A^{Z+}B^{Z-}$ is introduced into the dielectric, an excess of anions and cations is accumulated at the positive and negative plate, respectively. This causes a screening effect so that the electric field in the bulk vanishes. At $T = 0$ the entire excess charge would be closely attracted to the plates. However, at $T > 0$, owing to the thermal motion which blurs the distribution of particles, the screening acquires some length which determines the size of the region of net charge. The entire surface region including the charge on the plate and the diffuse charge in solution is called the electric (or diffuse) double layer which on the

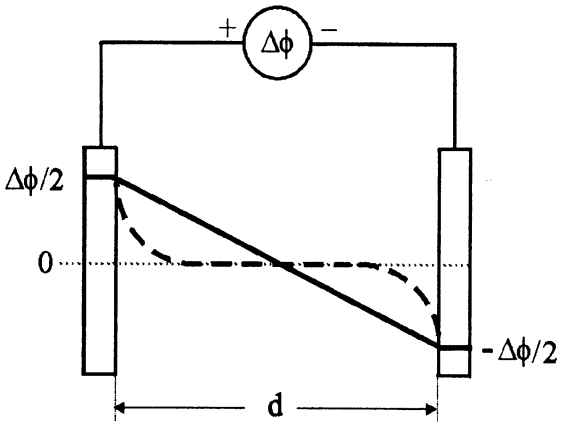

Fig. 2. Potential profile in a plane capacitor with a dielectric in the absence (solid line) and the presence (broken line) of an electrolyte $A^{Z+}B^{Z-}$.

whole is neutral but has a dipole moment. The field intensity in the diffuse double layer is much larger than the field in the absence of the electrolyte (see Fig. 2). Hence the external source has to supply additional charge to the plates in order to maintain the same value of $\Delta\phi$. The potential profile and the distribution of charge in the double layer are a typical example of a self-consistent phenomenon. This means that the field arises from the surface and mobile charges, but the distribution of the mobile charges is also determined by this very field.

In a dielectric the Poisson equation in the one-dimensional form reads (cf. Eqn. 13)

$$d^2\phi/dx^2 = -\rho(x)/\varepsilon \tag{32}$$

where x denotes a space coordinate perpendicular to the surface of the plate which points into the electrolyte solution and has its origin on the surface. For the symmetric electrolyte $A^{Z+}B^{Z-}$ the volume density $\rho(x)$ is related to the space-dependent ion concentrations $c_A(x)$ and $c_B(x)$ by

$$\rho(x) = Z\, e\, N_A\, [c_A(x) - c_B(x)] \tag{33}$$

where N_A denotes Avogadro's number. Since the electrochemical potential of both ionic species has to be constant throughout the dielectric (cf. section 2.2) one obtains from Eqns. 1 and 4

$$c_A(x) = c_b \exp[-Z\, e\, \phi(x)/(kT)]\,,$$

$$c_B(x) = c_b \exp[Z\, e\, \phi(x)/(kT)] \tag{34}$$

where c_b denotes the bulk concentration of the electrolyte. Combining Eqns. 32–34 yields the Poisson-Boltzmann equation, which in electrochemistry is known as the Gouy-Chapman equation

$$e/(kT)\, d^2\phi/dx^2 = \sinh[Z\, e\, \phi(x)/(kT)]/(Z\, \lambda^2) \tag{35}$$

The quantity λ called Debye length is defined as

$$\lambda = [\varepsilon kT/(2e^2 N_A Z^2\, c_b)]^{1/2} \tag{36}$$

and can be interpreted as a screening length. The value of λ tends to zero for T approaching 0; it decreases with increasing c_b, and is in the nm range for typical values of c_b (see section 2.3 in chapter 2).

In the small-potential approximation $Ze\phi/(kT) << 1$, Eqn. 35 is simplified to what is called the Debye equation,

$$d^2\phi/dx^2 = \phi/\lambda^2 \tag{37}$$

With the boundary conditions $\phi \to 0$ for $x \to \infty$ and $\phi(0) = \phi_s$, Eqn. 37 has the solution

$$\phi(x) = \phi_s \exp(-x/\lambda) \tag{38}$$

The quantity ϕ_s is called the *surface potential* and is equal to the difference between the potential at the membrane surface and in the bulk. The electric field on the surface is

$$E_s = -\, d\phi/dx \,|_{x=0} = \phi_s/\lambda \tag{39}$$

Hence, by means of Eqn. 27 with $\varepsilon_1 E_{1,n} = 0$ (metal plate) and $\varepsilon_2 E_{2,n} = \varepsilon E_s$, we obtain

$$\sigma = \varepsilon\, \phi_s/\lambda \tag{40}$$

If we consider the diffuse double layer as a capacitor, we obtain for its specific capacitance (cf. Eqn. 11)

$$C/A = \sigma/\phi_s = \varepsilon/\lambda \tag{41}$$

which is equal to the specific capacitance of a plane capacitor with a distance λ between the plates. In the general case, i.e. if the Debye approximation does not hold, the specific capacitance of the diffuse double layer depends on the surface potential,

$$C/A = (\varepsilon/\lambda) \cosh[Z\, e\, \phi_s/(2kT)] \tag{42}$$

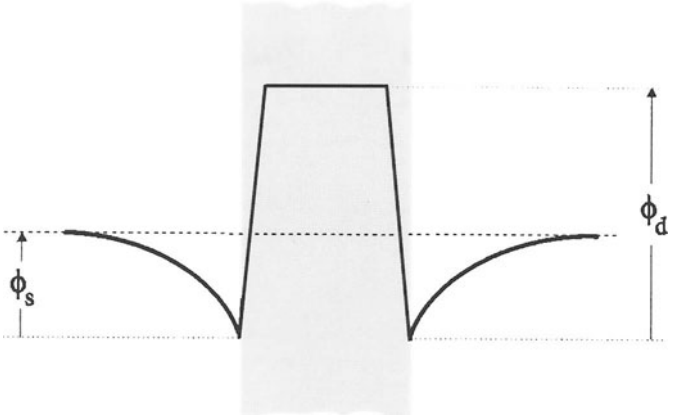

Fig. 3. Potential profile across a membrane with surface potentials ϕ_s and dipole potentials ϕ_d (symmetrical case).

The one-dimensional approximation usually used (cf. Eqn. 32) implies an averaging over the membrane surface. Experimental studies of the electrical properties of lipid bilayers show that the Gouy-Chapman equation works quite well in the one-dimensional approximation within a broad range of potentials [2]. At first glance, this seems surprising because the membrane surface formed by the polar head groups of the lipids is rather heterogeneous. However, the liquid state features a rapid lateral mixing of the lipids, which is equivalent to an averaging.

2.3.4. Potential profiles in lipid membranes: Consider a membrane between two aqueous solutions. The polar head groups of the lipids usually carry dipoles which are assumed to be symmetrically arranged such that the negative charge of the dipoles faces the aqueous phase. The dipoles give rise to a potential difference at each surface of the membrane, which is known as the *dipole potential* ϕ_d (Fig. 3). Dipole potentials depend mainly on the nature of the lipids, but are essentially insensitive to changes in the ionic composition of the solutions (see also section 2.4 in chapter 2). In the following figures dipole potentials will be omitted for the sake of simplicity.

The surface potential ϕ_s depends on the surface charge density σ and the ion concentration c_b in the solution (cf. Eqns. 36 and 40)

$$\phi_s = \sigma \lambda/\varepsilon = \sigma/(\varepsilon K c_b^{1/2}) \tag{43}$$

where

$$K = [\varepsilon kT/(2e^2 N_A Z^2)]^{1/2} \tag{44}$$

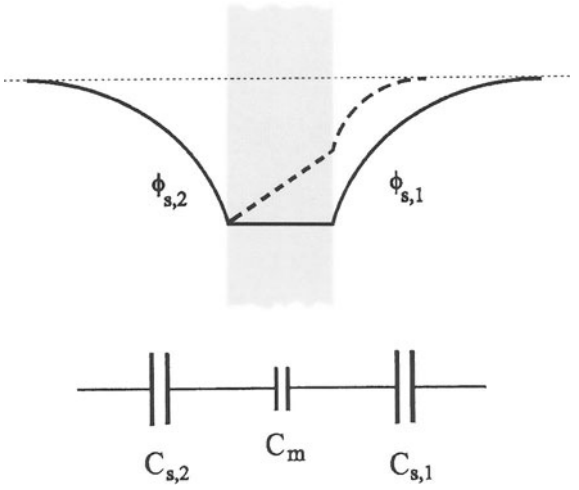

Fig. 4. Dependence of the potential profile on the ion concentration c_b in the bulk aqueous solutions for a short-circuited membrane ($\Delta\phi_m = 0$). If c_b is equal in both solutions $\phi_{s,1} = \phi_{s,2}$ (solid line) but $\phi_{s,1} < \phi_{s,2}$ if c_b is larger in solution 1 than in solution 2 (broken line). An equivalent electric circuit of the membrane is shown on the bottom.

is a constant, and ε is the permittivity of the aqueous solution. Hence if c_b is the same in both solutions the surface potentials are also equal and the potential profile for a short-circuited membrane is as shown by the solid line in Fig. 4. If, however, c_b is larger in one of the solutions the pertinent screening length λ and thus also ϕ_s are decreased, and the potential profile becomes as shown by the broken line in Fig. 4.

From the electrostatic point of view, the low-conducting membrane between electrolyte solutions is equivalent to three capacitors connected in series, the capacitors with capacitances C_{s1} and C_{s2} associated with the diffuse layers and a capacitor with capacitance C_m representing the membrane (Fig. 4). In view of Eqns. 29 and 41 the ratio between the capacitance of the membrane and one of the diffuse layers is

$$C_m / C_s = \varepsilon_m \lambda / (\varepsilon d) \tag{45}$$

where ε_m and d are the permittivity and the thickness of the membrane, respectively. Inserting typical values for the parameters in Eqn. 45 shows that C_m/C_s is of the order of 0.01. The electric potential is known to drop most across the smallest of the in-series capacitors. This implies that a variation of the transmembrane potential difference $\Delta\phi_m$ has virtually no effect on the surface potentials but is almost entirely manifested by a variation of the intramembrane potential difference $\Delta\phi_{im}$.

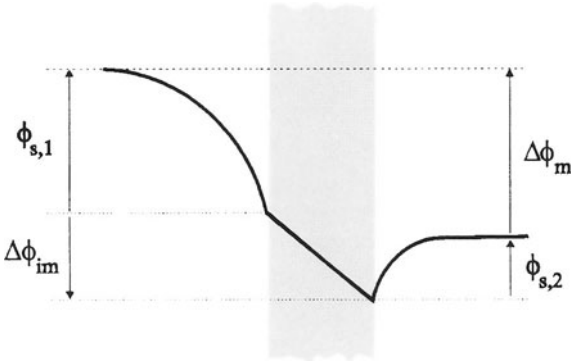

Fig. 5. Components of the transmembrane potential difference $\Delta\phi_m$.

The potential profile across a membrane for a typical case is shown in Fig. 5. The transmembrane potential difference $\Delta\phi_m$ comprises the two surface potentials ϕ_{s1} and ϕ_{s2}, and the intramembrane potential difference $\Delta\phi_{im}$. The magnitudes of $\Delta\phi_m$ and $\Delta\phi_{im}$ are determined by ion transport processes occurring across the membrane and/or by an externally applied field. The magnitudes of ϕ_{s1} and ϕ_{s2} are determined by the surface charge densities, which may change due to adsorption/desorption of ions or a shift in pH, as well as by the ion concentrations in the solutions. The potential profile inside the membrane is linear, but decays more or less exponentially (or exactly exponentially if $\varepsilon\phi_s$ /kT << 1) in the diffuse double layers. In a most general case dipole potentials may be present and the potential profile has to be modified as shown in Fig. 3. In this case $\Delta\phi_{im}$ may also include a contribution from the dipole potentials if the membrane is not symmetric. The components of the membrane potential play various functional roles (see also section 5 in chapter 2). The value of $\Delta\phi_{im}$ influences the ion flows and the stability of the membrane. The values of the surface potentials determine the cell motion in an external field, cell-cell interactions, adsorption of charged particles, and affect the concentrations of mobile ions in the membrane.

3. Methods for measuring membrane potentials

3.1. Electrophoresis

Cells or liposomes with a surface charge experience a force in an electric field E. In the steady state this force is balanced by the viscous

drag and the particles migrate at a constant velocity v (electrophoresis). According to Smolukhovsky's formula

$$v = \varepsilon E \zeta/\eta \tag{46}$$

where ε and η denote, respectively, the permittivity and the viscosity of the medium. The quantity ζ called zeta (or electrokinetic) potential is the electrical potential at the plane of shear, i.e. the boundary between the water layer, which migrates with the particle due to the adhesion of water on the surface, and the bulk phase. Obviously ζ is not identical with the surface potential ϕ_s, but it can be estimated using the Gouy-Chapman theory. Thus, the migration velocity v measured in an electrophoresis experiment can be used to determine ϕ_s, although this value is somewhat ambiguous because of the uncertainty associated with locating the correct position of the plane of shear (see also section 3.1 in chapter 2).

3.2. Measurement of membrane conductivity

This method is applicable to bilayer lipid membranes for determining the surface potential as a function of the ionic composition of the solutions. The same concentrations of impermeable ionic species are used for both solutions (background electrolyte), and a monovalent lipophilic ion, which can permeate through the membrane, is added at a small concentration. The concentration c_m of the lipophilic ion in the membrane is

$$c_m = K_p c_b \exp [- e \phi_s /(kT)] \tag{47}$$

where K_p is the partition coefficient and c_b the concentration in the bulk. The conductivity g_m of the membrane is proportional to the mobility u of the lipophilic ion in the membrane,

$$g_m \propto u c_m \tag{48}$$

If $g_m(c_i)$ is measured for different concentrations in the background electrolyte, symbolized by the argument c_i, it follows from Eqns. 47 and 48 that

$$\Delta\phi_s(c_i) = (kT/e) \ln [g_m(c_i)/g_m(c_s)] \tag{49}$$

where c_s denotes an arbitrarily chosen standard composition. Using the function $\Delta\phi_s(c_i)$ one can then calculate the surface charge density of the membrane by means of the Gouy-Chapman theory.

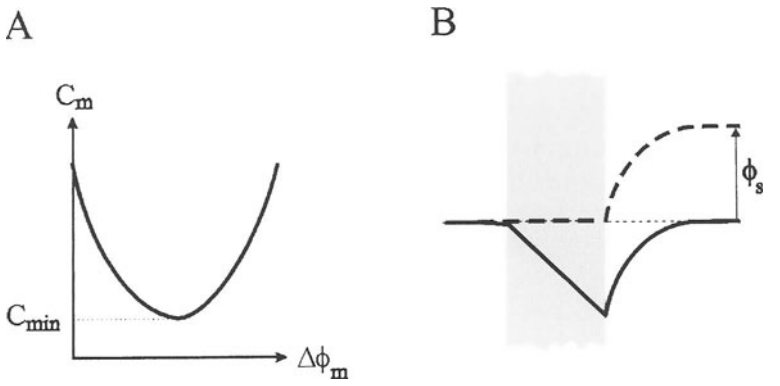

Fig. 6. Method of intramembrane field compensation. (A) Dependence of membrane capacitance C_m on transmembrane potential difference $\Delta\phi_m$. The minimum C_{min} is attained if $\Delta\phi_{im} = 0$. (B) Potential profiles across the membrane for $\Delta\phi_m = 0$ (solid line) and $\Delta\phi_{im} = 0$ (broken line).

3.3. The method of intramembrane field compensation

This method is suitable for measuring the intramembrane field and the surface potential of bilayer lipid membranes. It was experimentally shown that the capacitance of the membrane is a parabolic function of the transmembrane potential difference $\Delta\phi_m$, with a minimum C_{min} at the point where $\Delta\phi_{im} = 0$ (Fig. 6A). This result can be interpreted as arising from a membrane electrostriction under the action of the intramembrane field. The parabolic function of the membrane capacitance then arises if the change in membrane thickness Δd is proportional to $1/\Delta\phi_{im}^2$, since C_m is proportional to $1/d$ (cf. Eqn. 29). Following Alvarez and Latorre [3], consider a membrane formed from two monolayers one of which is charged and the other is neutral. If $\Delta\phi_m$ is clamped to zero the potential profile is as shown by the solid line in Fig. 6B, i.e. $\Delta\phi_{im}^2 > 0$ and hence $C_m > C_{min}$. If $\Delta\phi_m$ is chosen such that $C_m = C_{min}$ the potential profile is as shown by the broken line in Fig. 6B and $\Delta\phi_m = \phi_s$ since $C_m << C_s$ (see section 2.3.4). Moreover, $\Delta\phi_m$ is equal to $\Delta\phi_{im}$ in the case of the short-circuited membrane. The same protocol can be used for a symmetrically charged membrane, but then the composition of the background electrolyte on one side of the membrane is varied as described in section 3.2 which yields the function $\phi_s(c_i)$. Using this function one can calculate the surface charge density of the membrane by means of the Gouy-Chapman theory. Several modifications of this method are described in the literature [4, 5].

3.4. Optical probes

Using electrodes to measure membrane potentials (cf. section 3.1 in chapter 2) is not always possible particularly for small-sized cells, subcellular particles and liposomes. In these cases the use of probes whose optical properties depend on $\Delta\phi_m$ is the method of choice (see also section 3.2 in chapter 2). The signal of such probes has to be calibrated which is most commonly done with the K^+/valinomycin system. Valinomycin causes a substantial increase of the membrane permeability selectively for K^+ ions, and $\Delta\phi_m$ is then approximated by the Nernst potential for K^+ (see Eqn. 5) using the concentrations of this ion outside and inside the cell or liposome. While the concentration in the suspending medium can be controlled, the concentration inside may not always be precisely known. Moreover, this calibration can depend unfortunately on the number of particles used.

Optical probes are customarily classified into intrinsic and extrinsic probes. The former include carotenes whose spectral properties change in an electric field, a phenomenon called electrochromism. The advantage of such probes is their fast response, but their use is confined to the carotene-containing membranes. The change in adsorption at 515 nm is measured, and the calibration is done by means of the K^+/valinomycin system. Attempts to synthesize electrochromic probes have so far failed although styryl derivatives behave in a similar way.

Extrinsic probes include a vast number of compounds which are constantly being expanded. The most popular of the extrinsic probes are cyanine dyes (diS-C3-(5)) and carbocyanine dyes (di-O-C5) which are positively charged, and oxonols which are negatively charged. They can permeate through the lipid bilayer and have characteristic time constants of about 1s. In contrast the negatively charged merocyanines fail to permeate through the bilayer in spite of their lipophilicity, but their response is fast with characteristic time constants of less than 0.1 ms. Other probes behaving like merocyanines are safranine and ANS. As a rule, calibration of extrinsic probes is done with the K^+/valinomycin system.

Consider in brief the mechanism of action of extrinsic optical probes by way of example with oxonol VI [6]. Oxonols are successfully used to measure $\Delta\phi_m$ in cases where the inner region of the vesicles is positively charged. The main point is that the fluorescence of optical probes in the lipid phase is significantly higher than in the aqueous phase. Hence the basic fluorescence of oxonol in buffer (Fig. 7, curve 1) increases if liposomes are added (Fig. 7, curve 2). Oxonol partitions between the external solution and the intravesicular space according to Nernst's law (Eqn. 5), and hence is concentrated in the liposomes, but also in the inner monolayer because of the high partition coeffi-

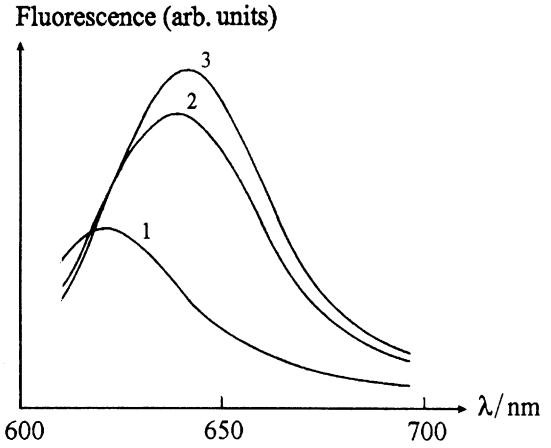

Fig. 7. Fluorescence spectra of oxonol VI in buffer (1), after the addition of liposomes (2), and in the presence of K^+/valinomycin (3) which causes $\Delta\phi_m$ = 36 mV (positive inside the liposomes). After Apell and Bersch [6].

cient in favor of the lipid phase which gives rise to the increased fluorescence. Adding valinomycin and K^+ to the suspending solution causes an increase of the transmembrane potential difference according to the Nernst equation (Eqn. 5), which in turn causes a further increase in fluorescence (Fig. 7, curve 3). With this technique a calibration curve between $\Delta\phi_m$ and fluorescence can be established, which can be used to determine $\Delta\phi_m$ of any vesicles or cells [6]. The transmembrane potential difference of the liposomes in the absence of valinomycin can then be calculated by means of the fluorescence with and without valinomycin.

The mechanism of action of merocyanines and other "fast" probes differs from that of the "slow" probes. Merocyanine appears to partition between the external aqueous phase and the membrane phase, and thus is localized in the outer monolayer close to the surface. In this way, its distribution "senses" the potential between this plane of adsorption and the external solution.

An alternative method of calibration consists of the null-point procedure. Consider this approach by example of measuring $\Delta\phi_m$ in erythrocytes [7]. The transmembrane potential difference in these cells is determined by the transport system of Cl^- ions, and is negative inside. Therefore, it is convenient to use the positively charged cyanine dye, which is distributed according to the Nernst law and yields a certain fluorescence signal reflecting $\Delta\phi_m(Cl^-)$. Adding a sufficient amount of valinomycin imposes a potassium potential $\Delta\phi_m(K^+)$ upon the cell, and cyanine is redistributed accordingly which leads to a change in the

fluorescence signal. The concentration of K^+ in the suspending medium is then adjusted such that the fluorescence is the same as without valinomycin, i.e. $\Delta\phi_m(K^+) = \Delta\phi_m(Cl^-)$. If the K^+ concentration in the erythrocytes is known, $\Delta\phi_m(K^+)$ and thus $\Delta\phi_m(Cl^-)$ can be calculated with the Nernst equation (Eqn. 5). With this method a value for $\Delta\phi_m(Cl^-)$ of about 5 to 9 mV was found, which is consistent with the results of other measurements.

4. Methods of electrical measurements on bilayer lipid membranes

Figure 8 depicts schematically a setup used to study the electrical properties of bilayer lipid membranes. Design in measuring cells, methods of membrane formation, and the features of electrical measurements are described in detail in Ref. 8 (see also section 4.2 in chapter 3). Here the conducting properties of the membrane has to be taken into account, in contrast with the conditions discussed in the previous sections where current flow across the membrane could be neglected. Hence, an equivalent circuit of the membrane consists of a capacitor C_m and a leakage resistor R_m (representing the membrane conductance) connected in parallel, while a resistor R_s represents the resistance of the electrolyte solutions and the electrodes (Fig. 9). In general the elements of the circuit are a function of the potential differences across them and may change during the course of the experiment. A standard technique in kinetic studies is to disturb the equilibrium or the stationary state of the system and record its relaxation to a new state. In line with the electrochemical terminology, we shall classify the methods of affecting the system as follows:

(1) potentiostatic: a preset protocol $\Delta\phi_m(t)$ for the transmembrane potential difference is applied (usually steps or square pulses [9]) and the membrane current, charge or capacitance are measured,
(2) galvanostatic: a preset current is passed through the system and the membrane potential is measured,
(3) coulomb-static: the membrane is charged up to a preset value and the relaxation of the transmembrane potential difference is measured.

With the typical parameter values C_m = 1–10 nF, R_m = 1–100 GΩ, R_s = 0.1–1 kΩ, the time constant of the cell $\tau_c = C_m R_s$ is less than 10 μs. The condition of voltage clamp on the membrane, i.e., the correspondence of the voltages across C_m and across the generator output is provided on a wide time scale only if both the time constant of the cell, τ_c, and of the entire circuit, τ, are significantly smaller than the

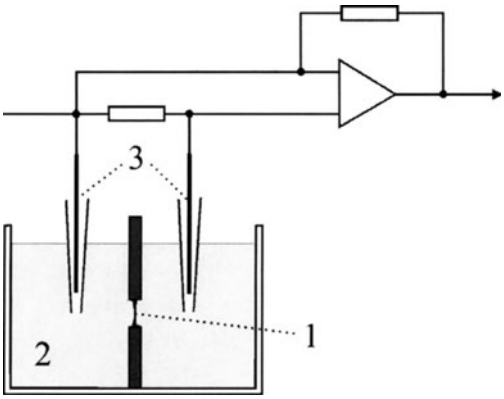

Fig. 8. Schematic diagram of a setup used to study electrical properties of bilayer lipid membranes. The membrane (1) is formed on a hole of a supporter immersed in a cuvette with an aqueous solution (2). The transmembrane potential difference $\Delta\phi_m$ is monitored with two electrodes (3).

time of observation. This imposes certain limitations on the output impedance of the generator, R_g, and the input impedance of the current amplifier, R_a, since $\tau = C_m (R_s + R_g + R_a)$. The modern operational amplifiers, for instance the Keithley-427 current/voltage converter with a range of measured currents between 10^{-13} and 10^{-3} A, behave as a current amplifier with essentially zero input impedance R_a. At the gain coefficient of 10^6 V/A, the value of the rise-time, τ_r, of this instrument is 15 μs which is close to τ_c. If the sensitivity is increased τ_r increases too, and the response thus becomes slower. This difficulty can be overcome by means of a two-electrode potentiostat, which compensates the ohmic losses in the cell, and τ can be lowered by almost one order of magnitude. This method virtually coincides with the voltage-clamp technique widely used in electrophysiology. The recorders suitable for these studies are standard equipment and need not be further specified.

In strong electric fields the major events which lead to the change in the conducting properties of the membrane develop within shorter times than several microseconds, i.e. close to the time span of the potentiostatic measurements. Such processes can be investigated by the coulomb-static method of charge relaxation [10]. The method consists of the fast charging of the membrane by a current pulse, followed by the recording of its relaxation owing to the self-discharge of the system (see Fig. 9). The major technical problem here is the necessity to rapidly disconnect the charging generator from the cell. The rate of self-discharge is determined by the capacitance and resistance of the membrane. Even in a strong electric field the capacitance of the membrane changes by no more than several percent, whereas the resist-

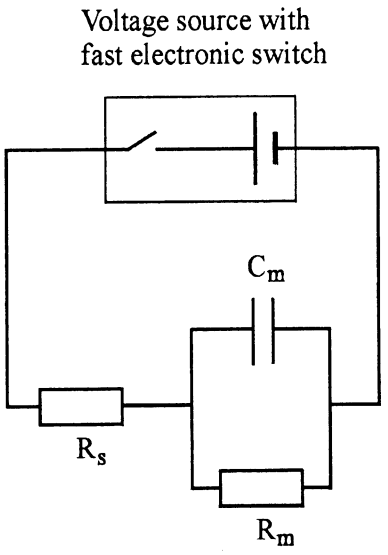

Fig. 9. Equivalent electric circuit for a measuring cell with a bilayer lipid membrane (cf. Fig. 8). The voltage source with a fast electronic switch is used in the coulomb-static method of charge relaxation as described in the text.

ance decreases by several orders of magnitude. Thus, the time course of self-discharge can be used to judge the character of changes in its resistance. It is true, though, that the data obtained by this method are hard to interpret because, during the self-discharge, the membrane potential constantly decreases and it is exactly $\Delta\phi_m$ that determines the conductance of the membrane. Another problem is the switching-off of the external source which limits the beginning of the recording to approximately a fraction of a microsecond. But, as is evident from the results reported in Ref. 9, the conductance has then already dropped by many orders of magnitude and remains almost constant within the entire time span of measurement. This shows that the crucial events occur in the nanosecond range where no direct recording is feasible. Thus, the potentiostatic method and the charge relaxation method are complementary. The first one makes it possible to record the changes in conductivity from 10^{-8} to 10^{-1} Ω^{-1} cm^{-2} at a resolution of 5 to 10 μs. The second one allows one to elucidate how soon the conducting state emerges (ns), but does not make it possible to follow its evolution on larger time scales.

Acknowledgements

I wish to thank Dieter Walz for helpful discussions and enormous editorial work. This work was supported by the CNRS and by a "Bourse pour chercheur de haut niveau" from the French Ministère de la Recherche.

References

1 Parsons R (1954) Equilibrium properties of charged interfaces. In: JO'M Bockris (ed.): *Modern aspects of electrochemistry*. Butterworth Scientific Publishers, London, 123–208.
2 McLaughlin S (1977) Electrostatic potentials at membrane-solution interface. In: F Bronnen, A Kleinzeller (eds.) *Current topics in membranes and transport*. Academic Press, New York, Vol. 9, 70–144.
3 Alvarez OA, Latorre R (1978) Biophys. J. 21: 1–7.
4 Chizmadzhev YA, Abidor IG (1980) Bioelectrochem. Bioenerg. 7: 83–100.
5 Sokolov VS, Cherny VV, Simonova MV, Markin VS (1990) Bioelectrochem. Bioenerg. 23: 27–44.
6 Apell H-J, Bersch B (1987) Biochim. Biophys. Acta 903: 480–489.
7 Bashford CL, Smith JC (1979) Potential-sensitive optical probes. In: S Fleischer, L Packer (eds.) *Methods of enzymology*. Academic Press, New York, Vol. LV part F – Biomembranes, 569–586.
8 Tien HT (1974) Bilayer Lipid Membranes (BLM). Marcel Dekker Inc, New York, 655
9 Chernomordik LV, Chizmadzev YA (1989) Electric breakdown of lipid bilayer membranes. In: E Neumann, A Sowers, C Jordan (eds.): *Electroporation and electrofusion in cell biology*. Plenum Press, New York, London, 83–95.
10 Zimmermann U, Scheurich P, Pilwat G, Benz R (1981) Angew. Chem. 20: 325–344.

Bioelectrochemistry of Membranes
ed. by D. Walz, J. Teissié and G. Milazzo†

CHAPTER 2
Membrane potentials: measurement, occurrence and roles in cellular functions

Paul O'Shea
Cell Biophysics Group, School of Biomedical Sciences, University of Nottingham, Nottingham NG7 2UH, United Kingdom

1. Introduction – the occurrence of membrane potentials in nature

Over a quarter of a century ago, the publication of the now familiar fluid-mosaic model of biological membranes (Fig. 1) described by Singer and Nicolson [1] was a landmark in cell biology. It provided a sound rubric for the future studies of the profound roles membranes play in cellular and physiological functions. And, indeed, a colossal expansion of both the information and understanding of the central role that membranes play in all aspects of cell function [2] has been seen. Apart from effectively defining the cell both morphologically as well as functionally, we have the beginnings of an understanding of how membranes feature in cellular development, cell recognition, metabolism, signal transduction and pathology etc. but many molecular details of the mechanisms remain elusive.

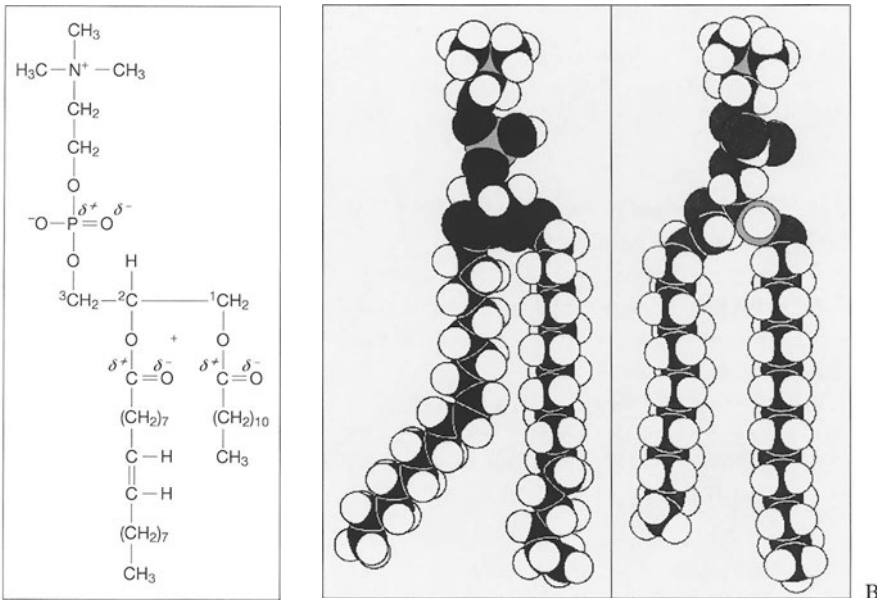

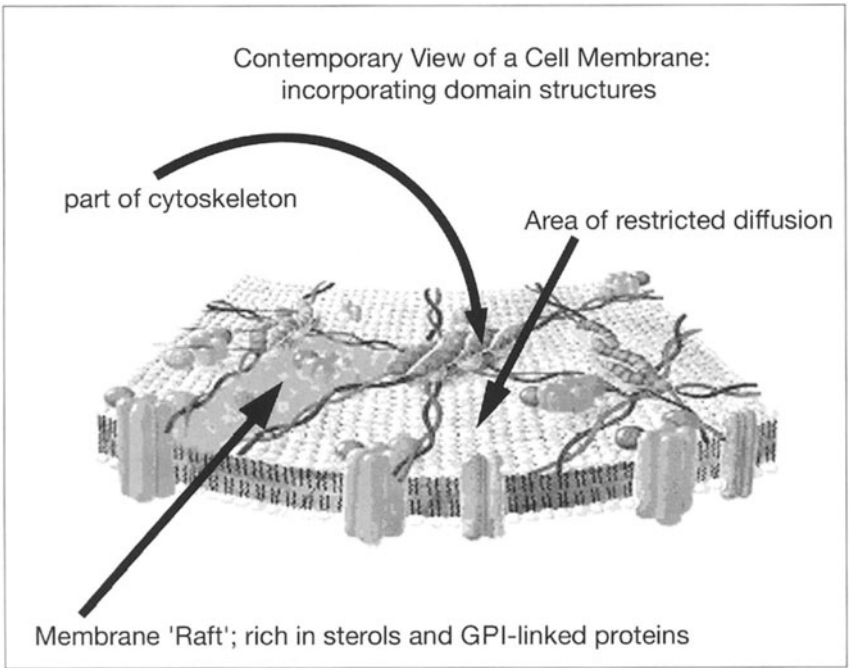

Fig. 1. The membrane bilayer; evolving complexity *in vivo*. (A) A typical phospholipid (phosphatidylcholine) also showing dipolar arrangement of functional groups. (B) Space-filling models of phosphatidylcholine (left) and sphingomyelin (right). (C) A more complex membrane including the cytoskeleton (after Ref. 2).

The majority of these processes are considered to reside in the highly specific "ligand-receptor" interactions conferred on particular membrane systems by virtue of their complement of integral protein components. Ironically, and in many ways, the abiding impression which seems to have evolved, however, is that the principal role of the membrane is to compartmentalise cellular components simply by acting as a selective permeability barrier. Thus, the barrier function is provided by the properties of the bilayer phospholipid and selective solute permeability, transport or transmembrane signalling is conferred by the proteinacious membrane components. This is certainly not an incorrect view but it is rather simplistic, for membranes possess many other fundamental and fairly ubiquitous properties which are likely to be as influential, but evidently not as well-known or perhaps understood, as the barrier functions. In this chapter, the importance of the barrier function will not be undervalued but the role of some of these additional membrane properties will be outlined.

In the past, studies of the fabric of the membrane were directed mostly towards the roles played by lipids, but these tended to be less of interest to cell biologists and more to biophysicists. The latter have often made little attempt to justify the relevance of their observations within the context of a biological problem. Similarly, cell biologists were not too inclined to consolidate such physical observations with their own particular frame of reference. Lately, these slightly parochial strategies have been superseded by truly multidisciplinary approaches which have proved to be enormously fruitful and informative. A good example of this involves the recently identified membrane microdomain components known as *Rafts*; these structures are stabilized by the physical forces which underlie the phase-separation of sterols such as cholesterol and sphingolipids in the membrane bilayer (Fig. 1). They appear to "recruit" glycosylphosphatidylinositols (GPI) and GPI-linked proteins [3]. Rafts appear to be of major biological importance [4] as their attendant (GPI-linked) proteins play significant roles in cell signalling and endocytosis. Similarly, e.g., Aderem and McLaughlin [5] have combined biophysical views with experiments in cell biology to both answer and pose questions dealing with signal transduction. With these examples in mind, the principal theme of the present chapter is directed towards the contributions that some ubiquitous physical properties of membranes play in cellular functions. The main focus will revolve around the various types of physical (i.e. mainly electrical) potentials associated with membranes.

Membrane potentials are manifest in a number of forms which have quite different origins and properties. Unfortunately, there seems to be noteworthy confusion associated with some of these potentials both in terms of their origins, identity and not least, their nomenclature, as well as with their influence on a number of important biolog-

ical processes. Consequently, it is not unexpected that a clear understanding of the explicit roles some of these processes play in biology are not widely appreciated. Presently, there are three types of membrane potential that merit separate consideration.

The "membrane potential" which has received the most experimental attention and is certainly the best-documented, is associated with a gradient of electrical charge across the phospholipid bilayer (cf. Fig. 1). These charge gradients are engineered and maintained by the translocation of charged solutes (e.g., ions) or electron transport across the membrane. To be established, they require an input of energy in one form or another. This field of endeavour is known as bioenergetics, and initially tended to deal exclusively with eucaryotic plastid and bacterial membranes [6]. A common feature of these gradients is that either or both an ionic concentration difference or the electrical gradient across the membrane may be utilised depending on the biological application. The gradient of electric charge gives rise to what is known as *the* membrane potential and is usually referred to by the symbol $\Delta\psi$ [6, 7]. Electrical potential differences of very similar origins are also described by electrophysiologists in plasma and organellar membranes in both plants and animals and are also explicitly referred to as membrane potentials [2]. Authoritative reviews of the manifold roles these gradients play in biological processes can be found in the earlier volumes of this series on bioelectrochemistry and in several cell biology and biochemistry university texts [2]. In view of this, a much less comprehensive description is presently necessary of the many roles these "membrane potentials" play in biological functions. For the sake of clarity, this membrane-associated potential will be referred to as the *transmembrane potential difference* (in fact, this ought to be referred similarly in the wider scientific literature). It is also worth emphasising that related to the transmembrane potential difference, another gradient of electric charge is known to exist which is the source of what is known as the Donnan potential. The Donnan potential arises from the inability of larger charged macromolecules or other fixed charges to move across the membrane.

The second "membrane potential" of major significance is known as the *membrane surface potential* and its existence has been established for some time. Unfortunately, with its roots in quite complex interfacial physics and electrochemistry (see below), it has only recently been appreciated by cell biologists to be an important and influential phenomenon. Nevertheless, the underlying physical theory is well developed and robust with congruency between many biological surfaces that possess such a potential with a similar commonality of formal description [8, 18] and in a membrane context, reviews by McLaughlin [9] and Cevc [10] offer sound and eloquent expositions of the nature of this membrane potential. With this in mind, there is

much compelling experimental evidence that indicates the surface potential is a major player in membrane biology.

The final manifestation of a "membrane potential" described as the *membrane dipole potential* considered in this review deals with the contribution that molecular polarisations or electrical dipoles make to the properties of biological membranes [11]. The membrane dipole potential is thought to have its origins in the molecular polarisations associated with the carbonyl group and the oxygen-bonded-phosphates components of most membranes (see Fig. 1). These occur at the membrane surfaces or perhaps just within what textbooks would describe as the hydrophobic phase of the membrane. In addition individual molecules of water are thought to adopt an organised structure along the membrane surface by virtue of their permanent molecular dipoles and so may also make a contribution [8]. This dipole potential, therefore, occupies the regions at or near the membrane surface but is also located just within what is usually regarded as the interior of the membrane. The dipole potential, however, is both the least well-documented and the least well-understood of all of these so-called membrane potentials. The appearance and influences that it may play in particular biological processes, therefore, remains somewhat poorly appreciated. Evidence is accumulating, however, which indicates, that the manifestation of this "membrane potential" is likely to be at least as influential as the others.

2. The nature of the membrane potentials: What are potentials?

Membrane potentials have their physical origins in both surface electrochemistry and interfacial physics. The appropriate terminology for their descriptions, therefore, comes from both sources; classical texts as reference to this include *Modern Electrochemistry* [12], *Introduction to colloid and surface chemistry* [13], and *Electromagnetism* [14]. The confusion in the literature about the nomenclature used for each of the "membrane potentials" is all too evident; biochemists seem unaware of the fact that a well-defined nomenclature for electrical potentials was developed in electrochemistry (see section 2.2 in chapter 1) long before electrochemistry became relevant to biochemical problems. Hence names and symbols were sometimes chosen and evolved into general usage that are not consistent with the electrochemical conventions. Another layer of complication to the nomenclature is also evident as within the discipline of classical physics, i.e. electromagnetism [14], offers alternative symbols for electrical potentials (e.g., the dipole potential as Φ_r). In a subject that is becoming genuinely multidisciplinary such a confused multinotational nomenclature is extremely counter-productive. Thus, the notations

adopted in this review are derived from the "elder" discipline of electrochemistry for reasons of clarity; all "membrane potentials" then map to the "internal" (i.e. the so-called "Galvani") potential whose symbol is ϕ. Accordingly the transmembrane potential difference would be denoted by $\Delta\phi_m$ (instead of $\Delta\psi$), and the membrane surface potential by ϕ_s (instead of ψ). Finally, the symbol for the membrane dipole potential is ϕ_d (instead of Φ_r) although the symbol for a dipole potential (unfortunately also called surface potential) in electrochemistry is χ. The view that the membrane dipole potential is a type of Galvani potential, however, seems more logical. For the sake of clarity these symbols will be reiterated in the subtitles of the subsequent sections.

2.1. (Electro)chemical potential: an expression of (potential!) thermodynamic activity

In the simplest terms, the term chemical potential μ_i is used to describe the thermodynamic activity of a chemical species i. When this species also possesses a net electrical charge as indicated by the charge number Z_i, an electrical term comprising the electrical potential ϕ of the phase is also included explicitly in the expression. The electrical and chemical potential are commonly combined and described by the symbol $\tilde{\mu}$ (see section 2.2 in chapter 1)

$$\tilde{\mu}_i = \mu_i + Z_i e\phi = \mu_i^o + kT \ln (c_i/c^o) + Z_i e\phi \qquad (1)$$

Here μ_i^o is the standard chemical potential, e the elementary charge, k the Boltzmann constant, T the absolute temperature, c_i the concentration, and c^o a standard concentration (usually 1 M).

The electrochemical potential $\tilde{\mu}_i$ is defined as the partial derivative of the Gibbs energy (or free enthalpy) G of the system with respect to the mole number n_i of the species, with other parameters (temperature, pressure, and mole number of other species) kept constant. Hence any spatial gradient of $\tilde{\mu}_i$, as well as a difference of $\tilde{\mu}_i$ between phases or compartments, constitutes a thermodynamic driving force and a "potential" for performing useful work. Vanishing gradients or differences of $\tilde{\mu}_i$ then indicate that species i has reached an equilibrium state.

2.2. The transmembrane electrical potential difference $\Delta\phi_m$

Membranes represent permeability barriers to the movement of ions (and electrons). Thus, the transport of net charge across the insulator

offered by the membrane will establish an electrical potential difference $\Delta\phi_m$ across the membrane. The transport of electrical charge across a membrane may take the form of cation, anion (both inorganic and organic) or electron transport. It can be passive due to membrane leaks or mediated by catalysts (e.g., valinomycin which facilitates the transport of K^+ and Rb^+). In this case the transport is driven by the difference in electrochemical potential of the particular ion between the two phases separated by the membrane. In biological membranes, however, the transport is frequently coupled either to the movements of other ions due to co- or anti-porting enzymes, or to chemical reactions as in the case of oxidative phosphorylation or hydrolysis of ATP. The value of $\Delta\phi_m$ established in such complex systems is governed by the relation

$$\sum_i Z_i J_i = 0 \tag{2}$$

where the sum has to include all flows J_i of charged species across the membrane [15]. When Eqn. 2 is satisfied, charging of the membrane capacity has ceased, and a (pseudo-)steady state with a (approximately) constant $\Delta\phi_m$ is then attained. Its value depends on the difference in chemical potential $\Delta\mu_i$ of all transported species and on the affinities of coupled chemical reactions. The pertinent relations are usually transcendental and cannot be solved explicitly except for some special cases. In particular, if only one species permeates through the membrane, a true equilibrium state is reached and the resulting transmembrane electrical potential difference is described by what is known as the Nernst equation (cf. Eqn. 5 in chapter 1)

$$\Delta\phi_m = (\phi_o/Z_i) \ln (c_{i,1}/c_{i,2}) \tag{3}$$

with the abbreviation

$$\phi_o = kT/e = RT/F \tag{4}$$

Here R and F are the gas constant and the Faraday constant, respectively, while $c_{i,1}$ and $c_{i,2}$ denote the concentrations of the species in the two phases separated by the membrane. Moreover, equal values of μ_i^o in both phases are assumed. Equation 3 should not be confused with another relation also called Nernst equation which relates the redox potential to the concentrations of the species of a redox couple [16, 17]. The redox potential is not a transmembrane electrical potential difference but is measured between an inert metal and a reference electrode, both in the same phase. It represents the chemical potential of the electron [17] and not its electrochemical potential as sometimes erroneously claimed. Much of this is reviewed eloquently and com-

prehensively by Walz [17] in one of the first attempts to rationalize and generalize this emerging truly, multidisciplinary science.

2.3. The membrane surface potential ϕ_s

In order for this potential to become manifest, the membrane must exist as a separate phase to that offered by the surrounding aqueous media, and the fixed charges must sit at the interface between a phase which possesses a low dielectric permittivity (i.e. non-polar) and another which possesses a high dielectric permittivity (i.e. the aqueous medium). This state of affairs, of course, is exactly the circumstances that occur at membrane surfaces within living systems, for not only is it necessary for the surface potential to become manifest but it is an absolute requirement for the stabilisation of the structure of the membrane via the so-called hydrophobic effect [1, 2]. The properties of a charged cell surface or more particularly the surfaces of all the membranes associated with the cell which are in contact with an aqueous medium containing salt, results in the presence of an electric field on the membrane surface and an electrical potential difference, ϕ_s, between the surface of the membrane and a point infinitely distant from the interface within the surrounding water-based bulk phase [9, 18].

The physical origins of the potential are worth outlining, and much of the history of the development of these ideas as directed towards metal surfaces in aqueous media (i.e. electrodes) may be found in the comprehensive electrochemistry text by Bockris and Reddy [12]. Although ions may be attracted towards the charged membrane surface, the radius of the hydrated ions in the layers adjacent to the surface prevents them from moving to the membrane surface without becoming actually adsorbed. The initial treatments of this phenomenon by Gouy and Chapman considered the ions as point charges. A modification of this model was presented by Stern who combined the much earlier Helmholtz-Perrin model with that of Gouy-Chapman (described in Refs. 12 and 13). The Helmholtz-Perrin model described the double-layer concept that counter-ions formed an ionic "sheet" upon a charged surface, the ions being at least partially dehydrated in the direction of the surface. The forces involved in the specific ionic-interactions with membranes were initially thought to be predominantly electrostatic and van der Waals in nature, and large enough to counter the thermal motion/diffusion of the ions away from the interface to the bulk medium. Later, it was suggested that water molecules may adopt a specific orientation upon the charged surface due to their permanent dipoles, and this latter concept has some bearing on an understanding of the dipole potential to be discussed in section 2.4. The Gouy-Chapman-Stern model was formalised by considering the

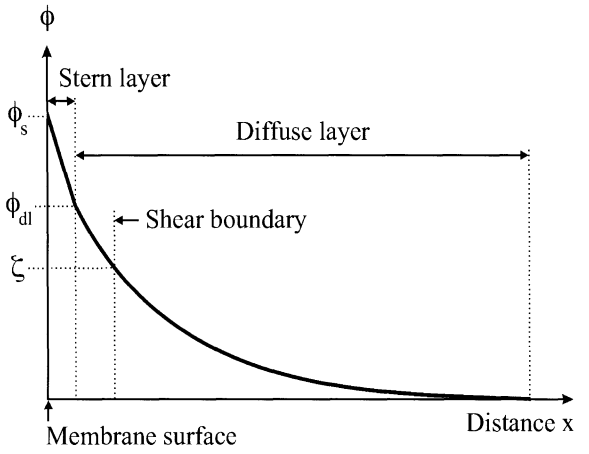

Fig. 2. Qualitative profile of electrical potential ϕ from the membrane surface to the aqueous bulk phase. Various models of the nature of the membrane-solution interface yield different predictions of the magnitude of the electrical potential at various distances from the membrane surface. The Stern layer consists of contact-adsorbed counterions and oriented water molecules. The diffuse layer comprises an inhomogeneous distribution of mobile ions of both signs according to the Gouy-Chapman model. A moving membrane carries an adhering aqueous layer, as indicated by the shear boundary, which gives rise to the zeta potential (ζ).

adsorption of counter-ions only, the process being approximated by a Langmuir-type adsorption isotherm [9, 13].

Several phases or layers have been identified which are thought to exist adjacent to the surfaces of membranes (see Fig. 2). These include the so-called Stern layer which represents contact-adsorbed counterions (either totally or partially dehydrated ions with charge opposite to that on the membrane surface) and oriented water molecules. The plane running through the centre of the contact adsorbed ions is referred to as the inner Helmholtz plane. The first layer of hydrated ions is then referred to as the outer Helmholtz plane. Adjacent to the Stern layer is the diffuse layer which is described by a combination of the Poisson equation and the Boltzmann equation. In the one-dimensional form the Poisson equation reads (cf. Eqn. 32 in chapter 1)

$$d^2\phi/dx^2 = -\rho(x)/(\varepsilon_r\,\varepsilon_0) \tag{5}$$

Here ε_r and ε_0 denote, respectively, the relative permittivity (or dielectric constant) and the absolute permittivity (or permittivity in vacuum), while x is a space coordinate perpendicular to the membrane surface which points into the electrolyte solution and has its origin on the surface. The charge density ρ can be expressed by the concentrations c_i of the charged species,

$$\rho(x) = \sum_i Z_i c_i(x) \tag{6}$$

where the sum has to be taken over all species. The Boltzmann equation for the species i reads

$$c_i(x) = c_{i,b} \exp [-Z_i \phi(x)/\phi_o] \tag{7}$$

where $c_{i,b}$ denotes the concentration in the bulk phase. It is obtained from Eqn. 1 with the assumption that the species is at equilibrium throughout the diffuse layer, i.e. $\tilde{\mu}_i$ = const (see section 2.1). Inserting Eqns. 6 and 7 into Eqn. 5 yields the Poisson-Boltzmann equation, which in general cannot be integrated analytically [9, 10, 15]. For the special case of an isolated membrane surface without a Stern layer and in contact with a symmetrical electrolyte, i.e. $Z_1 = -Z_2 = Z$ (e.g., NaCl), the integration is tractable and yields for the surface potential:

$$\phi_s = (2\phi_o/Z) \text{ Arsinh } [Z\phi_\sigma/(2\phi_o)] \tag{8}$$

with ϕ_o as in Eqn. 4 and the abbreviation

$$\phi_\sigma = \sigma \lambda/(\varepsilon_r \varepsilon_0) \tag{9}$$

Here σ denotes the surface charge density, and

$$\lambda = [\varepsilon_r \varepsilon_0 kT/(2e^2 N_A I_c)]^{1/2} \tag{10}$$

is known as the Debye length. At 25 °C $[\varepsilon_r \varepsilon_0 kT/(2e^2N_A)]^{1/2}$ = 0.304 nm $M^{1/2}$ for an aqueous phase with $\varepsilon_r \approx 80$. The quantity I_c is called ionic strength and is generally defined as

$$I_c = {}^1/_2 \sum_i Z_i^2 c_{i,b} \tag{11}$$

with the sum including all charged species i. For a symmetric electrolyte $I_c = Z^2 c_b$. In case of a membrane with a low and a high surface charge density Eqn. 8 can be approximated by

$$\phi_s \approx \phi_\sigma \text{ for } \phi_\sigma/\phi_o << 1 \tag{12a}$$

and

$$\phi_s \approx (2\phi_o/Z) \ln [Z\phi_\sigma/\phi_o] \text{ for } \phi_\sigma/\phi_o >> 1 \tag{12b}$$

respectively. The potential profile in the diffuse layer is given by

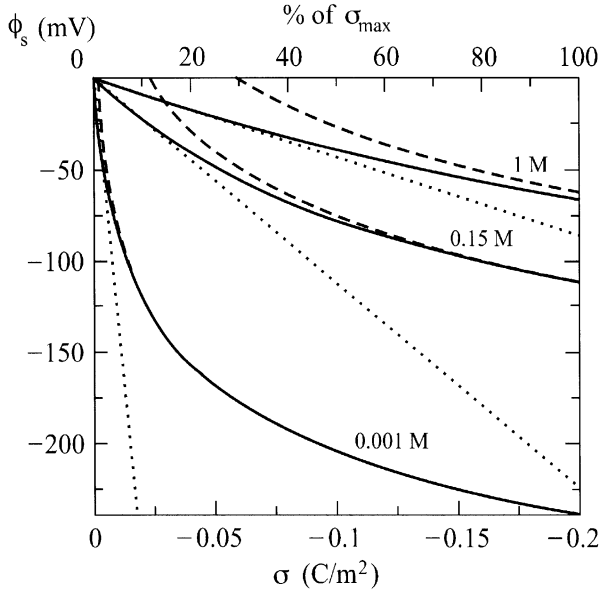

Fig. 3. Dependence of membrane surface potential ϕ_s on surface charge density σ and concentration of a univalent electrolyte. The scale on top shows σ as percentage of the maximal value $\sigma_m = -0.2$ C/m^2, which corresponds to one elementary charge per 0.8 nm^2, i.e., the approximate area occupied by one phospholipid head group. Solid lines represent Eqn. 8, while the approximations for a low and a high value of σ are represented by dotted (Eqn. 12a) and broken (Eqn. 12b) lines, respectively. Temperature 25 °C, $\varepsilon_r = 80$, electrolyte concentrations as indicated.

$$\phi(x) = \phi_o \ln \frac{1 + \tanh(\phi_s/2\phi_o) \exp(-x/\lambda)}{1 - \tanh(\phi_s/2\phi_o) \exp(-x/\lambda)} \quad \text{for } x \geq 0 \qquad (13)$$

The examples shown in Figs. 3 and 4 demonstrate that the nature and concentration of the ions in the solution surrounding the membrane have a profound effect on the surface potential ϕ_s. Any change in the concentration of the ions in the bulk phase promotes changes in the surface potential for a constant σ (Fig. 3). This phenomenon is illustrated in Table 1 when the zeta potentials (which reflect the surface potentials, see Fig. 2 and below) of erythrocytes are observed to become reduced in the presence of elevated levels of electrolyte. The other factor is the net excess charge density σ (i.e. the number of net charges per unit area) on the membrane surface. This phenomenon could well have some bearing on the interactions of molecules with cell membranes (see Table 1). On the other hand, ϕ_s not only depends upon the presence of the ions but also acts upon them. The potential profile in the membrane surface environment (Fig. 4) is a function of the surface potential (Eqn. 13). As is evident from the Boltzmann

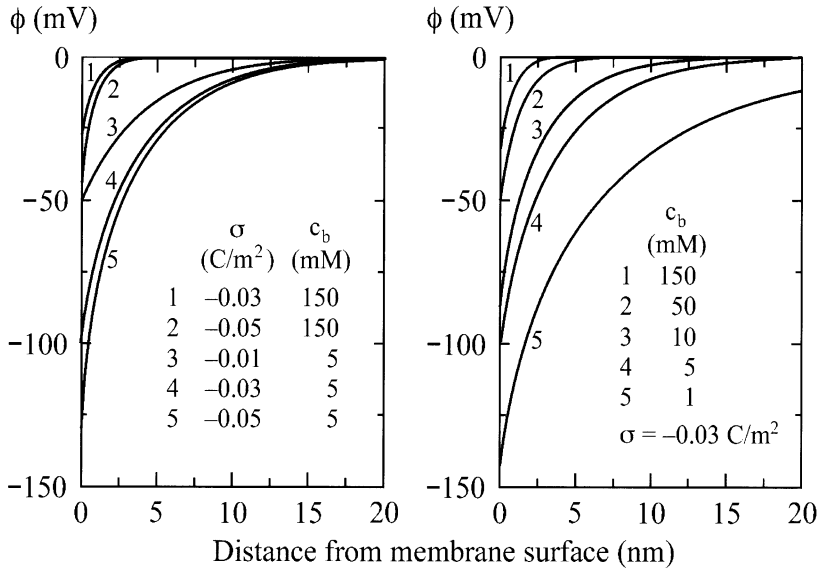

Fig. 4. Electrical potential ϕ from the surface of the membrane to the aqueous bulk phase; effect of surface charge density and electrolyte concentration. The profiles were calculated with Eqns. 8 and 13, using the values for the surface charge density, σ, and the bulk concentration of a univalent electrolyte, c_b, as indicated. Temperature 25 °C, $\varepsilon_r = 80$.

Table 1 Zeta potential measurements of human cells: effects of medium and proteins

Cell type	Suspension medium	Zeta potential (to nearest mV)
Lymphocytes	Low ionic strength	- 27
	Physiological ionic strength	- 18
Erythrocytes	Low ionic strength	- 40
	Low ionic strength [35]	- 39
	Physiological ionic strength	- 19
	Physiological ionic strength + 2.2 mg ml^{-1} albumin	- 65
	Physiological ionic strength + 200 μg ml^{-1} λRG57 [55]	- 72

Data without a reference were obtained in the authors' laboratory (see Ref. 31). Zeta potentials were calculated on the basis of the observed electrophoretic mobilities of the cells in the respective media [31]. For each determination, not less than 20 different measurements of each cell type were taken. λRG57 is an immunoglobulin light chain.

equation (Eqn. 7) this causes an uneven distribution of ions in the aqueous phase at the surface of the membrane. Ions of the same charge to that of the membrane surface are repelled, while ions of the opposite charge are attracted.

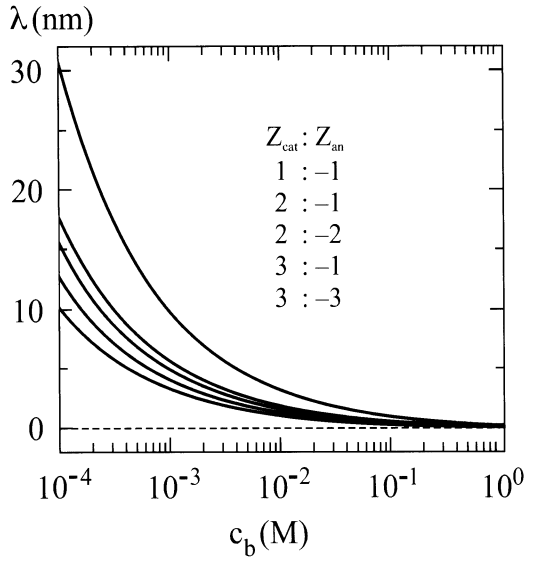

Fig. 5. Dependence of Debye length λ on bulk concentration, c_b, as well as on charge numbers of electrolyte. The curves were calculated with Eqns. 10 and 11, and pertain in the same order to the listed charge numbers Z_{cat} and Z_{an} for cation and anion, respectively; temperature 25 °C, $\varepsilon_r = 80$.

An important feature that emerges from such descriptions of the membrane surface is the membrane charge screening property of the medium. This is described by the Debye length λ (Eqn. 10) which provides a measure of the extent of the influence of the surface potential away from the surface. The Debye length is sensitive to a number of factors as shown in Fig. 5. As an example, for a membrane in contact with a monovalent and symmetrical electrolyte (1:1 in Fig. 5) at 1 mM, the Debye length is about 10 nm, which reduces to about 1 nm at 100 mM. At even higher concentrations the Debye length shortens to subnanometer dimensions (e.g., $\lambda = 0.215$ nm at $I_c = 2$ M). Under these conditions the diffuse layer will tend to a single sheet composed of counterions at the membrane surface as described by the Stern model, and is in fact quite similar to Helmholtz's original conception of an ionic double-layer [12, 13].

The question of the spatial influence of the surface potential from the surface out into the bulk medium as described above has a corresponding problem as to what extent does the electric field originating on the surface penetrate the interior of the membrane. In fact the above considerations apply to an isolated membrane surface, i.e. an "infinitely thick" membrane with no electric field (for a treatment of membranes with finite thickness see, e.g., Ref. 15). This has some relevance to the following section with a description of the electric field

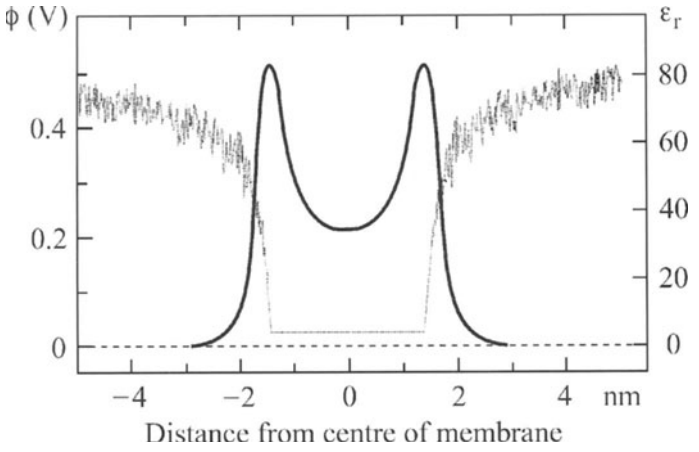

Fig. 6. Profiles of electrical potential ϕ and dielectric constant ε_r across a lipid membrane. The electrical potential profile (solid line) was constructed by means of the results obtained with molecular dynamics simulations shown in Fig. 4 of Ref. 20. The dielectric constant profile (dotted line) was determined according to observations of Vaz et al. [44] and Wall et al. [51]. The membrane boundaries are at about ±1.6 nm.

associated with the membrane shown in Fig. 6. McLaughlin [9] has also suggested a description of the extent of the field within the hydrophobic core of the membrane due to fixed charges at the membrane surface.

2.4. The membrane dipole potential ϕ_d

Molecular polarisation is an important property of many molecules but its influence on the behaviour of biological membranes is a relatively recent consideration. The likely arrangements of the multipole or dipolar configurations of simple phospholipids which make up many common membranes are shown in Fig. 1A. Both the $C^{\delta+}=O^{\delta-}$ and $O^{\delta-}-P^{\delta+}$ moieties are anticipated to exhibit polarisation on each phospholipid "head" group, and the organisation of these groups has been verified from neutron diffraction studies and NMR spectroscopy [11, 19]. Figure 6 indicates what would seem to be a "*pre-dipole potential*" consensus view of the nature of the electric field within the body of the membrane. This figure is constructed using results of molecular dynamics simulations of a membrane [20] which, however, treats all atomic charges as point charges with integer charge numbers, and so takes no account of molecular dipoles. In many ways, this kind of model is reminiscent of the earlier (i.e. simplistic) descriptions of the ionic relationships between an interface and the surrounding elec-

trolyte solution (e.g., Helmholtz model as compared to the Gouy-Chapman-Stern model). Thus, although these models certainly evolved in sophistication (e.g., to consider ion-solvation), they were unsatisfactory (or at least incomplete) descriptions of the real state of affairs at the membrane surface.

Although the membrane dipole potential ϕ_d appears to have its origins in the dipole moments of polar groups from the lipidic components of the bilayer, it seems likely that the water molecules in the transition region between the phases may also make a contribution [11]. The dipolar groups are thought to be oriented in a way such that the hydrophobic interior of the membrane is positive with respect to the external aqueous phases, and ϕ_d is thought to have a magnitude of several hundred millivolts (typically about 300 mV).

A vector drawn from the point of the negative charge –Q to the positive charge +Q of a dipole is called the electric dipole moment **p**. Its magnitude is Q a, with a denoting the distance between the points of the charges. The potential at some point with a position vector **r** with respect to the centre of the dipole can be expressed as

$$\phi = \mathbf{p}\,\mathbf{r}/(4\pi\varepsilon_r\varepsilon_0\, r^3) = p\cos\theta/(4\pi\varepsilon_r\varepsilon_0\, r^2) \quad \text{for} \quad r >> a \qquad (14)$$

where θ is the angle between **r** and **p**. Higher order terms should be included if the condition $r >> a$ is not fulfilled. Whilst Eqn. 14 considerably simplifies the formal description of the dipole potential, the relative permittivity (or dielectric constant) ε_r cannot be considered to possess the same value throughout the multiphase system represented by a membrane in an aqueous medium. Inspection of the permittivity profile shown in Fig. 6 indicates that ε_r changes from about 78 in the bulk aqueous phase to between 20 and 30 in the diffuse layer at the interface [44, 51] then to around 2 in the membrane interior. The denominator in Eqn. 14 must be expanded to include these complexities in the form of a distance-dependent dielectric constant. Nevertheless, based on Eqn. 14, an attempt shown in Fig. 7 has been made to describe the influence of the dipole potential within the membrane. The contribution of oriented water, however, is not shown. It is evident from Eqn. 14 that the potential "decays" as $1/r^2$ rather than the 1/r dependence of an isolated point charge. Accordingly the magnitude of the dipole potential decreases very steeply during passage from the water/membrane interface into the body of the membrane. The resulting forces on a polarised body would decline just as steeply, however, as it moved more deeply into the body of the membrane, until it encounters the dipoles located towards the other bilayer leaflet.

The factors which influence the dipole potential are not the same as those which affect the surface potential. Thus, the ionic strength of the

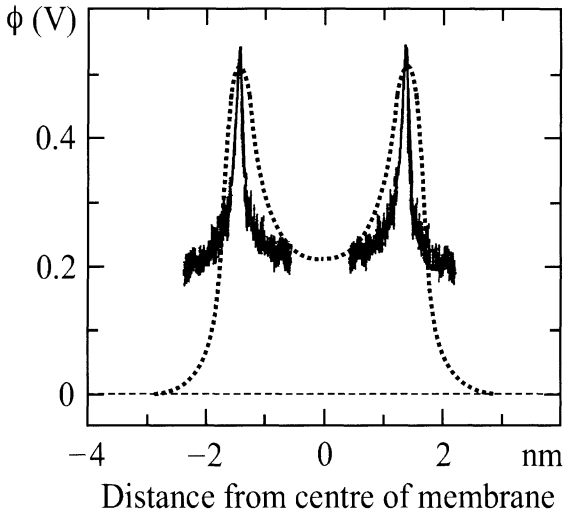

Fig. 7. Profile of the dipole potential. The profile was calculated by means of Eqn. 14 which, however, does not include the change in dielectric constant shown in Fig. 6. It is superimposed on the electrical potential profile of Fig. 6 (dotted line).

electrolyte surrounding the membrane whilst having a profound effect on the surface potential (see Figs. 4 and 5) has no direct effect on the magnitude or extent of the electrical influence of the dipole potential. It appears, however, that the solvation pressure and the dipole potential may be connected [11], so the ionic strength may influence the dipole potential through this agency. Thus, the structured water adjacent to the membrane also involved in contributing to the dipolar properties of the membrane, will undoubtedly be affected by solvation pressure (other aspects of this are discussed in the next section). Similarly, if reorganization of molecular dipoles on the membrane are likely to affect their contribution to the potential, it is possible that integral and peripheral membrane proteins also may both influence and be influenced by such dipoles.

2.5. Other physical factors which influence reactions with membranes

There have been many studies of the interactions of molecules with membranes but perhaps surprisingly very few globally successful attempts to provide a rational (i.e., predictive) basis for understanding such interactions have been achieved. This of course is a major preoccupation of the pharmaceutical industry with their twin desires to have a truly rational basis for building membrane-permeant proper-

ties into therapeutic agents as well as that of receptor-mediated therapeutic targets (such as G-proteins). These properties need to be optimised for drug delivery as molecules that are too 'membranephilic' may not leave membranes and lead to a diminished pharmacoavailability that would compromise their effectivity. Thus, the pharmaceutical industries have assembled a catalogue of behaviour based on molecular properties that are available for "drug design". Many of these rely on the so-called LogP of a given compound to gauge its membrane affinity. This parameter is defined as the octanol-water partition coefficient and is a general guide to such membrane affinity. The construction of a "master" equation to describe the membrane affinity for any molecule has also been attempted. It obviously involves LogP and has been further elaborated to incorporate parameters such as hydrogen-bonding capacity, explicit charge and many other parameters (see e.g. Ref. 23). Many of these therapeutic molecules, however, are much simpler than the biological macromolecules that life scientists need to understand.

Related to the search for a "master" equation describing molecular interactions with membranes, the orientation of "structured" water on the membrane surface as a candidate for affecting membrane interactions appears to have many latent possibilities and would benefit from inclusion into any such general theory. Parsegian and colleagues in particular have discussed this at some length [21] in which this property of membranes is essentially a special case of (poly-)molecular "hydration" and the complemenary effect on the molecular interactions seems extremely important.

White and Wimley [22] were amongst the first to try to catalogue and rationalize the multitude of possible reactions which may take place. Since then a number of reviews have appeared, to at least increase the awareness of the potential complexities involved in what hitherto had seemed to be a rather simple interaction [23, 24]. The most obvious of these is the hydrophobic effect which may "drive" the interaction between an apolar peptide or other molecule and the membrane. Seelig and Ganz [25] considered some earlier work which indicated that the binding of the potential-sensitive dye 2-p-toluidinylnaphthalene-6-sulfonate (TNS) to phospholipid membranes seemed to be driven by enthalpy and not by entropy. Since the reaction was anticipated to be hydrophobic in nature, a "non-classical" hydrophobic type of interaction was suggested. In a similar manner, we have found that under some circumstances exothermic binding enthalpies occur with the interactions of peptides with some membranes; with ΔH-values up to about 50 kJ/mol but with a binding entropy around zero [26]. In these cases, therefore, an enthalpic binding interaction may also be invoked. On the other hand, the concept of an equilibrium partition of a peptide from the water phase into mem-

branes is also not as simple as it may sound. White and Wimley [22], for example, eloquently reviewed concerns [27] that because of their relatively much larger molecular size than the solvent (exacerbated by the fact that water is the smallest solvent), peptides may interact with very many solvent molecules and lead to underestimates of entropic changes on a mole fraction basis of the partition phenomenon. Sharp et al. [27] refer to revision of this as the Flory-Huggins Corrected Volume-Fraction (FHCVF) problem. On this basis, White and Wimley [22] re-analysed a substantial body of published partition data of peptides of a variety of sizes and properties and found that they could only be reconciled in a logically consistent manner with appropriate thermodynamic parameters if the FHCVF units were included. Thus, the solvent-accessible surface area of delineated peptides seems to have a major bearing on how they may interact with membranes.

There are a number of other factors which appear to have powerful influences on the interactions of molecules with membranes (see Table 2); some of these are outlined in reviews by White and Wimley [22, 24] and Roberts et al. [23]. It is worth emphasising the widely reported ability of peptides and proteins to adopt secondary structure motifs within membranes. The driving force behind this is believed to be the avoidance of the peptide bonds partition energetic cost through hydrogen bonding. It has been recently reported that the free energy reduction per residue accompanying the folding of an α-helix peptide in the membrane interface is about 1.7 kJ/mol [28] whereas a value of 2.5 kJ/mol per residue has been observed for β-sheet formation by a hexapeptide model system [24, 29]. α-helices are the most abundant type of secondary structure found in membrane proteins and they represent one of the main paradigms of structural membrane biology. Table 2 summarizes some intermolecular interactions which ought not be neglected if a rational basis for the understanding of membrane interactions is sought.

3. The measurement of membrane potentials

A number of quite different techniques have evolved to make measurements of each type of electric potential associated with membranes (see also section 3 in chapter 1) but particular measurements must rely on the physical differences between the potentials. In order to avoid interpretative difficulties due to interference between each potential, however, it is of course necessary to have a very clear understanding of the physical nature of both the potential as well as the measurement technique. In addition, however, membranes also possess other properties which often complicate assignments of specific values for the membrane potentials.

Table 2. Intermolecular interactions important during encounters of peptides with membranes

Nature of molecular interaction (between functional groups on peptide and membrane)	Symbol	Magnitude of energy ΔG ($kJ\ mol^{-1}$)
Electrostatic effect between charges and dipoles of functional groups of peptide and membrane; affected by		
Transmembrane potential difference	$\Delta\phi_m$	Many and complex
Surface potential	$\phi_s \Leftrightarrow$ charge on peptide	
Dipole potential	ϕ_d membrane $\Leftrightarrow$ ϕ_d peptide	
Hydrophobic effect		
Entropic effect (but possible enthalpic contribution)	$\Delta G_{hydrophobic}$	~ +80
Hydrogen bonding capacity of peptide groups (maxium preferred)	$\Delta G_{hydrogen\ bond\ capacity}$	~ +80
Lipid disorder vs. order from acyl chain and peptide side chains		
Desolvation of peptide upon insertion into membrane:		
Helix insertion		~ +160
Random structure insertion		~ −120
Specific functional groups	–OH	+16
	$-NH_2$	+20
	–COOH	+20
	–C=O	+8
	–C=O $\Leftrightarrow$ –NH	+2

3.1. Electrodes

Perhaps the most obvious technique for measuring electrical potentials involves the use of an electrode; i.e. comparison of the potential at a measuring electrode with that of a reference electrode yields some estimation of the potential in question. Penetration of a membrane (such as that of an organelle or a plasma-membrane patch) when compared to a reference electrode potential, for example, facilitates an estimation of the transmembrane potential $\Delta\phi_m$. Despite the elegance and reliability as well as the great sensitivity of techniques such as patch-clamping [30], depending on the desired application, related techniques may offer less assured interpretations. There are many reasons why fully penetrating a plasma membrane system with

an electrode is unsatisfactory – even a microelectrode compared to the size of a cell is essentially a very large object (it has been said for example that penetrating a cell with an electrode is analogous to penetrating a cat with a baseball bat!) and so, use of an electrode may actually perturb the value of the measurement (e.g., by affecting cellular metabolism which underlies the transmembrane potential). On the other hand if control and related transmembrane current measurements of the transmembrane potential are all that is desired there is no doubt that electrodes offer a very powerful tool.

Measurements of the membrane surface potential ϕ_s may be similarly undertaken in principle, by bringing an electrode very close to the surface of a membrane and comparing the measured potential to that of a remote reference electrode. The remaining (and as it originated in the 19th century one might even suggest – almost traditional) method of making measurements of ϕ_s involves passing a current between electrodes and determining the rate of movement of the membranous particles. The current generates an electric field which acts on membrane-located charges and leads to bulk electrophoresis of the particles. In order for this technique to be applied, the membrane system must exist as a relatively homogenous particulate suspension but may be routinely used with liposomes or with human cells (see Table 1). By application of the Helmholtz-Smolukhovsky equation (see Eqn. 46 in chapter 1, and references below), the quantity ζ known as the *zeta potential* (also called electrokinetic potential) is obtained. This bears some relation to ϕ_s (see Fig. 2), although it is not formally well defined and is conceded to be a major interpretative difficulty [8, 31]. Nevertheless, particle microelectrophoresis has been implemented in a number of membrane systems, including those in my own laboratory, to make measurements of the binding of macromolecules to human cells [31]. As well as these applications to relatively simple systems, other studies have been directed towards non-mammalian eucaryotic cellular systems, artificial surfaces [32, 33] and colloidal systems of plant origin [34] but cannot be applied to adherent cells. The results appear to be consistent and reliable but the nature of the particle electrophoresis technique does not permit any time resolution of these events even in principle because the technique requires that the surface is in electrical equilibrium over the time scales of the measurements. This leads to a serious experimental difficulty for if further changes at the cell surface take place following ligand binding (e.g., as with receptor-mediated endocytosis) then due to the relatively long time periods that measurements of zeta potential require, resulting data may be misleading.

Table 1 indicates measurements of the zeta potentials of cells in various media and in the absence and presence of representative types of protein which are anticipated to bind to the cell surface. Some data

from Maeda et al. [35] are also illustrated for comparison. These authors reported that the electrophoretic mobility of erythrocytes in a low salt medium was 3 $\mu m\ s^{-1}/(V\ cm^{-1})$ which corresponds to a zeta potential of –39 mV (for calculation with specific reference to erythrocytes see Refs. 34, 36 and 37). The slight discrepancy (i.e., 1 mV) between our evaluation and that of Maeda et al. [35] is most probably due to the differing sources of the erythrocytes; i.e. we have found in our studies that erythrocytes possess differing amounts of sialic acid which results in different surface potentials (see also section 6). The data in Table 1 also show the anticipated effects of electrolytes on the zeta potential of human cells.

Finally, measurements of the dipole potential may also be accessible utilizing electrode technology. Brockman [11] has eloquently reviewed several such applications but it must be conceded that they also leave much to be desired.

The most recent technological development involving the application of electrodes to membranes involves the use of the scanning tunnelling microscope or more recently, the Atomic Force Microscope (AFM, see Ref. 38). With this instrument, it proved possible to map the surface morphology and also it proved possible to estimate the electrostatic nature of the surface. Thus, quantitative estimations of the membrane surface potential may be attempted, but at this stage it is not clear whether the membrane dipole potential may also have an effect on this value. Despite the apparent extravagance of using such tools for surface potential measurements and even ignoring the possibility that the dipole potential may well interfere with such estimations, $\Delta\phi_m$ across a membranous structure is not accessible using AFM technology. Nevertheless, this is one of the few emerging techniques available which offers spatial information about any of the membrane potentials.

3.2. Spectroscopic measurements of membrane potentials

Notwithstanding the recent developments of the AFM as directed towards the cell surface, the other less-sophisticated applications of electrodes are really rather less than satisfactory. Presently, therefore, the most widely used techniques tend to involve spectroscopy in one manner or another; in both invasive and non-invasive regimes. Of the latter, NMR spectroscopy has been applied to interrogate membranes in many different ways and has yielded an enormous amount of valuable information about the structures of both lipid and protein membrane components [39]. In addition, NMR may also be utilised to obtain information of the membrane potential trinity. More particularly, NMR has been used recently to develop a clearer understanding

of the nature of the membrane dipole-potential and actually more than a decade ago as a tool to monitor the membrane surface charge [40].

Whilst NMR techniques directed towards membranes have been either totally non-invasive or effectively non-invasive by isotopic substitution of appropriate atomic nuclei, a number of other techniques rely on the inclusion of probe molecules to report the membrane properties [41, 42]. Numerous spectroscopic membrane probes have been developed to study a number of membrane properties (see Fig. 8). These technologies appear to be fairly simple to use and to be very versatile. Further details may be found in Ref. 42, and a large amount of useful information may be found in the updated Molecular Probes™ Inc. catalogue which references the many applications of its products. Whilst in general these technologies have been well-documented, the remaining parts of this section will deal with a brief outline of the use of some other newly-developed probe molecules that have emerged as powerful spectroscopic tools.

3.2.1. Spectroscopic measurements of the transmembrane potential difference: This area of study has been fairly well established and usually involves assessing the redistribution of membrane-permeant indicators which migrate according to the transmembane potential difference $\Delta\phi_m$ as embodied in the Nernst equation (Eqn. 3). The first developments of this strategy involved counting the distribution of radioactive membrane-permeant indicators across a membrane [6, 43]. It was found, however, that the added advantage of using spectroscopic indicators which could respond to $\Delta\phi_m$ was that they also offered the possibility of obtaining kinetic information of the changes of potential. Thus an enormous range of studies have been performed using many different optical intrinsic or extrinsic probes which exhibit potential-dependent properties [42].

3.2.2. Spectroscopic measurements of the membrane surface potential: Amongst the techniques developed for obtaining electrostatic details of the membrane surface using spectroscopic probes [10, 42], applications with two categories of probe seem to have evolved. Probe molecules either redistribute themselves and/or change their spectral properties according to the magnitude of an electrical potential at the membrane surface [44–46]. These include 5-dimethylamino-naphthalene-1-sulphonyl, dansyl [44], anthraniloyl, Lucifer yellow, N-1-pyrenesulphonyl-PE, pyrene-PE [47] and a series of lipoid indicators: coumarin-alkyl adjuncts [48–50]. The structures of representatives of these groups are shown in Fig. 8. Cevc [10] has discussed and strongly criticized the relative merits of many of these implementations with artificial membranes. One of the main criticisms for example, resides in problems of the uncertainty as to the exact location of the probes

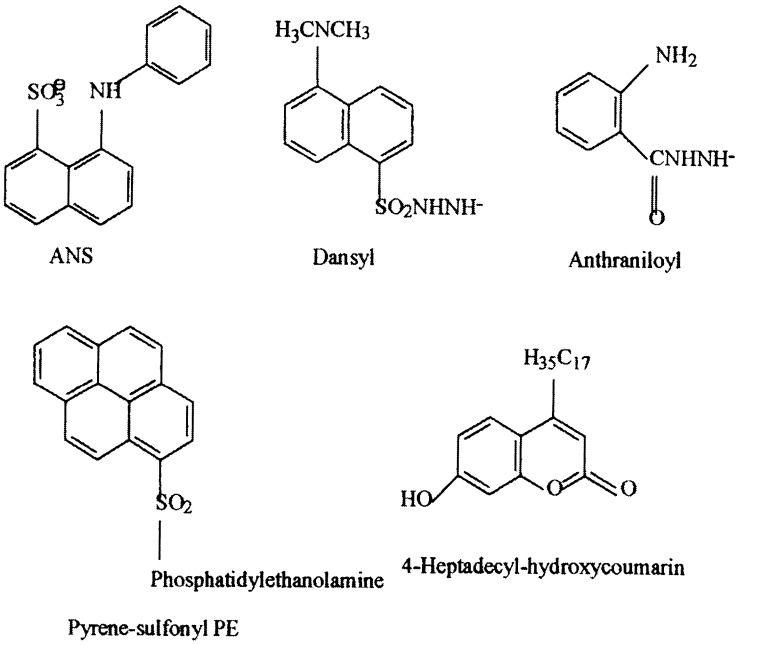

Fig. 8. Examples of spectroscopic membrane probes. Biological applications of these probes may be found in Ref. 42 as well as in the Molecular Probes™ Inc. catalogue.

during the course of measurements. We have addressed many of these problems and introduced the use of a family of fluorophores attached to a phospholipid molecule. These have the advantage of being virtually non-invasive as they are used at very low concentrations and do not perturb the membrane.

One such probe molecule, FluoresceinPhosphatidylEthanolamine (FPE), has proved to be a hugely versatile indicator of the electrostatic nature of the membrane surface in both artificial and cellular membrane systems [26, 31, 51]. FPE is sensitive to changes in the surface potential ϕ_s at the membrane-solution interface because the fluorescent moiety of the FPE lies precisely at the membrane solution interface. Any changes in the number of surface charges at the membrane, such as the binding of an inorganic ion or a charged oligopeptide, will cause an alteration in ϕ_s, as discussed in section 2.3. According to the Boltzmann equation (Eqn. 7) the concentration of a charged species at the membrane surface is

$$c_{i,s} = c_{i,b} \exp [-Z_i F \phi_s /(RT)] \quad (15)$$

which, when dealing explicitly with protons and introduced into the Henderson-Hasselbalch equation, yields upon rearranging

$$\log(c_B/c_{HB}) = pH - [pK - F\,\phi_s/(RT\ \ln 10)] \quad (16)$$

Here $pH = -\log(c_{H,b})$, while c_B and c_{HB} denote the concentrations of the dissociated and protonated species of an acid-base pair, respectively [26, 31, 44]. The quantity $pK - F\,\phi_s/(RT\ \ln 10)$ can be considered as an apparent pK for proton binding of an acid-base pair on the membrane surface. Equation 16 shows that the protonation state c_B/c_{HB} of the probe is altered if ϕ_s changes at constant pH, which results in a change in the fluorescence yield. This technique has been utilised to measure the time course of the interactions of charged molecules such as Ca^{2+}, peptides, and proteins with synthetic and biological membranes with great sensitivity. By performing rapid-kinetic studies, it has also proved possible to monitor the early events during the interactions of oligopeptides with artificial membrane systems [51–54] and with cells [55].

3.2.3. Spectroscopic measurements of the membrane dipole potential: Since the possibility that the dipole potential ϕ_d may have some influence on cellular function was the last to be appreciated, techniques designed to make measurements have not become either as well established or as varied. Nevertheless, experiences with measurement strategies for the other potentials has meant that measurements of ϕ_d are at least as sophisticated as those used for other membrane potentials. Recently, a series of potentiometric fluorescent indicators have been introduced that function by putative electrochromic mechanisms. Loew's group in particular introduced the use of a fluorescent dye, 1-(3-sulfonatopropyl)-4-[β[2-(di-n-octylamino)-6-naphthyl] vinyl] pyridinium betaine (known as di-8-ANEPPS) [56]. The use of these dyes has been successfully applied to the measurement of ϕ_d [57, 58] using the dual-wavelength ratiometric fluorescence method [41, 54, 59–61]. This method forestalls problems arising from small differences in dye concentration between different samples, dye bleaching or the influence of light scattering on the fluorescence measurements [39].

The excitation spectrum of di-8-ANEPPS in phosphatidylcholine (PC) membranes is significantly altered when 15 mole% of either 6-ketocholestanol (KC) or phloretin are added to such membranes. These sterol-like compounds promote changes in the membrane dipole potential, and significant variations of the intensity and position of the excitation maximum are observed when these sterols are incorporated into the membrane bilayer. Montana et al. [57] have pointed out that such intensity variations may be due in part to a potential-dependent shift in the emission spectrum which gives a change in intensity at the fixed emission wavelength used for the excitation scan. To determine the changes resulting only from the spectral shift, the areas of the excitation spectra must be normalized to the

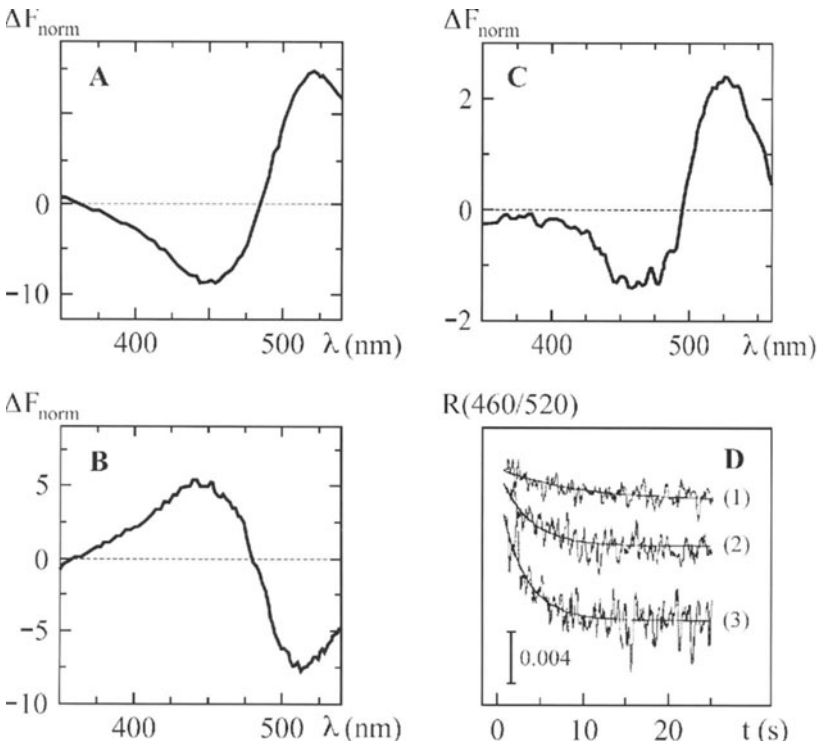

Fig. 9. Fluorescence measurements of the dipole potential; effects of sterols and addition of a peptide. The fluorescence difference spectra were obtained by subtracting the excitation spectrum of di-8-ANEPPS-labelled phosphatidylcholine membranes from the spectrum of similar membrane preparations which include 15 mole% of phloretin (A) or 6-ketocholestanol (B), and from the same membrane preparation treated with a signal peptide known as p25 (C). Prior to subtraction the spectra were divided by the integrated areas, thus yielding the normalized fluorescence signal F_{norm}, in order that the difference spectra reflect only the spectral shifts. Concentrations were 4 μM for di-8-ANEPPS, 200 μM for lipids, and 15 μM for p25; emission wavelength 580 nm. In (D) the time-course of the change in dipole potential upon addition of the signal peptide p25 is shown. The change is assessed by the quantity R(460/520) which is the ratio of the fluorescence signals at 580 nm for excitation at 460 nm and 520 nm, respectively (dual-wavelength ratiometric technique). Changes of R(460/520) as a result of the addition of 15 mM p25 to various membrane systems with the following compositions of lipids (in mole%): 85 PC, 15 phloretin (trace 1), 100 PC (trace 2), 85 PC, 15 KC (trace 3); PC, phosphatidylcholine. Further details may be found in Ref. 61.

same integrated intensity and then subtracted [57, 61]. This procedure yields the difference spectra shown in Fig. 9. In the case of phloretin the difference spectrum has a minimum at 450 nm and a maximum at 520 nm (Fig. 9A). In the case of KC, however, the difference spectrum has a maximum at 450 nm and a minimum at 520 nm (Fig. 9B), which is the opposite effect to that of phloretin. Therefore, recording the

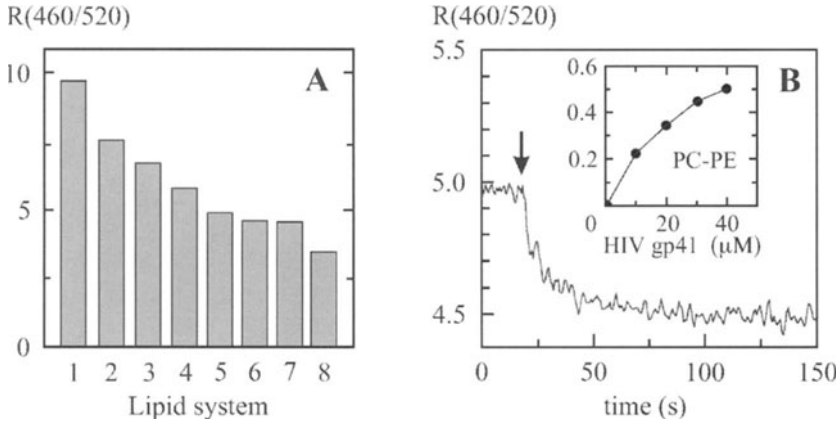

Fig. 10. Dependence of dipole potential on membrane composition. The dipole potential was determined with the dual-wavelength ratiometric technique (see legend to Fig. 9). (A) Compositions of lipid systems in mole% are (1) 85 PC, 15 KC; (2) 70 PC, 30 cholesterol; (3) 35 PC, 50 PE, 15 KC; (4) 100 PC; (5) 50 PC, 50 PE; (6) 35 PC, 50 PE, 15 PHL; (7) 25 PC, 50 PE, 25 ganglioside; (8) 85 PC, 15 PHL. Abbreviations: PC, phosphatidylcholine; KC, 6-ketocholestanol; PE, phosphatidylethanolamine; PHL, phloretin. (B) Time-course of the change in dipole potential after addition of the HIV gp41 fusion peptide. The inset shows the maximal change in R(460/520) as a function of the HIV gp41 concentration. The amino acid sequence of the fusion peptide is Ala-Val-Gly-Ile-Gly-Ala-Leu-Phe-Leu-Gly-Phe-Leu-Gly-Ala-Ala-Gly. PC-PE vesicles (200 μM lipid) labelled with 10 μM di-8-ANEPPS, temperature 37 °C; for further details see Ref. 54.

ratio R of fluorescence excited at the two wavelengths with the maximum positive and negative changes provides a method for measuring spectral shifts originating from changes of the local electric field and avoiding artifactual variations in intensity. The feasibility of measuring the membrane dipole potential by measuring R has been explored by other laboratories [57, 58] and the possibility of using the ratiometric method to measure variations of the membrane dipole potential has been reported [41, 59, 60]. In agreement with these studies an increase of the membrane dipole potential occurs due to the presence of KC and a decrease caused by phloretin.

A more comprehensive illustration of the dependence of the relative magnitude of the dipole potential on the membrane lipidic composition is given in Fig. 10A. Of more interest, however, was the observation that di-8-ANEPPS may be used to indicate the interactions of some macromolecules with membranes [61]. The ratiometric spectrum obtained following the exposure of a membrane labelled with di-8-ANEPPS to model peptides yields a spectral shift similar in profile to that obtained with KC (see Fig. 9C). The time course of the interaction of the peptide with the membrane is shown in Fig. 9D, and cor-

relates well with other studies which indicate that this signal change relates to the insertion and folding of the peptide. In further studies we were able to show that the dipole potential also has an effect on the structure of the peptide within the membrane [61]. We also measured a membrane dipole potential decrease caused by the interaction of the simian [54] and human (Fig. 10B) immunodeficiency virus fusion peptides with model membranes. These are short hydrophobic sequences known to insert into the lipid bilayer [62, 63]. It can be deduced from our findings that the magnitude of ϕ_d is strongly influenced by peptides which insert at least partially into the membrane, since experiments with other hydrophilic and non-amphiphatic sequences (e.g., bacitracin and penetratin) cause a much lower level of perturbation.

4. Spatial disposition of membrane potentials; quantitative imaging

The last decade or so has seen an enormous increase in the applications of various types of imaging technologies to biological problems. This has already been alluded to with respect to comments about the AFM in section 3.1 and many of these technologies involve fluorescence microscopy. The spatial variation over the cell surface of the transmembrane potential difference $\Delta\phi_m$ has been achieved using fluorescent probes in a dual-excitation or emission mode (Molecular Probes™ Catalogue) but this is the only type of membrane potential which has been interrogated in any kind of routine manner. Lately, by utilising appropriate probes (e.g., di-8-ANEPPS, see section 3.4), Loew and colleagues have extended such imaging procedures to visualize the membrane dipole potential ϕ_d. To date, however, there have been no published reports of measurements of the spatial imaging of the membrane surface potential ϕ_s.

With this latter hiatus in mind, and as well as introducing the use of the FPE-family of ϕ_s indicators of both artificial and cellular membranes, my colleagues and I have explored similar applications in an imaging mode. Figure 11B, for example, indicates that it is indeed possible to obtain high-resolution images of the spatial variation of the electrostatic potential of the cell surface (i.e., the outer bilayer leaflet of the plasma membrane). The fine detail in this image is striking as it illustrates the heterogeneity of the potential and there are clearly a number of "hot" and "cold" spots of electrical potential. In common with a number of other cells which have been imaged in a similar way, perhaps the most striking feature of this image is a "collar" of electropositive potential which seems to partially encircle the nuclear region. In fact, comparison of the "electrostatic" image with that of the bright field (Fig. 11A) indicates that this collar is associated with

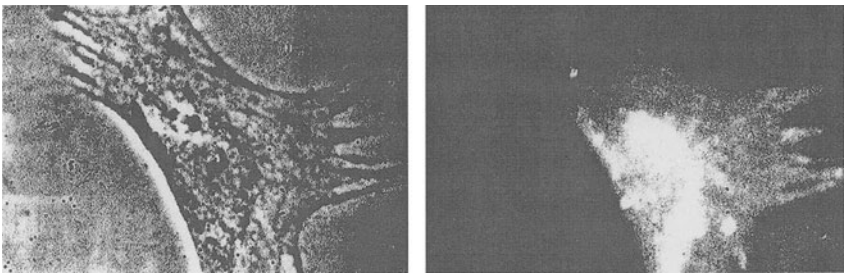

Fig. 11. Spatial imaging of the surface potential at the outer surface of the fibroblast plasma membrane. (A) Bright field image of the fibroblast. (B) The outer-bilayer leaflet of the plasma membrane of a fibroblast cell line was labelled with the fluorescent probe FPE as described [31]. FPE was excited at 490 nm and fluorescence collected above 518 nm. The image was obtained using an inverted fluorescence microscope coupled to a high-resolution CCD camera in a fluorescence configuration.

the trans-golgi apparatus and rough ER near to the nucleus. One possible explanation of this phenomenon, therefore, is that newly-synthesised proteins may have been inserted into the plasma membrane and perhaps the punctate electrostatic "hot" spots around the periphery of the cell also reflect new protein/vesicle insertion into the plasma membrane. By extending the interpretation it has proved possible to utilise the FPE fluorescence signals in a quantitative mode. Thus, as the signals may change during (say) protein binding to parts of the cell surface and as long as the net charge on the protein is known, it is possible to deduce the number of protein molecules which have become bound. These are clearly exciting prospects which seem to offer a new kind of imaging technology to address biological problems.

5. The role of membrane potentials in cellular functions

The various electrical potentials associated with membranes are involved in a large number of cellular processes and underline the opening comments that membranes are very much more than permeability barriers. In fact, membranes offer biology (and evolution in particular) all the possibilities of surface chemistry and physics, as well as chemistry with an additional dielectric phase over and above that provided by solution biochemistry, or on a much larger scale than that offered by the micro-domains within proteins (e.g., as within the active sites of enzymes or antibodies).

The monumental role that the transmembrane potential difference $\Delta\phi_m$ plays in cell physiology is well documented in numerous reviews and several monographs (see, e.g., Ref. 6). Similarly, the basic para-

digms of how this potential features in cell biology are fairly well established and may be arranged broadly into two major classifications. The most ubiquitous action of $\Delta\phi_m$ is that it acts as a labile reservoir of energy or power, as elucidated in subcellular structures and micro-organisms principally by Mitchell [7]. This property also features in a very similar manner in eucaryotic plasma membranes etc. [64, 65]. The second major duty of $\Delta\phi_m$ is that it takes part in or behaves as an element within the many signal transduction processes which have been identified. These range from nervous conduction along and between neurons to second messenger systems [2]. The particular roles that $\Delta\phi_m$ plays will not be further described here since there are many examples and reviews which outline its properties and functions (see, e.g., Refs. 66 and 67), and a further discussion of these particular properties in the available space of this chapter would be redundant. Before moving on to the other membrane potentials, however, it ought to be emphasised that there are additional aspects of $\Delta\phi_m$ in that it may be also involved in macromolecular structural changes during the interactions of proteins with(in) membranes. It has been suggested that $\Delta\phi_m$ may play a role in affecting or controlling the structure and thus perhaps also the activity of certain membrane-located proteins [68]. On this basis, it also seems possible that $\Delta\phi_m$ may be accessed to drive or import proteins into the body of the membrane itself or indeed into subcellular compartments [69]. In fact there is now much evidence that a transmembrane potential difference does indeed promote protein transport in many membrane systems [70, 71].

The possibility that in addition to $\Delta\phi_m$, the membrane surface potential ϕ_s plays an important role in a number of cell functions is also worth emphasising. By and large, most cell membranes tend to possess a net negative charge. So, on the face of it, electrostatic repulsion between plasma membranes, and hence their parent cells, would seem to be the most obvious manifestation of the effects of a significant surface potential. Such repulsion, for example, is thought to be the dominant parameter which prevents the aggregation of eythrocytes [35, 72]. Similarly, the zeta potential has been implicated in many related surface interactions between cells. Of the latter, our research programme directed towards the physical properties of the fungal cell surface has involved characterisation of ϕ_s as an important factor in fungal pathogenicity [33, 46, 73] and bacterial infection [50, 74]. It has also been emphasised [9, 18, 75] that electric fields on the surface of biological membranes (as well as those within the membrane due to $\Delta\phi_m$, see section 2.3.4 in chapter 1) may influence the conformation and activity of many surface-located molecules including proteins [8, 10]. In addition, Arcangeli et al. [76] suggested that some reagents which induce cell transformation [77] do so by promoting changes in ϕ_s, although a specific molecular mechanism was not identified.

As well as electrostatic repulsion (or attraction), for example involved in binding reactions of many molecules [78], the clearest effect of surface potentials, however, is that they may lead to the accumulation or depletion of charged solutes at the membrane surface. This property seems to underlie the formerly curious observation that divalent ions may promote a positive shift in the conductance-voltage relations as embodied in the Hodgkin-Huxley equations of nerve or muscle tissue. McLaughlin et al. [79] showed that such influences were the result of changes in the electrostatic potential at the cell surface. Closely related to this effect, the activities of enzymes which depend upon the concentration of charged substrates for their action would be anticipated to respond to the "effective" concentration of the substrates which would be a function of ϕ_s according to Eqn. 15. In fact, this behaviour seems to have been identified [8, 80]. In other words, a membrane-bound enzyme which acts upon a charged substrate would be anticipated to exhibit a K_m which was related to the magnitude of ϕ_s [81]. This may be altered in many ways. Thus, a striking effect of this phenomenon would occur if an enzyme in a solution of low ionic strength were turning over at a steady state and the surface potential was rapidly changed (e.g., by the addition of salt). A change in the rate of catalysis would be anticipated, provided the substrate was charged and the salt did not directly affect the enzyme. The elevation of the ionic strength reduces the magnitude of ϕ_s, consequently the effective concentration of the substrate at the membrane surface must also change and lead to changes in enzymatic activity [82].

In some cases, however, membrane-located enzymes which utilize charged substrates may not appear to act in this manner, i.e., do not exhibit an ionic strength-dependent activity. Such observations are ostensibly inconsistent with the doctrines of the membrane surface potential and perhaps might even be considered to cast some doubt on the basic theory. The effect of the surface potential, however, may also pertain to other factors which could conceivably affect enzymatic activity. This is particularly important if ionizable functional groups are involved in either enzyme catalysis *per se* or binding (release) of substrates (products). Equation 16 implies that the apparent pK of a sensitive group must change with ϕ_s [31]. The corresponding changes in protonation may affect catalysis/binding, and thus could conceivably oppose the changes in effective concentrations of substrate or product at the membrane surface.

Alternatively, enzyme kinetics with a non-compliance with Eqn. 16 may offer a more revealing picture of the functional structure of the enzyme within the membrane. The behaviour of such an enzyme would be expected to abide by the Boltzmann relation only if the region about the active site was able to respond to a surface potential. In other words the membrane surface together with the attendant

proteins, including any cavities represented by the active site, acts as an electrostatic continuum. In the event that the active site was not effectively in easy communication with the membrane surface the enzyme may not respond to changes in the concentration or nature of the electrolyte. This is not difficult to visualise if the active site were to be either buried deep within the enzyme or within the core of the membrane and thus remote from electrical influences at the membrane surface.

The other major area of cellular function that the surface potential appears to influence strongly are those which include the interactions of macromolecules with the membrane surface [83]. In fact this represents (by far) a major classification of cell biology research, as virtually all specific research topics eventually require that, in order to place a given process in the context of cell function, some consideration of the interactions of (macro)molecules with membranes must be undertaken. Work in our laboratory directed towards elucidating these topics can be found in some recent publications [26, 31, 51, 55, 61].

Consideration of the possible roles that the dipole potential ϕ_d may play in cellular physiology are less well documented. To date, the effect of membrane dipoles has been shown to influence the translocation of hydrophobic ions through lipidic bilayers [84]. It has also been found that preparations of phospholipid membranes supplemented with a number of different sterols cause changes in ϕ_d in a controlled manner (cf. Figs. 9 and 10). Thus, phloretin, a sterol-analogue that significantly reduces the magnitude of the dipole potential, was found to increase the translocation rate of hydrophobic cations whilst decreasing the rate for anions. On the other hand, 6-ketocholestanol (KC) which increases the dipole potential affects the translocation rates of hydrophobic ions in a direction opposite to that of phloretin. In my own laboratory, we have found that by manipulating ϕ_d it is possible to affect the extent of the penetration of peptides within membranes (Fig. 9D) and perhaps more importantly, the manner in which they fold into secondary structures [61]. The interesting additional possibility exists, therefore, that by controlling the magnitude and directions of membrane dipoles in a systematic manner, their influence on protein-protein interactions may be explored. There have been few other studies on the relationship between peptides and proteins such as gramicidin [85, 86], phospholipase A [87] or signal sequences [88].

All these studies illustrate the effect of ϕ_d on peptide structure and function and, together with the reported ability of sterols to modify ϕ_d, leads to an important implication of general biological interest. These data point towards the very likely importance of the dipole potential in the behaviour of peptides or proteins within the cholesterol-rich microdomains referred to as "rafts". These structures are thought to

function by preferentially associating with specific proteins while excluding others and have been implicated in membrane sorting in polarized cells, endocytosis and signal transduction from cell surface receptors and entry of viruses into the cell [4, 89]. It is known that depletion of cholesterol inhibits some signalling processes associated with rafts and the sorting of apical membrane proteins and apically secreted glycoproteins. Cholesterol is thought to act as a linker for the different raft components promoting segregation from a liquid crystal to a liquid ordered phase [90]. The relationship between dipole potential and peptide-membrane interaction adds an additional property to be taken into account. Thus, sterols within the raft structure are likely to significantly alter ϕ_d compared to that of the surrounding lipid. It is quite feasible therefore, that the partition and conformations of raft-associated proteins in either side of the membrane and of receptors, particularly G-protein coupled receptors, within the plasma membrane will respond to the magnitude of the local dipole potential of the membrane raft. It should be borne in mind that, whilst the raft structures are likely to alter the properties of proteins and peptides resident within the microdomain, addition of peptides themselves may also alter the local dipolar properties of the region of membrane to which they bind, a process that may perhaps elicit formation of a raft structure and offer a clue to their biological control.

6. Future directions and biological speculations

As well as the huge (but obviously unequal) knowledge-base already in existence concerning the biological roles of the trinity of membrane potentials outlined above, a number of new questions and exciting possibilities spring to mind (see, e.g., Ref. 96). In particular, once the properties of each type of potential as well as how they may be modified together with the roles they may confer on membranes are identified, an understanding of the huge diversity of lipid types present in biological membranes may seem more rational. Each potential, for example, is affected in quite different ways by the lipidic components of membranes.

Taking each potential in turn; the factors which affect the magnitude of the transmembrane potential difference $\Delta\phi_m$ are probably fairly well understood. The main points are that depending on the effective membrane capacity and the rate of charge translocation across the membrane [15, 43], a large or small $\Delta\phi_m$ can be maintained. An essential factor, however, is the leakage of ions across the membrane which also determines the steady-state value of $\Delta\phi_m$ at least in some membrane systems [91, 92]. It was shown that the electrical permeability of many membranes depends on $\Delta\phi_m$ and this may be tailored physio-

logically by adjustment of the ionic leakage rate. To put it another way, the membrane-dependent leakage rate seemed to depend upon the lipid constitution of the membrane [93], in this manner, a biological system could well adjust the efficiency of energy conversion which, for example, may well have some bearing on physiological states in humans, such as obesity [92]. The variability of membrane lipids in mitochondria that includes, e.g., cholesterol, therefore appears enigmatic and other related roles seem to offer the most likely explanations of these observations (see below).

The membrane surface potential ϕ_s may be modified simply by incorporating a greater or lesser percentage of charged phospholipids or charged proteins into the membrane. The presence of sialic acid moieties attached to glycophorin, for example, confers upon erythrocytes negative charge. For reasons which are not clear, however, the amount of sialic acid attached to glycophorin varies signifycantly and is especially reduced during disease conditions such as uncontrolled diabetes [94]. This means that the erythrocytes of such patients are subject to aggregation with all the attendant medical problems of thrombosis and stroke. The question of how diabetes may lead to differences in the occurrence of sialic acid linked to glycophorin, however, is as yet not really clear. Other roles of ϕ_s may include more exotic properties such as the control of the formation of specific domains within membranes [95]. Such domains appear to be involved in signal transduction and, in addition, an electrostatic-switch process also related to signalling has been proposed by Aderem and McLaughlin [5]. These interesting combinations of biophysics and cell biology are presently areas of highly active study.

At this stage the biological significance or roles of the membrane dipole potential ϕ_d are clearly open to many speculations. The effects of sterols, which markedly modify ϕ_d, on the penetration of ions may complement the work mentioned above concerning the metabolic control of membrane permeability [92]. The question of why the inner mitochondrial membrane, for instance, is made up of about 5% cholesterol has been somewhat on an enigma since it was first identified. If its role is to modify the membrane permeability to certain types of hydrophobic ions (e.g., fatty acids) and can be modified by say diet, however, it may be possible to build up a clearer picture of the control of metabolism. Cholesterol, however, is a multirole molecule which also affects the membrane fluidity and the lipid phase behaviour besides acting as a skeleton for the bile salts and steroid hormones. With the observations that sterols, through the agency of ϕ_d, also affect the penetration and more importantly the folding of proteins within membranes [54, 61] it may be possible to add one more property to their repertoire. Thus, the cell may well be able to tailor protein-protein reactions and modify the folding of membrane proteins in mem-

brane domains with different sterol or lipid components which alter the ambient dipole potential [96]. In mitochondria, therefore, the effects of cholesterol on protein-protein interactions may feature, e.g., in the formation of the "permeability-complex" involved in the phenomenon of the permeability transition. Similarly, in the plasma membrane, membrane domain including incipient Caveolae possess similar such properties, and other such domains appear to be present in many types of cell [4], much more research work needs to be done!

Acknowledgements

I would like to acknowledge the great help that my many research colleagues have given during the evolution of my views about living systems and their membranes. These very splendid people include: Fayad Ayoub, Neil Chadborn, Richard Cherry, Josep Cladera, George Georgiou, Angus Bain, Jason Bryant, Lorraine Jones, Carole Hobden, Paul Gouldson, Pete Winn, Marcus Thelen, Jon Wall and Caroline Golding, and their contributions over a number of years are very much appreciated. Financial support from the BBSRC, EPSRC and the Wellcome Trust is also gratefully acknowledged. Dieter Walz also merits thanks for his efforts to keep this chapter consistent with the others.

References

1 Singer SJ, Nicolson GL (1972) The fluid mosaic model of the structure of cell membranes. Science 175: 720–731.
2 Voet D, Voet JG (1995) *Biochemistry*, 2nd Edition. J. Wiley & Son Inc., Chichester.
3 Hooper NM (1992) More than just a membrane anchor. Curr. Biol. 2: 617–619.
4 Simons K, Ikonen E (1997) Functional rafts in cell membranes. Nature 387: 569–572.
5 Aderem A, Mclaughlin S (1995) The myristoyl-electrostatic switch – a modulator of reversible protein-membrane interactions. Trends Biochem. Sci. 20: 272–276.
6 Nicholls D, Ferguson S (1992) *Bioenergetics*, 2nd Edition. J. Wiley & Son, Inc., Chichester.
7 Mitchell PD (1968) *Chemiosmotic Coupling and Energy Transduction*. Glynn Research, Cornwall.
8 McLaughlin S (1977) Electrostatic potentials at membrane solution interfaces. Curr. Top. Membr. Trans. 9: 71–144.
9 McLaughlin S (1989) The electrostatic properties of membranes. Annu. Rev. Biophys. Chem. 18: 113–136.
10 Cevc G (1990) Membrane electrostatics. Biochim Biophys Acta 1031: 311–382.
11 Brockmann H (1994) Dipole potential in lipid membranes. Chem. Phys. Lipids 73: 57–79.
12 Bockris JO'M, Reddy AK (1970) *Modern Electrochemistry*. MacDonald, London.
13 Shaw DJ (1970) *Introduction to colloid and surface chemistry*, 2nd Edition. Butterworth & Co., London.
14 Grant I, Phillips WR (1975) *Electromagnetism*. J. Wiley & Sons Ltd. Chichester.
15 Walz D (1990) Biothermokinetics of processes and energy conversion. Biochim. Biophys. Acta 1019: 171–224.
16 Wood PM (1985) What is the Nernst equation. Trends Biochem. Sci. 10: 106–107.
17 Walz D (1979) Thermodynamics of oxidation-reduction reactions and its application to bioenergetics. Biochim. Biophys. Acta 505: 279–353.
18 O'Shea P (1988) Physical fields and cellular organisation. Experientia 44: 684–694.
19 Bechinger B, Seelig J (1991) Interaction of electric dipoles with phospholipid headgroups. A ^{2}H and ^{31}P NMR study of phloretin and phloretin analogues in phosphatidylcholine membranes. Biochemistry 30: 3923–3929.

20 Jakobsson E (1997) Computer simulation studies of biological membranes: progress, promise and pitfalls. Trends Biochem. Sci. 22: 339–344.
21 Parsegian VA. (2002) Protein-water interactions. Int. Rev. Cytol. 215: 1–31.
22 White SH, Wimley WC (1994) Peptides in lipid bilayers – structural and thermodynamic basis for partitioning and folding. Curr. Opin. Struct. Biol. 4: 79–86.
23 Roberts MS, Pugh WJ, Hadgraft J (1996) Int. J. Pharmaceutics 132: 23–32.
24 White SH, Wimley WC (1999) Membrane protein folding and stability: physical principles. Annu. Rev. Biophys. Biomol. Struct. 28: 319–365.
25 Seelig J, Ganz P (1991) Non-classical hydrophobic effect in membrane-binding equilibria. Biochemistry 30: 9354–9359.
26 Golding CA, O'Shea PS (1995) The interactions of signal sequences with membranes. Biochem. Soc. Symposium 23: 971–976.
27 Sharp KA, Nicholls A, Friedman R, Honig B (1991) Extracting hydrophobic free energies from experimental data: relationship to protein folding and theoretical models. Biochemistry 30: 9686–9697.
28 Ladokhin AS, White SH (1999) Folding of amphiphatic α-helices on membranes: energetics of helix formation by melittin. J. Mol. Biol .285: 1363–1369.
29 Wimley WC, Hristova K, Ladokhin AS, Silvestro L, Axelsen PH, White SH (1998) Folding of β-sheet membrane proteins: a hydrophobic hexapeptide model. J. Mol. Biol. 277: 1091–1110.
30 Nilius B, Viana F, Droogmans G (1997) Ion channels in vascular endothelium. Annu. Rev. Physiol. 59: 145–170.
31 Wall JS, Ayoub F, O'Shea PS (1995) The interactions of macromolecules with the mammalian cell surface. J. Cell Sci. 108: 2673–2682.
32 O'Shea P (1991) The role of electrostatic and electrodynamic forces in fungal morphogenesis and host infection. In: JP Latge, D Boucias (eds.): *Fungal Cell Wall and Immune Response*. NATO ASI series, Springer Verlag, Heidelberg, 285–302.
33 Jones L, O'Shea P (1994) The electrostatic nature of the cell surface of *Candida albicans*: a role in adhesion. Experimental Mycology 18: 110–120.
34 O'Shea P, Walters J, Ridge I, Wainright M, Trinci APJ (1990) Zeta potential mesurements of cell wall preparations of *Regnellidium diphyllum* and *Nymphoides peltata*. Plant, Cell and Environment 13: 447–454.
35 Maeda N, Imaizumi K, Sekiya M, Shiga T (1984) Rheological characterisation of desialylated erythrocytes in relation to fibrinogen-induced aggregation. Biochim. Biophys. Acta 776: 151–158.
36 Levine S, Levine M, Sharp KA, Brooks DE (1983) Theory of the electrokinetic behaviour of human erythrocytes. Biophys. J. 42: 127–13.
37 Donath E, Voigt A (1986) Electrophoretic mobility of human erythrocytes: on the applicability of the charged layer model. Biophys. J. 49: 493–499.
38 Butt H-J, Wolf EK, Gould SA, Dixon Northern B, Peterson CM, Hansma PK (1990) Imaging cells with the atomic force microscope. J. Struct. Biol. 105: 54–61.
39 Campbell I, Dwek R (1984) *Biological Spectroscopy*. Benjamin Cummings, Inc., London.
40 Seelig J, Macdonald PM, Scherer PG (1987) Phospholipid head groups as sensors of electric charges in membranes. Biochemistry 26: 7535–7541.
41 Ross E, Bedlack RS, Loew LM (1994) Dual-wavelength ratiometric fluorescence measurement of the membrane dipole potential. Biophys. J. 67: 208–16.
42 Loew LM (1988) *Spectroscopic Membrane Probes*. Vol. 1–3. CRC Press, Boca Raton.
43 Nicholls D (1981) *Bioenergetics*. J. Wiley & Son. Inc., Chichester.
44 Vaz WL, Nicksch A, Jähnig F (1978) Electrostatic interactions at charged lipid membranes. Eur. J. Biochem. 83: 299–307.
45 Kim J, Mosior M, Chung LA, Wu H, McLaughlin S (1991) Binding of peptides with basic residues to membranes containing acidic phospholipids. Biophys. J. 60: 135–148.
46 Jones L, Hobden C, O'Shea PS (1995) Use of a real-time fluorescent probe to study the electrostatic properties of the cell surface of *Candida albicans*. Mycological Research 99: 969–976.
47 Winiski AP, Eisenberg M, Langner M, McLaughlin S (1988) Fluorescent probes of electrostatic potential 1 nm from the membrane surface. Biochemistry 27: 386–92.
48 Fromherz P, Masters B (1974) Interfacial pH at electrically charged lipid monolayers investigated by the lipoid pH-indicator method. Biochim. Biophys. Acta 356: 3270–275.

49 Fernandez M (1981) Determination of the surface potential in liposomes. Biochim. Biophys. Acta 646: 23–26.
50 Afolabi P, Davies K, O'Shea PS (1995) The electrostatic nature of the spore of Pasteuria Penetrans, the bacterial parasite of root-knot nematodes. J. Appl. Bacteriol. 79: 244–249.
51 Wall JS, Golding C, van Veen M, O'Shea PS (1995) The use of fluoresceinphosphatidyl-ethanol-amine as a real-time probe for peptide-membrane interactions. Mol. Membr. Biol. 12: 181–190.
52 Wolfe C, Cladera J, O'Shea P (1998) Amino acid sequences which promote and prevent the binding and membrane insertion of surface active peptides: comparison of melittin and promelittin. Mol. Membr. Biol. 15: 221–227.
53 Wolfe C, Cladera J, Lahda S, Senior S, Jones R, O'Shea P (1999) Membrane interactions of the putative fusion peptide (MFalphaP) from Fertilin-alpha, the mouse sperm protein complex involved in fertilization. Mol. Membr. Biol. 16: 257–263.
54 Cladera J, Martin I, Ruysschaert JM, O'Shea P (1999) Characterization of the sequence of interactions of the fusion domain of the simian immunodeficiency virus with membranes. J. Biol. Chem. 274: 29951–29959.
55 Wall JS, Ayoub F, O'Shea PS (1996) A study of the interactions of immunoglobulin λ light chains with B-lymphocyte membranes. Frontiers in Biosciences 11: 46–58.
56 Loew LM, Scully S, Simpson L, Waggoner AS (1979) Evidence for a charge-shift electrochromic mechanism in a probe of membrane potential. Nature 281:497–499.
57 Montana V, Farkas DL, Loew LM (1989) Dual-wavelength ratiometric fluorescence measurements of membrane potential. Biochemistry 28:4536–4539.
58 Loew LM, Cohen L, Dix J, E Fluhler, Montana V, Salama G, Wu J (1992) A napthyl-analog of the aminostyrylpyridinium class of potentiometric membrane dyes shows consistent sensitivity in a variety of tissue, cell, and model membrane preparations. J. Membr. Biol. 130: 1–10.
59 Clarke RJ (1997) Effect of lipid structure on the dipole potential of phosphatylcholine bilayers. Biochim. Biophys. Acta 1327: 269–278.
60 Clarke RJ, Kane DJ (1997) Optical detection of membrane dipole potential: avoidance of fluidity and dye-induced effects. Biochim. Biophys. Acta 1323: 223–239.
61 Cladera J, O'Shea P (1998) Intramembrane molecular dipoles affect the membrane insertion and folding of a model amphiphilic peptide. Biophys. J. 74: 2434–2442.
62 Martin I, Schaal H, Scheid A, Ruysschaert J-M (1996) Lipid membrane fusion induced by the human immunodeficiency virus type 1 gp41 N-terminal extremity is determined by its orientation in the lipid bilayer. J. Virol. 70: 298–304.
63 Agirre A, Flach C, Goñi FM, Mandelsohn R, Valpuesta JM, Wu F, Nieva JL (2000) Interactions of the HIV-1 fusion peptide with large unilamellar vesicles and monolayers. A cryo-TEM and spectroscopic study. Biochim. Biophys. Acta 1467: 153–164.
64 Berteloot A (1985) Cation, pH and Membrane-potential dependencies of intestinal glutamic-acid transport. Federation Proceedings 44 No.3: 444.
65 Volotovski I, Khovratovich V (1986) Coupling between transmembrane calcium-transport and membrane-potential in retinal rod disks. Proc. Royal Soc. (London) 228: 97–108.
66 Grinstein S, Dixon SJ (1989) Ion-transport, membrane-potential and cytoplasmic pH in lymphocytes – changes during activation. Physiol. Rev. 69: 417–481.
67 Smith PM, Pritchard JB, Miller DS (1988) Membrane-potential drives organic cation-transport into teleost renal proximal tubules. Am. J. Physiol. 255: 492–499.
68 Wyatt K, Cherry RJ (1992) Effect of membrane-potential on band-3 conformation in the human erythrocyte-membrane detected by triplet-state quenching experiments. Biochemistry 31: 4650–4656.
69 Leenhouts JM, de Grier J, de Kruijff B (1993) A novel property of a mitochondrial presequence. FEBS Lett. 327: 172–176.
70 Pfanner N, Neupert W (1986) Transport of f1-atpase subunit-beta into mitochondria depends on both a membrane-potential and nucleoside triphosphates. FEBS Lett. 209: 152–156.
71 Keibler M, Becker K, Pfanner N, Neupert W (1993) Mitochondrial protein import – specific recog-nition and membrane translocation of preproteins. J. Membr. Biol. 135: 191–207.

72 Izumida Y, Seiyama A, Maeda N (1991) Erythrocyte aggregation: bridging by macromolecules and electrostatic repulsion by sialic acid. Biochim. Biophys. Acta 1067: 221–226.
73 Hobden C, Teevan C, Jones L, O'Shea PS (1995) The hydrophobic properties of the cell surface of Candida albicans: a role in aggregation. Microbiology 141: 1875–1881.
74 Davies K, Afolabi P, O'Shea PS (1996) Adhesion of *Pasteuria Penetrans*, to the cuticle of root-knot nematodes (*Meloidogyne* spp.) inhibited by fibronectin: a study of electrostatic and hydrophobic interactions. Parasitol. 113: 1–7.
75 O'Shea P (1989) Biophysical mechanisms of development: signal transduction and self-organisation. In: J Krekule, F Seidlova (eds.) *Signals in Plant Development.* SPB Academic Publishing, The Hague, 25–44.
76 Arcangeli A, Carla M, Del Bene M, Becchetti A, Wanke E, Olivotto M (1993). Polar/apolar compounds induce differentiation by modulating cell-surface potential. Proc. Natl. Acad. Sci. USA 90: 5858–5862.
77 Gurdon J (1987) Embyronic induction – molecular prospects. Development 99: 285–306.
78 Terzi E, Hölzemann G, Seelig J (1994) Alzheimer β-amyloid peptide (25–35): Electrostatic inter-actions with phospholipid membranes. Biochemistry 33: 7434–7441.
79 McLaughlin S, Szabo G, Eisenmann G (1971) Divalent ions and the surface potential of charged phospholipid membranes. J. Gen. Physiol. 58: 667–687.
80 Katchalski A, Silman I, Goldman R (1971) Effect of the microenvironment on the mode of action of immobilised enzymes. Adv. Enzymol. 24: 445–451.
81 Kimmich GA, Randles J (1988) Membrane-potential dependent K_m values for Na^+ in Na^+-sugar transport. Faseb J. 2: A751.
82 Laidler KJ, Bunting PS (1980) The kinetics of immobilised enzyme systems. Meth. Enzymol. 64: 227–232.
83 Stankowski S (1991) Surface charging by large multivalent molecules: Extending the Gouy-Chapman treatment. Biophys. J. 60: 341–351.
84 Franklin JC, Cafiso DS (1993) Internal electrostatic potentials in bilayers: measuring and controlling dipole potentials in lipid vesicles. Biophys. J. 65: 289–299.
85 Rokitskaya TI, Atonenko YN, Kotova EA (1997) Effect of the dipole potential of a bilayer lipid membrane on gramicidin channel dissociation kinetics. Biophys. J. 73: 850–854.
86 Shapovalov V, Kotova EA, Rokitskaya TI, Antonenko YN (1999) Effect of gramicidin A on the dipole potential of phospholipid membranes. Biophys. J. 77: 299–305.
87 Maggio B (1999) Modulation of phospholipase A2 by electrostatic fields and dipole potential of glycosphingolipids in monolayers. J. Lip. Res. 40: 930–939.
88 Voglino L, McIntosh TJ, Simon SA (1998) Modulation of the binding of signal peptides to lipid bilayers by dipoles near the hydrocarbon-water interface. Biochemistry 37: 12241–12252.
89 Brown DA, London E (2000) Structure and function of sphingolipid and cholesterol rich membrane raft. J. Biol. Chem. 275: 17221–17224.
90 Brown DA, London E (1998) Functions of lipid rafts in biological membranes. Annu. Rev. Cell Dev. Biol. 14: 111–136.
91 O'Shea P, Azzi A (1984) On the location of the electrogenic step(s) during the process of dioxygen reduction by cytochrome c oxidase. Biochem. J. 224: 1053–1057.
92 Porter RK, Hulbert AJ, Brand MD (1996) Allometry of mitochondrial proton leak: Influence of membrane surface area and fatty acid composition. Am. J. Physiol. – Regulatory Integrative and Comparative Physiology 40: R1550–R1560.
93 O'Shea P, Petrone G, Casey RP, Azzi A (1984) The current-voltage relationships of liposomes and mitochondria. Biochem. J. 219: 719–726.
94 Rogers ME, Williams DT, Niththyananthan R, Rampling MW, Heslop KE, Johnston DG (1992) Decrease in erythrocyte glycophorin sialic-acid content is associated with increased erythrocyte aggregation in human diabetes. Clin. Sci. 82: 309–313.
95 Buser CA, Kim J, McLaughlin S, Peitzsch RM (1995) Does the binding of clusters of basic residues to acidic lipids induce domain-formation in membranes? Mol. Memb. Biol. 12: 69–75.
96 O'Shea P (2003) Intermolecular Interactions with/within cell membranes and the trinity of membrane potentials; kinetics & imaging. Biochem. Soc. Trans. 31: 990–996.

Bioelectrochemistry of Membranes
ed. by D. Walz, J. Teissié and G. Milazzo†

CHAPTER 3
Lipids

Alfred Blume
Martin-Luther-Universität Halle-Wittenberg, Department of Chemistry, Institute of Physical Chemistry, Halle/Saale, Germany

1. Introduction

All living cells are separated from the surrounding medium by a barrier, the cell or plasma membrane. This barrier is a prerequisite for the normal function of living cells. In fact, the cell as an entity being distinct from the surrounding environment, is essentially defined by this plasma membrane.

Membranes not only separate the cell interior from the surroundings and the different compartments inside the cell, but they also have important and fundamental biochemical functions. For instance, they control the passage of ions and molecules from one side of the membrane to the other. Many important biological functions and reactions

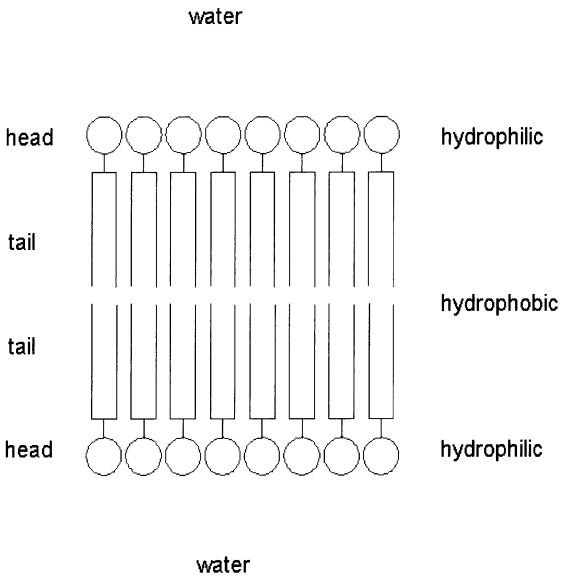

Fig. 1. Schematic diagram of the bimolecular lipid membrane as proposed by Gorter and Grendel [4].

occur at membranes, because only then is it possible to separate the products from the educts by vectorial transport [1, 2].

Over 100 years ago Overton [3] recognized from permeability studies that membranes must contain lipids, as he observed a correlation between the permeability of membranes to non-electrolytes and their lipid solubility. The development of the "Langmuir trough" by I. Langmuir in 1917 for studying monolayers of amphiphilic molecules at the air-water interface was one other important step towards the understanding of membrane structure. In 1925, Gorter and Grendel found that lipids extracted from erythrocytes covered an area on the Langmuir trough corresponding roughly to twice the surface area of the erythrocyte and suggested the bimolecular leaflet as the essential entity of a membrane [4] (see Fig. 1). The hydrophobic tails of the lipid molecules of the opposing monolayers were suggested to be in contact with one another, and the hydrophilic groups of the lipids were thought to be exposed to water. This concept of the bimolecular lipid membrane, though based on incorrect determinations of the surface area of the erythrocytes and incomplete extraction of the lipids (luckily these two errors compensated), was very important for the development of the current models for membrane structure. Ten years after Gorter and Grendel, Danielli and Davson [5] included proteins adsorbed to both sides of the bilayer lipid membrane in their membrane model. Various improvements of this model followed, until

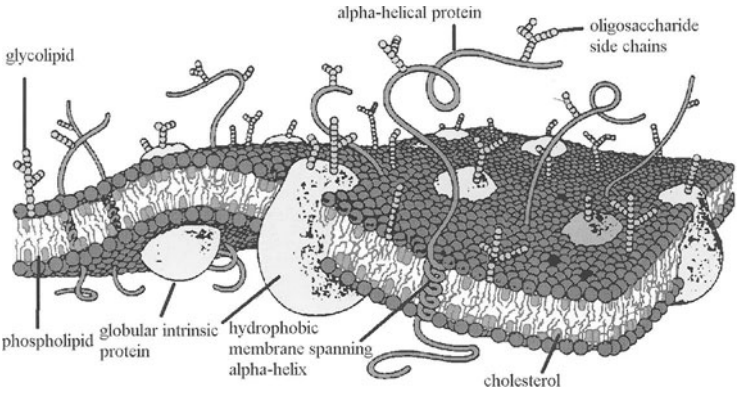

Fig. 2. Fluid-mosaic membrane model as proposed by Singer and Nicolson [6]. Adapted from Ref. 7.

finally the current view of membrane structure, the fluid-mosaic model of Singer and Nicolson evolved [6] (Fig. 2).

It was recognized early that the bilayer matrix is "fluid" in the sense that proteins and also the lipid molecules themselves can rapidly diffuse in the plane of the bilayers. Biological membranes were found to be asymmetric with respect to the distribution of lipids and protein to the two opposing monolayers [7]. The passive redistribution of lipids, the so-called lipid flip-flop, is a slow process with half times between hours and days, the rate depending on the amphiphilic nature of the lipid molecules. Transmembraneous proteins, once incorporated into the membrane, are unlikely to show flip-flop across the membrane, unless they are small and have mostly hydrophobic amino acids.

From studies of lipid extracts of biological membranes and from the studies of lipid model systems, it was recognized that lipid bilayers can exist in physical states of different order and fluidity, depending on the temperature, the chemical structure of the lipid, the composition, and the pH of the aqueous phase [8]. Because much of our understanding of biological membranes is based on results obtained on lipid model membranes consisting of lipids of defined chemical structure [9–11], we will now discuss the various lipid classes occurring in biological membranes and how membrane behavior is related to the chemical structure of the lipids building up the bimolecular leaflet.

2. Chemical structure of membrane lipids

Biological membranes are composed of lipids, proteins, and small amounts of carbohydrates linked either to lipids (glycolipids) or as

Table 1. Chemical composition of various cell membranes [2,12]

Membrane's major function	Percent dry weight of membrane			Protein/lipid (w/w)
	Protein	Lipid	Carbohydrate	
Permeability barrier				
Myelin	18	79	3	0.23
Transport				
Various eukaryotic cells	46–60	37–54	1.5–10	0.85–1.6
Mitochondrial outer membrane	52	48	2–4	1.1
Nuclear membrane	59	35	2.9	1.6
Sarcoplasmic reticulum	67	33	–	2
Outer membrane of S. typhimurium	43	~19	–	2.26
Biosynthesis, secretion				
Microsomes, rat liver	62	32	–	1.9
Signal transduction				
Retinal rods, bovine	51	49	4	1
Energy transduction				
Mitochondrial inner membrane	76	26	1–2	3.2
Chloroplast thylakoid membrane	70	30	6	2.3
Multiple functions				
Plasma membranes of				
Salmonella typhimurium	60	~24	–	2.5
Gram positive bacteria	75	25	~10	3

part of glycoproteins. The protein/lipid ratio can vary between ca. 0.25 and 5. Table 1 shows the chemical composition of various cell and intracellular membranes [2, 12].

Membrane lipids are amphiphilic in nature, i.e. they have hydrophilic moieties which are exposed to water, and hydrophobic parts. Membrane lipids show a great diversity in chemical structure, the hydrophobic moieties consisting in most cases of long aliphatic chains. Most lipids are soluble in non-polar solvents, such as benzene, chloroform, or chloroform/methanol mixtures. The solubility depends on the length and degree of unsaturation of the hydrocarbon chains and, more importantly, on the size and polarity of the hydrophilic head group. More than 1000 different fatty acids have been identified occurring in lipids of prokaryotes and eukaryotes [13]. Table 2a shows the structure, nomenclature, and length of some common fatty acids found in membrane lipids, and Table 2b some less common fatty acids, usually found in prokaryotic membrane systems.

One of the major classes of lipids occurring in prokaryotic as well as eukaryotic membranes are glycerophospholipids. The principal chemical structure of phospholipids is shown in Fig. 3a. The stereospecific numbering (*sn*) system is normally used to distinguish between different enantiomers. In natural phospholipids the phosphate group is bound to the *sn*-3 hydroxyl group of the glycerol and the molecule has

Table 2a. Common fatty acids found in membrane lipids

Common name	Chemical structure	Chain length: unsaturation
Lauric acid	$CH_3(CH_2)_{10}COOH$	12:0
Myristic acid	$CH_3(CH_2)_{12}COOH$	14:0
Palmitic acid	$CH_3(CH_2)_{14}COOH$	16:0
Stearic acid	$CH_3(CH_2)_{16}COOH$	18:0
Arachidic acid	$CH_3(CH_2)_{18}COOH$	20:0
Behenic acid	$CH_3(CH_2)_{20}COOH$	22:0
Lignoceric acid	$CH_3(CH_2)_{22}COOH$	24:0
Cerotic acid	$CH_3(CH_2)_{24}COOH$	26:0
Palmitoleic acid	$CH_3(CH_2)_5CH{=}CH(CH_2)_7COOH$	16:1 (9-cis)
Oleic acid	$CH_3(CH_2)_7CH{=}CH(CH_2)_7COOH$	18:1 (9-cis)
Vaccenic acid	$CH_3(CH_2)_5CH{=}CH(CH_2)_9COOH$	18:1 (11-cis)
Linoleic acid	$CH_3(CH_2)_4CH{=}CHCH_2CH{=}CH(CH_2)_7COOH$	18:2 (9-cis,12-cis)
α-Linolenic acid	$CH_3CH_2(CH{=}CHCH_2)_2CH{=}CH(CH_2)_7COOH$	18:3 (9,12,15-all-cis)
γ-Linolenic acid	$CH_3(CH_2)_4(CH{=}CHCH_2)_2CH{=}CH(CH_2)_4COOH$	18:3 (6,9,12-all-cis)
Arachidonic acid	$CH_3(CH_2)_4(CH{=}CHCH_2)_4(CH_2)_2COOH$	20:4 (5,8,11,14-all-cis)

Table 2b. Less common fatty acids

Name	Chemical structure
iso-branched fatty acid	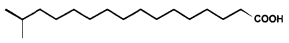
anteiso-branched fatty acid	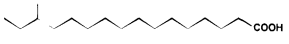
Cyclopropane fatty acid	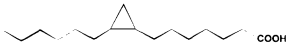
Phytanoic acid	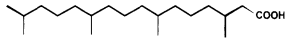
ω-Cyclohexyl fatty acid	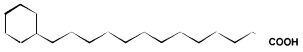
Bicyclopentane fatty acid	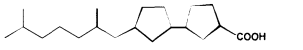

an L-configuration. The phosphate group is normally present in the form of a diester group because various short chain alcohols are linked to it.

The hydrophilic head group of lipids can be zwitterionic or negatively charged. 1,2-diacylphosphoglycerides are the most common form of phospholipids. Fig. 3b shows common phosphoglycerides with their different head groups, the short-hand notation, and the generic

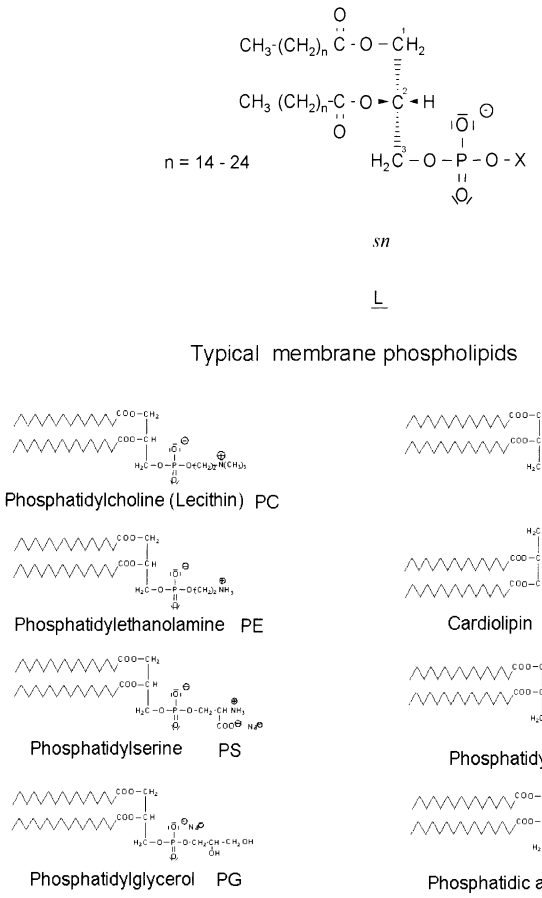

Fig. 3. Top: Stereochemical configuration and *sn*-numbering of phospholipids. X indicates short chain alcohols esterified to the phosphate group. Bottom: Phospholipids with two palmitoyl chains esterified to glycerol with different polar head groups. In the abbreviations used the first two letters indicate the two fatty acyl chains (DP, dipalmitoyl; DM, dimyristoyl), while the next two letters indicate the head group structure: PC, phosphatidylcholine; PE, phosphatidylethanolamine; PS, phosphatidylserine; PG, phosphatidylglycerol; PA, phosphatidic acid; PI, phosphatidyl inositol.

name usually used to characterize the structure of the head group and the linkage and position of the chains. The complete name for a phospholipid such as DPPC is 1,2-dipalmitoyl-*sn*-glycero-3-phosphocholine, in a more abbreviated form it is also called 1,2-dipalmitoylphosphatidylcholine. In plasmalogens, the chain in the *sn*-1 position is linked to the glycerol *via* an α-β-unsaturated ether linkage. Most plasmalogens have ethanolamine, choline or serine as head groups (Fig. 4).

Sphingolipids are derived from the long chain amino alcohol sphingosine. In phosphosphingolipids, the hydrophobic residue ceramide is esterified with phosphoric acid to which similar short chain alcohols

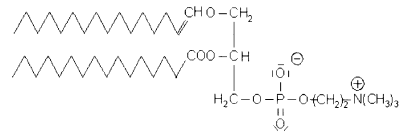

Choline plasmalogen

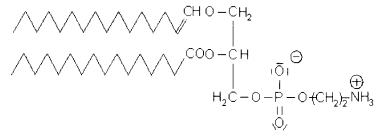

Ethanolamine plasmalogen

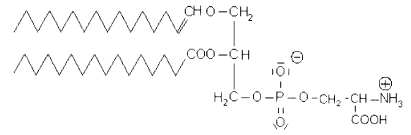

Serine plasmalogen

Plasmalogens

Fig. 4. Chemical structure of three common plasmalogens.

are linked as found in phosphoglycerides. One of the most important lipids of this class is sphingomyelin (see Fig. 5). Most other sphingolipids have sugar residues as hydrophilic head groups and thus belong to the large class of glycolipids. In glycoglycerolipids the sugar residues are directly bound to the glycerol backbone by a glycosidic linkage. Figure 6 shows some representative examples of glycoglycerolipids.

Most sphingolipids are glycosphingolipids, in which carbohydrate residues of varying length and complexity are linked to the ceramide backbone by a glycosidic bond (see Fig. 7). Gangliosides are glycosphingolipids that have negatively charged head groups due to one or more sialic acid (N-acetyl-neuraminic acid) residues. Gangliosides have important physiological functions. The large carbohydrate head groups of gangliosides extend from the surface of the membrane into the aqueous phase. These molecules act as receptors for certain glycoprotein hormones but also for proteins like cholera toxin and plant lectins and take part in processes such as cell-cell recognition, cell differentiation, oncogenic transformation, and neurotransmission [14, 15]. Figure 8 shows the structure of the ganglioside G_{M1} and the short hand notation of some other important gangliosides.

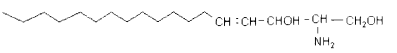

Sphingosine

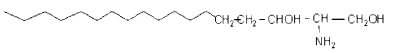

Dihydrosphingosine

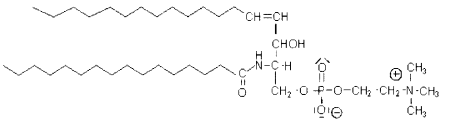

Sphingomyelin

Sphingolipids

Fig. 5. Chemical structure of palmitoyl sphingomyelin and the two sphingosine bases commonly found in sphingophospholipids.

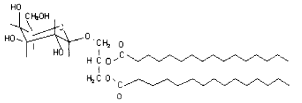

Monogalactosyldiglyceride (MGDG)

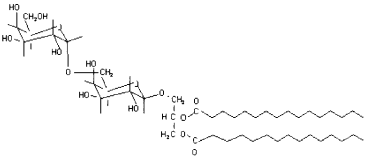

Digalactosyldiglyceride (DGDG)

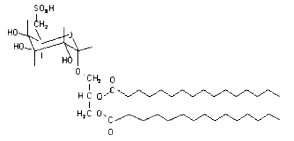

Sulfolipid

Glycoglycerolipids

Fig. 6. Chemical structure of some glycoglycerolipids with two palmitoyl chains.

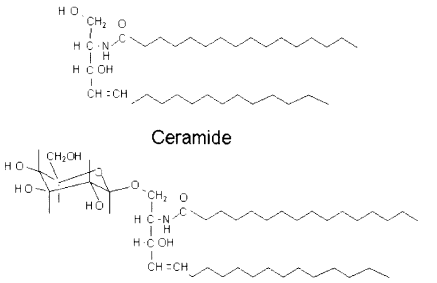

Ceramide

Glucocerebroside (Glucosylceramide)

Galactosylceramide : Gal-Cer

Glucosylceramide : Glc-Cer

Lactosylceramide : Gal-Glc-Cer

Trihexosylceramide : Gal-Gal-Glc-Cer

Globoside : GalNAc-Gal-Gal-Glc-Cer

Abbreviations:

Gal: Galactose, Glc: Glucose

GalNAc: N-Acetylgalactosamine, Cer: Ceramide

Glycosphingolipids

Fig. 7. Chemical structure of glycosphingolipids and the commonly used short-hand notation.

The major amphiphilic components of the outer membrane of Gram-negative bacteria, such as *E. coli* or *S. minnesota*, are lipopolysaccharides, their lipid residue being the so-called lipid A. The quite unusual form of this lipid with its six or seven chains is shown in Fig. 9 [16, 17].

Bacteria living in extreme environments, such as volcanic lakes, geothermal soils, hot springs or waste dumps have membranes consisting of very unusual long chain compounds. Thermophiles possess a large content of longer saturated and predominantly branched-chain fatty acids, mostly of the C_{15} to C_{19} iso- or anteiso-type (see Table 2). Some species, for instance *B. acidocaldarius*, contain fatty acids with ω-cyclohexyl groups. Remarkable are the diether and tetraethers of halophiles and of *Thermoplasma* and *Sulfolobus*, in which the hydrophobic parts consist of two C_{20} or C_{40} saturated isoprenoid-branched chains with ether linkages to the glycerol [18, 19]. The biphytanyl chains may also contain cyclopentane rings as shown in Fig. 10. Archaebacteria also contain other di- and tetraterpenoides like the carotenoids shown in Fig. 11 [20].

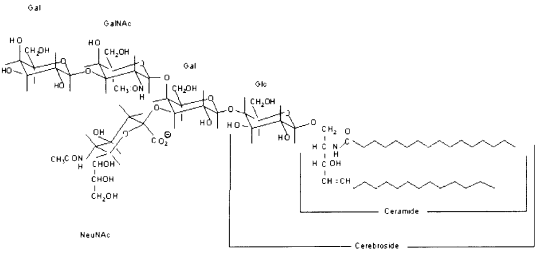

Ganglioside G_{M1}

G_{M3} : NeuNAc-Gal-Glc-Cer

G_{M2} : GalNAc-Gal-Glc-Cer
NeuNAc

G_{M1} : Gal-GalNAc-Gal-Glc-Cer
NeuNAc

G_{D1} : NeuNAc-Glc-GalNAc-Gal-Glc-Cer
NeuNAc

G_{T1} : NeuNAc-Gal-GalNAc-Gal-Glc-Cer
NeuNAc-NeuNAc

Abbreviations:
Gal: Galactose, Glc: Glucose, Cer: Ceramide
GalNAc: N-Acetyl-galactosamine, NeuNAc: N-Acetyl-neuraminic acid

Gangliosides

Fig. 8. Chemical structure of the ganglioside G_{M1} and short-hand notation for other important gangliosides with different head groups.

Sterols are found in animal, plant and some microbial membranes. The major sterol in the plasma membranes of all animal cells is cholesterol [21, 22]. Sterols are rigid, compact molecules derived from a system of four fused saturated rings, the parent compound cyclopentanoperhydrophenanthrene (see Fig. 12). Plant membranes contain no cholesterol, but other sterols such as stigmasterol, β-sitosterol and ergosterol. Prokaryotic cells characteristically contain almost no cholesterol. The only exception is *Mycoplasma*, a prokaryote without a cell wall, which obtains these compounds from its hosts [23].

The prokaryotic polyterpenoids can serve as substitutes for cholesterol [24, 25]. The pentacyclic hopanoids are found in many prokaryotic cells in comparable quantities to cholesterol present in eukaryotic membranes [20]. They can also be found in some eukaryotic cells, such as *Tetrahymena pyriformis* and *Zymomonas* [20, 26]. Figure 13 shows characteristic chemical structures of hopanoids.

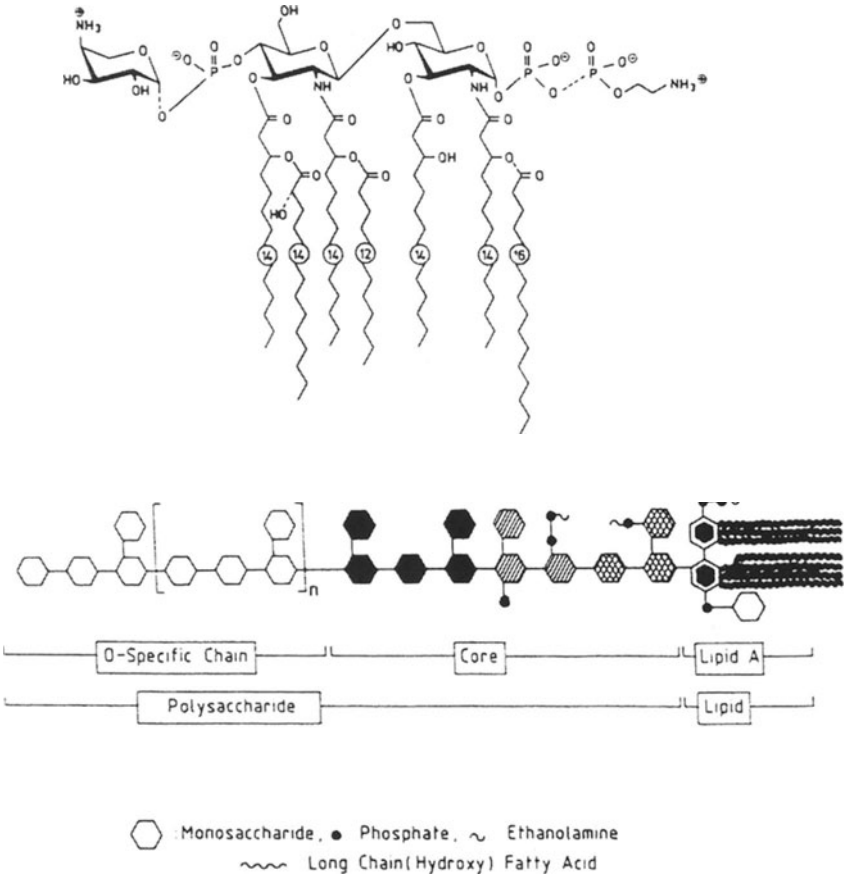

Fig. 9. Chemical structure of the Lipid A from *Salmonella minnesota* and schematic structure of lipopolysaccharides from *Salmonella*. Adapted from Refs. 16 and 17.

3. Aggregation forms of lipids

Depending on the balance between the hydrophobic moieties and the hydrophilic head group, lipids can form various forms of aggregation structures. The driving force for the association into aggregates is the decrease in chemical potential when alkyl chains are removed from an aqueous surrounding and transferred into a non-polar hydrocarbon environment [27–30]. This self-association in water is a manifestation of the hydrophobic effect, i.e. the large negative entropy contribution at room temperature arising from the rearrangement of water molecules when they come into contact with "hydrophobic groups". A characteristic feature of the "hydrophobic effect" is the occurrence of a change in apparent molar heat capacity ΔC_p when non-polar groups

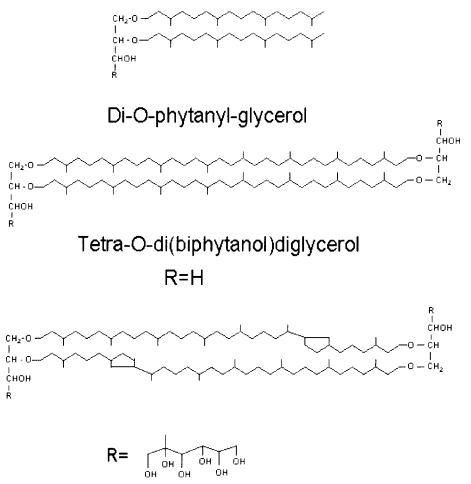

Fig. 10. Chemical structure of diether and tetraether compounds found in prokaryotic membranes [18, 19].

are transferred from hydrocarbon solution into water. This ΔC_p is positive and leads to a strong temperature dependence of the "hydrophobic effect" [29–31].

Israelachvili et al. have shown that lipids will form micelles, lamellar phases or inverted hexagonal phases, depending on whether the molecules can be modeled as cones, cylinders or inverted cones [28]. Figure 14 shows examples for different types of lipid classes and their aggregates. Isralachvili [28] proposed a geometrical packing model where a critical packing parameter N_c is defined as

$$N_c = V/(lA) \tag{1}$$

Here V is the volume of the lipid molecule, while l is an effective length, and A an effective surface area. The effective length l can be estimated from the length of an extended hydrocarbon chain with n methylene groups according to

$$l/nm = 0.15 + 0.127\ n \tag{2}$$

The effective surface area A of the head group can be estimated from molecular models. However, for charged amphiphiles, A depends on

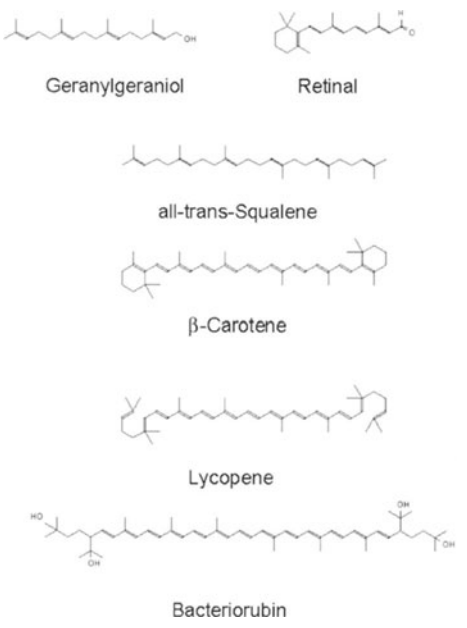

Fig. 11. Chemical structure of isoprenoids and carotenoids found in prokaryotic membranes [20].

electrolyte and surfactant concentration. Phospholipids dispersed in water can exist in different aggregation forms, a phenomenon called lyotropic mesomorphism [28, 32]. Transitions between these different phases can be induced by changes in temperature, water content, ionic strength or pH.

3.1. Lamellar phases

In lamellar phases, lipid bilayers are stacked upon each other repetitiously, the bilayers being separated by water layers of defined thickness. Several lamellar phases are known. At high temperature, normally an L_α-phase is formed, a so-called liquid-crystalline lamellar phase. This phase is characterized by a high mobility of the individual lipid molecules, the molecules can rotate rapidly around their molecular long axis and they can also diffuse freely in the plane of the bilayer. The long hydrocarbon chains show trans-gauche isomerization by restricted rotation around C–C single bonds. The properties of the liq-

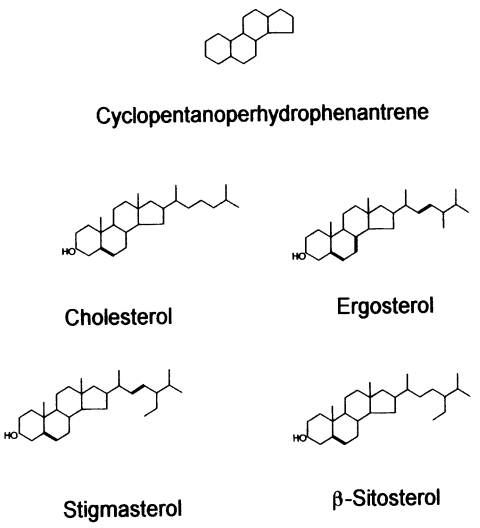

Fig. 12. Chemical structure of sterols found in animal and plant membranes.

uid-crystalline L_α-phase are relevant for biological systems because almost all biological membranes are in this liquid-crystalline state. The dynamic properties of liquid-crystalline bilayers are accurately described when the various reorientational modes are taken into consideration. Data for these various processes are shown in Table 3.

When the temperature is lowered, normally more ordered lamellar phases are formed, called "gel phases" [33]. This gel-like behavior is caused by a considerable reduction of the mobility of the individual lipid molecules in the lamellae. Rotational motions of the molecules and particularly lateral diffusion and trans-gauche isomerization in the chains are reduced and the hydrocarbon chains are now predominantly in an all-trans conformation. Several lamellar gel phases, distinguished by the orientation of the chains with respect to the bilayer normal, by the packing of the hydrocarbon chains, by the degree of hydration of the head groups and by the presence or absence of surface distortions, have been found [34]. Figure 15 shows, as a typical example, the major phase transformations of phosphatidylcholines and phosphatidylethanolamines with saturated fatty acids. The partially dehydrated phases found at lower temperatures are called L_c-phases. Lamellar phases with tilted chains are designated by a prime, such as $L_{c'}$.

The temperatures at which transitions between different lamellar phases occur depend on the length of the fatty acyl chains, the chem-

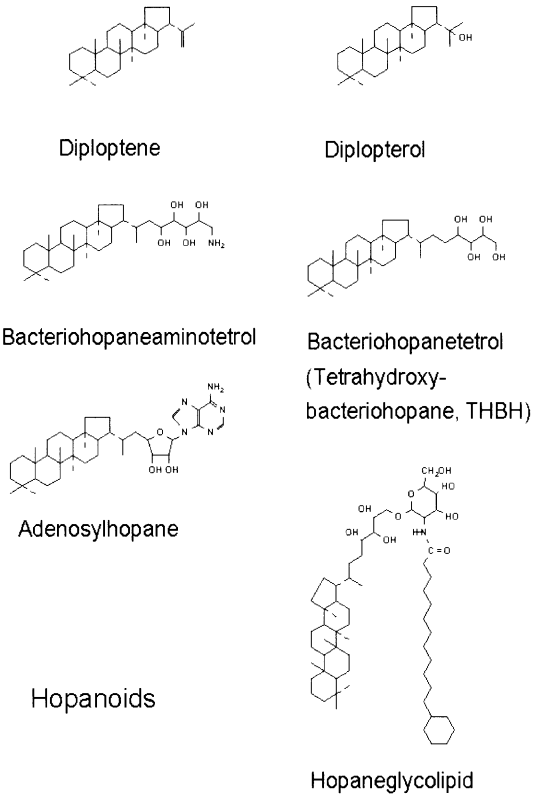

Fig. 13. Chemical structure of some hopanoids found in prokaryotic membranes as sterol replacement [20].

ical structure of the phospholipid head group and on lipid concentration. Figure 16 shows a phase diagram of the DPPC/water system [34]. Similar phase diagrams are observed for phosphatidylglycerols. Phosphatidic acids and phosphatidylethanolamines convert from an L_β-phase to an L_α-phase upon heating. Figure 17 shows typical differential scanning calorimetric (DSC) scans of phospholipids with different chain lengths dispersed in excess water showing the peaks observed when phase changes induced by temperature occur [35, 36].

When a lipid has two chains of unequal length, partly or completely interdigitated ordered gel phases can be observed [37]. In these phases, the thickness of the lamellae is reduced due to chain interdigitation; it is essentially a lipid monolayer. These lamellar phases are also observed for diether phosphatidylcholines with equal chain lengths and for diacyl phosphatidylcholines when dispersed in ethanol/water mixtures [38] (see Fig. 18).

The influence of variations in head group and fatty acyl chain structure on lipid dynamics have been extensively studied. Lipid mobility

Lipid	N_c	Critical packing shape	Structures formed
Single-chained lipids (surfactants) with large head-group areas: *SDS in low salt*	< 1/3	Cone 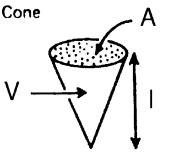	Spherical micelles 
Single-chained lipids with small head-group areas: *SDS and CTAB in high salt, nonionic lipids*	1/3-1/2	Truncated cone 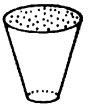	Cylindrical micelles 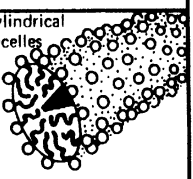
Double-chained lipids with large head-group areas, fluid chains: *Phosphatidyl choline (lecithin), phosphatidyl serine, phosphatidyl glycerol, phosphatidyl inositol, phosphatidic acid, sphingomyelin, DGDG[a], dihexadecyl phosphate, dialkyl dimethyl ammonium salts*	1/2-1	Truncated cone 	Flexible bilayers, vesicles 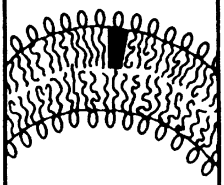
Double-chained lipids with small head-group areas, anionic lipids in high salt, saturated frozen chains: *phosphatidyl ethanolamine, phosphatidyl serine + Ca^{2+}*	~1	Cylinder 	Planar bilayers 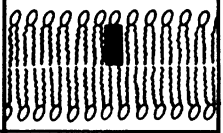
Double-chained lipids with small head-group areas, nonionic lipids, poly *(cis)* unsaturated chains, high *T*: *unsat. phosphatidyl ethanolamine, cardiolipin + Ca^{2+} phosphatidic acid + Ca^{2+} cholesterol, MGDG[b]*	> 1	Inverted truncated cone or wedge 	Inverted micelles 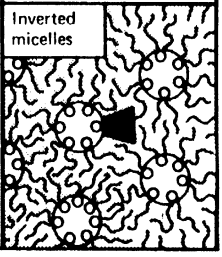

Fig. 14. Schematic diagram of the various structures formed by amphiphilic molecules, depending on the critical packing parameter N_c (see Eqn. 1) as suggested by Israelachvili [28].

is reduced when the head groups are capable of intermolecular hydrogen bonding, such as that observed for phosphatidylethanolamine and phosphatidic acid [39–43]. Phospholipids with unsaturated chains have been viewed as increasing the "fluidity" of the bilayers. How-

Table 3. Approximate correlation times τ_c for various motional modes in the different phases of phosphatidylcholines and phosphatidylethanolamines

Phase	Chain isomerization by rotation around single bonds	Long axis rotation	Wobbling of chain axis	Order director fluctuations
$L_c(L_{c'})$	$< 10^{-3}$ s	$< 10^{-3}$ s	–	–
$L_\beta(L_{\beta'})$	10^{-9}–10^{-5} s	10^{-6}–10^{-5} s	10^{-5}–10^{-3} s	–
L_α	10^{-12}–10^{-9} s	10^{-9}–10^{-8} s	10^{-9}–10^{-7} s	$\approx 10^{-3}$ s

ever, NMR examinations show that bilayers with polyunsaturated chains are relatively ordered and that the molecules have longer correlation times for intramolecular reorientational chain motions [44]. This shows that the term "fluidity" is ill-defined and does not correctly describe bilayer properties. For a proper description, conformational order, chain fluctuations, and correlation times for intra- and intermolecular motions have to be considered. How changes in these properties will influence other properties of bilayers, such as elasticity, compressibility, permeability, thermal stability and stability towards fusion, is still under intensive investigation.

3.2. Hexagonal phases

In the geometric model proposed by Israelachvili [28], the critical packing parameter N_c (see Eqn. 1) determines the type of the lipid aggregate. If $N_c \neq 1$ a spontaneous curvature of the surface is induced. Specifically, if $N_c < 1$ spherical and cylindrical micelles are the predominant aggregation forms. For $N_c = 1$ planar bilayers are stable, and for $N_c > 1$ an inverted hexagonal phase H_{II} can be formed. In the H_{II}-phase, the lipid molecules are arranged in cylindrical, rod-like inverted micelles, which are packed in a hexagonal array [34, 45] (see Fig. 19). Very common is a temperature-induced phase transition from a lamellar liquid-crystalline L_α-phase to an H_{II}-phase at higher temperature. This type of phase behavior is observed with phosphatidylethanolamines with unsaturated fatty acyl chains.

Different contributions to the total free energy arising from head group interactions including hydration, from curvature energy of the monolayers, and from chain interaction and packing constraints have to be considered when predictions about the existence of inverted hexagonal phases are made. These different contributions can change with temperature, hydration, composition of the aqueous phase, and pH. Consequently transitions from lamellar to hexagonal phases can be induced by a change of one or several of these parameters [46].

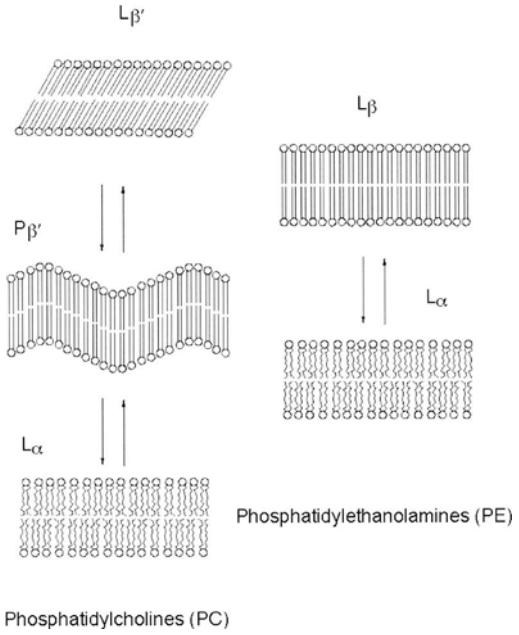

Fig. 15. Schematic diagram of the phase transitions between different lamellar phases for phosphatidylcholines and phosphatidylethanolamines.

The different forces acting at the hydrophilic surface, i.e. the area of the head group exposed to water, and at the hydrophobic surface can lead to a spontaneous curvature of the monolayer in the minimum energy configuration. Helfrich [47, 48] has shown that the energy of elastic bending per unit area of a thin layer is

$$U_{ben} = \chi\,(1/R_1 + 1/R_2 - 1/R_0)^2/2 + \chi_G\,/(R_1\,R_2) \qquad (3)$$

with χ and χ_G being the bending rigidity and the elastic modulus of Gaussian curvature, respectively. R_1 and R_2 are the principal radii of curvature and R_0 the radius of spontaneous curvature. U_{ben} will be minimal if $(1/R_1 + 1/R_2 - 1/R_0) = 0$, i.e., if the net curvature is equal to the spontaneous curvature. For the cylindrical micelles of the H_{II}-phase, the Gaussian curvature $1/(R_1\,R_2) = 0$ because $1/R_2 = 0$ in the case of a cylinder, and only the net curvature contributes to the total elastic bending energy. The spontaneous curvature $1/R_0$ is a thermodynamic property of the system, resulting from the difference in forces at different planes located at the head groups or the tails of the molecules. The curvatures $1/R_1$ and $1/R_2$ are the physically observed curvatures resulting from the minimization of the first term in the equation.

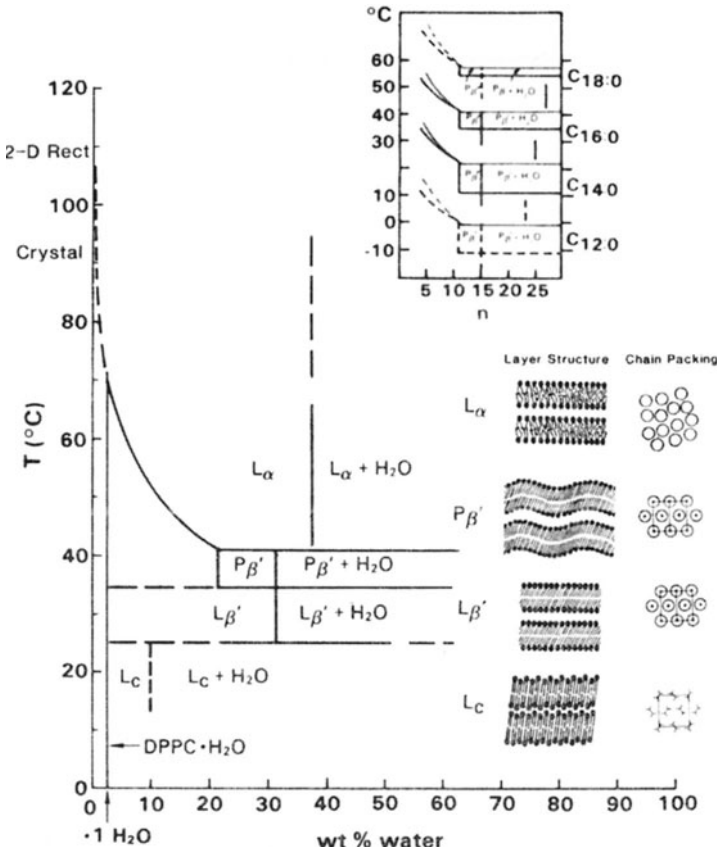

Fig. 16. Phase diagram for DPPC as a function of water content. Inset: schematic phase diagrams for other saturated phosphatidylcholines (adapted from Ref. 34).

Luzatti first found examples for H_{II}-forming lipids in brain lipids composed of mixtures of phosphatidylethanolamine (PE), phosphatidylcholine (PC) and phosphatidylinositol (PI) [49]. Later it was recognized that effects which expand the hydrophobic region relative to the head group region will lead to non-lamellar phases. A prime example is the different phase behavior of PCs and PEs. PCs have relatively large, well hydrated head groups. Even chain unsaturation with the concomitant expansion of the hydrophobic region will not increase the critical packing parameter sufficiently that inverted hexagonal phases are not formed.

This is different for phosphatidylethanolamines. PEs have stronger intermolecular interactions between head groups *via* H-bonds and the headgroups are less hydrated compared to PCs. In the geometric

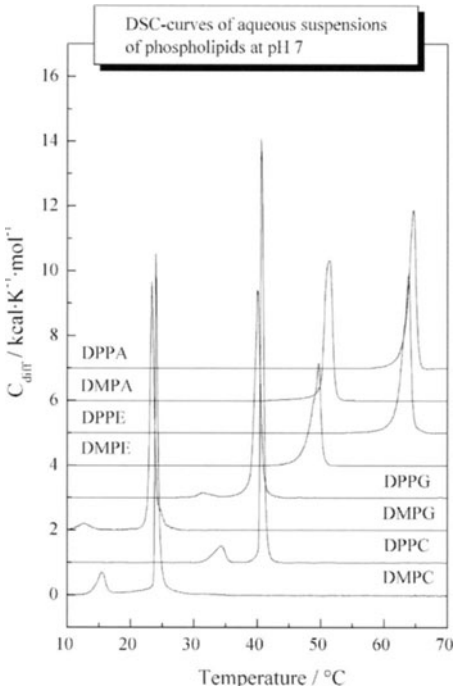

Fig. 17. Differential scanning calorimetric curves of the phase transitions of PCs and PEs with different chain length [35, 36].

model this reduces the effective surface area A. Consequently PEs are "H_{II}-prone" lipids, they show a transition into the H_{II}-phase when the temperature in the L_α-phase is increased [45]. For short saturated chain PEs this transition occurs above 100 °C, but when the chain length is increased, the transition temperatures (T_h) into the H_{II}-phase decrease below 100 °C as is the case for diacylphophatidylethanolamine (DAPE) (see Fig. 20) [50].

For phosphatidylethanolamines with ester instead of ether bonds, the transition temperature T_h is reduced because the head group region is now less hydrophilic due to the absence of the carbonyl oxygens. Addition of NaCl reduces T_h even more, PEs with long chains now convert directly from an ordered L_β into a disordered H_{II}-phase [50] (see Fig. 20).

The transition temperature T_h is also reduced when PEs have unsaturated fatty acids. The phase behavior of dioleoylphophatidylethanolamine (DOPE) in water has been systematically characterized using various methods [45, 51–54]. In excess water, the transition from the L_α to the H_{II}-phase occurs at 5–10 °C and the H_{II} lattice parameter (the distance between the cylinder axes) is 80 Å, decreasing con-

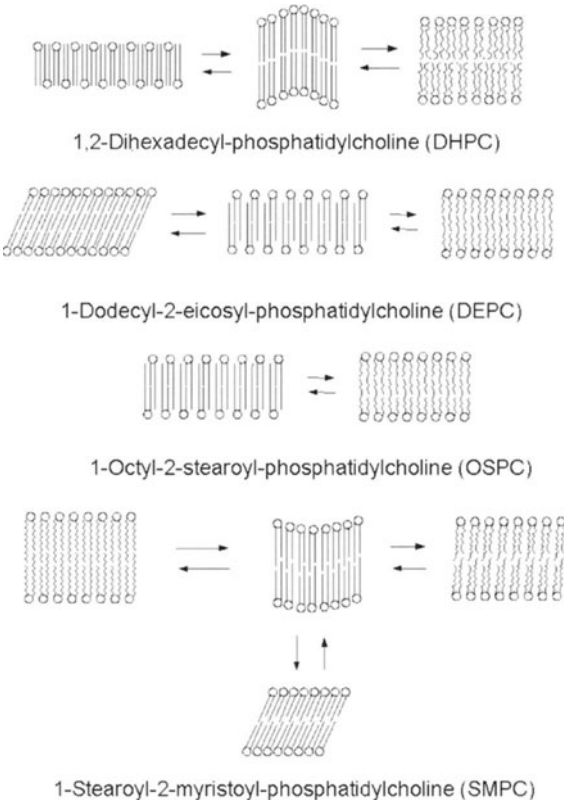

Fig. 18. Schematic diagrams of the phase transitions of phospholipids which form interdigitated gel phase bilayers [37, 38].

tinuously with temperature. An effective packing of the inverted cylinders can only be accomplished when the hydrophobic interstices between the rods are filled to minimize the interaction energies between the hydrocarbon chains. This packing problem can be relieved when alkanes are added to the DOPE/water system, T_h is now decreased to temperatures below 0 °C because the alkane molecules are accumulated between the rods [45]. A much larger effect on T_h was observed for dioleoylphosphatidylcholine (DOPC)/DOPE (3:1) mixtures [45, 53]. This mixture converts to an H_{II}-phase at ca. 55 °C, the H_{II} lattice parameter being 75 Å just above T_h. Addition of a few percent of dodecane relieves the chain packing constraints. The transition to the H_{II}-phase is now reduced to 0 °C or below. Recently, the significance of phase transitions from the fluid lamellar phase to the inverted hexagonal phase was again discussed with respect to the possible significance for membrane fusion processes [46, 55, 56].

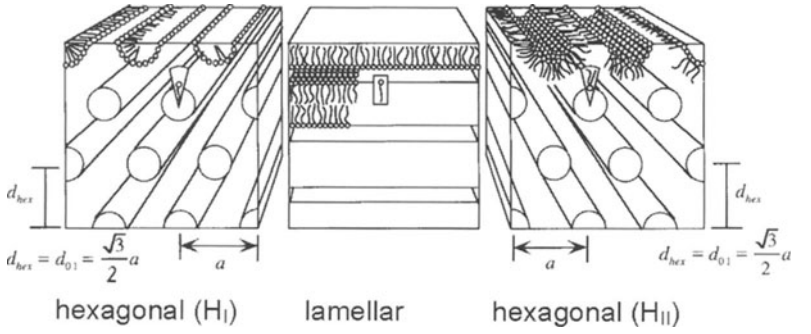

Fig. 19. Arrangement of the lipid molecules in the hexagonal H_I, the lamellar, and the hexagonal H_{II}-phase. Adapted from Ref. 32.

3.3. Cubic phases

Quite a few lipid/water systems convert directly from a lamellar L_α-phase to the H_{II}-phase [45, 46, 55, 56]. An interesting problem is how this transition develops. The mechanism of this transition has been discussed intensively, and it was suggested that the transition proceeds *via* the formation of so-called "lipidic particles", which are in fact inverted micelles localized in between the two opposing monolayers [56–58]. While in many systems, particularly mixed lipid systems, these lipidic particles can be detected by, for instance, freeze fracture electron microscopy, other systems like pure PEs show no "lipid particles" in the fracture faces. Siegel and Epand [56] have suggested that these "inverted micellar intermediates" (IMIs) are one possible step towards the formation of the H_{II}-phase. They proposed that when the density of the IMIs is high enough, they will fuse into "rod micellar intermediates" (RMIs) and thus form line defects. These eventually are the nuclei for the formation of the H_{II} phase. Figure 21 shows schematically how this transition could proceed.

Another possibility is the formation of interlamellar attachments (ILA). This is essentially a fusion of two bilayers leading to a channel connecting the two bilayers [58]. If the concentration of ILAs is high enough they can coalesce to form a bicontinuous cubic phase, a structure is shown in Fig. 22. This cubic phase has a periodic minimal surface (PMS). These surfaces are three-dimensional, periodic, free from self-intersections, and have zero curvature everywhere, i.e. the sum of the principal curvatures $1/R_1 + 1/R_2$ is zero, every point on the surface is a saddle point. The volumes occupied by the water and by the lipid chains are continuous throughout the whole phase [92].

Cubic phases of this type always occur in between the lamellar and inverted hexagonal phases. Not very many examples of cubic phases

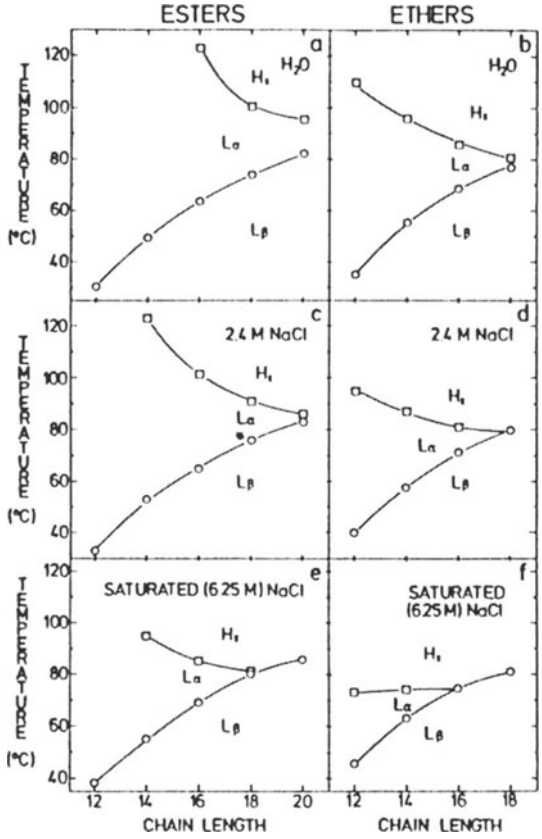

Fig. 20. Chain length dependence of the transition temperature from the gel phase into the L_α- and H_{II}-phase for phosphatidylethanolamines with ether and ester bonds [50].

formed by lipids with two chains exist. In DOPE, the cubic phase can be formed by repeated temperature cycling through the L_α-H_{II} transition. The cubic phase formed is then very stable, the reverse transition seems to be kinetically hindered. Monogalactosyldiglyceride/digalactosyldiglyceride (MGDG/DGDG) mixtures, found in chloroplasts, also form cubic phases [59].

A number of membrane perturbers can also induce the formation of cubic phases, such as anesthetics and gramicidin, though mostly the H_{II} phases are more readily formed [60].

The phenomenon of spontaneous curvature has important biological implications. While the existence of H_{II}-phases in biological systems is still unclear, the occurrence of transient structures, such as IMI and ILA, in biological events which require a disruption of the bimolecular leaflet, namely fusion of membranes, endocytosis and exocyto-

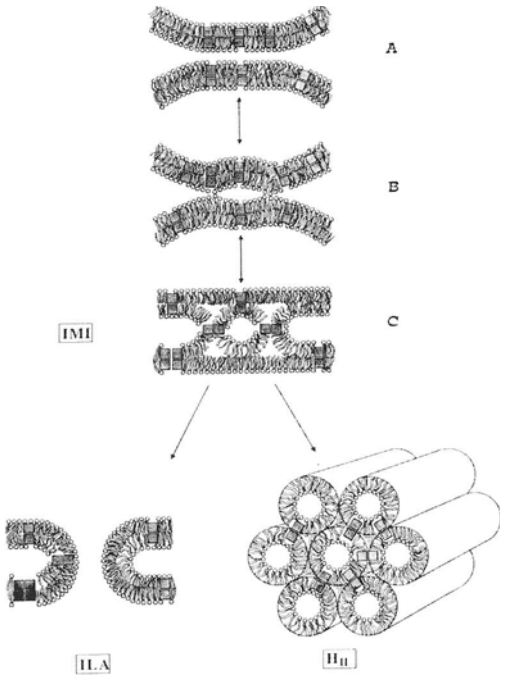

Fig. 21. Scheme of possible transformations of the lamellar phase into the H_{II}-phase *via* "inverted micellar intermediates" (IMI), which can also form "interlamellar attachments" (ILA) [58].

sis, is very likely. Another important effect of H_{II}-prone lipids may be to facilitate the lipid flip-flop from one side of the lipid bilayer to the other *via* IMIs. And finally, a hypothesis which has to be proved, H_{II}-prone lipids could also affect the permeability of bilayers to ions and small molecules.

Cubic phases have recently been used for the crystallization of membrane proteins [61]. Also, the biological significance of cubic phases in biological systems is intensively discussed [62]. For practical applications, it seems possible to use lyotropic phases as drug delivery systems [63, 64].

4. Lipid model systems for biological membranes

Much of our understanding of the functions of biological membranes has been gained from investigations of model systems. Biological membranes can be readily isolated, but experiments with these systems are complicated by the fact that they are very complex and that the lipid composition is diverse. In addition, due to variations in mem-

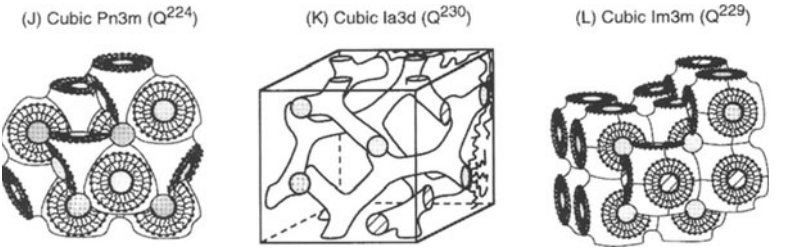

Fig. 22. Structure of bicontinuous cubic phases of lipids and their nomenclature. Shading indicates the connectivity of the water channels. The surface of the middle of the bilayers is an infinitely periodic minimal surface (IPMS) with zero mean curvature. Adapted from Ref. [32].

brane composition in the biological system and/or artificially introduced by the preparation procedures, these systems are not well defined in the sense that the various physical parameters which control the membrane properties cannot be influenced in a precise way.

Model systems are much easier to understand and investigate. Their chemical composition can be chosen and changed at will. Various physicochemical properties can be studied using different methods. Proteins can be reconstituted into lipid bilayers, regenerating functional properties like transport or other enzymatic activities. The simplicity of these model systems as compared to their biological counterparts is at the same time their greatest disadvantage. Properties which require the presence of all constituents of the membrane cannot be mimicked by a simple model membrane. As the behavior of a complex system cannot be predicted by just adding the properties of the individual components, the study of simple systems may lead to wrong conclusions. Nevertheless, without the study of model systems our understanding of biological membranes would be still very limited.

Mainly three different model systems have been used and studied in quite detail, namely lipid monolayers, so-called bilayer (or black) lipid membranes (BLM) and lipid bilayers in the form of lipid vesicles or liposomes and planar lipid bilayers.

4.1. Lipid monolayers

Amphiphilic molecules such as detergents and also membrane lipids can be spread at the air/water interface to form stable lipid monolayers [65]. As mentioned in the introduction, the results from spreading experiments with erythrocyte lipids by Gorter and Grendel led to the

concept of the bimolecular lipid membrane as the basic feature of all biological membranes [4]. The traditional apparatus for studying insoluble monolayers is the Langmuir film balance or trough (see Fig. 23). A known amount of lipid dissolved in an organic solvent is applied to the water surface in between the two barriers. The solvent evaporates and the water surface is now covered by a monolayer of lipid molecules, their hydrophilic groups being solvated and the hydrophobic groups pointing away from the water surface. The advantage of this setup is that the state of the monolayer can be controlled by changing the temperature, the composition of the aqueous subphase, and the available area, as one of the barriers can be moved to compress the film. The surface pressure $\pi = \gamma_0 - \gamma$, i.e. the difference between the surface tension γ_0 of pure water and γ of the water surface covered with the monolayer, respectively, can be measured from the forces acting on the other floating barrier using a torsion balance (Langmuir method) or by the Wilhelmy method, where the forces acting on an immersed small plate are measured. A typical pressure/area curve for a phospholipid, in this case the compound 1,2-dimyristoylphosphatidic acid (DMPA), is shown in Fig. 24 (Garidel and Blume, unpublished observations).

For phospholipids, transitions between different monolayer states can be observed. At high surface pressure, the monolayer is in a solid-analog state, the molecules are tightly packed with their chains perpendicular to the water surface. The area cannot be reduced any further, the film will collapse when the surface pressure is increased [66, 67]. The molecular area in these solid surface films depends on the nature of the lipid head group. For lipids with small head groups the cross-sectional area of the two chains is the limiting factor. Values of ca. 40 $Å^2$/molecule are found, characteristic for the cross-sectional area of two alkyl chains being tightly packed. In phosphatidylcholines, the head groups are larger and are therefore the limiting factor. The PC monolayer can only be compressed to ca. 44–45 $Å^2$/molecule.

When the monolayer area is slightly increased, a change in slope of the π-A curve is observed when it changes into the liquid-condensed phase. On further expansion an almost horizontal isotherm occurs. This plateau region is characteristic for a transition from the so-called liquid-condensed (LC) to the liquid-expanded (LE) state [66, 67]. The plateau region occurs at consecutively higher lateral pressures when the temperature is increased (see Fig. 24). In the plateau-region a phase equilibrium between LC and LE phase should exist when this transition is of first order or weakly first order.

This is indeed observed by epifluorescence techniques [68–73]. In this method a fluorescent lipid probe is mixed with the other lipids at low concentration and the surface fluorescence is observed through an optical microscope. The fluorescent dye accumulates in the

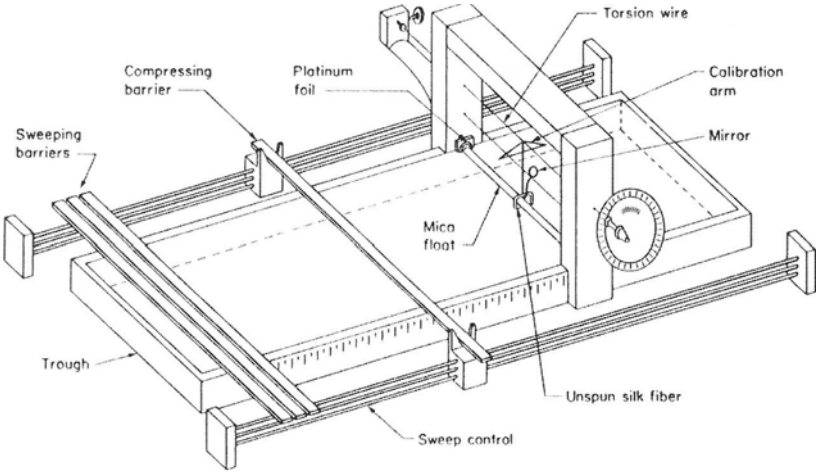

Fig. 23. Principle arrangement of a Langmuir trough used for investigations of lipid monolayers at the air-water interface. In modern instruments the torsion wire is replaced by an electronic pressure detection system, such as a position sensitive inducer. The surface pressure can also be measured by the Wilhelmy plate method using an electro balance [65].

domains of the LE state, the LC domains show no fluorescence. Figure 25 shows a series of fluorescence micrographs obtained in the plateau region of the lipid DMPA. The growth of the LC domains at the expense of the LE domains can clearly be seen. This proves that the LE-LC transition in monolayers is a first order transition [70].

The LC domains observed upon compression of the monolayers can adopt a variety of different forms. If the compression is slow enough they represent "equilibrium" shapes. When two enantiomeric phospholipids, such as D-DPPC or L-DPPC are used, the domains can have opposite chirality. The shape of the domains is mainly determined by the line tension between LC and LE phase [69] (see Fig. 26). Incorporation of small amounts of cholesterol reduces the line tension, because it accumulates at the LC-LE interface. This leads to a thinning of the domain widths [71, 72] and spiral domains are formed.

Whereas in the beginning the visualization of domains in monolayers could only be achieved using a fluorescence microscope and fluorescent probes incorporated into the monolayer, the development of Brewster Angle Microscopy (BAM) has made it possible to visualize domains with a probe free technique [74, 75].

When lipid monolayers are used as a model for lipid bilayers the correct surface pressure has to be chosen. From experimental results [66, 76–78], as well as from theoretical arguments using as a basis the hydrophobic free energy density [78] and from model calculations [79], it is now accepted that at a surface pressure of ca. 30–35 mN/m

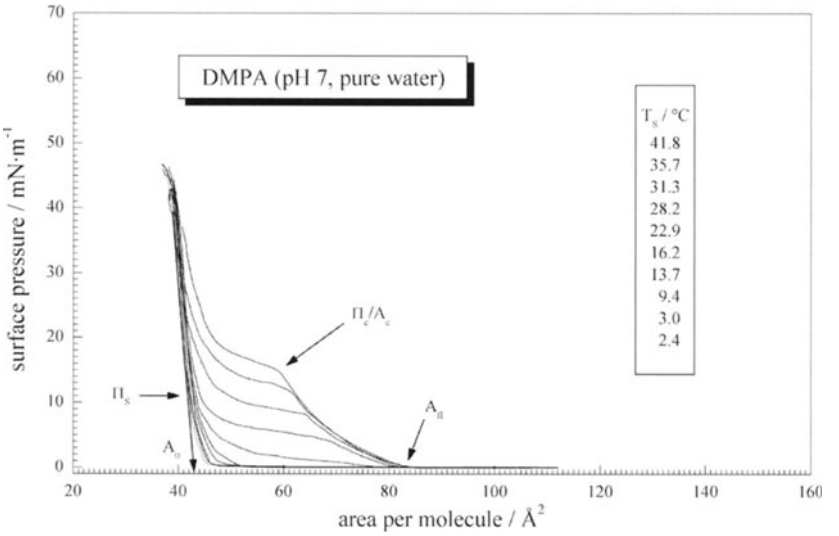

Fig. 24. Surface pressure-area (π-A)-isotherms for the mono-sodium salt of DMPA at various temperatures (Garidel and Blume, unpublished observations).

the lipid molecules in the monolayer are in a similar arrangement as in a bilayer, i.e. their head group area at the air/water interface is the same. When monolayer isobars are recorded, then the LC-LE transition is clearly discernible by a sudden increase in surface area (see Fig. 27). At a surface pressure of approximately 30 mN/m, the absolute area in the LC-phase and the area change at the LC-LE transition are very similar to the values found for the gel to liquid-crystalline bilayer transition [66]. However, the transition temperatures T_m for the monolayer transition are ca. 4–10 °C lower. This difference is obviously caused by the absence of the opposing monolayer. The relatively small shift in T_m shows that the coupling between the two monolayers in bilayers is weak [79].

The influence of changes in subphase composition on the monolayer behavior can be easily followed. The pH can be changed, the effect of ionic strength of the aqueous subphase, and the binding of divalent cations to negatively charged phospholipids can be studied [80]. Proteins can be incorporated into or adsorbed to monolayers and the effect on film compressibility and stability be followed [81]. A classical example for monolayer investigations with water-soluble proteins are studies on the activity of phospholipase A_2 as a function of film pressure. These studies led to the conclusion that the molecular arrangements of lipid molecules in monolayers are similar to the arrangement in bilayers when the monolayer pressure is ca. 30–35 mN/m [76]. Other examples are the binding of cytochromes b5 and

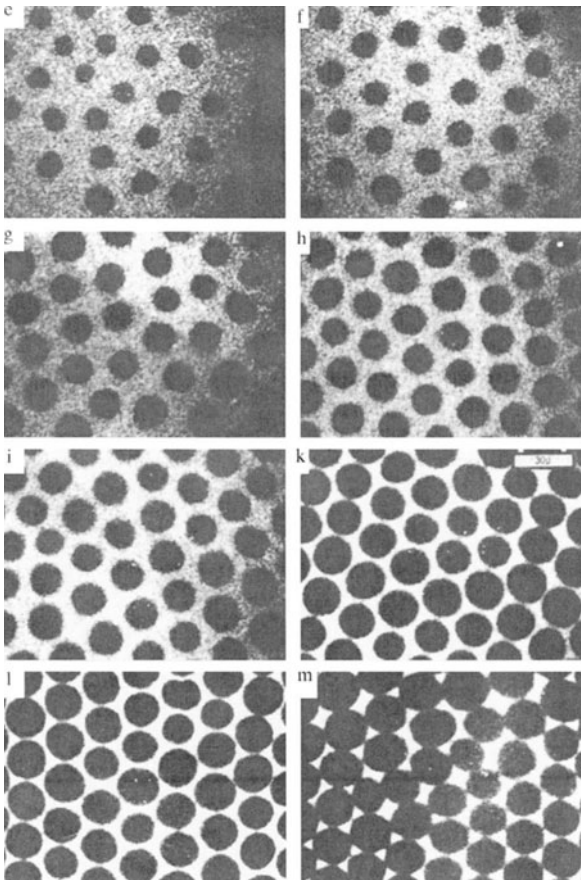

Fig. 25 Epifluorescence micrographs of a DMPA monolayer in the LE-LC transition region. Dark areas correspond to LC domains from which the fluorescent probe dipalmitoyl-NBD-PE (see Fig. 62) is excluded. The surface pressure increases from e) to m) [70].

c to lipids using a protein labeled with a fluorescent probe. The protein distribution in the monolayer can then be studied by epifluorescence techniques using an optical microscope [82]. Other studies are new epifluorescence experiments with phospholipase A_2, showing that the enzymatic action of phospholipase starts specifically at the boundary lines between LE and LC domains and that the activity can be increased by incorporation of smaller peptides [83, 84].

Significant progress has also been made in the application of X-ray and neutron scattering techniques for studying surfactant and lipid monolayers [70, 71, 85, 86]. The X-ray or neutron beam is oriented in such a way that it hits the surface of the monomolecular film at an angle below that corresponding to total reflection (~ 0.1°). When the

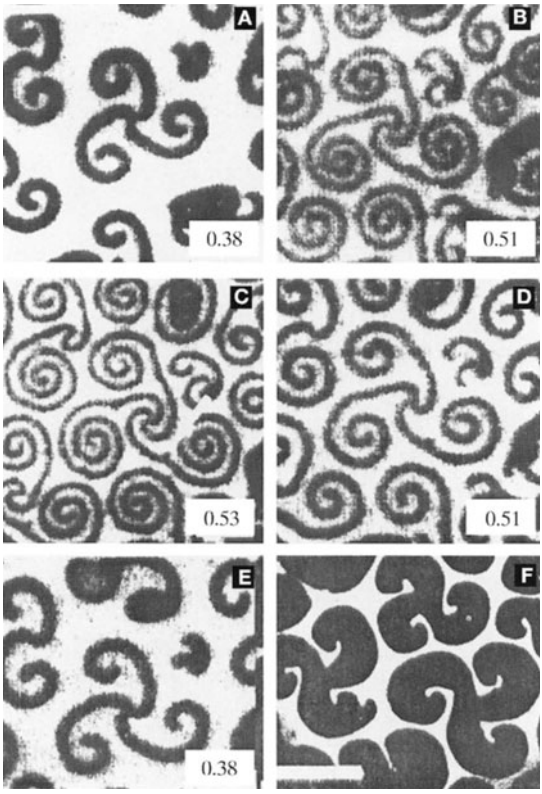

Fig. 26. Epifluorescence micrographs of R-DPPC with 2 mole% cholesterol. Numbers indicate the fraction of the surface covered by the LC domains. The bar is 10 μm [73].

specular reflection is measured as a function of the incident angle, information on the electron density distribution parallel to the normal to the surface is obtained. Measuring the diffracted intensity at fixed incidence as a function of the in-plane diffraction angle yields information on the lattice structure. These experiments can be performed at different surface pressures corresponding to different points on the pressure-area isotherm. An example for DMPA monolayers is shown in Fig. 28 [70]. From the peak maximum the lattice constant for the (1,0) spacing of the hexagonal lattice (ca. 4.2 Å) can be derived. This value corresponds closely to the lattice spacing found in L_β-phases of lipids.

In the last years, the application of Fourier-Transform-Infrared-Spectroscopy (FT-IR) to investigation of lipid monolayers has considerably increased due to progress in technical developments and sensitivity of detectors. The technique of Infrared Reflection Absorption Spectroscopy (IRRAS) will be described below.

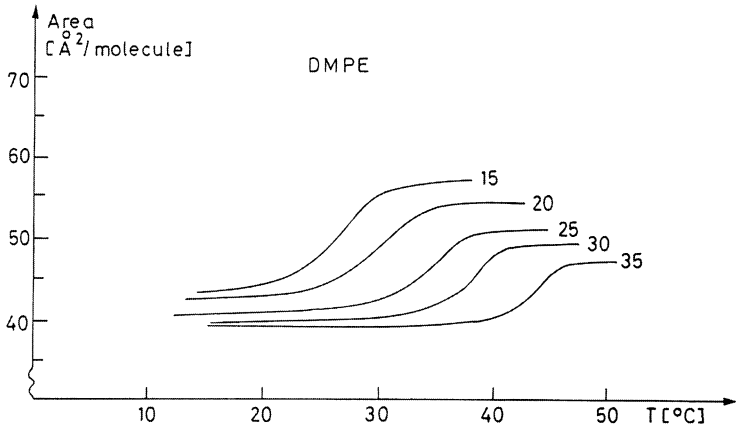

Fig. 27. Monolayer isobars of DMPE at increasing surface pressure π from 15 to 35 mN/m. At the LC-LE transition the monolayer expands, the differences between the areas in the LC and LE phase being dependent on the surface pressure [66].

4.2. Bilayer lipid membranes (BLM)

Much of our knowledge of the electrical and transport properties of lipid membranes has come from studies of BLMs, the so-called "bilayer (or black) lipid membranes" [87–89]. A BLM is formed on a small hole of about 1 mm diameter in a Teflon wall, separating two compartments filled with aqueous solution (Fig. 29, see also section 4 in chapter 1). A small volume of the lipid dissolved in an organic solvent, such as n-decane or hexadecane, is applied to the hole using a syringe, and the formation of the BLM is observed in reflected white light using a microscope. When the bilayer thins due to flow and dispersing of the solvent, the light is at some thickness no longer reflected and the bilayer seems "black", hence the name "black lipid membrane" was first coined. Later the name "bilayer lipid membrane" has become more common. The major drawback of the use of BLMs prepared by this method is that residual solvent can influence the properties of the BLM. Several methods are now available with which essentially solvent-free BLMs can be produced. Also asymmetric BLMs can be made from monolayer films [90].

BLMs have specific advantages for measuring transport processes because the composition of the aqueous solution on either side of the BLM can be manipulated at will as long as the BLM remains stable. Electrical measurements can be made by placing electrodes in both compartments. The electrical properties are measured under direct current or with alternating currents in the frequency range up to 1000 kHz. The specific resistance R_m of planar membranes can be as

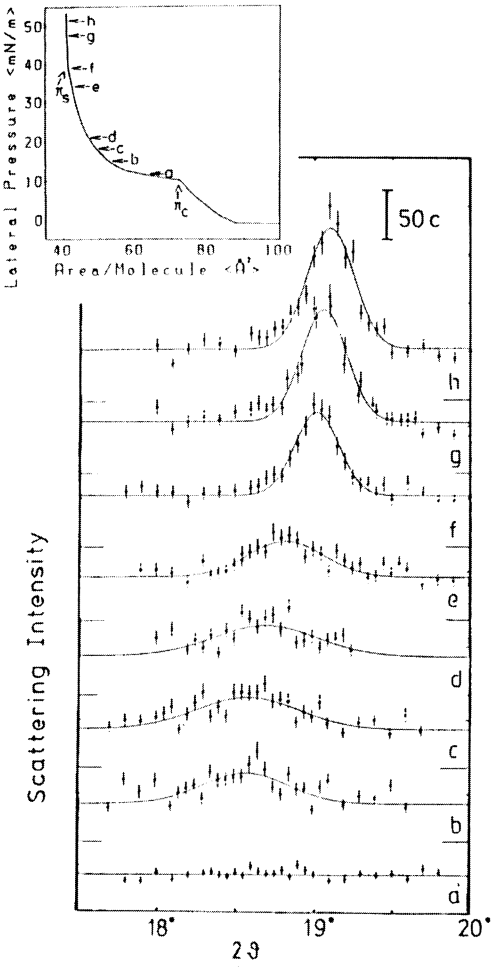

Fig. 28. X-ray scattering from DMPA monolayers at different surface pressures as indicated in the π-A-curve in the inset. With increasing π the molecules orient perpendicular to the surface and a maximum in the scattering intensity at an angle corresponding to a spacing of 4.2 Å develops [71].

high as 10^5 to 10^7 Ω cm^2, much higher than the resistance of cell membranes which is between 1 and 10^4 Ω cm^2. The BLM not only has a resistance, but also a capacitance C_m, which can be determined by a simple experiment assuming an equivalent circuit with a capacitor C_m in a parallel with a resistor R_m (Fig. 30A). When a current I is suddenly turned on at t = 0, the transmembrane potential difference $\Delta\phi_m$ will rise to a final value $\Delta\phi_{m,\infty}$ according to

$$\Delta\phi_m(t) = \Delta\phi_{m,\infty} [1 - \exp(-t/\tau_m)] \quad (4)$$

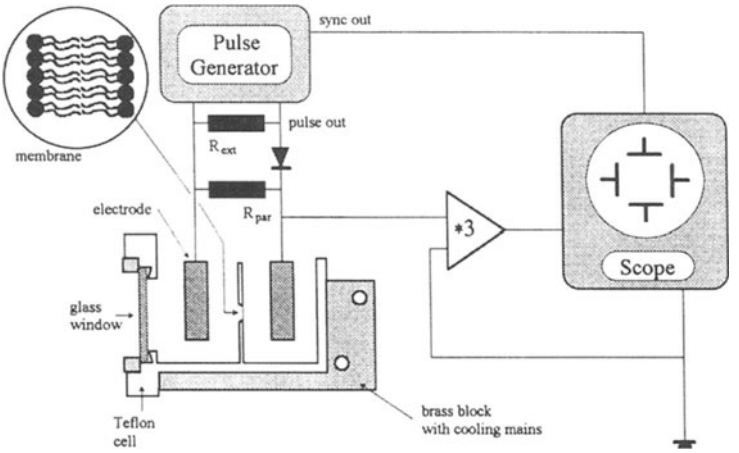

Fig. 29. Schematical arrangement of the chamber and electrical setup used for the study of black lipid membranes (BLM). Adapted from Ref. 89.

with the relaxation time $\tau_m = R_m C_m$ (Fig. 30B). The resistance R_m can be obtained from $\Delta\phi_{m,\infty} = I R_m$ and the capacitance C_m can then be calculated from the relaxation time τ_m. The specific capacitance C_m of BLMs ranges between 0.3 and 1 $\mu F\ cm^{-2}$.

BLMs can also be used to measure the various types of membrane potentials by means of suitable electrodes placed into the two compartments. A transmembrane potential difference $\Delta\phi_m$ may have a variety of sources, e.g. diffusion potentials, different surface potentials due to fixed charges of the BLM-forming lipids and/or adsorption of ions (see also sections 2 in chapters 1 and 2). The diffusion of ions and their concentrations in the two compartments influence these potentials [88].

BLMs have been used extensively to study ion transport mediated by carriers and channel forming molecules [90]. Examples for carriers are valinomycin, a K^+-specific carrier molecule. It is a cyclic depsipeptide having twelve amino acids with the sequence $(D\text{-Val-L-Lac-L-Val-D-Hyi})_3$. Valinomycin forms a complex with K^+ in which the six C=O groups of the amide bonds chelate the K^+ ion. The K^+ ion is now buried inside the molecule, its hydrophobic side chains pointing outwards. In this conformation the complex is highly lipid soluble and K^+ ions can be shuttled across the bilayer. Other ionophores are nigericin, monensin, both polyethers with carboxyl groups, and A23187, a carrier for Ca^{2+} ions [90].

An example for a pore forming molecule is the linear polypeptide gramicidin A with 15 residues. The formation of gramicidin channels specific for monovalent cations can be followed by the conductance of

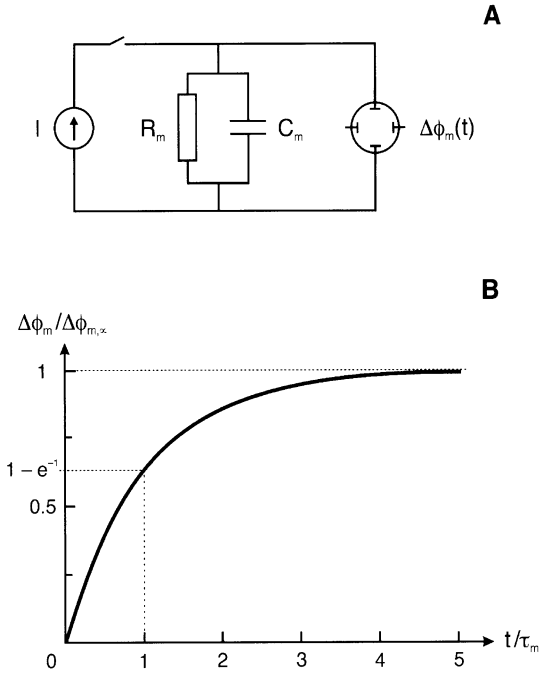

Fig. 30. Equivalent circuit for a BLM with resistance R_m and capacitance C_m (A) and time dependence of transmembrane potential difference $\Delta\phi_m$ after turning on the current I (B). In (A) the resistance of the electrolyte solutions is neglected because it is much smaller than R_m. The circles labeled with I and $\Delta\phi_m(t)$ represent a current source and an oscilloscope, respectively. For $\Delta\phi_m(t)$ in (B) see Eqn. 4.

BLMs into which gramicidin molecules have been incorporated. When a transmembrane potential difference $\Delta\phi_m$ is applied, the current shows characteristic step-wise fluctuations due to the formation and dissociation of gramicidin dimers, which form the open pore. The lifetimes of the dimers are between 10 ms and 1 s. The single-channel conductance of the gramicidin channel is about 30 pS per channel. The channel is about 25–30 Å long and has a diameter of about 4 Å. Water can also move through the channel at a high rate [91, 92].

The prime example for a voltage-dependent channel is the antibiotic alamethicin. At a low $\Delta\phi_m$ no current across the BLM will be observed. If $\Delta\phi_m$ exceeds a certain threshold, the conductance suddenly increases through the formation of open alamethicin channels. The single channel conductance is about 5000 pS at 1 M KCl. This shows that the pore formed by alamethicin must have a large diameter. It probably comprises 8 to 12 monomers forming a barrel type channel [93].

BLMs have been used to study a variety of proteins forming channels or pores in membranes and also membrane proteins which have

transport functions [88, 90, 94]. The technique has been refined to be able to study functions in intact membrane patches adsorbed to BLMs [95, 96].

The process of electroporation can also be studied by means of BLMs, and significant progress has been made in understanding this process ([89, 97]; see also chapter 5).

4.3. Liposomes and vesicles

Many phospholipids "swell" spontaneously when brought into contact with water. This process leads to multilamellar aggregates in which the stacked lipid bilayers are separated by water layers. After addition of excess water, these large aggregates can be broken up by mechanical agitation, i.e. vigorous shaking, rapid stirring with a high speed stirrer or ultrasonication. Depending on the time and intensity of agitation, liposomes and/or lipid vesicles form [8, 27, 28, 33, 98]. They are ideal model systems for studying the physical properties of pure lipid bilayers because the preparation method is easy and reproducible.

Figure 31 shows schematically the structure of multilamellar vesicles (MLVs), small unilamellar vesicles (SUVs), intermediate unilamellar vesicles (IUVs) and large unilamellar vesicles (LUVs) [167, 169]. SUVs have different physicochemical properties because the high curvature of the bilayers induces additional disorder and strain. This is greatly reduced in bilayers of IUVs and LUVs, which are therefore to be preferred for model membrane studies.

MLVs can be simply prepared by drying down a lipid solution in an organic solvent on the inner surface of a round bottom flask using a rotary evaporator [98, 99]. To the film a buffer solution or pure water is added and the flask is mechanically agitated by shaking or by rotation using the rotary evaporator. The temperature of the solution should be kept above the transition temperature of the respective lipid. MLVs can also be produced by adding buffer or water to the dry lipid and vortexing the solution vigorously at temperatures above T_m for several minutes. Further homogenization of the resulting very turbid dispersion can be achieved by mild sonication in a bath type sonicator. Multilamellar vesicles (MLVs) prepared by these methods usually have diameters between 200 and 2000 nm with a broad distribution of sizes.

The lower limit for the diameter of small unilamellar vesicles (SUVs) is ca. 15–20 nm. In SUVs the lipid membrane is highly curved. Packing problems arise when these vesicles are cooled below their transition temperature. T_m values are generally several degrees lower for SUVs than for MLVs and the width of the phase transition region is much larger. Due to the high curvature, and because the inner diam-

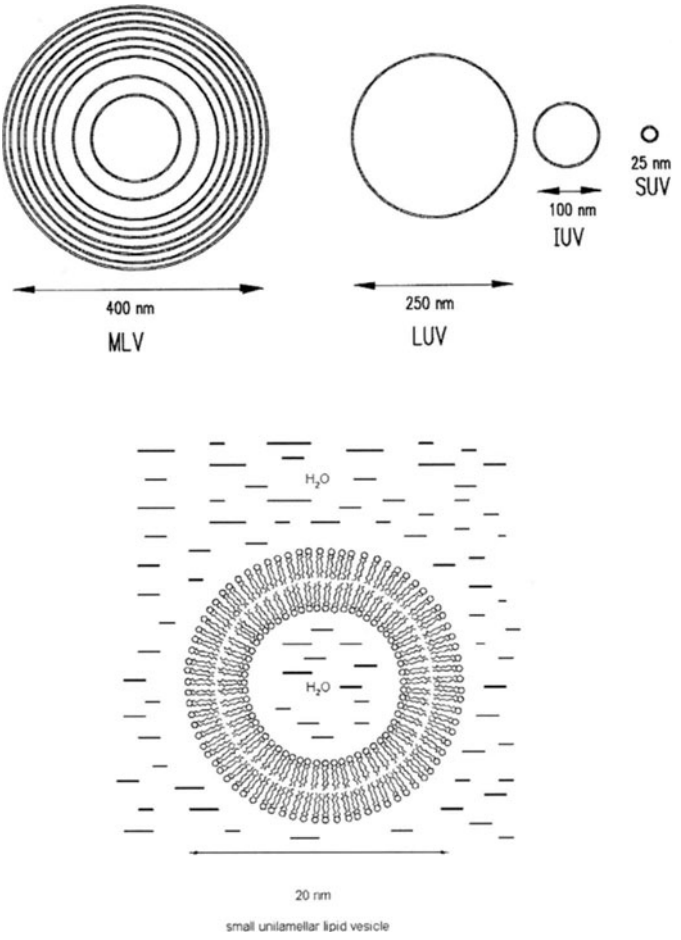

Fig. 31. Schematic comparison of vesicle sizes of multilamellar (MLV), large unilamellar (LUV), intermediate unilamellar (IUV), and small unilamellar (SUV) vesicles.

eter is only 5–10 nm, bilayer thickness being ca. 5 nm, approximately 2/3 of the lipid is in the outer and only 1/3 in the inner monolayer. SUVs are prepared by extensive sonication of MLV suspensions with a probe type sonicator [98, 99]. Larger vesicles can be removed by centrifugation, chromatography on Sepharose 2B or 4B, or by filtration through membranes with pore diameters > 30 nm.

Intermediate and large unilamellar vesicles (IUVs and LUVs) are to be preferred for model membrane studies. Numerous techniques have been developed for the preparation of unilamellar vesicles of different sizes with diameters between 100 and 200 nm and with reasonable homogeneities in vesicle diameters using extrusion tech-

niques [99, 100]. An extrusion procedure through polymer membranes with defined pore sizes is today the method of choice. Commercial setups of various sizes using this procedure are available. The lipid suspension is passed 5–10 times through these membranes, preferably at temperatures above the transition temperature of the lipid. MLVs will be broken down to mostly unilamellar vesicles with an average diameter of approximately the pore size of the membrane [101].

Unilamellar vesicles of intermediate size can also be prepared by injection of a solution of lipids in an organic solvent into water or aqueous buffer [98]. The size of the unilamellar vesicles produced by the ethanol injection method can be controlled in a certain range by the concentration of the lipid in the ethanol solution. The vesicle concentration is limited by the final ethanol content of the buffer which should not exceed 5 to 7%. Ethanol has to be removed afterwards by dialysis. A similar method uses diethyl ether as a solvent. Injection into the aqueous phase at 60 °C should be performed slowly so that the ether completely evaporates during the injection.

With reverse phase evaporation (REV) LUVs with high trapping efficiencies can be produced [98, 102]. The lipids are dissolved in diethyl ether or in isopropyl ether/chloroform mixtures. Buffer is injected into this organic solution up to a specific organic phase/water ratio to produce a stable "water-in-oil" emulsion by sonication. The organic solvent is then removed under reduced pressure until a stable "gel" has formed. This gel is than subjected to vortexing or mild sonication, and evaporation of the solvent is continued. When the LUV suspension has formed, residual solvent is removed by dialysis against buffer. LUVs with diameters of up to 500 nm can be produced by this procedure.

The detergent dialysis method produces vesicles with diameters between 100 and 250 nm [98, 103]. The lipids are solubilized in detergent solutions, for instance desoxycholate or octylglucoside, to form mixed micelles. The detergent is then removed by extensive dialysis over several days and vesicles are spontaneously formed.

Giant unilamellar vesicles are spontaneously formed by slow hydration with water or sugar solutions from the anhydrous state. Though the yield is low, enough of them are formed to be able to select and aspirate a vesicle with a micropipette. Figure 32 shows a giant unilamellar DMPC (dimyristoyl-phosphatidylcholine) vesicle of ca. 15 mm diameter aspirated to a micropipette at temperatures in the L_β, the P_β, and the L_α-phase [104]. With giant unilamellar vesicles, thermoelastic properties of lipid bilayers, i.e. values for the bending elastic modulus, the bilayer tension, the elastic area compressibility modulus, and the thermal area expansivity can be determined. Also, experiments on vesicle-vesicle adhesion using different types of lipid mixtures were performed [47, 104–106].

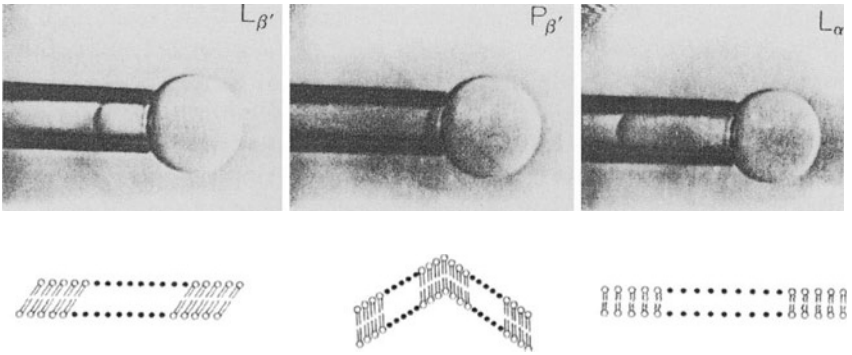

Fig. 32. Giant unilamellar vesicle of DMPC with a diameter of 15 μm in its three lamellar phase states aspirated to a micropipette tip. Adapted from Ref. 104.

5. Physical methods for the study of lipids in membranes

A wide range of methods applicable for studies of lipid-water systems exist. The methods can be differentiated according to the type of information which can be obtained with them.

Thermotropic and structural properties of lipids can be studied by differential scanning calorimetry (DSC), isothermal titration calorimetry (ITC), and scattering methods, such as X-ray and neutron scattering. The scattering methods give information on the phase structure and symmetry and on the packing properties of lipids, whereas the calorimetric methods yield information on the phase transition temperatures and enthalpies. Phase properties and morphologies can also be studied by electron microscopy where particularly the freeze fracture techniques can give information on non-periodic structures. Cryo-electron microscopy is well suited to visualize liposome shapes and sizes. Turbidity or light-scattering measurements as a function of temperature are fast methods to determine phase transition temperatures. Dynamic light scattering (DLS) is routinely used to measure liposome sizes.

Conformational and dynamical properties of lipid molecules are best studied by spectroscopic techniques. Vibrational spectroscopy (infrared and Raman) gives an instantaneous picture of the conformational properties of the lipid molecules and their interactions with the surrounding molecules. In electron spin resonance (ESR) spectroscopy spin-labeled membrane probes are used to measure dynamics and order in lyotropic phases. The line shapes of ESR spectra of these probes are sensitive to motions in the time regime between 10^{-10} to 10^{-8} s. Nuclear magnetic resonance (NMR) methods are very versatile because different nuclei can be studied. The time regime in which NMR spectra are sensitive to motions lies between 10^{-7} and

10^{-1} s. Fluorescence spectroscopy can be applied in a number of ways. When the time dependence of the fluorescence anisotropy of a probe is measured, information on the reorientational motion of the probe molecule can be obtained. Lateral diffusion of fluorescence probes can be measured by excimer techniques or by fluorescence recovery after photobleaching (FRAP). The kinetics of the transition between different phases is usually studied by relaxation techniques, such as temperature jump or pressure jump methods. As detection methods, light scattering, fluorescence changes of incorporated probes, and time-resolved X-ray scattering have been used.

5.1. Differential scanning calorimetry (DSC)

DSC is one of the most widely used techniques for studying lipid behavior. Its application has continuously increased due to the availability of commercial instruments of high sensitivity and good base line reproducibility [8, 35, 36, 60, 107–111]. Figure 17 shows transition curves of a variety of different phospholipids differing in their head group structure and in the length of the acyl chains. The transition peaks observed here are due to transitions between lamellar phases of different order (see above). For modern instruments, only 0.1–1.0 mg of lipid is needed to get good and reproducible DSC curves. For transitions with a half width of 20–30 degrees, as occurs in lipid mixtures and in natural membranes, the concentration has to be increased by a factor of 5–10.

As shown in Fig. 17, DSC can be used to determine transition temperatures T_m as well as transition enthalpies ΔH of lipids. The latter are calculated by integration of the calorimetric peaks and the transition entropies ΔS are then given by $\Delta H/T_m = \Delta S$ because $\Delta G = 0$ at $T = T_m$. Plots of ΔH versus chain length are essentially linear for the gel to liquid-crystalline phase transition of phospholipids with saturated chains. ΔH increases by about 1.9 to 2.1 kJ mol^{-1} per additional CH_2 group. Similar linear plots are obtained for the transition entropy ΔS.

The sharpness of the DSC peaks are determined by three parameters: a) the response time of the DSC instrument (a slow response time leads to instrumental broadening); b) the purity of the lipid (impurities lead to a depression of the "melting point" and a concomitant transition broadening); c) the nature of the phase transition, whether it is truly or only weakly first order. A first order transition would give an indefinitely sharp melting point with the cooperativity going to infinity. For weakly first order transitions the size of the cooperative unit n can be calculated from the ratio $\Delta H_{v.H}/\Delta H_{cal}$ with ΔH_{cal} being the calorimetrically determined transition enthalpy and $\Delta H_{v.H}$ the van't Hoff transition enthalpy calculated from the relation

$$\Delta H_{v.H} = 4\,RT_m^2\,(d\Theta/dT)_{Tm} = 4\,RT_m^2\,C_{max}/\Delta H_{cal} \quad (5)$$

Here Θ is the degree of transition which ranges between 0 and 1, $(d\Theta/dT)_{Tm}$ is the slope of the transition curve obtained by integration and normalization of the DSC peak at $T = T_m$, and C_{max} is the value of the heat capacity maximum at $T = T_m$. Equation 5 only holds for a truly symmetrical two-state transition [112].

With high sensitivity instruments it is possible to determine the apparent molar heat capacities of lipids in dispersion. These are calculated from the shift of the base line when recording the DSC curve of a lipid dispersion in relation to a water/water base line and the known specific volumes of the lipid. Apparent molar heat capacities of several phospholipids were determined using this procedure [108, 113]. They contain important information on the hydration of apolar moieties of the lipids.

DSC has been widely used to study phase diagrams and miscibility properties in binary and ternary lipid mixtures, lipid-protein interactions, and effects of addition of lipid soluble solutes, such as drugs, to the aqueous phase [21, 29, 33, 60, 114, 115].

From the analysis of phase diagrams of pseudo-binary phospholipid mixtures, one can obtain information on the miscibility properties in the different lamellar phases [36, 110, 115–120]. Figure 33 shows DSC curves of pseudo-binary mixtures of DMPC with DPPG (dipalmitoylphosphatidylglycerol) at two different pH-values. The phase diagrams in Fig. 34 were obtained by simulations of the DSC peaks on the basis of regular solution theory with an additional cooperativity parameter to account for the reduced cooperativity of the transition in mixed systems [116]. The non-ideality parameters obtained from this analysis indicate that it is possible to induce domain formation in the liquid-crystalline L_α-phase by partly protonating the phosphatidylglycerol component in the mixture. Several other examples for this possibility have been found in pseudo-binary mixtures of zwitterionic lipids mixed with at pH 7 anionic lipids [117, 120].

Because the phase behavior of anionic lipids depends on the ionic composition and ionic strength of the aqueous phase, numerous studies of the effects of ion binding on the thermotropic properties have been performed [39, 42, 121–123]. Figure 35 shows as an example the changes in thermotropic properties of DMPG when divalent cations such as Ca^{2+} or Mg^{2+} are added with increasing concentration [36, 124]. Particularly Ca^{2+} binds very strongly to the phosphate groups of phospholipids, dehydrates the interface and induces lamellar phases with high order.

DSC measurements have been routinely used to study lipid-protein interactions [125]. From the changes of the DSC peaks as a function of protein content one can obtain information on the site of incorpo-

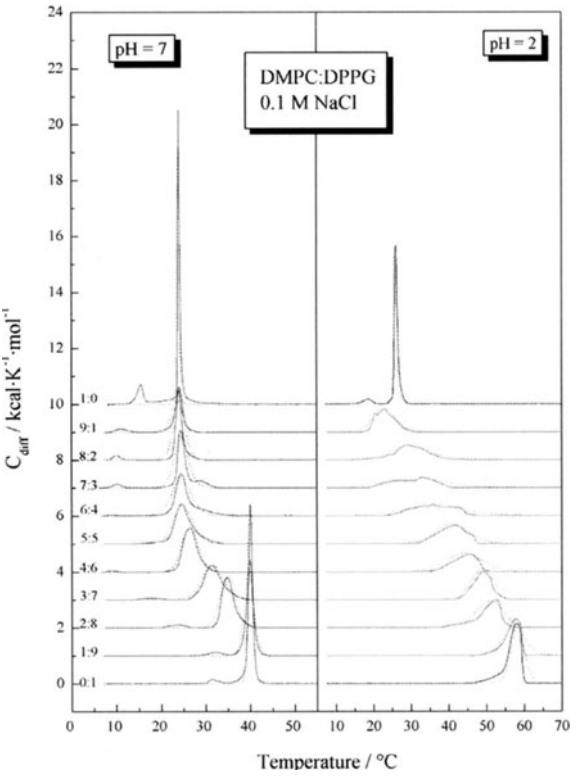

Fig. 33. DSC heat capacity curves obtained for DMPC/DPPG mixtures at two different pH-values and various molar ratios. The dotted lines represent heat capacity curves simulated as described in Refs. 116 and 118.

ration of the protein. Proteins or peptides incorporated into the lipid bilayers have different effects on the DSC peaks compared to those interacting only with the membrane surface by electrostatic interactions. An example for this type of application is shown in Fig. 36. Here a water soluble protein, the sphingolipid activator protein for the ganglioside GM1, was added to unilamellar vesicles of different lipids [36, 126]. The activator protein specifically interacts with the sugar headgroup of GM1 but also shows some non-specific electrostatic binding to anionic lipids. The binding causes the appearance of a shoulder on the high temperature side of the DSC peaks. Proteins incorporated into lipid bilayers usually lead to a broadening of the transition and a shift to lower temperature.

This list of possible applications is far from being complete. In summary, DSC is a fast and convenient method for obtaining data on the

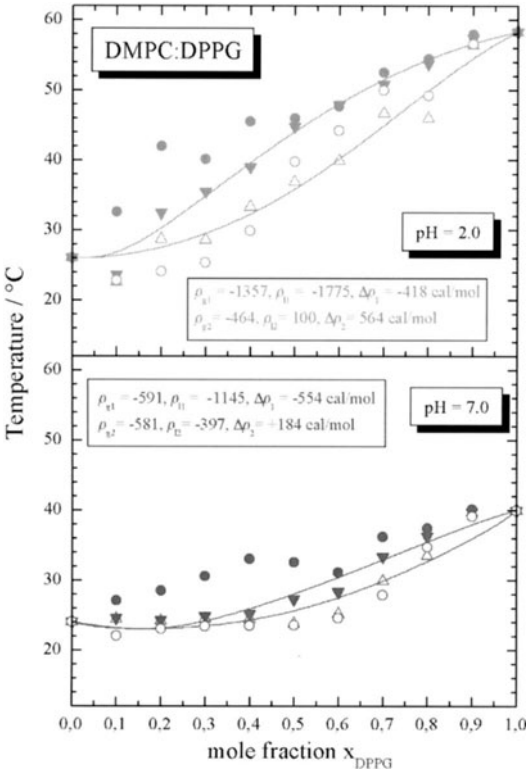

Fig. 34. Pseudobinary phase diagrams for the system DMPC/DPPG at pH 2 and pH 7 constructed from the simulated heat capacity curves. Triangles are T(–) and T(+) values obtained from the simulation of the cp-curves [116], circles are $T^{exp}(-)$ and $T^{exp}(+)$ values obtained by the usual empirical procedure. The solid lines are the coexistence lines calculated using the four-parameter model described in Refs. 116 and 118 with the nonideality parameters ρ_{l1} and ρ_{l2} for the liquid crystalline phase and ρ_{g1} and ρ_{g2} for the gel phase, respectively. The differences $\Delta\rho_1 = \rho_{l1} - \rho_{g1}$ and $\Delta\rho_2 = \rho_{l2} - \rho_{g2}$ are also shown.

thermotropic properties of lipid-water systems which can serve as a basis for further more detailed investigations.

5.2. Isothermal titration calorimetry (ITC)

Isothermal titration calorimetry (ITC) has emerged as a very powerful method for studying the interaction or binding of molecules [35, 36, 110, 127]. For membrane and lipid studies, ITC is suitable to measure the enthalpic effects arising from the binding of ions or other molecules to lipids, from the partitioning of hydrophobic molecules into

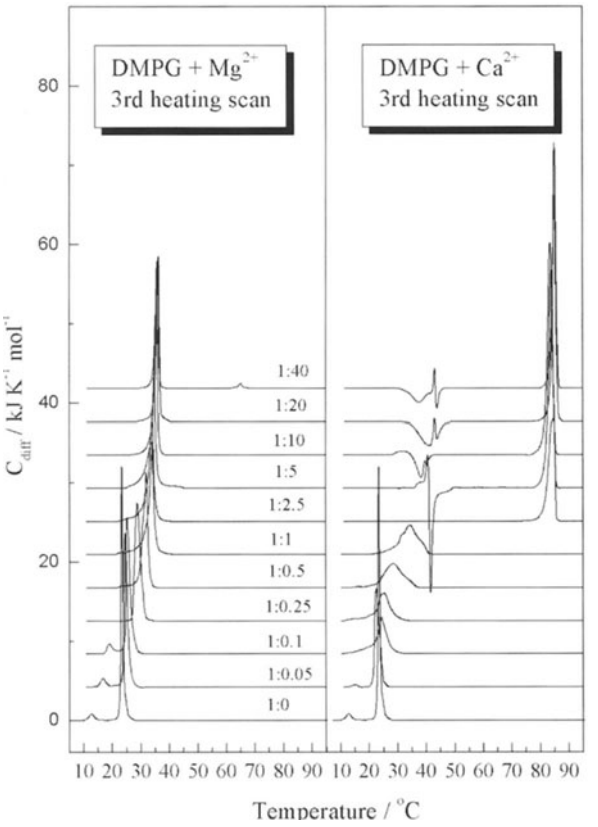

Fig. 35. DSC-curves for DMPG at pH 7 with increasing molar ratios of Mg^{2+} (left panel) and Ca^{2+} (right panel). For the DMPG:Mg^{2+}-complex, a phase transition at ca. 40 °C develops, whereas the Ca^{2+}-complex has a much higher transition temperature of 80–85 °C. In addition exothermic peaks can be seen which indicate the formation of metastable phases upon cooling [124].

bilayers, and from the incorporation of peptides and proteins into membranes [36, 109, 110, 123, 127]. Figure 37 shows as an example the heat effects observed when the negatively charged lipid DMPA is titrated with NaOH. With increasing pH, the second proton of the phosphate head group is dissociated. After subtraction of the heats of dilution of NaOH and the heat of neutralization, the molar enthalpy of dissociation is obtained. Besides obtaining a titration curve by adding NaOH, it is also possible to measure the total heat by titration of a DMPA vesicle solution into 0.01 M NaOH. The combination of ITC with DSC data leads to a complete enthalpy-temperature diagram for the two dissociation states of DMPA (see Fig. 38) [123].

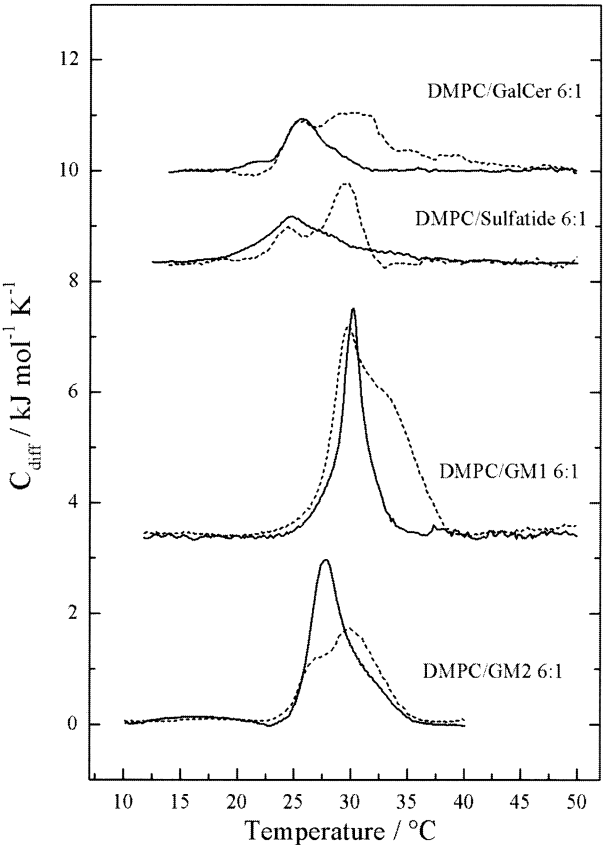

Fig. 36. DSC-curves of DMPC/ganglioside mixtures with molar ratios as indicated in 150 mM phosphate buffer at pH 6.8 with (- - -) and without (—) GM2-activator protein in a molar ratio of 10:1 (ganglioside:protein) [126].

In a similar way, the binding of other cations to negatively charged lipids can be studied, though in many cases the titration with a solution of, for instance, divalent cations such as Mg^{2+} or Ca^{2+}, is not possible because of the drastic change of the phase properties induced by the binding of these ions. In this type of titration experiment it is usually not possible to reach equilibrium states. The reversed experiment is in most cases still feasible. Figure 39 shows the total heat of binding for Mg^{2+} and Ca^{2+} to DMPG (dimyristoylphosphatidylglycerol) bilayers as a function of temperature [36, 124]. The slope of the enthalpy-temperature diagram yields the change in heat capacity ΔC_p, a parameter which contains information on the change in hydration of the lipid-water interface. Binding of divalent cations usually leads to a dehydration of the polar groups but also to a reduction of contacts of water molecules with hydrophobic moieties. The latter is connected

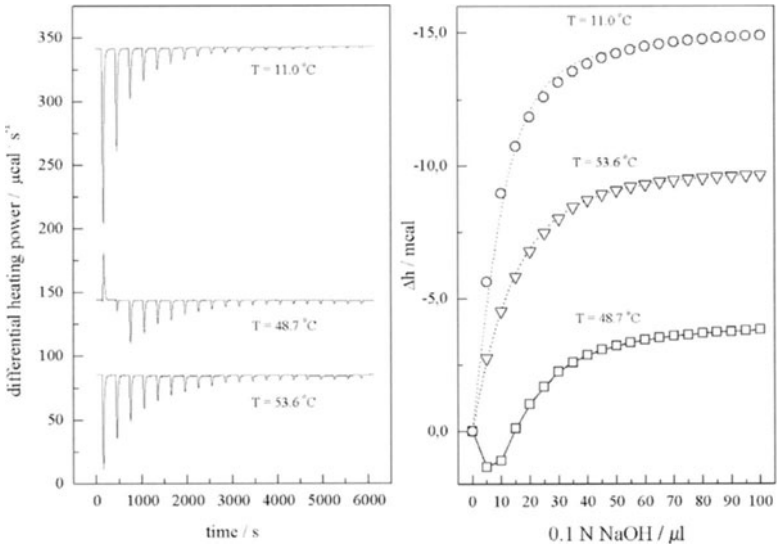

Fig. 37. Heat effects observed when titrating a 1 mM DMPA (pH 7) vesicle suspension with 0.1 M NaOH by stepwise addition of aliquots of 5 µl of NaOH solution. At 11 °C and 53.6 °C the heat effects arise from the heat of neutralization, the heat of dilution of NaOH, and the heat of dissociation for the second proton in the L_β- and L_α-phase of DMPA. At 48.7 °C additional heat effects arising from the pH-induced transition into the La-phase are superimposed for the first few additions of NaOH. Left: calorimetric titration peaks; right: integrated heat effects. Adapted from Ref. 123.

with a decrease in heat capacity, while the former usually leads to an increase in C_p. The negative slope of the enthalpy-temperature diagrams at low temperature shows that the reduction of "wetting" of hydrophobic groups after ion binding overcompensates the reduction in hydration of the polar group.

A most useful application of ITC has been found for studying micellar systems and for the interaction of surfactants with lipid vesicles. The demicellization of surfactants can be easily studied by just diluting a micellar solution of a surfactant into water. A sudden decrease in the observed heat effects indicates that the critical micellar concentration (*cmc*) is reached. These studies can be performed over a wide range of temperature. The *cmc* is determined from the first derivative of the titration curves [128–130]. These contain also information on the distribution function for the aggregation numbers of monomers within the micelles. The temperature dependence of the enthalpy of micellization again yields information on the "wetting" of hydrophobic groups in the micelles. An example for this type of experiment is shown in Fig. 40 for the surfactant nonyl glucoside (NG) [130]. The steepness of the titration curves contain information on the

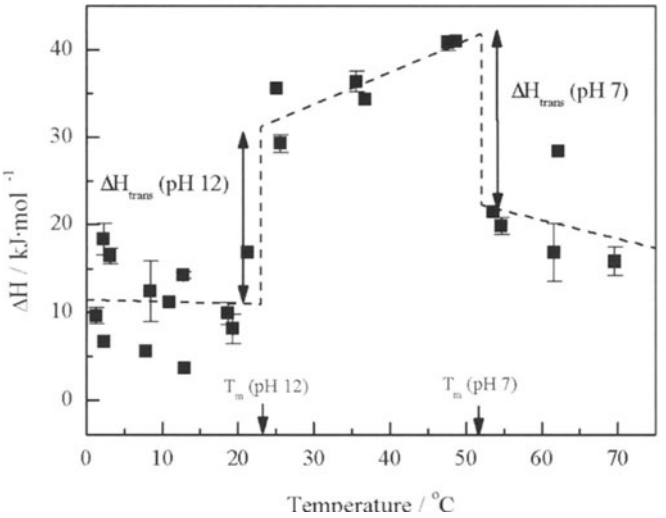

Fig. 38. Complete enthalpy *versus* temperature diagram of $DMPA^-$ and $DMPA^{2-}$ as obtained by DSC and ITC measurements. Vertical bars are the transition enthalpies for the two forms determined by DSC, arrows represent the heat effects observed by ITC for complete titration to $DMPA^{2-}$. Adapted from Ref. 123.

aggregation number n of the detergent in the micelle in the vicinity of the *cmc*. For the determination of n the titration curves have to be simulated using a mass action model for the aggregation. The simulations then yield the equilibrium constant for aggregation, the aggregation number and the enthalpy of aggregation. For NG at different temperatures, the aggregation number was determined to approximately 60 and the ΔH and ΔG-values for the demicellization as a function of temperature are shown in Fig. 40 [130]. It is clearly evident, that the enthalpy of micellization is strongly temperature dependent, whereas the change in Gibbs energy ΔG is almost constant over the same temperature range. This means that the terms ΔH and TΔS run almost parallel. This "enthalpy-entropy compensation" is consistently found when hydrophobic effects are involved.

The interaction of surfactants with lipid bilayers has recently been increasingly studied by ITC [131–134]. When excess surfactant is added to lipid vesicles the vesicles become "solubilized", meaning that mixed micelles of surfactant and lipid are formed. This process can be easily studied by ITC. At low surfactant concentration, the surfactant molecules are first incorporated into the lipid bilayers. The partition coefficient of surfactants can be studied by either titrating monomeric surfactant solutions to lipid vesicles or *vice versa*. When high surfactant concentrations are added the transition of vesicles into micelles is observed. The schematic "phase diagram" observed in sys-

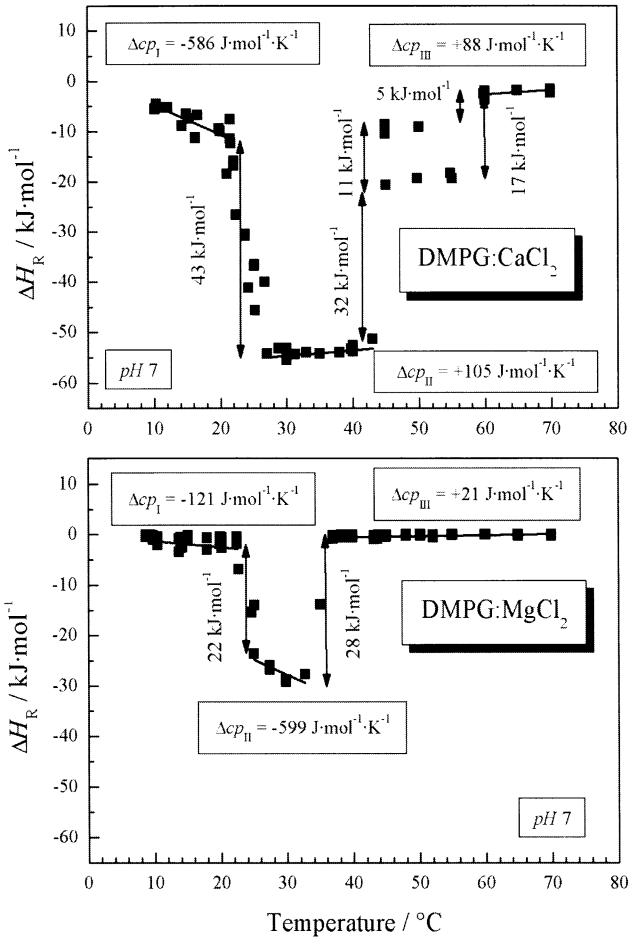

Fig. 39. Enthalpy *versus* temperature diagram for the binding of Ca^{2+} (top) and Mg^{2+} (bottom) to DMPG at pH 7. The titration calorimetric experiments were performed by injecting a DMPG vesicle suspension into a salt solution containing excess divalent cations. The slopes of the curves correspond to changes in heat capacity caused by the binding and the change of the phase structure. The sudden jumps are caused by ion-induced isothermal transition from the liquid-crystalline to the gel phase [124].

tems with high water content is shown in Fig. 41 [132]. The partitioning experiment according to arrow (3) in this diagram yields heat effects as shown in Fig. 42 from which the partition coefficient can be calculated using appropriate models [131, 132, 134].

When a micellar solution of surfactant is added to a vesicle suspension of low concentration the solubilization process is evident from a sudden deviation of the heat effects from a continuous curve. Figure 43 shows for comparison the titration of a micellar solution of octylglucoside into water and into a DMPC vesicle solution. The devi-

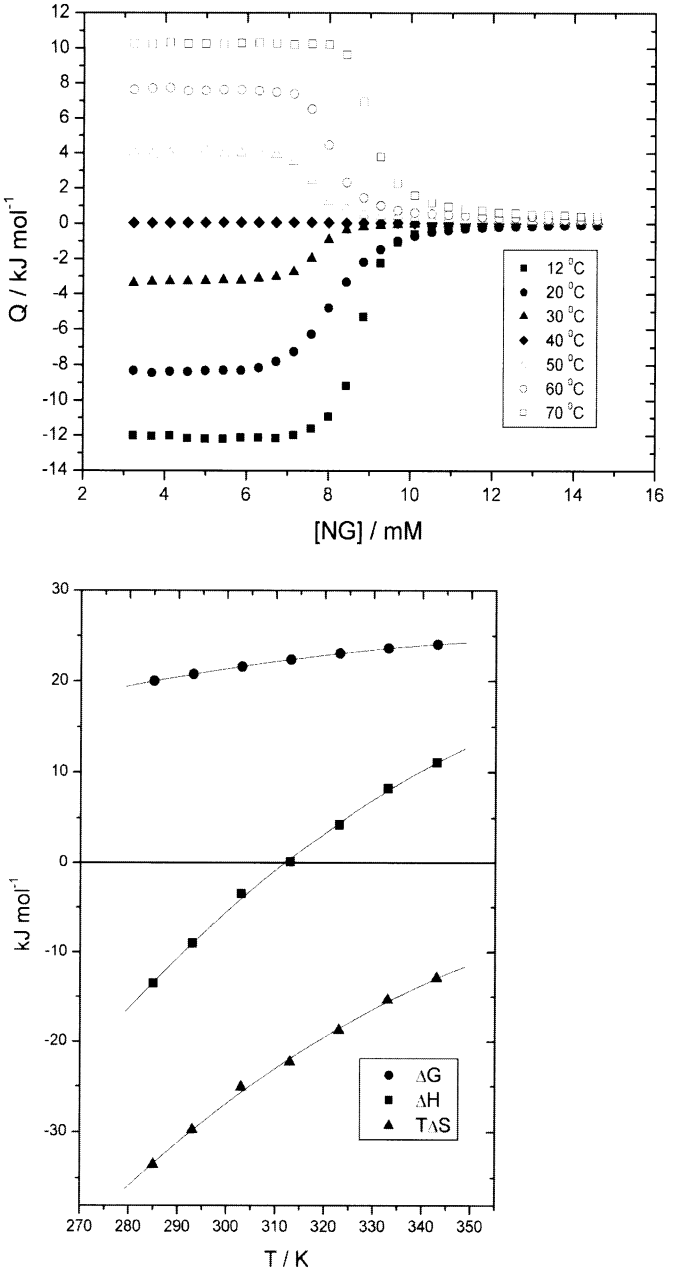

Fig. 40. Top: Heat evolved during the injection of 122 mM nonyl glucosid solution (NG) into water at different temperatures. The initial heat effects are caused by the demicellization of the surfactant. The heat effects at the end of the experiments are caused by dilution of micelles. Bottom: Enthalpy of demicellization ΔH, Gibbs energy of demicellization ΔG, and entropic term T ΔS for NG demicellization as a function of temperature. ΔH is strongly temperature dependent, while ΔG is only slightly increasing with temperature because the temperature dependence of ΔH and T ΔS is more or less the same. This "enthalpy-entropy-compensation" is always found when hydrophobic effects are involved [130].

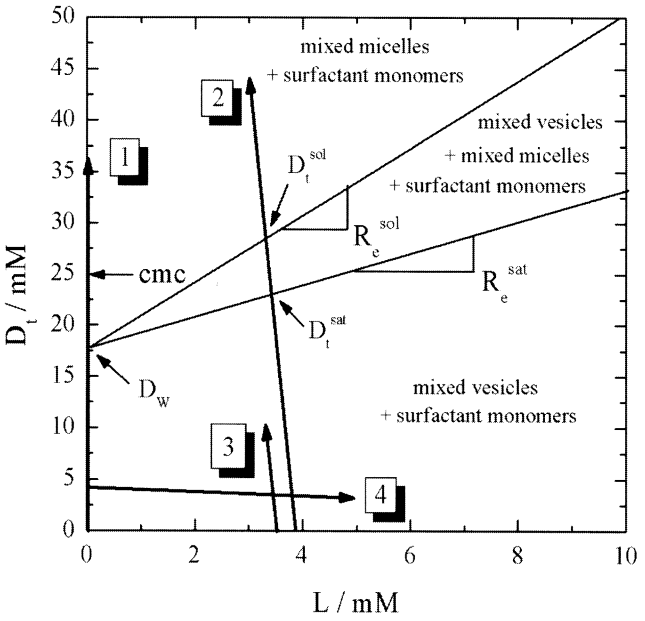

Fig. 41. Schematic phase diagram for a phospholipid/surfactant/water mixture in excess water. The arrows designate the different calorimetric titration experiments that can be performed. Arrow 1 corresponds to the demicellization of OG, arrows 2 and 3 are experiments where surfactant is added to lipid vesicles. In experiment 3, the vesicles are "solubilized" into micelles. Arrow 4 corresponds to the addition of lipid vesicles to monomeric surfactant to determine partition coefficients. Adapted from Ref. 132.

ations are observed when the phase boundaries are crossed, as shown in Fig. 41, arrow (4). The resulting "phase diagrams" obtained for lipids with different head groups are shown in Fig. 44. A clear dependence on the type of lipid head group is observed. Phospholipids with strong intermolecular interactions between head groups, such as phosphatidylethanolamines or phosphatidic acids, are difficult to transform into micelles [Keller and Blume, unpublished observations]. This is much easier for phosphatidylglycerols and phosphatidylcholines. Remarkable is the fact that in almost all cases the surfactant concentration needed for "solubilization" of phospholipids is below the *cmc* of the pure surfactant [36, 110, 132, 134].

5.3. X-ray and neutron scattering

X-ray scattering techniques are widely employed to study the phase structure of lipid-water systems. Time resolved experiments have become feasible in the last years due to the availability of synchro-

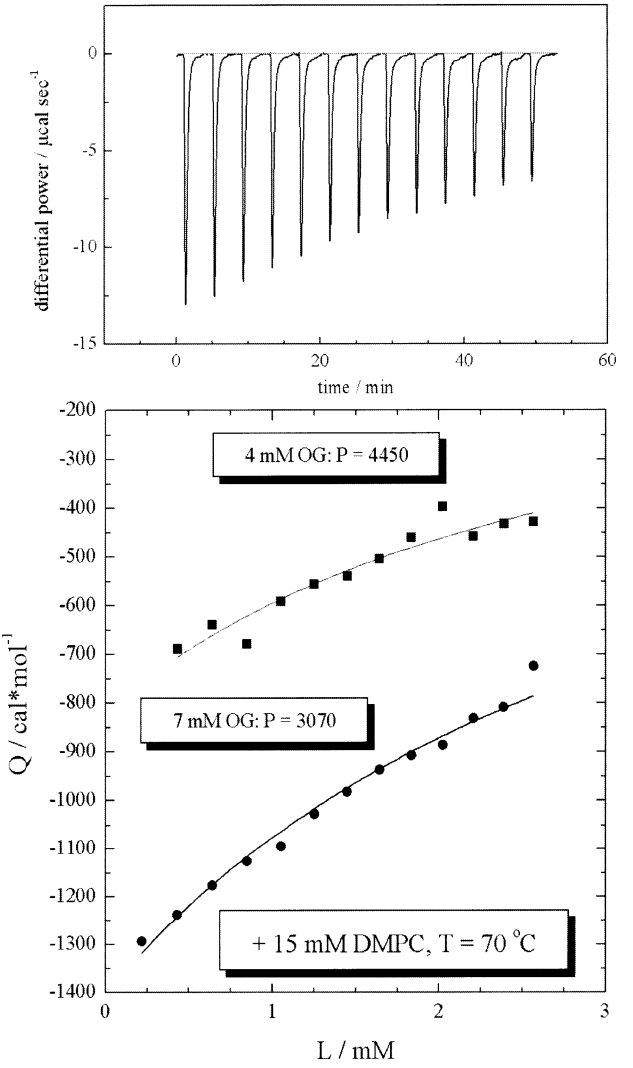

Fig. 42. Calorimetric peaks (top) and heat effects (bottom) observed when titrating 15 mM DMPC vesicles into monomeric octylglucoside (OG) solutions of different concentration as indicated. The partition coefficients P, determined as described in Refs. 132 and 134, are indicated.

trons as intense X-ray sources [49, 135–138]. Because lipids are difficult to crystallize, X-ray diffraction studies on single crystals are scarce. Compared to the large number of proteins which have been successfully crystallized and the structure being determined, the number of crystal structures of lipids is very small. The first pioneering work was the elucidation of the crystal structure of dilauroylphosphatidylethanolamine (DLPE) in 1974 by Hitchcock et al. [139]. A

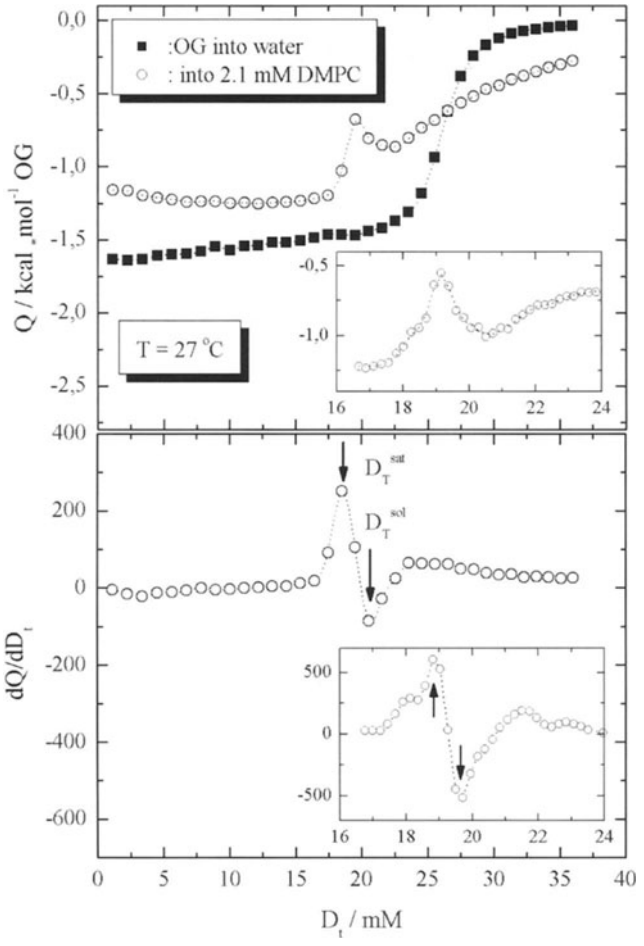

Fig. 43. Top: Enthalpograms for the demicellization of OG in comparison to the solubilization of DMPC vesicles by OG at 27 °C. Bottom: first derivative of the solubilization enthalpogram for the determination of the points on the phase boundaries D_T^{sat} and D_T^{sol}. The insets show the solubilization region in the vicinity of D_T^{sat} and D_T^{sol} obtained with a larger number of data points. Adapted from Ref. 132.

similar conformation of the lipid chains was found later in phosphatidylcholine (DMPC) crystals [140], whereas in phosphatidic acids and for one of the phosphatidylglycerol molecules in the unit cell, the orientation of the glycerol back bone is almost parallel to the bilayer surface [141, 142]. Figure 45 shows the conformations of some lipids in the crystalline state.

For the structure elucidation of lipid-water mesophases, small- (SAXS) and wide-angle X-ray scattering (WAXS) methods are used. Lamellar mesophases may be quasi-crystalline in two dimen-

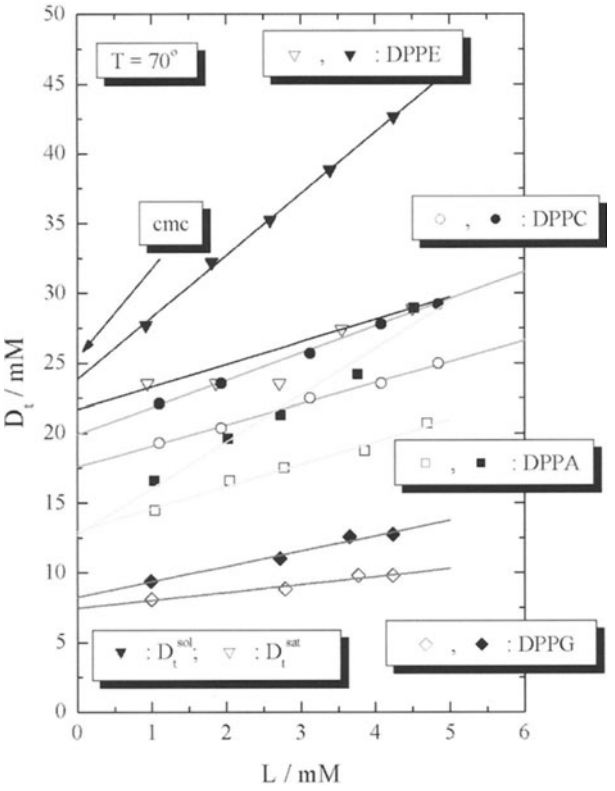

Fig. 44. Phase boundaries D_t^{sat} and D_t^{sol} determined by ITC for four different phospholipids. Particularly the negatively charged phospholipid dipalmitoylphosphatidylglycerol (DPPG) is easily transformed into micelles (Keller and Blume, unpublished observations).

sions, but ordering in the third dimension perpendicular to the layer surface is usually far from being perfect. The low-angle region contains information on the long-range order of the lipid mesophase. Depending on whether the lipids are in lamellar, H_{II} or cubic phases, Bragg reflections with characteristic reciprocal spacings $s_{hkl} = 1/d_{hkl}$ are observed, where d_{hkl} is the spacing of the lattice planes with the Miller indices h, k, and l. In lamellar phases long-range order is restricted to one dimension perpendicular to the bilayer plane, in H_{II}-phases order extends in two, and in cubic phases in three dimensions [49, 52].

In lamellar systems of low water content, the electron density profile across the bilayer can be determined from the lamellar reflections if the phases of the peaks are correctly assigned [136]. This problem can be solved by trial and error, by swelling methods, and by isomorphous replacement and heavy atom methods.

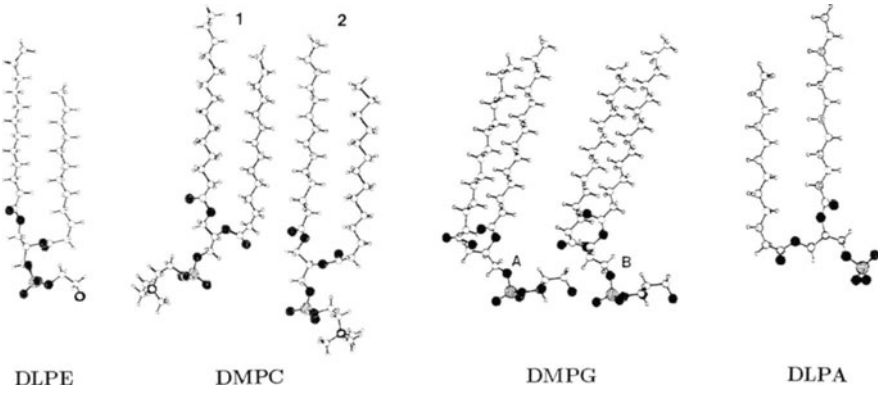

Fig. 45. Structures of some phospholipids as determined by X-ray crystallography on lipid crystals [139–142].

The proof for the existence of a specific lipid mesophase can only by found using X-ray scattering, though other methods may give a hint about the most likely structure. In particular, spectroscopic methods show whether motional averaging can occur only in two dimensions as in a bilayer membrane, or in addition around a H_{II}-phase cylinder, or in three dimensions as in cubic phases. A special packing arrangement of the lipid molecules, such as found in the interdigitated phases, can only be proved by X-ray scattering and by the determination of the electron density profile. The details of this procedure can be found in numerous original papers and reviews [137, 143–146]. An example for the X-ray scattering curves, the electron density profile, and the schematic packing of the lipids is shown in Fig. 46 for the case of DPPC and DHPC (dihexadecylphosphatidylcholine).

While the scattering intensities in the low angle region and their spacing contain information on the large repeat distances and therefore on the type of mesophase (lamellar, hexagonal, cubic) the wide angle reflections give information on the packing of the chains in the sub-cells and possible tilting of the chains. The analysis of the wide angle reflections has made some progress in recent years due to a combination of simulation procedures for different chain packing modes together with calculations of the resulting energy landscapes [147–149].

Neutron scattering is a very similar method with respect to the underlying principles [150, 151]. Whereas X-rays are scattered by the electrons in the molecule, the neutrons are scattered by the nuclei. The typical X-ray wave length is 1.54 Å for the Cu K_α-line. The wave length is therefore in the size range of atoms and the interatomic separations. The scattering intensity depends therefore on the scattering

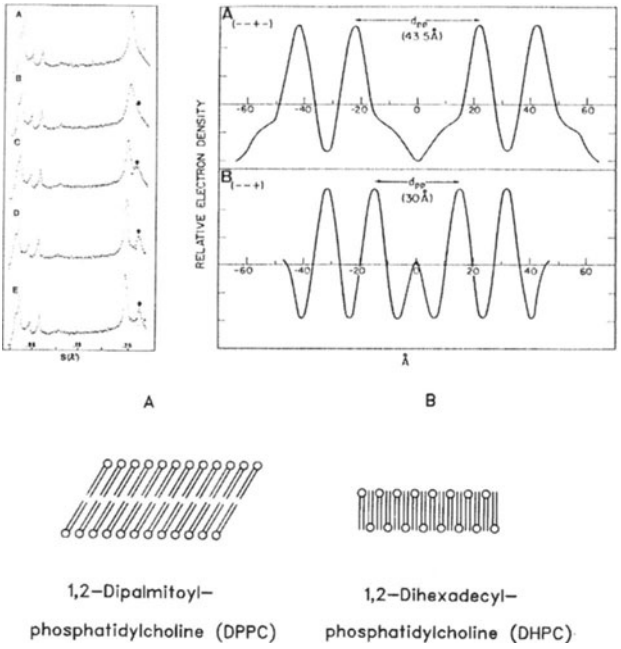

Fig. 46. Top left: X-ray diffraction patterns for dihexadecyl-phosphatidylcholine (DHPC) in the interdigitated phase at different temperatures: 20 °C (A), 10 °C (B), 5 °C (C), 0 °C (D), and –2 °C (E). Top right: Electron density profile for DPPC in the $L_{\beta'}$-phase (A) and DHPC in the interdigitated phase (B) [145]. Bottom: Schematic arrangement of the molecules in the $L_{\beta'}$-and the interdigitated phase.

angle. The de Broglie wave length of neutrons at 600 K is ca. 1 Å and is thus comparable to the wave length of X-rays. However, because the nuclei have only dimensions of ca. 10^{-5} Å , they behave as point scatterers and the neutrons are scattered isotropically.

The main advantage of neutron scattering is that differences in scattering lengths between isotopes of the same element exist, and that light elements, such as hydrogen, have a similar scattering power as carbon or oxygen. Particularly useful is the difference in scattering length between hydrogen and deuterium, which is -3.74×10^{-13} cm for H and $+6.67 \times 10^{-13}$ cm for D. This difference in sign of the scattering length can be used to vary the contrast between the aqueous phase and the solute, i.e. the lipid phase, by changing the H_2O/D_2O ratio of the aqueous solution. In addition, it offers the possibility to investigate membranes of specifically deuterated lipids [152, 153]. At the position of the labeled carbon atom higher scattering intensities will occur. Thus the position of the CD_2 groups relative to the bilayer surface can be located [153].

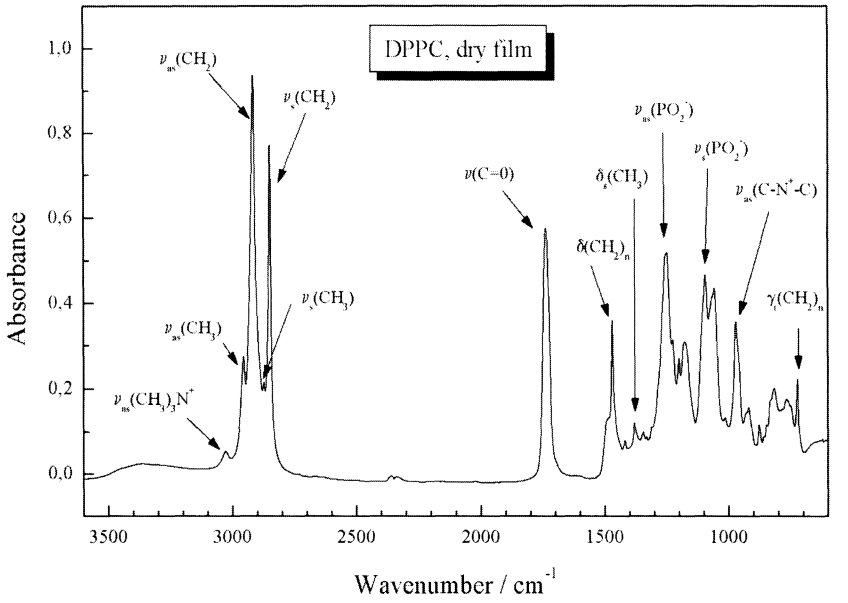

Fig. 47. FT-IR spectrum of a dry DPPC lipid film on a ZnSe ATR crystal. Some of the characteristic absorption bands used for the IR-analysis of lipids are indicated (see Table 4).

5.4. Infrared (IR) and Raman spectroscopy

5.4.1. IR spectroscopy: Infrared and Raman spectroscopy have been used for a long time for the characterization of lipid phase behavior [154, 155]. Because of the development of Fourier-Transform (FT) techniques in IR spectroscopy and the ease of data acquisition, this method of vibrational spectroscopy is presently favored over Raman spectroscopy [156]. With modern FT-IR spectrometers systematic investigations of lipid/water systems have become feasible due to the greatly reduced recording times. Increased sensitivity of the detectors, the use of reflection techniques, such as attenuated total reflection (ATR) [157–159] and infrared-reflection-absorption-spectroscopy (IRRAS) [160, 161], the improvement in data analysis [162] and band shape simulation techniques [163, 164] have contributed to the power of vibrational spectroscopy.

Lipids are compounds with long aliphatic chains and show characteristic IR spectra in the mid infrared range between 600 and 4000 cm^{-1} dominated by the vibrations of the CH_2 groups. Figure 47 shows a spectrum of a dry lipid film. Indicated are some of the characteristic vibrational bands used for the analysis of lipid phase behavior and conformational properties of lipids. The bands belonging to the various vibrational modes of the CH_3- and CH_2-groups are sensitive to the conformational state of the chains. In phospholipids, the ester car-

Table 4. Important infrared group frequencies of phospholipids

Wavenumber (cm^{-1})	Assignment[a]	Symbol
3400	HOH-stretch	ν(OH)
3028	choline-CH_3-as-stretch	$\nu_{as}(CH_3)_3N^+$
2956	CH_3-as-stretch	$\nu_{as}(CH_3)$
2918	CH_2-as-stretch	$\nu_{as}(CH_2)$
2875	CH_3-sym-stretch	$\nu_s(CH_3)$
2849	CH_2-sym-stretch	$\nu_s(CH_2)$
2212	CD_3-as-stretch	$\nu_{as}(CD_3)$
2178	CD_2-as-stretch	$\nu_{as}(CH_2)$
2155	CD_3-sym-stretch	$\nu_s(CD_3)$
2094	CD_2-sym-stretch	$\nu_s(CH_2)$
1740	ester-carbonyl-stretch	ν(C=O)
1470	CH_2-bending (scissoring)	$\delta(CH_2)_n$
1380	CH_3-sym-bending	$\delta_s(CH_3)$
1342–1180	CH_2-wagging (progression)	$\gamma_w(CH_2)_n$
1250–1220	phosphate-diester-as-stretch	$\nu_{as}(PO_2^-)$
1170	ester(C-O)-as-stretch	ν_{as}(CO-O-C)
1086–1072	phosphate-diester-sym-stretch	$\nu_s(PO_2^-)$
1085	ester(C-O)-sym-stretch	ν_s(CO-O-C)
1070	phosphate-ester-stretch	ν(C-O-PO_2^-)
970	choline-as-stretch	ν_{as}(C-N^+C)
930	choline-sym-stretch	ν_s(C-N^+C)
725	CH_2-rocking	$\gamma_r(CH_2)_n$
640	CD_2-rocking	$\gamma_r(CD_2)_n$

[a]as, antisymmetric; sym, symmetric

bonyl stretching vibration, and the symmetric and anti-symmetric PO_2^--vibrations are particularly sensitive to the interactions of the lipid head groups with water and ions. For lipids with specifically deuterated or perdeuterated chains the symmetric and antisymmetric CD_2 stretching vibrations appear in a frequency range normally void of other interfering bands. In addition to the vibrational bands indicated in Fig. 47, a number of other characteristic bands appear as summarized in Table 4.

The investigation of lipid/water systems is complicated by the fact that water itself has very intense infrared absorption bands. The region above 3100 cm^{-1} is obscured by the symmetric and antisymmetric stretching bands of H_2O. Another intense band is due to the H_2O bending mode located at 1645 cm^{-1}. For observations in this frequency region it is advisable to change the solvent to D_2O, because the D_2O-bending vibration is shifted to 1215 cm^{-1} due to the vibrational isotope effect. Deuterated lipids have to be investigated in H_2O because the D_2O stretching modes obscure the CD_2-vibrations.

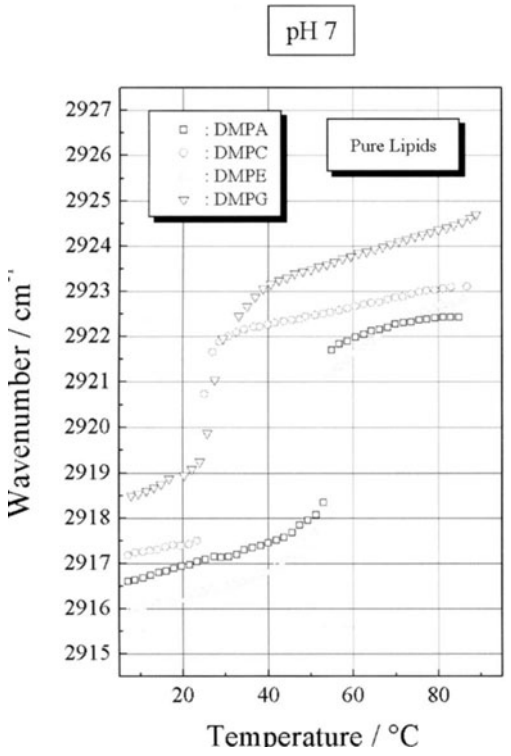

Fig. 48. Temperature dependence of the antisymmetric CH_2-vibrational band for four different phospholipids (Garidel and Blume, unpublished observations).

Depending on which spectral window has to be observed, either H_2O or D_2O has to be used as a solvent.

At the main phase transition of lipids from the gel to the liquid-crystalline phase an abrupt increase in frequency of the CH_2-stretching bands is observed. The concomitant changes in intensity and the increase in half width of both methylene stretching bands is caused by an increase in gauche conformers in the liquid-crystalline phase. Plots of the frequency of the symmetric or antisymmetric CH_2 stretching vibration as a function of temperature are a convenient way to determine the phase transition temperature. Figure 48 shows as a typical example the frequency *versus* temperature plots of the antisymmetric CH_2-vibration for several phospholipids with different head groups [165]. For specifically deuterated lipids, the frequencies of the CD_2-groups, and the frequency shifts observed at the phase transition, depend on the position of the CD_2-group in the fatty acyl chain [166].

When lipid mixtures are being investigated, a lipid with perdeuterated chains can be used as one of the components, because then both

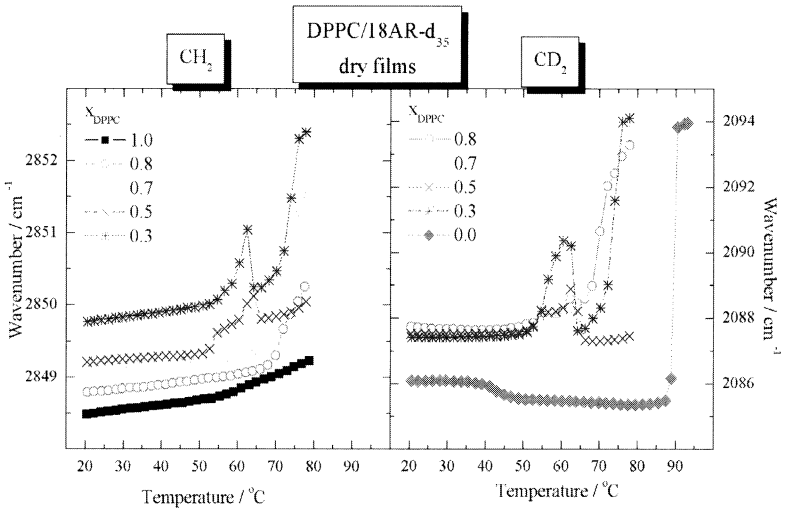

Fig. 49. Frequencies of the antisymmetric CH_2 vibration of DPPC and the antisymmetric CD_2 vibration of 5-n-octadecyl-resorcinol (18AR) with a perdeuterated chain in dry films of DPPC/18AR-d_{35} mixtures (Hoffmann and Blume, unpublished observations).

components can be observed separately in their conformational and melting behavior in the range of the CH_2 or CD_2 vibrations. Figure 49 shows curves for mixtures of phospholipids with a 5-n-alkylresorcinol, a single chain amphiphile ([167]; Hoffmann and Blume, unpublished observations). The different melting behaviors of the two compounds can be clearly distinguished.

More detailed information on the conformational order of the fatty acyl chains in the liquid-crystalline phase can be determined from an analysis of the CH_2-wagging vibrations. The bands in the region between 1380 and 1320 cm^{-1} can be attributed to g^+tg^- (kinks) and other gtg conformers (1356 cm^{-1}), to double gauche (gg) (1340 cm^{-1}) and to end-gauche conformers (1320 cm^{-1}). The integral intensities of these bands are calibrated using spectra of micellar systems or alkanes and applying Flory's rotational isomeric state model to calculate the distribution of conformers. With this approach the total number of gauche conformers per chain has been evaluated for several lipids with different head groups as a function of temperature [165, 168]. The analysis shows that the head group interactions have notable effects on the conformational behavior of the chains [165, 167].

For all-trans chains, as they occur in the gel state, a wagging progression, i.e. a number of bands of low intensity, appears between 1320 and 1100 cm^{-1} superimposed on the other vibrational bands [169]. The number of bands is directly related to the maximum length of the all-trans chain. The wagging progression disappears at temperatures in

the liquid-crystalline phase as now the all-trans segments are very short.

Even more detailed information can be obtained by the analysis of the rocking modes of specifically deuterated lipids. Several CD_2 rocking bands appear between 600 and 650 cm^{-1} due to different sequences of gauche and trans conformations in the chains. Thus a profile of the conformational properties along the fatty acyl chain can be determined [170, 171].

Interactions at the lipid-water interface can be monitored by following vibrations of specific groups in the molecule located in this region. For instance, the frequency and shape of the C=O ester stretching band is sensitive to hydration of the head group region. Its frequency changes with the transition into the liquid-crystalline state. ^{13}C-labelling of one of the C=O groups in the phospholipid leads to the appearance of two C=O bands due to the vibrational isotope effect, the one with the lower frequency originating from the ^{13}C=O vibration [163, 172–174]. Both C=O vibrational bands can be decomposed again into at least two overlapping bands of different frequency. The lower frequency band was shown to be caused by hydrogen-bonding of water molecules to the carbonyl groups. The carbonyl bands can thus be used to monitor changes in hydration at the bilayer water interface. Figure 50 shows the characteristic changes of the C=O bands of ^{13}C-labelled DMPC in its three different lamellar phases [163].

Attenuated total reflection (ATR) spectroscopy can be used to study planar oriented bilayers prepared by deposition of lipids from organic solutions on the surface of an ATR-crystal (ZnSe or Ge) by a self-assembly process or by Langmuir-Blodgett techniques [157, 159, 173, 175, 176]. The hydration of the films is achieved by controlling the relative humidity of water vapor (H_2O or D_2O). The orientation of certain groups can be studied by measuring the IR-dichroism of the appropriate vibrational bands. The dichroic ratio of the absorbance of a vibrational band is determined by the orientational distribution function of the transition dipole moment with respect to the laboratory frame. For a determination of the orientation of specific molecular groups the relative orientation of the transition dipole moment with respect to the molecular frame has to be known. This is not always the case. Therefore, mainly relative changes of the IR-dichroism as a function of hydration or temperature can be interpreted. In the case of the CH_2-stretching vibrations, it can be safely assumed that the transition dipole moment is perpendicular to the chain axis. Then, for gel phase lipids the chain orientation with respect to the bilayer surface can be determined from the dichroic ratio of the symmetric or antisymmetric CH_2-vibration. For other group vibrations, such as the C=O and PO_2^- vibrational bands, only the orientation of transition

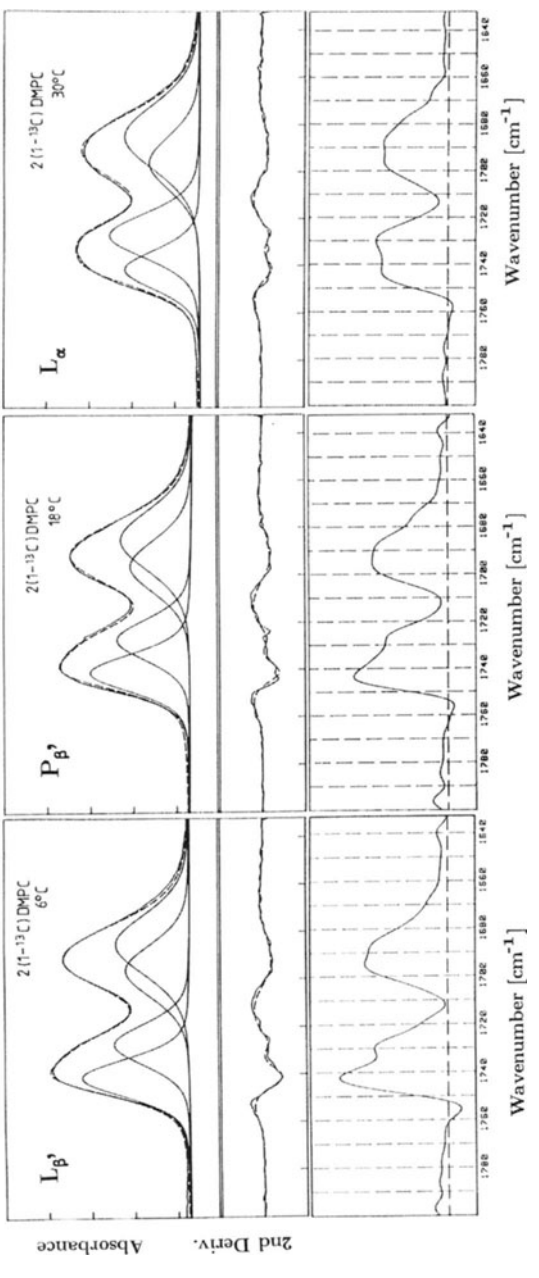

Fig. 50. Top panel: C=O stretching bands for 2(1-^{13}C)DMPC at 6°C (left), 18°C (middle), and 30°C (right) with pertinent lipid aggregations shown schematically on the top. The component bands were obtained by band shape fitting using the wave numbers for the components as determined from the 2nd derivative (middle panel) and from Fourier-self-deconvolution of the spectra (bottom panel). The high frequency maximum corresponds to the ^{12}C=O band and the lower frequency band to the ^{13}C=O group at the *sn*-2 position [163].

dipole moments with respect to the director can be determined. Experiments of this type have been performed for a variety of dry and hydrated phospholipids as well as glycolipids [157–159, 173, 175–177].

Sensitivity of FT-IR spectroscopy has been increased to such an extent that the investigation of lipid monolayers at the air/water interface has become possible in the last years [160, 161, 178–180]. This IRRAS-technique is particularly useful for studying the orientation and packing of lipid molecules at the air/water interface as a function of surface pressure, the binding of ions to mixed monolayers, and the binding of proteins to lipid monolayers.

5.4.2. Raman spectroscopy: The application of laser Raman spectroscopy to analysis of lipid bilayer membranes started in the seventies [181, 182]. Because Raman spectroscopy uses visible light, the problem of high absorption due to water, as present in the IR-region, is not existent. A vibrational Raman spectrum of a lipid is similar to an IR spectrum though the vibrational Raman bands have different intensities compared to the IR-bands due to the different selection rules. For instance, the C–C stretching modes between 1050 and 1150 cm^{-1} can easily be observed in Raman spectra and provide valuable information on the chain conformation, whereas in IR spectra these bands are weak due to their vanishing transition dipole moments and are in addition superimposed on the phosphate stretching modes [181, 182]. The CH_2-streching bands can also be used in Raman spectroscopy to follow the phase transition as described before, but the band profile is more complex than in the IR spectra [183]. The symmetric and antisymmetric methylene stretching modes appear at ca. 2845 and 2880 cm^{-1}. Additional bands belonging to the symmetric and asymmetric stretching modes of the C–H groups of terminal methyl groups show up at a 2935 and 2954 cm^{-1} [184]. In the liquid-crystalline phase, the intensity at 2935 cm^{-1} increases. This increase is partly due to the fact that an infrared-active antisymmetric methylene stretching mode becomes Raman active because the chain symmetry is lowered. Also the Fermi resonance between the symmetric C–H stretching mode of the terminal methyl groups and the first overtone of the CH_2-bending vibration changes. Concomitantly the intensity of the 2880 cm^{-1} band decreases, its frequency shifting to higher wave numbers, and its half width increasing [184].

To monitor the progress of the phase transition several ratios of band intensity I at two wavelengths can be used, for instance the ratios I_{2935}/I_{2880} or I_{2850}/I_{2880} in the methylene region or I_{1090}/I_{1130} in the C–C stretching region. The I_{2850}/I_{2880} ratio measures primarily changes in intermolecular order, while inter- as well as intramolecular effects contribute to the I_{2935}/I_{2880} ratio. The I_{1090}/I_{1130} parameter specifically measures intramolecular order of the chains, as this ratio

is sensitive only to the length of the all-trans segments in the acyl chains.

With the introduction of FT-Raman spectroscopy the field of applications has broadened, in particular for biological materials such as the *stratum corneum* of skin and the composition of membranes of eye lenses [185–187].

5.5. Electron spin resonance (ESR) spectroscopy

Numerous books and reviews exist in which the application of ESR spectroscopy in lipid research is described in detail [188, 189]. Molecules containing a nitroxide (N–O) group are the most commonly employed spin probes (see Fig. 51). The ^{14}N nucleus has a spin $I = 1$. Consequently three electronic transitions are observed, separated by the hyperfine coupling constant between the electron and the ^{14}N nucleus. The hyperfine splitting and the resonance frequency (g-value) depend on the polarity of the medium. This effect can be utilized to study partition coefficients of spin probes between water and the apolar lipid bilayer membrane, which in turn are affected by the phase state of the lipid membrane. Thus phase transition temperatures can be determined with spin probes such as 2,2,6,6-tetramethylpiperidine-1-oxide (TEMPO) (see Fig. 51).

Other suitable spin probes are fatty acids or phospholipids carrying the reporter group at certain positions in the acyl chains, which are mixed with the lipids under study. Due to the high sensitivity of ESR spectroscopy, the concentration of the spin probes in the bilayers can be kept well below 1 mole%. The major application of these spin probes is the study of lipid dynamics and order. This is possible because g-value as well as hyperfine coupling (A-value) depend on the orientation of the nitroxide group with respect to the external magnetic field. The spectra are sensitive to motional averaging by isotropic as well as anisotropic motions. Spin probes dissolved in isotropic media give ESR spectra with orientationally averaged hyperfine splittings due to rapid isotropic tumbling. The correlation time for this motion has to be short on the ESR time scale, i.e. 10^{-9} s or shorter. Longer correlation times lead to gradual broadening of the ESR lines, for instance, when the viscosity of the solvent is increased. The spectra are particularly sensitive to motions in the intermediate time regime when the correlation times are between 10^{-9} and 10^{-7} s [189].

When lipid spin probes are dissolved in membranes, the reorientational motions are anisotropic. Because the correlation time for the long axis rotation increases when the lipid passes into the gel phase, marked changes in spectral line shape occur at the phase transition. The line shapes are sensitive to the order parameter

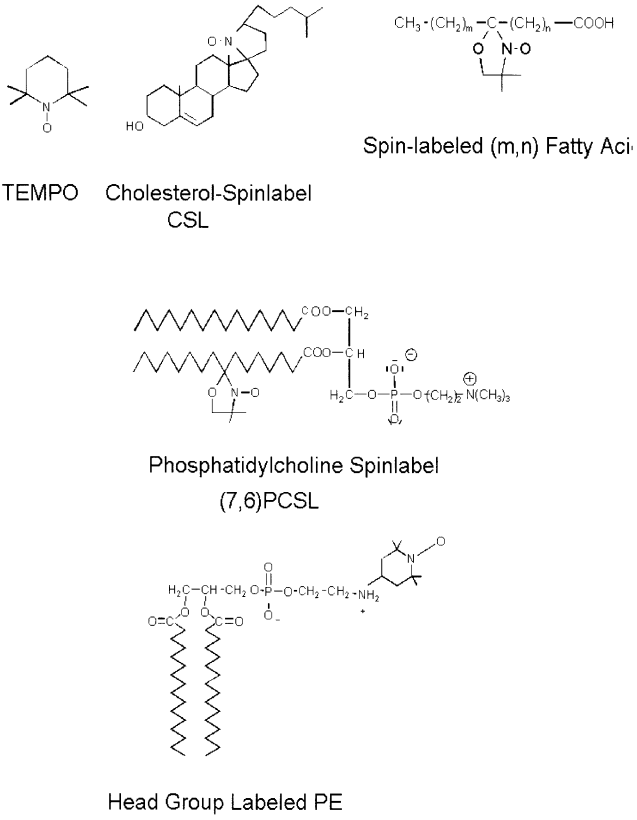

Fig. 51. Chemical structure of spin labels and spin labeled lipids used in ESR spectroscopy.

$$S = \langle {}^1/_2 \, (3 \cos^2 \vartheta - 1) \rangle \tag{6}$$

which describes the time average of the extent of the angular excursions of the molecular long axis, ϑ being the angle between the long axis and the membrane normal. An example of the results of ESR spectroscopy with chain labeled spin probes in DMPC membranes is shown in Fig. 52. The rigid body order parameter of the molecule and the correlation times of the various intra- and intermolecular reorientational motions as obtained from line shape analysis are shown in comparison to the results obtained by ^{2}H-NMR spectroscopy [190].

The ESR method has also been successfully employed to study lateral and transverse (flip-flop) diffusion in lipid bilayers [191–194]. Lateral diffusion can be studied because ESR spectra are sensitive to spin exchange. This effect becomes larger with higher spin probe con-

centration due to an increase in the collision frequency between the spin-labeled molecules by lateral diffusion. The collision or exchange frequency can be determined by computer simulations of the experimental spectra. From the exchange frequency the lateral diffusion coefficient is calculated applying a two-dimensional random-walk model. With this technique the first data on lateral diffusion coefficients in lipid bilayers were determined by Träuble and Sackmann [191] and Devaux and McConnell [192]. Lipid flip-flop, i.e. transverse diffusion, can also be measured using a lipid molecule spin-labeled at the lipid head group as the nitroxide group can be reduced by ascorbic acid to the corresponding hydroxylamine [193].

One of the major applications of ESR spectroscopy is the determination of the extent and specificity of the interactions of lipids with intrinsic membrane proteins. Lipids in the first and second annulus around a membrane protein are somewhat reduced in their mobility. In the ESR spectra, line shapes are observed, which in a first order approximation can be described as arising from a superposition of a spectrum of spin labels in an unperturbed lipid matrix and an "immobilized" (more precisely, motionally restricted) component corresponding to lipids in the annulus around the intrinsic protein [195]. Using a variety of spin-labeled phospholipids Marsh and coworkers and other groups determined the lipid specificity for various membrane proteins and their apparent relative binding constants [195–197]. With few exceptions, the observed specificities are not very pronounced. Some examples for lipid specificity are cytochrome c oxidase, which has a preference for the binding of cardiolipin, with a relative binding constant of $K \sim 5$ for cardiolipin in relation to phosphatidylcholine, and Na^+/K^+-ATPase which has a preference for negatively charged lipids [195].

The recent development of 2-dimensional spectroscopic techniques in ESR has increased the possibility to determine lipid dynamics in bilayers [198, 199].

5.6. Nuclear magnetic resonance (NMR) spectroscopy

For the detailed theory of NMR and its application to lipid bilayers the reader is referred to textbooks and review articles [43, 200–203]. The advantages of NMR are that it is an intrinsic method and thus does not require the introduction of a potentially perturbing label or probe. When a nuclear spin probe such as ^2H, ^{13}C, and ^{15}N is introduced, the chemical structure of the molecule is not changed and its intermolecular interactions are almost unaltered.

Lipid bilayers and biological membranes are anisotropic systems, free isotropic reorientational motions of the molecules are not possible. The orientation-dependent interactions, such as dipolar interac-

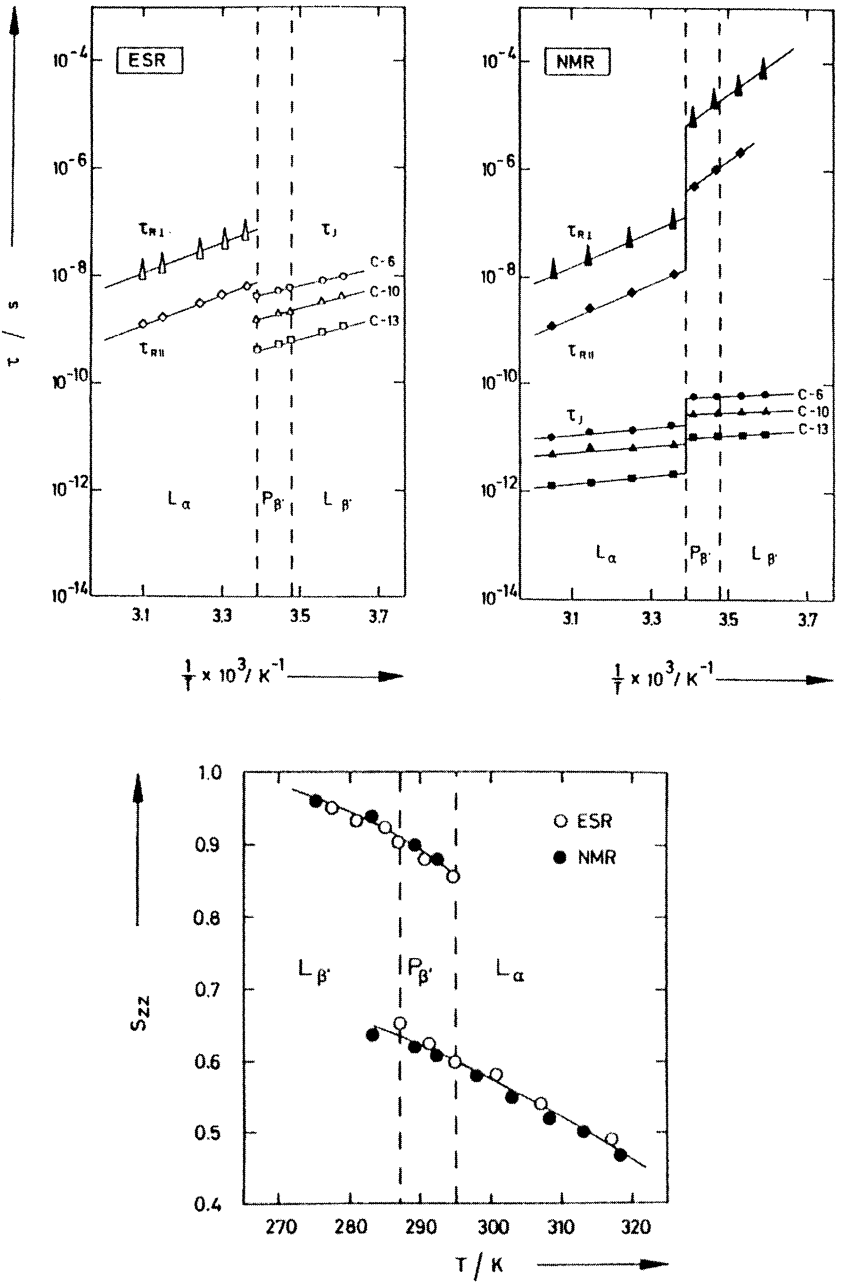

Fig. 52. Top left: Temperature dependence of the correlation times τ_J (chain isomerization), $\tau_{R\parallel}$ (long axis rotation), and $\tau_{R\perp}$ (hindered wobbling motion of the long axis) of DMPC spin-labeled at three different positions in the chains. Top right: Corresponding correlation times determined by ^{2}H-NMR spectroscopy of ^{2}H-labeled DMPC. Note the differences in correlation times induced by the spin label. Bottom: Rigid body order parameter of DMPC as a function of temperature obtained by the two methods [190].

tions, chemical shift anisotropy, and quadrupolar interactions, are therefore not completely averaged. The broad lines observed in NMR spectroscopy applying solid state techniques contain information on the extent, type and correlation times of the reorientational motions [202, 204–206]. The determination of relaxation times for longitudinal and transverse relaxation can provide additional information on lipid dynamics [207, 208].

For the analysis of chemical shift anisotropies ^{31}P spectroscopy is a well suited spectroscopic technique in systems containing phospholipids, because there is usually only one ^{31}P nucleus in a phospholipid molecule. The dipolar interactions with the protons are normally removed by broad band decoupling of the protons during the acquisition time [202, 203, 209]. Similarly only one prominent line is observed in ^{13}C-NMR spectroscopy, when the molecule is enriched with a ^{13}C nucleus at a certain site in the molecule. The observed line shapes can then be quantitatively analyzed.

The chemical shift anisotropy can be expressed as a second rank tensor which is diagonal in its principal axis system. This coordinate system is fixed in the molecular frame, its orientation being *a priori* not known. In the case of a single crystal, in which no motions are present, the chemical shift component σ_{zz} parallel to the external magnetic field is of interest. This is related to the principal components of the shift tensor σ_{11}, σ_{22}, and σ_{33} by rotations through the Euler angles ϑ and φ [202]. For a crystal of a compound with only one ^{31}P nucleus, a single line at a resonance frequency being dependent on the orientation of the crystal with respect to the magnetic field, i.e. on the Euler angles ϑ and φ would be observed. For a crystal powder a superposition of signals from all orientations is observed, giving rise to a so-called powder pattern.

Molecular motion will lead to an averaging of the chemical shift. Fast isotropic reorientations lead to a sharp line at the isotropic chemical shift as observed in high resolution NMR. If the reorientational motions are anisotropic, characteristic broader lines are observed, their line shapes being dependent on the rate of the reorientational motions and the orientation of the main axis of the chemical shift tensor [202]. Figure 53 shows the characteristic line shapes observed for two different reorientational motions as a function of the reduced rate constants. These model calculations are the basis for the analysis of ^{31}P- and ^{13}C-NMR spectra of lipids.

^{31}P-NMR has been used extensively to study the transition from lipid L_α phases to the inverted hexagonal H_{II} phase [202, 203, 210–213]. In this case, an additional motional averaging in the H_{II} phase by rapid diffusion of lipid molecules around the H_{II} cylinders being perpendicular to the long axis of the lipids leads to a reduction in line width by a factor of two and an inversion of sign. Thus this type of

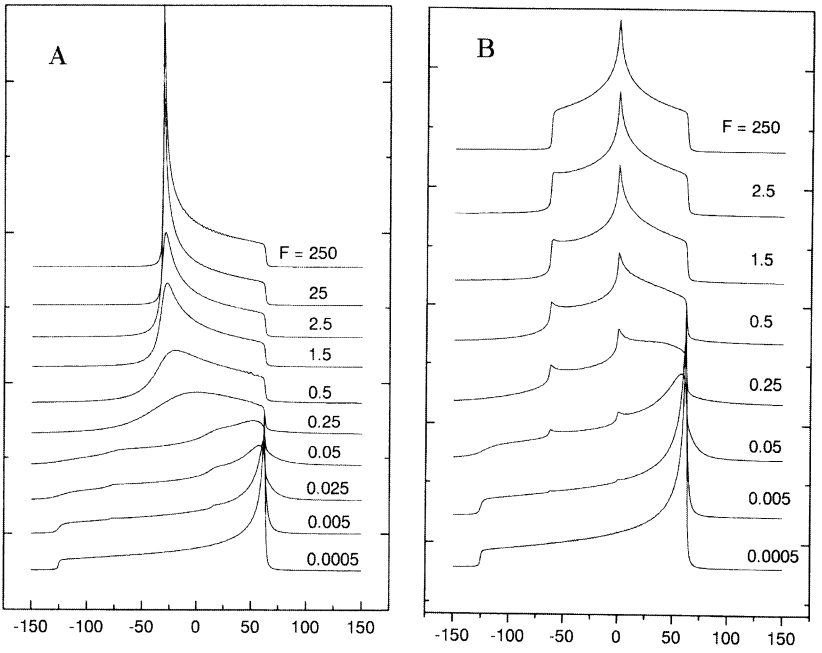

Fig. 53. (A) Calculated line shapes for an axially symmetric chemical shift tensor with the σ_{33} component oriented perpendicular to a rotation axis around which a three-fold jump is executed. F is a reduced rate constant defined as $F = k/\Delta\sigma$, where k is the jump rate constant and $\Delta\sigma = \sigma_{11}-\sigma_{33}$ is the width of the chemical shift tensor in Hz. (B) Calculated line shapes for an axially symmetric chemical shift tensor executing jumps between two sites with an angle of 109.4° between the sites. F is the reduced jump rate constant as in (A) [43, 202, 204].

transition can be easily detected by ^{31}P-NMR. Figure 54 shows a representative example for ^{31}P spectra and the corresponding ^{2}H-NMR spectra [214].

When phospholipids are cooled from the L_α-phase to the gel ($P_{\beta'}$ or L_{β}-phase), where motional averaging is reduced, the ^{31}P line shape changes abruptly at the main transition. Further decrease in temperature leads to gradual changes till, at very low temperatures, the so-called rigid limit is approached. All reorientational motions are then slow on the ^{31}P time scale with correlation times longer than 10^{-3} s. The line shapes in the intermediate time regime are very sensitive to the rates of motion. The spectra have been analyzed and simulated using various motional models [215, 216]. Figure 55 shows the line shapes and the simulations for DMPC observed upon cooling from the L_α through the $P_{\beta'}$ to the $L_{\beta'}$-phase [216].

^{13}C-NMR spectroscopy can be used in a similar way as ^{31}P-NMR spectroscopy. However, the natural abundance of the ^{13}C nucleus is low so that the acquisition times become very long. Application of magic angle spinning techniques (MAS) leads to high resolution spec-

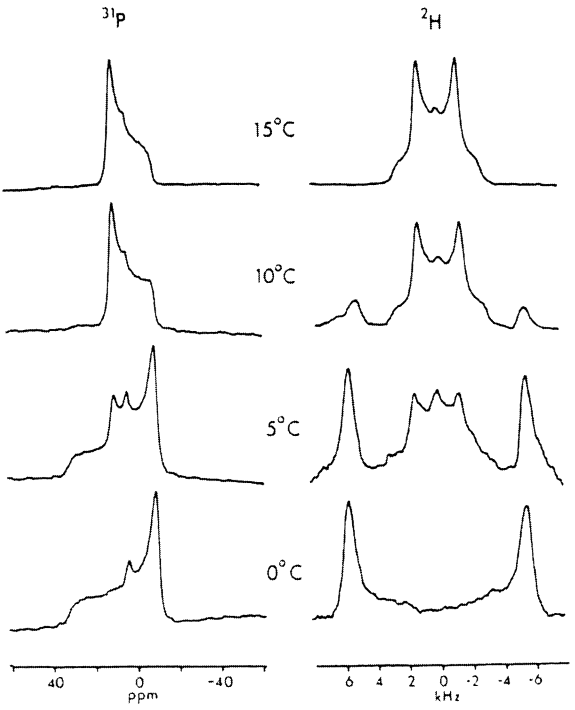

Fig. 54. Left: ^{31}P-spectra of fully hydrated DOPE as a function of temperature. The L_α-H_{II}-transition leads to a reduction of the ^{31}P line shape by a factor of two and a sign reversal. Right: Corresponding ^{2}H-NMR spectra of DOPE labeled at the 11-position of the chains. At 5 °C and 10 °C two component spectra are seen in the transition region [214].

tra in which the chemical shifts of the individual carbon atoms in the lipid molecules can be analyzed [217, 218]. Specific ^{13}C enrichment of one of the carbon atoms in the fatty acid ester groups leads to a prominent signal shifted away from the other resonances. The line shape of this signal can be analyzed as a function of temperature in a similar way to that described above for the ^{31}P line of phospholipids [219]. The analysis shows that below the main transition of phosphatidylcholines and phosphatidylethanolamines long axis rotation is still possible with correlation times shorter than 10^{-4} s. Figure 56 shows the ^{13}C line shapes observed for DPPC and DPPE (dipalmitoylphosphatidylethanolamine) as a function of temperature [219].

In the case of ^{2}H-NMR, the orientation-dependent interaction is the quadrupole interaction between the nuclear quadrupole moment and the electric field gradient (EFG) of the surrounding electrons in the particular C–^{2}H bond. Deuterons (^{2}H) have a spin I = 1. Consequently three different energy levels will arise when the nucleus is placed in a magnetic field. In high magnetic fields the quadrupole interaction can

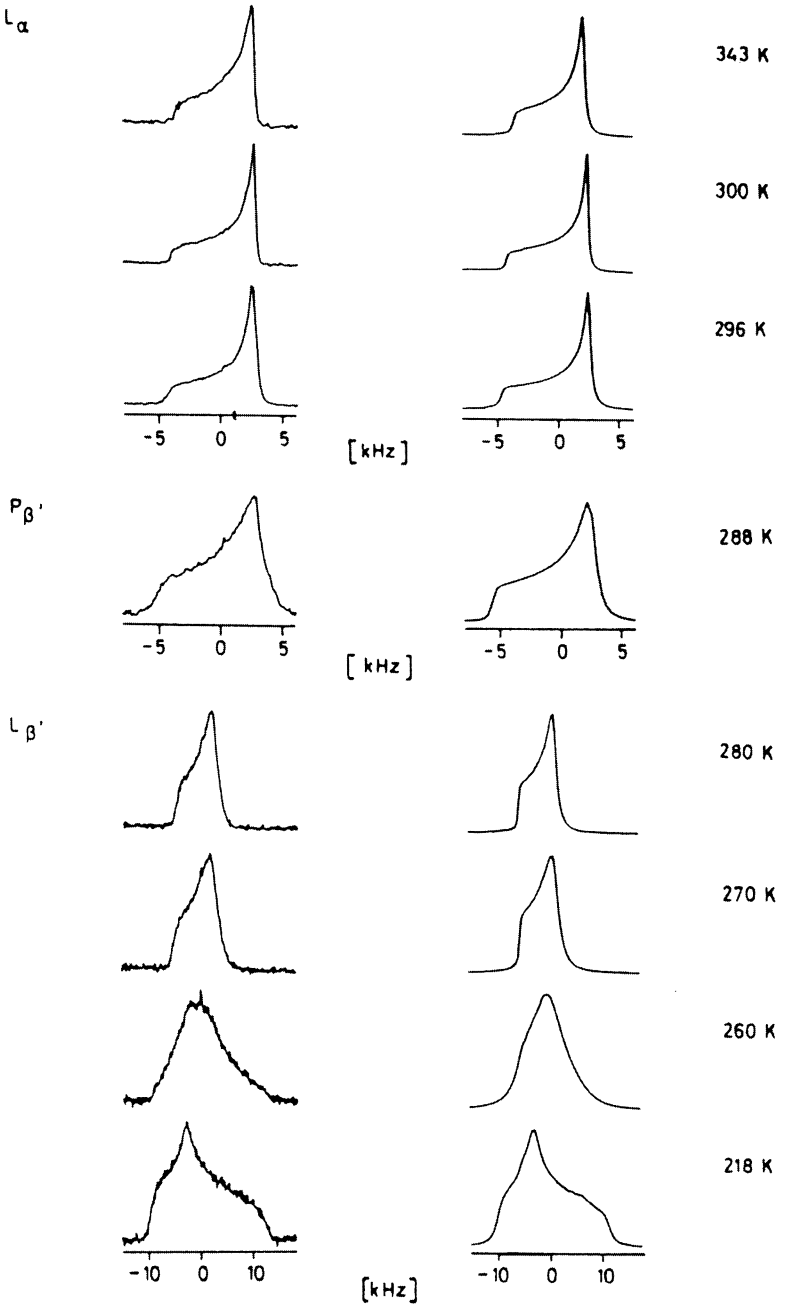

Fig. 55. ^{31}P-NMR spectra of DMPC at various temperatures together with line shape simulations [216].

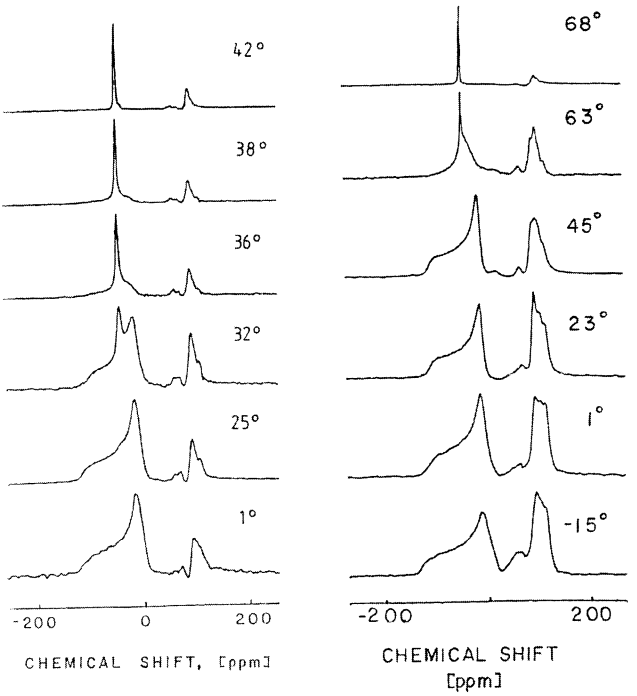

Fig. 56. ^{13}C-NMR spectra of 2(1-^{13}C)DPPC (left) and 2(1-^{13}C)DPPE (right) as a function of temperature. The prominent line at low ppm values is due to the labeled *sn*-2 C=O group, whereas the signals farther to the right arise from carbon atoms of natural abundance in the chains, the back bone, and the head group. The transition into the L_α-phase leads to the appearance of a narrow ^{13}C line, indicating that the orientation of the ^{13}C tensor is close to the magic angle [219].

be viewed as a perturbation of the Zeeman interaction [200, 201]. This additional perturbation leads to a change of the originally evenly spaced three energy levels, so that two transitions with different frequencies ν_+ and ν_-, being symmetric around the unperturbed frequency ν_o, are observed. The difference $\Delta\nu_Q = \nu_+ - \nu_-$ is called the quadrupole splitting and depends on the orientation of the EFG tensor with respect to the magnetic field [201, 202]. In the case of an aliphatic C–^{2}H bond, the EFG tensor is axially symmetric with $V_{xx} = V_{yy} \neq V_{zz}$. If the z-axis of the EFG is parallel to the magnetic field H_o we observe a splitting

$$\Delta\nu_{Q\|} (H_o \| zz) = {}^3/_2 \, (e\, Q/h)\, V_{zz} = {}^3/_2 \, (e^2\, q\, Q/h) \qquad (7)$$

with the abbreviation $e\, q = V_{zz}$ called the electric field gradient. The terms eQ and $e^2q\, Q/h$ denote the quadrupole moment of the nucleus

and the so-called quadrupole coupling constant, respectively, while e and h are the elementary charge and Planck's constant, respectively. For an aliphatic C–^{2}H bond $e^2q\,Q/h \approx 169$ kHz so that $\Delta\nu_{Q\|}$ becomes 250 kHz. This is a much larger separation than the effects arising from the chemical shift anisotropy. The quadrupole interaction does not depend on the magnetic field strength, in contrast to the chemical shift anisotropy. Consequently, $\Delta\nu_Q$ is expressed in Hz and not in ppm.

$\Delta\nu_Q$ depends on the orientation of the EFG with respect to the H_o field. For an axially symmetric EFG tensor we get for the orientation dependence

$$\Delta\nu_Q(\vartheta) = {}^3/_2(e^2qQ/h)\ {}^1/_2(3\cos^2\vartheta - 1) \tag{8}$$

with ϑ denoting the angle between H_o and V_{zz}. In a crystal powder, we again have a superposition of all possible orientations and observe a powder pattern as shown in Fig. 57B (a). The splitting $\Delta\nu_{Q\perp}$, i.e. the separation of the peaks of this powder pattern, is reduced by the presence of molecular motions. If this motion consists of fast rotation around a preferred axis the reduced splitting $\overline{\Delta\nu_{Q\perp}}$ is

$$\overline{\Delta\nu_{Q\perp}} = \Delta\nu_{Q\perp}{}^1/_2\,(3\cos^2\beta - 1) \tag{9}$$

with β now the angle between the C–^{2}H bond and the rotation axis. For $\beta = 90°$ a line shape as shown in Fig. 57B (c) is observed. The width of the powder pattern is reduced by a factor of 2. A line shape as in Fig. 57B (b) is observed, when a fast two-site jump is present with a angle of 109° between the two sites. Other more complicated reorientational motions give rise to line shapes as shown in Fig. 57B (d–g). If all motions are in the fast limit, the spectra look very similar. However, the line shapes are also very sensitive to the rate of reorientational motion. This is shown in Fig. 57A for a three-fold jump rotation with $\beta = 90°$.

In the fast limit of the ^{2}H-NMR experiment when the correlation times τ_c are shorter than 10^{-7} s, the splitting is related to the deuterium order parameter S_{CD} by

$$\overline{\Delta\nu_{Q\perp}} = {}^3/_4\,(e^2qQ/h)\,S_{CD} \tag{10}$$

where

$$S_{CD} = \langle {}^1/_2\,(3\cos^2\beta - 1)\rangle \tag{11}$$

is the order parameter of the C–D bond [201] and describes the time average of the fluctuation of this bond with respect to the director, the preferred axis around which all motional reorientations occur.

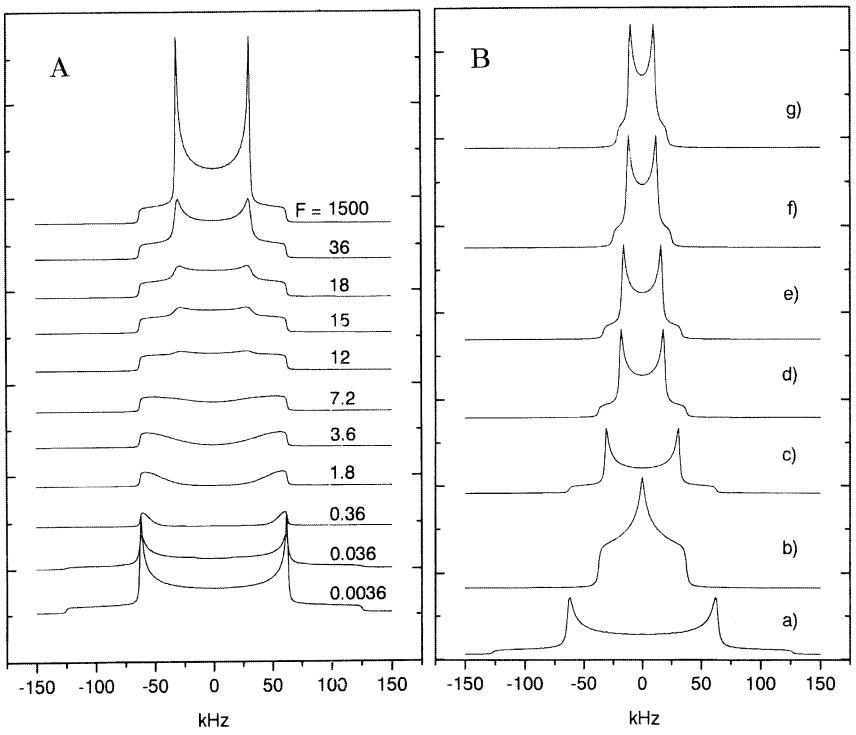

Fig. 57. (A) Calculated ^{2}H-NMR quadrupole echo line shapes for a three-fold rotational jump motion with the C-D axis perpendicular to the rotation axis. F is the reduced jump rate, i.e. k divided by the quadrupole coupling constant e^2q Q/h = 168 kHz for a CD_2-group. (B) Calculated line shapes for various fast limit (k = 5×10^8 s) reorientational motions. a) rigid limit powder pattern; b) two site jump with $\beta = 109.4°$; c) fast three-fold jump rotation with $\beta = 90°$; d) as in c) but with additional trans-gauche isomerization with 20% gauche probability; e) as in d) but with additional wobbling motion with an angle of ±10°; f) as in d) but with 30% gauche probability; g) as in d) but with additional wobbling motion with an angle of ±20° [43, 202, 204].

Frequently the order parameter S_{mol} is also used. It describes the order of the direction normal to the plane spanned by the C–D segment [201]. It is related to S_{CD} by $S_{mol} = -2\ S_{CD}$.

The order parameter concept has been widely used to describe conformation and dynamics of lipid molecules in the liquid-crystalline phase. Selective deuteration of the acyl chains at different positions shows that the motional freedom increases towards the chain ends. This order parameter gradient determined by ^{2}H-NMR spectroscopy is shown in Fig. 58. It has been postulated that S_{mol} is a product of at least two order parameters, a segmental order parameter, describing motional averaging of each segment by trans-gauche isomerization, and a rigid body order parameter describing the wobbling motions of

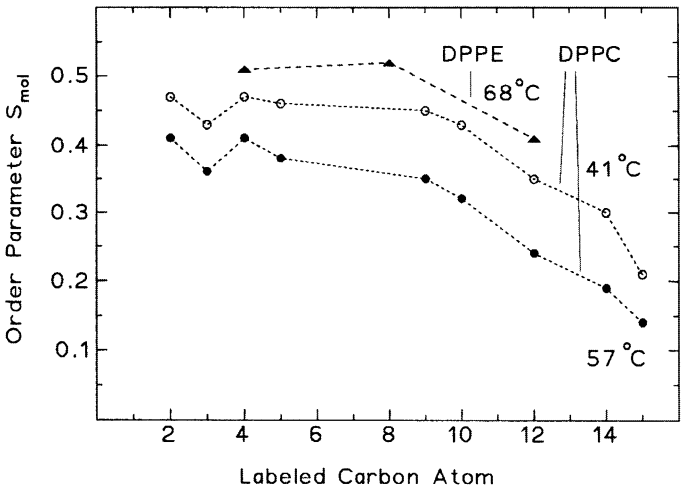

Fig. 58. Order parameter S_{mol} for DPPC and DPPE in the L_α-phase as a function of position of the CD_2-group [201, 222].

the molecular long axis of the molecule [220]. A separation of these two contributions can only be achieved by using information from additional experiments, such as ^2H-T_1- and T_2-relaxation [206, 208], FT-IR data [165, 167, 171] (see above), and fluorescence spectroscopy measurements (see below).

Line shape simulations of experimental spectra of gel phase lipids yield detailed information on the correlation times of the motional modes. This has been used extensively to study motions in gel phase phosphatidylcholines [43, 44, 190, 201, 205, 206, 221], phosphatidylethanolamines, [222, 223], glycolipids [207, 224], lipid/cholesterol [207, 221, 225, 226] and other binary lipid mixtures [41, 227–229]. Figure 59 shows ^2H-NMR spectra of three different phosphatidylcholines. The gel phase spectra are much wider but are not rigid-limit spectra, indicating that even in the gel phase reorientational motions are possible.

The use of oriented lipid bilayers can give additional information because the motional model used for the simulation must also quantitatively describe the angular dependence of the spectral line shapes. Figure 60 shows ^2H-NMR spectra of oriented bilayers of 1,2(4,4-d_2)DMPE with different orientations with respect to the magnetic field [223]. The spectra can be described by using a three-fold axial jump process for the long axis rotation and a two-fold jump for trans-gauche isomerization. The successful simulation of the experimental spectra proves that the motions of PE molecules in the gel phase mainly consist of long axis rotation in a quasi-hexagonal lattice.

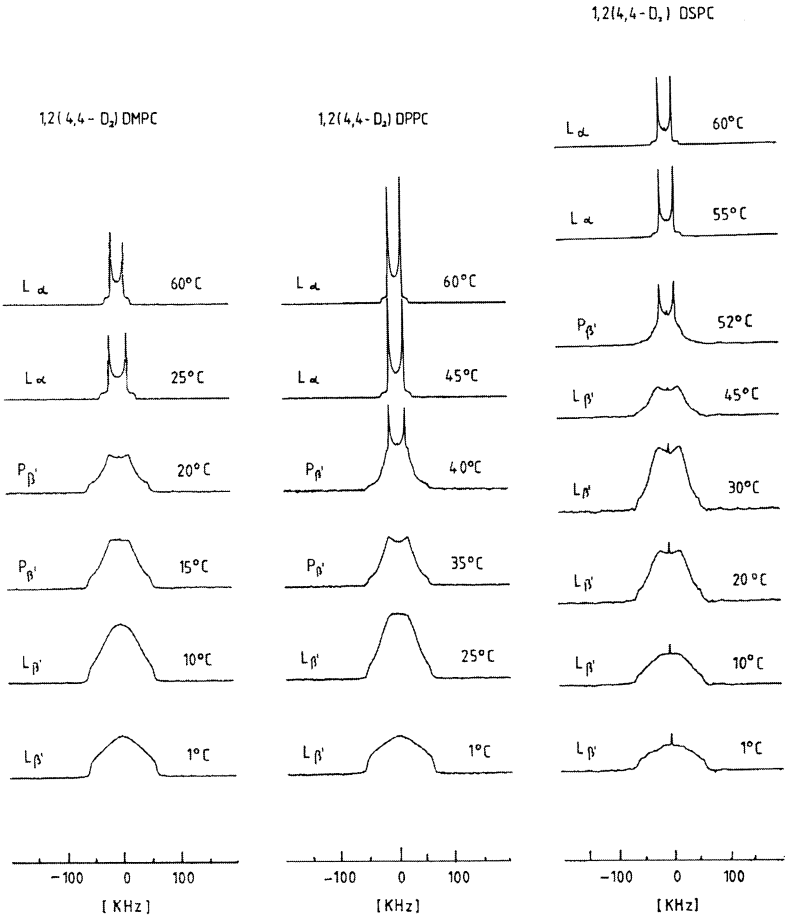

Fig. 59. ^{2}H-NMR spectra of three different phosphatidylcholines as a function of temperature. The line shapes in the gel phases indicate rotational motions in the intermediate time regime [41, 43].

Lipids with perdeuterated chains have been used extensively to study order parameter gradients in bilayers of pure and mixed lipids. Lipids with perdeuterated chains offer the advantage of higher signal to noise ratio and the possibility to extract the complete smoothed order parameter profile for the liquid-crystalline phase. To assign the individual splitting a dePakeing procedure is used [230]. In lipid mixtures the labeling can be reversed to study the behavior of the two components separately. An example for this type of experiment is shown in Fig. 61 for mixtures of DMPC with DMPA, and of DPPC with DMPA. The average order parameters S_{CD} for the pure components are different. This is somewhat reduced in the mixtures but the

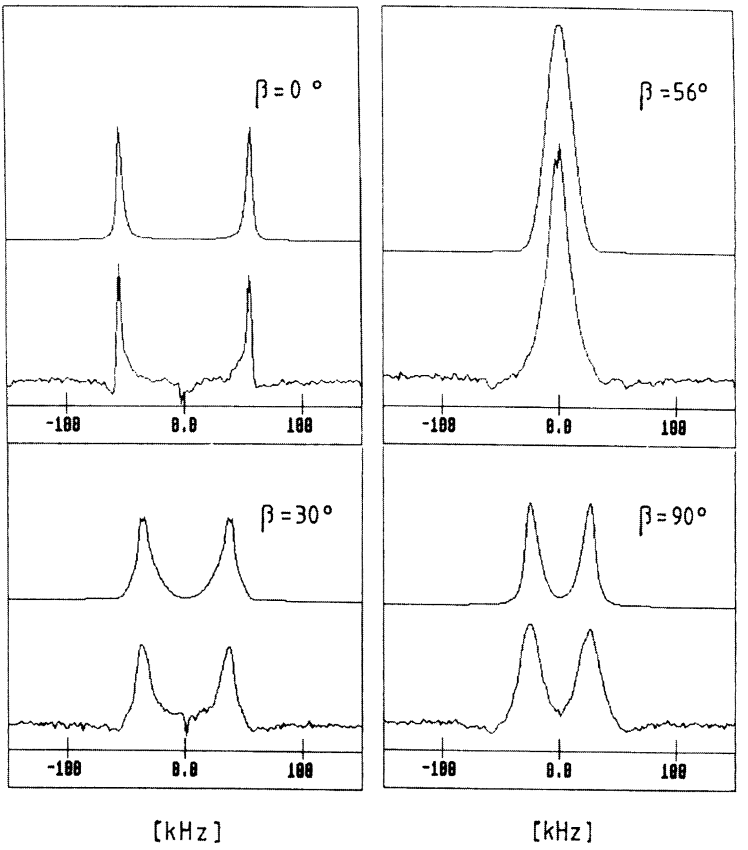

Fig. 60. ^{2}H-NMR spectra (bottom) and line shape simulations (top) of oriented bilayers of 1,2(4,4-D_2)DMPE in the gel phase at different angles β of the membrane normal with respect to the magnetic field. The simulations were performed using a three-fold jump model for long axis rotation with $R_{rot} = 3.1 \times 10^6$ s^{-1} and additional 5% trans-gauche isomerization with a rate $R_{tg} = 3 \times 10^5$ s^{-1} [223].

chains of the two components still have distinctive conformational properties [167].

5.7. Fluorescence spectroscopy

Fluorescence spectroscopic techniques can be used in a variety of ways, namely to study lateral diffusion in membranes, to measure dynamics and order of fluorescent probes incorporated into the lipid bilayers, to probe intermolecular interactions and distances by quenching and energy transfer processes, and for following the formation of

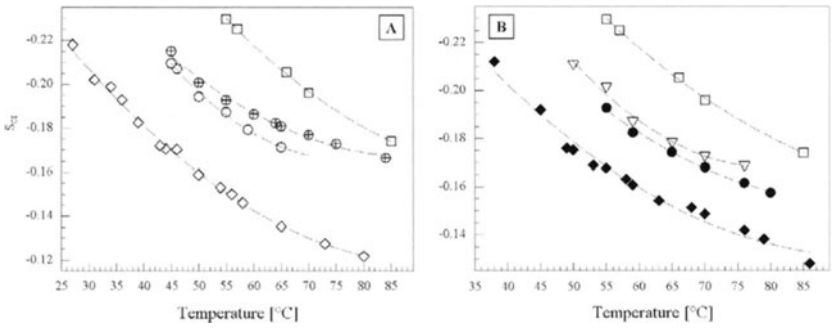

Fig. 61. Temperature dependence of the average order parameter S_{CD} of the perdeuterated acyl chains of some lipids and their respective binary 1:1 mixtures, all in H_2O at pH 7. (A) DMPA-d_{54} (■), DMPC-d_{54} (◇), DMPA-d_{54}/DMPC (⊕), and DMPC-d_{54}/DMPA (○). (B) DMPA-d_{54} (□), DPPC-d_{62} (◆), DPPC-d_{62}/DMPA (●), and DMPA-d_{54}/DPPC (▽) [167].

excimers [231–234]. In all cases, a fluorescent label has to be used which can be covalently attached to the lipid molecule. Figure 62 shows a variety of fluorescent probes used in membrane studies.

Information on order and dynamics in lipid bilayers can be obtained by measuring the time dependence of fluorescence anisotropy of rod-like probe molecules, such as diphenylhexatriene (DPH) or DPH attached to amphiphilic molecules (see Fig. 62). The fluorescence anisotropy

$$r(t) = [I_{\parallel}(t) - I_{\perp}(t)]/[I_{\parallel}(t) + 2\, I_{\perp}(t)] \tag{12}$$

with $I_{\parallel}$ and $I_{\perp}$ being the fluorescence intensities with polarization directions parallel and perpendicular to the polarization of the exciting beam, should in the simplest case decay with a simple exponential

$$r(t) = r_{\infty} + (r_o - r_{\infty}) \exp(-t/\tau_c) \tag{13}$$

Here τ_c is the correlation time for rotations perpendicular to the long axis of the probe, while r_{∞} and r_o are the anisotropy at time $t = 0$ and $t \rightarrow \infty$, respectively. In many cases only steady state and not time resolved measurements of the fluorescence anisotropy are performed. The steady state anisotropy $\bar{r}$ changes at the phase transition temperature into the L_{α}-phase because both, r_{∞} and τ_c, are decreased. When only one correlation time τ_c is observed, $\bar{r}$ depends on r_{∞} and τ_c as follows [235, 236]

$$\bar{r} = r_{\infty} + (r_o - r_{\infty})\, \tau_c /(\tau_c + \tau_f) \tag{14}$$

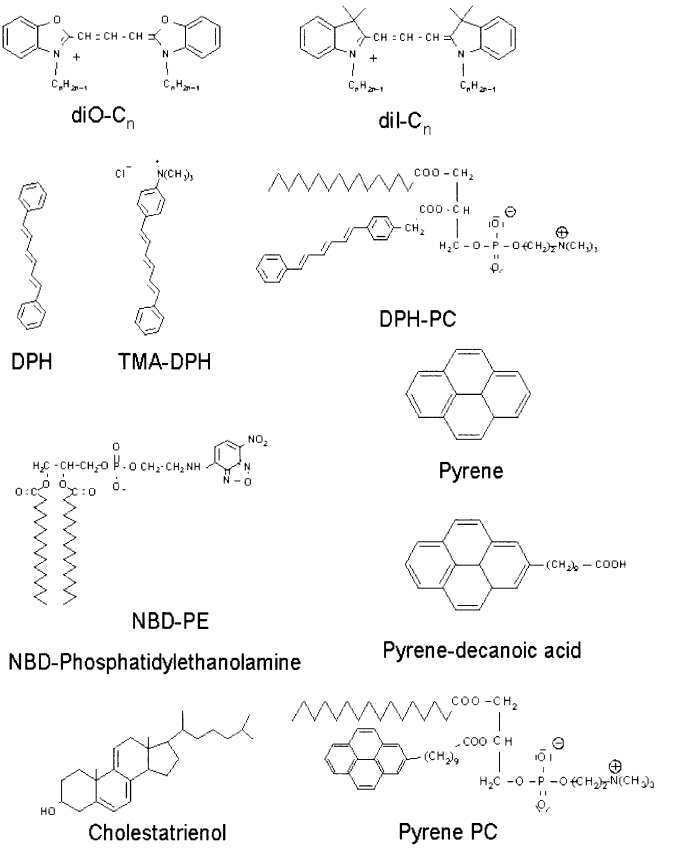

Fig. 62. Fluorescent probes and lipids with fluorescent labels used for fluorescence spectroscopy in lipid bilayers.

with τ_f being the fluorescence life time of the probe molecule. The values r_o and r_∞ are related to the order parameter S of the fluorescent probe (cf. Eqn. 6) by

$$S = [r_\infty/r_o]^{1/2} \tag{15}$$

Thus, S can be determined from time dependent measurements of r, providing the correlation time τ_c is not much longer than the fluorescence life time τ_f [235].

Numerous papers have been published on fluorophore dynamics in lipid membranes [231, 236, 237]. One particular disadvantage of this

method is the fact that the location of the fluorescent probe has to be known before conclusion on the dynamics and order of the surrounding lipids can be made. It has been verified recently by neutron scattering that DPH itself is not necessarily located in the bilayer parallel to the lipid chains. Hence TMA-DPH can have two different orientations, the populations depending on temperature and phase state of the lipid [237]. Any analysis of time-resolved fluorescence decay curves has to take into account that this possibility exists and that the orientation and order parameters determined by fluorescent probes are not necessarily the same as those of the surrounding lipids [238]. However, recent new experiments on the location of the DPH residue of various DPH derivatives using the quenching effects of bromine atoms or spin labels attached to lipid chains came to the conclusion that the location of the fluorophore is always more or less the same, deep within the bilayer region [239]. Therefore the question seems to be unresolved and any conclusions on the order and orientation of the probe molecules have to be made with caution.

Lateral diffusion coefficients of lipids and proteins in bilayers can be determined using the Fluorescence Recovery After Photobleaching (FRAP)-technique with its various modifications [232, 233]. A lipid or protein with a covalently attached fluorescent residue is incorporated into planar lipid bilayers and distributes homogeneously in the plane of the membrane. An intense laser beam is then directed towards the surface and the fluorescent molecules in a small spot are irreversibly bleached. After this bleaching pulse, the fluorescence intensity in this spot is recorded as a function of time. Due to the movement of unbleached molecules into this area by lateral diffusion the fluorescence increases again. Figure 63 shows a schematic diagram of this experiment [232]. The lateral diffusion coefficient D_L of the fluorescent molecule is then given by

$$D_L = \omega^2 \gamma_D/(4t_{1/2}) \tag{16}$$

where $\gamma_D = t_{1/2}/\tau_D$ is the so-called bleaching parameter, ω the radius of the focused laser beam at the intensity e^{-2}, $t_{1/2}$ the half time of fluorescence recovery, and τ_D the diffusional recovery time. The FRAP technique can also be applied to study lipid diffusion in lipid monolayers at the air/water interface [240].

Another fluorescence method used for studying lipid diffusion is the excimer technique, using molecules with the pyrene moiety covalently attached to lipids or fatty acids (see Fig. 62). Pyrene forms excimers, the rate of the excimer formation being related to the concentration and the translational mobility of the probe molecules. Because the excimer technique measures diffusion over short distances, the lateral diffusion coefficients are not necessarily identical with those meas-

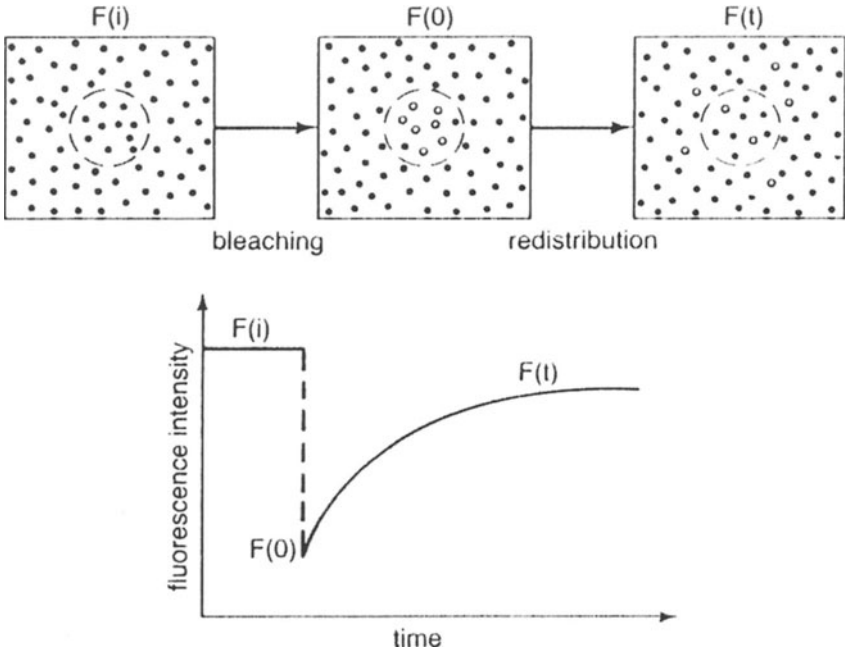

Fig. 63. Schematic illustration of a FRAP experiment and the resulting time dependence of the fluorescence recovery after the bleaching pulse [232].

ured by the FRAP method where diffusion is measured over distances of several μm [232, 241–243].

Fluorescence techniques have a particularly useful application in determination of lateral organization in membranes in the gel-liquid-crystalline coexistence region, but have also been used to address the question of fluid-fluid immiscibility in membranes [233, 244, 245]. The application of fluorescence spectroscopy in the form of epifluorescence microscopy to visualize domains in lipid monolayers in the region of lateral phase separation has been described above [68–72]. Fluorescence spectroscopy in its various forms is thus a powerful and sensitive technique for the investigation of lipid membranes and lipid monolayers.

5.8. Other physical techniques

Numerous other physical techniques have been employed to study lipid bilayer behavior, which will not be described here in detail. The reader is referred to the appropriate literature. Some other important techniques are:

a) Static and dynamic light scattering (DLS) techniques to study the size of lipid vesicles [246].
b) Electron microscopy (EM) to visualize lipid bilayers and vesicles. Different preparation techniques, such as transmission microscopy with negative staining, freeze fracture electron microscopy and cryo-electron microscopy are used [247–249].
c) Atomic Force Microscopy (AFM) for the visualization of Langmuir-Blodgett films and monolayers on solid supports [250, 251].
d) Surface plasmon resonance spectroscopy (SPR) for investigations of lipid-protein layers on solid supports [252].
e) Relaxation methods for the investigation of the kinetics of lipid phase transitions. Temperature jump and pressure jump with optical detection [253–255] and with X-ray detection applying synchrotron radiation have been applied [136, 137, 256, 257].
f) Stopped-flow kinetic measurements with optical detection to study binding kinetics of ions, peptides and other molecules, or phase transitions induced by the binding of ions or other molecules [258, 259]. The technique is also applicable to study the permeation of ions and other molecules through bilayers of lipid vesicles [260–262].

The list of methods mentioned above is far from being complete. Various combinations of different methods are used today, depending on the type of information necessary to be gained. In addition, the methods have to be adapted to the type of lipid systems under study, namely liposomes, unilamellar vesicles or oriented planar lipid bilayers.

6. Concluding remarks

The goal of this chapter was to give an introductory description of the chemical and physicochemical properties of bilayer forming lipids and the methods used in the area of research on lipid model membrane systems. This description could not cover all aspects of lipid structure and behavior. For additional information the reader is referred to other volumes of this series, and to the numerous books and review articles dealing with specialized topics as cited in this text. Likewise, not all of the physicochemical techniques applied in membrane research could be covered. The selection and the emphasis on some of the methods described above is biased towards those also present in the author's laboratory. However, the description should give an overview of those methods most widely used and enable the reader to take this chapter as a starting point for a further, more detailed search on specific topics.

Acknowledgments

Work from the author's laboratory was supported by grants from the Deutsche Forschungsgemeinschaft and the Fonds der Chemischen Industrie, which is gratefully acknowledged.

References

1 Voet D, Voet JG (1990) *Biochemistry*. John Wiley, New York.
2 Gennis RB (1990) *Biomembranes: Molecular Structure and Function*. Springer Verlag, New York.
3 Overton E (1895) Über die osmotischen Eigenschaften der lebenden Pflanzen und der Tierzelle. Vjsch. Naturf. Ges. Zürich 40: 159–201.
4 Gorter E, Grendel F (1925) Bimolecular layers of lipoids on chromocytes of blood. J. Exp. Med. 41: 439–443.
5 Danielli JF, Davson, H (1935) A contribution to the permeability of thin films. J. Cell Comp. Physiol. 5: 495–508.
6 Singer SJ, Nicolson GL (1972) The fluid mosaic model of the structure of cell membranes. Science 175: 720.
7 Bretscher MS (1985) The molecules of the cell membrane. Sci. Am. 253: 100–108.
8 Chapman D, Wallach DFH (eds) (1973) *Biological Membranes*. Academic Press, London and New York, Vol. 2.
9 Cevc G (ed) (1993) *Phospholipids Handbook*. Marcel Dekker, New York.
10 Lipowsky R, Sackmann E (eds) (1995) *The Structure and Dynamics of Membranes. Handbook of Biological Physics*. Vol 1, Elsevier Science, Amsterdam.
11 Lasic DD, Barenholz Y (eds) (1996) *Handbook of Nonmedical Applications of Liposomes*. Vol. 1–4, CRC Press, Boca Raton.
12 Datta DB (1987) *A Comprehensive Introduction to Membrane Biochemistry*. Floral Publishing, Madison.
13 Schmidt RD (1989) Unusual fatty acids and their scope in biotechnology. Fat. Sci. Technol. 89: 582–85.
14 Oettgen HF (ed) (1989) *Gangliosides and Cancer*. VCH, Weinheim.
15 Hakomori S-I (1991) Carbohydrate-carbohydrate interaction as an initial step in cell recognition. Pure & Appl. Chem. 63: 4473–482.
16 Lüderitz O, Freudenberg MA, Galanos C, Lehmann V, Rietschel ETh, Shaw DH (1982) Lipopolysaccharides of gram negative bacteria. Curr. Topics Membr. Transport 17: 79–151.
17 Rietschel ETh, Wollenweber HW, Brade H, Zähringer U, Lindner B, Seydel V, Bradeczek H, Barnickel G, Labischinski H, Giesbrecht P (1984) Structure and conformation of the lipid A component of lipopolysaccharides. In: ETh Rietschel (ed): *Handbook of Endotoxin*. Vol. 1, Elsevier Science Publishers B.V., Amsterdam, 187–220.
18 Langworthy TA (1982) Lipids of bacteria living in extreme environments. Curr. Topics Membr. Transport 17: 45–78.
19 Luzzati V, Gambacorta A, de Rosa M, Gulik A (1987) Polar lipids of thermophilic prokaryotic organisms. Ann. Rev. Biophys. Chem. 16: 25–47.
20 Ourisson G, Rohmer M, Roralla K (1987) Prokaryotic Hopanoids and Other Polyterpenoid Sterol Surrogates. Ann. Rev. Microbiol. 41: 301–33.
21 Demel RA, de Kruyff B (1976) The function of sterols in membranes review. Biochim. Biophys. Acta 457: 109–32.
22 Yeagle, PL (1985) Cholesterol and the cell membrane. Biochim. Biophys. Acta 822: 267–287.
23 Razin S (1982) Sterol in Mycoplasma Membranes. Curr. Topics Membr. Transport 17: 183–206.
24 Kannenberg E, Poralla K, Blume A (1980) A hopanoid from the thermo-acidophilic *Bacillus acidocaldarius* condenses membranes. Naturwiss. 67: 458–459.
25 Kannenberg E, Blume, A, McElhaney RN, Poralla K (1983) Monolayer and calorimetric studies of phosphatidylcholines containing branched-chain fatty acids and of their

interactions with cholesterol and with a bacterial hopanoid in model membranes. Biochim. Biophys. Acta 733: 111–116.
26 Bringer S, Härtner T, Poralla K, Sahm H (1985) Influence of ethanol on the hopanoid content and the fatty acid pattern in batch and continuous cultures of Zymomonas mobilis. Arch. Microbiol. 140: 312–316.
27 Tanford C (1980) *The Hydrophobic Effect*, 2nd ed., John Wiley, New York.
28 Israelachvili J (1992) *Intermolecular and Surface Forces*. 2nd ed., Academic Press, New York.
29 Privalov PL, Gill DJ (1988) Stability of protein structure and hydrophobic interaction. Adv. Protein Chem. 39: 191–234.
30 Blokzijl W, Engberts JBFN (1993) Hydrophobe Effekte – Ansichten und Tatsachen. Angew. Chem. 105: 1610–1648.
31 Privalov PL (1989) Thermodynamic problems of protein structure. Ann. Rev. Biophys. Chem. 18: 47–49.
32 Caffrey M, Cheng A (1995) Kinetics of lipid phase changes. Curr. Opin. Struct. Biol. 5: 548–555.
33 Chapman D (ed) (1968) *Biological Membranes*. Academic Press, London.
34 Small DM (ed) (1986) *The Physical Chemistry of Lipids. Handbook of Lipid Research.* Vol 4, Plenum Press, New York.
35 Blume A (1991) Biological calorimetry: membranes. Thermochim. Acta 193: 299–347.
36 Blume A, Garidel P (1999) Lipid model membranes and biomembranes. In: RB Kemp (ed) *Handbook of Thermal Analysis and Calorimetry*. Vol. 4 *From Macromolecules to Man.* Elsevier Science B.V., Amsterdam, 109–173.
37 Huang C, Mason JT (1986) Structure and properties of mixed-chain phospholipid assemblies. Biochim. Biophys. Acta 864: 423–470.
38 Simon SA, McIntosh TJ (1984) Interdigitated hydrocarbon chain packing causes the biphasic transition behavior in lipid/alcohol suspensions. Biochim. Biophys. Acta 773: 169–172.
39 Eibl H, Blume A (1979) The influence of charge on phosphatidic acid bilayer membranes. Biochim. Biophys. Acta 553: 476–488.
40 Marsh D, Watts A, Smith ICP (1983) Dynamic structure and phase behavior of dimyristoyl-phosphatidylethanolamine bilayers studied by deuterium nuclear magnetic resonance. Biochemistry 22: 3023–3026.
41 Hübner W, Blume A (1987) ^{2}H-NMR-spectroscopic investigations of phospholipid bilayers. Ber. Bunsenges Phys. Chem. 91: 1127–1132.
42 Boggs JM (1987) Lipid intermolecular hydrogen bonding: Influence on structure organization and membrane function. Biochim. Biophys. Acta 906: 353–404.
43 Blume A (1988) ^{2}H and ^{13}C-NMR-spectroscopy of lipid model membranes. In: C Hidalgo (ed) *Physical Properties of Biological Membranes and Their Functional Implications.* Plenum Press, New York, 21–70.
44 Baenziger JE, Jarell HC, Smith CP (1992) molecular motions and dynamics of a diunsaturated acyl chain in a lipid bilayer: implications for the role of polyunsaturation in biological membranes. Biochemistry 31: 3377–3385.
45 Tate MW, Eikenberry EF, Turner DC, Shyamsunder E, Gruner SM (1991) Nonbilayer phases of membrane lipids. Chem. Phys. Lipids 57: 147–164.
46 Siegel DP, Epand RM (1997) The mechanism of lamellar-to-inverted hexagonal phase transitions in phosphatidylethanolamine: implications for membrane fusion mechanisms. Biophys J 73: 3089–3111.
47 Helfrich W (1973) Elastic properties of lipid bilayers: Theory and possible experiments. Z Naturforsch 28c: 693–703.
48 Helfrich W (1995) Tension-induced mutual adhesion and a conjectured superstructure of lipid membranes. In: R Lipowsky, E. Sackmann (eds): *The Structure and Dynamics of Membranes. Handbook of Biological Physics*. Vol 1, Elsevier Science, Amsterdam, 691–722.
49 Luzzati V (1968) X-ray diffraction studies of lipid-water systems. In: D Chapman (ed.): *Biological Membranes*, Vol. 1, Academic Press, New York, 71–123.
50 Seddon JM, Cevc G, Marsh D (1983) Calorimetric studies of the gel-fluid (L_{β}-L_{α}) and lamellar inverted hexagonal (L_{α}-H_{II}). Phase transitions in dialkyl and diacylphophatidyl ethanolamines. Biochemistry 22: 1280–1289.

51 Tate MW, Gruner SM (1989) Temperature dependence of the structural dimensions of the inverted hexagonal (H_{II}) phase of phosphatidylethanolamine-containing membranes. Biochemistry 28: 4245–4253.
52 Gawrisch K, Parsegian VA, Hajduk DA, Tate MW, Gruner SM, Fuller NL, Rand RP (1992) Energetics of a hexagonal-lamellar-hexagonal-phase transition sequence in dioleoylphosphatidylethanolamine membranes. Biochemistry 31: 2856–2864.
53 Rand RP, Fuller NL, Gruner SM, Parsegian VA (1990) Membrane curvature, lipid segregation, and structural transition for phospholipids under dual-solvent stress. Biochemistry 29: 76–87.
54 Siegel DP (1993) Energetics of intermediates in membrane fusion: comparison of stalk and inverted micellar intermediate mechanisms. Biophys. J. 65: 2124–2140.
55 Kinnunen PKJ (1996) On the mechanisms of the lamellar → hexagonal H_{II} phase transition and the biological significance of the H_{II} propensity. In: DD Lasic, Y Barenholz (eds): *Handbook of Nonmedical Applications of Liposomes*, Vol I, CRC Press, Boca Raton, 153–171.
56 Siegel DP, Epand RM (1997) The mechanism of lamellar-to-inverted hexagonal phase transitions in phosphatidylethanolamine: implications for membrane fusion mechanisms. Biophys. J. 73: 3089–3111.
57 Lewis RN, McElhaney RN, Harper PE, Turner DC, Gruner SM (1994) Studies of the thermotropic phase behavior of phosphatidylcholines containing 2-alkyl substituted fatty acyl chains: a new class of phosphatidylcholines forming inverted nonlamellar phases. Biophys. J. 66: 1088–1103.
58 Siegel DP (1984) Inverted micellar structures in bilayer membranes. Biophys. J. 45: 399–420.
59 Siegel DP (1986) Inverted micellar intermediates and the transitions between lamellar, cubic, and inverted hexagonal lipid phases. I. Mechanism of the $L_{\alpha} \rightarrow H_{II}$ phase transitions. Biophys. J. 49: 1155–1170.
60 Lohner K (1991) Effects of small organic molecules on phospholipid phase transitions. Chem. Phys. Lipids 57: 341–362.
61 Ostermeier C, Michel H (1997) Crystallization of membrane proteins. Curr. Opin. Struct. Biol. 7: 697–701.
62 Luzzati V (1997) Biological significance of lipid polymorphism: the cubic phases. Curr. Opin. Struct. Biol. 7: 661–668.
63 Chang CM, Bodmeier R (1997) Swelling of and drug release from monoglyceride-based drug delivery systems. J. Pharm. Sci. 86: 747–752.
64 Lesile SB, Puvvada S, Ratna BR, Rudolph AS (1996) Encapsulation of hemoglobin in a bicontinuous cubic phase lipid. Biochim. Biophys. Acta 1285: 246–254.
65 Adamson AW, Gast AP (1997) *Physical Chemistry of Surfaces*. 6th Edition, John Wiley, New York.
66 Blume A (1978) A comparative study of the phase transition of phospholipid bilayers and monolayers. Biochim. Biophys. Acta 557: 32–44.
67 Albrecht O, Gruler H, Sackmann E (1978) Polymorphism of phospholipid monolayers. J. Phys. 39: 301–313.
68 Lösche M, Möhwald H (1984) Impurity controlled phase transitions of phospholipid monolayers. Eur. Biophys. J. 11: 35–42.
69 Weis RM, McConnell HM (1984) Two-dimensional chiral crystals of phospholipid. Nature 310: 47–49.
70 Lösche M, Duwe HP, Möhwald H (1988) quantitative analysis of surface textures in phospho-lipid monolayer phase transitions. J. Coll. Interf. Sci. 126: 432–444.
71 Möhwald H (1990) Phospholipid and phospholipid-protein monolayers at the air/water interface. Ann. Rev. Phys. Chem. 41: 441–476.
72 Knobler CM (1990) Recent developments in the study of monolayers at the air-water interface. Adv Chem. Phys. 77: 397–449.
73 McConnell HM (1991) Structures and transitions in lipid monolayers at the air-water interface. Ann. Rev. Phys. Chem. 42: 171–195.
74 Hönig D, Möbius D (1991) Direct visualization of monolayers at the air-water interface by Brewster angle microscopy. J. Phys. Chem 95: 4590–4592.
75 Henon S, Meunier J (1991) Microscope at the Brewster angle. Direct observation of first-order phase transitions in monolayers. Rev. Sci. Instrum. 62: 936–939.

76 Demel RA, Geurts von Kessel WSM, Zwaal RFA, Roelofson B, van Deenen LLM (1975) Relation between various phopholipase actions on human red cell membranes and the interfacial phospholipid pressure in membranes. Biochim. Biophys. Acta 406: 97–107.
77 Seelig A (1992) Interaction of substance P agonist and of substance P antagonists with lipid membranes. A thermodynamic model. Biochemistry 31: 2897–2904.
78 Marsh D (1996) Lateral pressures in membranes. Biochim. Biophys. Acta 1286: 183–223.
79 Zuckermann MJ, Pink DA, Costas M, Sanctuary BC (1982) A theoretical model for phase transitions in lipid monolayers. J Chem. Phys. 76: 4206–4216.
80 Demel RA, Yin CC, Lin BZ, Hauser H (1992) Monolayer characteristics and thermal behaviour of phosphatidic acids. Chem. Phys. Lipids 60: 209–223.
81 Demel RA, Jordi W, Lambrechts H, van Damme H, Hovius R, de Kruijff B (1989) Differential interactions of apo- and holocytochrome c with acidic membrane lipids in model systems and the implications for their import into mitochondria. J. Biol. Chem. 264: 3988–3997.
82 Heckl WM, Zaba BN, Möhwald H (1987) Interactions of cytochromes b5 and c with phospholipid monolayers. Biochim. Biophys. Acta 903: 166–176.
83 Grainger DW, Reichert A, Ringsdorf H, Salesse C (1990) Hydrolytic action of phospholipase A2 in monolayers in the phase transition region: direct observation of enzyme domain formation using fluorescence microscopy. Biochim. Biophys. Acta 1023: 365–379 .
84 Signor G, Mammi S, Peggion E, Ringsdorf H, Wagenknecht A (1994) Interaction of bombolitin III with phospholipid monolayers and liposomes and effect on the activity of phospholipase A2. Biochemistry 33: 6659–6670.
85 Als-Nielsen J, Jacquemain D, Kjaer K, Leveiller F, Lahav M, Leiserowitz L (1994) Principles and applications of grazing incidence x-ray and neutron scattering from ordered molecular monolayers a the air-water interface. Phys. Rep. 246: 251–313.
86 Thomas RK, Penfold J (1996) Neutron and X-Ray Reflectometry of interfacial systems in colloid and polymer chemistry. Curr. Opin. Colloid Interface Sci 1: 23–33.
87 Montal M, Mueller P (1972) Formation of bimolecular membranes from lipid monolayers and a study of their electrical properties. Proc. Natl. Acad. Sci. USA 64: 3561.
88 Tien HT (1985) Planar bilayer lipid membranes. Prog. Surf. Science 19: 169–274.
89 Winterhalter M (1996) Liposomes in electric fields. In: DD Lasic, Y Barenholz (eds): *Handbook of Nonmedical Applications of Liposome,* Vol. 1, CRC Press, Boca Raton 285–307.
90 Schindler H (1989) Planar lipid-protein membranes: strategies of formation and of detecting dependencies of ion transport functions on membrane conditions. Methods Enzymol. 171: 225–53.
91 Urry DW, Trapane TL, Venkatachalam CM, McMichens Rb (1989) Ion interactions at membranous polypeptide sites using nuclear magnetic resonance: determining rate and binding constants and site locations. Methods Enzymol. 171: 286–342.
92 Wallace BA (1990) Gramicidin channels and pores. Ann. Rev. Biophys. Chem. 19: 127–157.
93 Menestrina G, Voges KP, Jung G, Boheim G (1986) Voltage dependent channel formation by rods of helical polypeptides. J. Membrane Biol. 93: 111–132.
94 Darszon A (1986) Planar bilayers. A powerful tool to study membrane proteins involved in ion transport. Methods Enzymol. 127: 486–502.
95 Butt HJ, Fendler K, Bamberg E, Tittor JOD (1989) Aspartic acids 96 and 85 play a central role in the function of bacteriorhodopsin as a proton pump. EMBO J. 8: 1653–1657.
96 Haupts U, Bamberg E, Oesterhelt D (1996) Different modes of proton translocation by sensory rhodopsin I. EMBO J. 15: 1834–1841.
97 Wilhelm C, Winterhalter M, Zimmermann U, Benz R (1993) Kinetics of pore size during irreversible electrical breakdown of lipid bilayer membranes. Biophys. J. 64: 121–128.
98 Lasic DD (1993) *Liposomes: From Physics to Applications*. Elsevier, Amsterdam.
99 Woodle MC, Papahadjopoulos D (1989) Liposome preparation and size characterization. Methods Enzymol. 171: 193–217.
100 Hope MJ, Bally MB, Mayer LD, Janoff AS, Cullis PR (1986) Generation of multilamellar and unilamellar phospholipid vesicles. Chem. Phys. Lipids 40: 89–107.

101 MacDonald RC, MacDonald RI, Mence BPhM, Takeshita K, Subbarao NK, Hu LR (1991) Small-volume extrusion apparatus for preparation of large, unilamellar vesicles. Biochim. Biophys. Acta 1061: 297–303.
102 Szoka F, Papahadjopoulos D (1981) In: CG Knight (ed.): *Liposomes: From Physical Structure to Therapeutic Application*, Elsevier, Amsterdam, 51.
103 Allen JM (1984) In: G Gregoriadis (ed): Liposome Technology, Vol. 1, CRC Press, Boca Raton, Florida, 109.
104 Evans E, Needham D (1987) Physical properties of surfactant bilayer membranes: thermal transitions elasticity, rigidity, cohesion, and colloidal interaction. J. Phys. Chem 91: 4219–4228.
105 Evans E, Ritchie K, Merkel R (1995) Sensitive force technique to probe molecular adhesion and structural linkages at biological interfaces. Biophys. J. 68: 2580–2587.
106 Evans E, Ritchie K (1997) Dynamic strength of molecular adhesion bonds. Biophys. J. 72: 1541–1555.
107 Privalov PL, Plotnikov VV, Filimonov VV (1975) Precision scanning microcalorimeter for the study of lipids. J. Chem. Thermodynam. 7: 41–47.
108 Blume A (1983) Apparent molar heat capacities of phospholipids in aqueous dispersion effects of chain length and head group structure. Biochemistry 22: 5436–5442.
109 Blume A (1988) Applications of calorimetry to model membranes. In: C Hidalgo (ed.): *Physical Properties of Biological Membranes and Their Functional Implications.* Plenum Publishing Corp., New York, 71–121.
110 Blume A, Garidel P (1999) Lipid model membranes and biomembranes. In: RB Kemp (ed.): *Handbook of Thermal Analysis and Calorimetry. Vol 4. From Macromolecules to Man.* Elsevier Science B.V., Amsterdam, Chapter 3, 109–173.
111 Plotnikov VV, Brandts JM, Lin LN, Brandts JF (1998) A new ultrasensitive scanning calorimeter. Anal. Biochem. 250: 237–244.
112 Träuble H (1971) Phasenumwandlungsen in Lipiden. Mögliche Schaltprozesse in biologischen Membranen. Naturwiss. 58: 277–284.
113 Bendzko PI, Pfeil WA, Privalov PL, Tiktopulo EI (1988) Temperature-induced phase transitions in proteins and lipids. Volume and heat capacity effects. Biophys. Chem. 29: 301–307.
114 Lee AG (1977) Lipid phase transitions and phase diagrams. II. Mixtures involving lipids. Biochim. Biophys. Acta 472: 285–344.
115 Tenchov BG (1985) Nonuniform lipid distribution in membranes. Prog. Surf. Science 20: 273–340.
116 Johann C, Garidel P, Mennicke L, Blume A (1996) New approaches to the simulation of heat-capacity curves and phase diagrams of pseudobinary phospholipid mixtures. Biophys. J. 71: 3215–3228.
117 Garidel P, Johann C, Blume A (1997) Non-ideal mixing and phase separation in phosphatidylcholine-phosphatidic acid mixtures as a function of ph and chain length. Biophys. J. 72: 2196–2210.
118 Garidel P, Johann C, Mennicke L, Blume A (1997) The mixing behaviour of pseudobinary phosphatidylcholine-phosphatidylglycerol mixtures as a function of ph and chain length. Eur Biophys. J. 26: 447–459.
119 Garidel P, Blume A (1998) Miscibility of phospholipids with identical headgroups and acyl chain lengths differing by two methylene units: Effects of headgroup structure and headgroup charge. Biochim. Biophys. Acta 1371: 83–95.
120 Garidel P, Blume A (2000) The mixing behavior of pseudobinary phosphatidylethanolamine-phosphatidylglycerol mixtures as a function of pH and acyl chain length. Eur. Biophys. J. 28: 629–638.
121 Blume A, Eibl H (1979) The influence of charge on bilayer membranes. Calorimetric investigations of phosphatidic acids. Biochim. Biophys. Acta 558: 13–21.
122 Cevc G (1990) Membrane electrostatics. Biochim. Biophys. Acta 1031: 311–382.
123 Blume A, Tuchtenhagen J (1992) Thermodynamics of ion binding to phosphatidic acid bilayers. Titration calorimetry of the heat dissociation of DMPA. Biochemistry 31: 4636–4642.
124 Garidel P, Blume A (1999) Interaction of alkaline earth cations with the negatively charged phospholipid 1,2-dimyristoyl-*sn*-glycero-3-phosphoglycerol: a differential scanning and isothermal titration calorimetry study. Langmuir 15: 5526–5534.

125 McElhaney RN (1986) Differential scanning calorimetric studies of lipid-protein interactions in model membrane systems. Biochim. Biophys. Acta 864: 361–421.
126 Giehl A, Lemm T, Bartelsen O, Sandhoff K, Blume A (1999) Interaction of the GM2-activator protein with phospholipid/ganglioside bilayer membranes and with monolayers at the air/water interface. Eur. J. Biochem. 261: 650–658.
127 Seelig J (1997) Titration calorimetry of lipid-peptide interactions. Biochim. Biophys. Acta 1331: 103–116.
128 Paula S, Süs W, Tuchtenhagen J, Blume A (1995) Thermodynamics of micelle formation as a function of temperature: a high sensitivity titration calorimetry study. J. Phys. Chem 99: 11742–11751.
129 Garidel P, Hildebrand A, Neubert R, Blume A (2000) Thermodynamic characterization of bile salt micelle formation as a function of temperature and ionic strength using isothermal titration calorimetry. Langmuir 16: 5267–5275.
130 Majhi PR, Blume A (2001) Thermodynamic characterization of temperature-induced micellization and demicellization of detergents studied by differential scanning calorimetry. Langmuir 17: 3844–3851.
131 Heerklotz H, Lantzsch G, Binder H, Klose G, Blume A (1996) Thermodynamic Characterization of Dilute Aqueous Lipid/Detergent Mixtures of POPC and $C_{12}EO_8$ by Means of Isothermal Titration Calorimetry. J. Phys. Chem 100: 6764–6774.
132 Keller M, Kerth A, Blume A (1997) Thermodynamics of interaction of octyl glucoside with phosphatidylcholine vesicles: partitioning and solubilization as studied by high sensitivity titration calorimetry. Biochim. Biophys. Acta 1326: 178–192.
133 Opatowski E, Kozlov MM, Lichtenberg D (1997) Partitioning of octyl glucoside between octyl glucoside/phosphatidylcholine mixed aggregates and aqueous media as studied by isothermal titration calorimetry. Biophys. J. 73: 1448–1457.
134 Hildebrand A, Neubert R, Garidel P, Blume A (2002) Bile salt induced solubilization of synthetic phosphatidylcholine vesicles studied by means of isothermal titration calorimetry. Langmuir 18: 2836–2847.
135 Hauser H, Pascher I, Pearson RH, Sundell S (1981) Preferred conformation and molecular packing of phosphatidylethanolamine and phosphatidylcholine. Biochim. Biophys. Acta 650: 21–51.
136 Caffrey M (1989) Structural, mesomorphic and time-resolved studies of biological liquid crystals and lipid membranes using synchrotron x-radiation. Topics Curr. Chem. 151: 75–109.
137 Laggner P, Kriechbaum M (1991) Phospholipid phase transitions: kinetics and structural mechanisms. Chem. Phys. Lipids 57: 121–145.
138 Katsaras J (1995) X-ray diffraction studies of oriented lipid bilayers. Biochem. Cell Biol. 73: 209–218.
139 Hitchcock PB, Mason R, Thomas KM, Shipley GG (1974) Structural chemistry of 1,2 dilauroyl-DL-phosphatidylethanolamine: molecular conformation and intermolecular packing of phospholipids. Proc. Natl. Acad. Sci. USA 71: 3036–3040.
140 Pearson RH, Pascher I (1979) The molecular structure of lecithin hydrates. Nature 281: 499–501.
141 Harlos K, Eibl H, Pascher I, Sundell S (1984) Conformational and packing properties of phosphatidic acid: the crystal structure of monosodium dimyristoylphosphatidate. Chem. Phys. Lipids 34: 115–126.
142 Pascher I, Sundell S, Harlos K, Eibl H (1987) Conformation and packing properties of membrane lipids: The crystal structure of sodium dimyristoylphosphatidylglycerol. Biochim. Biophys. Acta 896: 77–88.
143 McIntosh TV, McDaniel RV, Simon SA (1983) Induction of interdigitated gel phase in fully hydrated phosphatidylcholine bilayers. Biochim. Biophys. Acta 731: 109–114.
144 Braganza LF, Worcester DL (1986) Hydrostatic pressure induces hydrocarbon chain interdigitation in single-component phospholipid bilayers. Biochemistry 25: 2596–2599.
145 Ruocco MJ, Simonovitch DJ, Griffin RG (1985) Comparative study of the gel phases of ether- and ester-linked phosphatiylcholines. Biochemistry 24: 2406–2411.
146 Katsaras J (1995) X-ray diffraction studies of oriented lipid bilayers. Biochem. Cell Biol. 73: 209–218.
147 Meister A, Förster G, Blume A (2000) Energy calculations related to aliphatic chain-packing modes. Progr. Coll. Interf. Sci. 115: 259–264.

148 Förster G, Meister A, Blume A (2000) Van der Waals energy contour map describing the orthorhombic hydrocarbon chain packing of symmetry Pbnm. Phys. Chem. Chem. Phys. 2: 4503–4508.
149 Förster G, Meister A, Blume A (2001) Chain packing modes in crystalline surfactant and lipid bilayers. Curr. Opin. Coll. Interf. Sci. 6: 294–302.
150 Worcester DL, Franks NP (1976) Structural analysis of hydrated egg lecithin and cholesterol bilayers. II neutron diffraction. J. Mol. Biol. 100: 359–378.
151 Seelig J, Seelig A (1980) Lipid conformation in model membranes and biological membranes. Quart. Rev. Biophys. 13: 19–61.
152 Knoll W, Schmidt G, Sackmann E (1983) Critical demixing in fluid bilayers of phospholipid mixtures. A neutron diffraction study. J. Chem. Phys. 797: 3439–3442.
153 Büldt G, Seelig J (1980) Conformation of phosphatidylethanolamine in the gel phase as seen by neutron diffraction. Biochemistry 19: 6170–6175.
154 Amey RL, Chapman D (1984) Infrared spectroscopic studies of model and natural membranes. In: D Chapman (ed): *Biomembrane Structure and Function*, Verlag Chemie, Weinheim, 199–256.
155 Mendelsohn R, Mantsch HH (1986) Fourier transform infrared studies of lipid-protein interaction. In: A Watts, JJHHM de Pont (eds.): *Progress in Protein-Lipid-Interaction* 2, Elsevier Science Publisher BV, Amsterdam, 103–146.
156 Griffiths PR, De Haseth JA (1986) *Fourier Transform Infrared Spectroscopy*. John Wiley, New York.
157 Fringeli UP (1977) The structure of lipids and proteins studied by attenuated total reflection (ATR) infrared spectroscopy. II Oriented layers of a homologous series: Phosphatidylethanolamine to phosphatidylcholine. Z. Naturforsch. 320: 20–45 .
158 Ter-Minassian-Saraga L, Okamura E, Umemura J, Takenaka T (1988) Fourier transform infrared-attenuated total reflection spectroscopy of hydration of dimyristoylphosphatidylcholine multibilayers. Biochim. Biophys. Acta 946: 417–423.
159 Okamura E, Umemura J, Takenaka T (1990) Orientation studies of hydrated dipalmitoylphosphatidylcholine multibilayers by polarized FTIR-ATR spectroscopy. Biochim. Biophys. Acta 1025: 94–98.
160 Dluhy RA (1989) Langmuir revisited: using infrared reflectance spectroscopy to determine monolayer structure at liquid interfaces. Proc. SPIE-Int. Soc. Opt. Eng. 1145: 22–27.
161 Dluhy RA, Reilly KE, Hunt RD, Mitchell ML, Mautone AJ, Mendelsohn R (1989) Infrared spectroscopic investigations of pulmonary surfactant. Surface film transitions at the air-water interface and bulk phase thermotropism. Biophys. J. 56: 1173–1181.
162 Mantsch HH, Moffatt DJ, Casal HL (1988) Fourier transform methods for spectral resolution enhancement. J. Molec. Struct. 173: 285–288.
163 Blume A, Hübner W, Messner G (1988) Fourier transform infrared spectroscopy of $^{13}C{=}O$ labeled phospholipids. hydrogen bonding to carbonyl groups. Biochemistry 27: 8239–8249.
164 Rahmelow K, Hubner W, Ackermann T (1998) Infrared absorbances of protein side chains. Anal. Biochem. 257: 1–11.
165 Tuchtenhagen J, Ziegler W, Blume A (1994) Acyl chain conformational ordering in liquid-crystalline bilayers: comparative FT-IR and ^{2}H-NMR studies of phospholipids differing in headgroup structure and chain length. Eur. Biophys. J. 23: 323–335.
166 Cameron DG, Casal HL, Mantsch HH, Boulanger Y, Smith ICP (1981) The thermotropic behavior of dipalmitoyl phosphatidylcholine bilayers. A. Fourier transform infrared study of specifically labeled lipids. Biophys. J. 35: 1–16.
167 Ziegler W, Blume A (1995) Acyl chain conformational ordering of individual components in liquid-crystalline bilayers of mixtures of phosphatidylcholines and phosphatidic acids. A comparative FT-IR and ^{2}H-NMR study. Spectrochim. Acta A 51: 1763–1768.
168 Senak L, Davies MA, Mendelsohn R (1991) A quantitative IR study of hydrocarbon chain conformation in alkanes and phospholipids: CH_2-wagging modes of disordered bilayers and H_{II} phases. J. Phys. Chem 95: 2565–2571.
169 Senak L, Moore D, Mendelsohn R (1992) Methylene wagging progressions as IR probes of slightly disordered phospholipid acyl chain states. J. Phys. Chem 96: 2749–2754.

170 Mendelsohn R, Davies MA, Brauner JW, Schuster H, Dluhy RA (1989) Quantitative determination of conformational disorder in the acyl chains of phospholipid bilayers by infrared spectroscopy. Biochemistry 28: 8934–8939.
171 Davies MA, Hübner W, Blume A, Mendelsohn R (1992) Acyl chain conformational ordering in 1,2-dipalmitoyl-phosphatidylethanolamine. integration of FT-IR and ^{2}H-NMR-results. Biophys. J. 63: 1059–1062.
172 Blume A, Hübner W, Müller M, Bäuerle HD (1988) Structure and dynamics of lipid model membranes. FT-IR and ^{2}H-NMR-studies. Ber Bunsenges Phys Chem 92: 964–973.
173 Huebner W, Mantsch HH (1991) Orientation of specifically ^{13}C=O labeled phosphatidylcholine multilayers from polarized attenuated total reflection FT-IR-spectroscopy. Biophys. J. 59: 1261–1272.
174 Lewis RNAH, McElhaney RN, Pohle W, Mantsch HH (1994) Components of the carbonyl stretching band in the infrared spectra of hydrated 1,2-diacylglycerolipid bilayers: a re-evaluation. Biophys. J. 67: 2367–2375.
175 Brandenburg K, Seydel V (1986) Orientation measurements on ordered multibilayers of phospholipids and sphingolipids from synthetic and natural origin by ATR Fourier transform infrared spectroscopy. Z. Naturforsch. 41c: 453–467.
176 Müller E, Giehl A, Sandhoff K, Schwarzmann G, Blume A (1996) Oriented 1,2-dimyristoyl-*sn*-glycero-3-phosphorylcholine/ganglioside membranes: a Fourier transform infrared attenuated total reflection spectroscopic study. Band assignments; orientational, hydrational, and phase behavior, and effects of Ca^{2+} binding. Biophys. J. 71: 1400–1421.
177 Hübner W, Blume A (1998) Interactions at the lipid-water-interface. Chem. Phys. Lipids 96: 99–123.
178 Mendelsohn R, Brauner JW, Gericke A (1996) External infrared reflection absorption spectrometry of monolayer films at the air-water interface. Ann. Rev. Phys. Chem. 46: 305–343.
179 Gericke A, Brauner JW, Erukulla RK, Bittman R, Mendelsohn R (1997) *In-situ* investigation of partially deuterated fatty acid and phospholipid monolayers at the air-water interface by IR reflection-absorption spectroscopy. Thin Solid Films 292: 330–332.
180 Gericke A, Kerth A, Blume A (1999) Infrared spectroscopic investigation of lipid and protein monolayers at the air-water interface. Bruker Application Note #51, 1–10.
181 Mendelsohn R, Maisano J (1978) Use of deuterated phospholipids in raman spectroscopic sudies of membrane structure. I. Multilayers of dimyristoyl phosphatidylcholine (and its -d_{54} derivative) with distearoyl phosphatidylcholine. Biochim. Biophys. Acta 506: 192–201.
182 Vogel H, Jähnig F(1981) Conformational order of the hydrocarbon chains in lipid bilayers. A Raman spectroscopic study. Chem. Phys. Lipids 29: 83–101.
183 Devlin MT, Levin IW (1989) Raman spectroscopic studies of the packing properties of mixed dihexadecyl- and dipalmitoylphosphatidylcholine bilayer dispersions. Biochemistry 28: 8912–8920.
184 Vincent JS, Levin IW (1991) Raman spectroscopic studies of dimyristoylphosphatidic acid and its interactions with ferricytochrome c in cationic binary and ternary lipid-protein complexes. Biophys. J. 59: 1007–1021.
185 Sato H, Borchman D, Ozaki Y, Lamba OP, Byrdwell WC, Yappert MC, Paterson CA (1996) Lipid-protein interactions in human and bovine lens membranes by Fourier transform Raman and infrared spectroscopies. Exp. Eye Res. 62: 47–53.
186 Wegener M, Neubert R, Rettig W, Wartewig S (1997) Structure of stratum corneum lipids characterized by FT-Raman spectroscopy and DSC. III. Mixtures of ceramides and cholesterol. Chem. Phys. Lipids 88: 73–82.
187 Lawson EE, Anigbogu AN, Williams AC, Barry BW, Edwards HG (1998) Thermally induced molecular disorder in human stratum corneum lipids compared with a model phospholipid system; FT-Raman spectroscopy. Spectrochim. Acta A Mol. Biomol. Spectrosc. 54A: 543–558.
188 Berliner LJ (1979) *Spin Labelling II: Theory and Application*, Academic Press, New York.
189 Berliner LJ, Reuben J (eds.) (1989) *Biological Magnetic Resonance*. Vol. 8. Plenum Press, New York.

190 Moser M, Marsh D, Meier P, Wassmer K-H, Kothe G (1989) Chain configuration and flexibility gradient in phospholipid membranes. Comparison between spin-label electron spin resonance and deuteron nuclear magnetic resonance, and identification of new conformations. Biophys. J. 55: 111–123.
191 Träuble H, and Sackmann E. (1972) Studies of the crystalline-liquid crystalline phase transition of lipid model membranes. III. Structure of a steroid-lecithin system below and above the lipid transition. J Am Chem Soc 94: 4499–4510.
192 Devaux P, McConnell HM (1972) Lateral diffusion in spin-labeled phosphatidylcholine multilayers. J. Am. Chem. Soc. 94: 4475–4481.
193 Kornberg Rd, McConnell HM (1970) Inside-outside transitions of phospholipids in vesicle membranes. Biochemistry 10: 1111–1120.
194 Shin YK, Freed JH (1989) Dynamic imaging of lateral diffusion by electron spin resonance and study of rotational dynamics in model membranes. Effect of cholesterol. Biophys. J. 55: 537–550.
195 Marsh D (1987) Selectivity of lipid-protein-interactions. J. Bioenergetics Biomembr. 19: 677–689.
196 Marsh D (1997) Stoichiometry of lipid-protein interaction and integral membrane protein structure. Eur. Biophys. J. 26: 203–208.
197 Marsh D (1997) Magnetic resonance of lipids and proteins in membranes. Curr. Opin. Coll. Interface Sci. 2: 4–14.
198 Patyal BR, Crepeau RH, Freed JH (1997) Lipid-gramicidin interactions using two-dimensional Fourier-transform electron spin resonance. Biophys. J. 73: 2201–2220.
199 Cassol R, Ge MT, Ferrarini A, Freed JH (1997) Chain dynamics and the simulation of electron spin resonance spectra from oriented phospholipid membranes. J. Phys. Chem B 101: 8782–8789.
200 Ernst RR, Bodenhausen G, Wokaun A (1987) *Principles of Nuclear Magnetic Resonance in One and Two Dimensions*. Oxford University Press, Oxford.
201 Seelig J (1977) Deuterium magnetic resonance: theory and application to lipid membranes. Q. Rev. Biophys. 10: 353–418.
202 Griffin RG (1981) Solid state nuclear magnetic resonance of lipid bilayers. Methods Enzymol. 72: 108–173.
203 Yeagle PL (1996) Characterization of liposomes and vesicles by ^{31}P-NMR. In: DD Lasic, Y Barenholz (eds.): *Nonmedical Applications of Liposomes*. Vol. 2, CRC, Boca Raton, Fla., 77–84.
204 Spiess HW (1985) Deuteron NMR – A new tool for studying chain mobility and orientation in polymers. Adv. Polymer Sci. 66: 23–57.
205 Meier P, Ohmes E, Kothe G, Blume A, Weidner J, Eibl HJ (1983) Molecular order and dynamics of phospholipid membranes. A deuteron magnetic resonance study employing a comprehensive line-shape model. J. Phys. Chem 87: 4904–4912.
206 Mayer C, Mueller K, Weisz K, Kothe G (1988) Deuteron NMR relaxation studies of phospholipid membranes. Liq. Cryst. 3: 797–806.
207 Siminovitch DJ, Ruocco MJ, Olejniczak ET, Das Gupta SK, Griffin RG (1988) Anisotropic deuterium nuclear magnetic resonance spin-lattice relaxation in cerebroside- and phospholipid-cholesterol bilayer membranes. Biophys. J. 54: 373–381.
208 Jarrell HC, Smith ICP, Jovall PA, Mantsch HH, Siminovitch DJ (1988) Angular dependence of deuteron NMR relaxation rates in lipid bilayers. J Chem. Phys. 88: 1260–1263.
209 Browning JL, Seelig J (1980) Bilayers of phosphatidylserine: A deuterium and phosphorous nuclear magnetic resonance study. Biochemistry 19: 1262–1270.
210 Tilcock CPS, Cullis Pr, Hope M, Gruner SM (1986) Polymorphic phase behavior of unsaturated lysophosphatidylethanolamines. A ^{31}P NMR and x-ray diffraction study. Biochemistry 25: 816–822.
211 Cullis PR, Hope MJ, Tilcock CPS (1986) Lipid polymorphism and the roles of lipids in membranes. Chem. Phys. Lipids 40: 127–144.
212 van Gorkom LCM, Cheetham JJ, Epand RM (1995) Ganglioside GD1a generates domains of high curvature in phosphatidylethanolamine liposomes as determined by solid state ^{31}P-NMR spectroscopy. Chem. Phys. Lipids 76: 103–108.
213 Marinov R, Dufourc EJ (1996) Thermotropism and hydration properties of POPE and POPE-cholesterol systems as revealed by solid state ^{2}H and ^{31}P-NMR. Eur. Biophys. J. 24: 423–431.

214 Tilcock CPS, Bally Mb, Farren SB, Cullis PR (1982) Influence of cholesterol on the structural preferences of dioleoyl-phosphatidylethanolamine-dioleoyl-phosphatidylcholine systems: A phosphorous 31 and deuterium nuclear magnetic resonance study. Biochemistry 21: 4596–4601.
215 Milburn MP, Jeffrey KR (1987) Dynamics of the phosphate group in phospholipid bilayers. A phosphorus-31 nuclear relaxation time study. Biophys. J. 52: 791–799.
216 Dufourc EJ, Mayer C, Stohrer J, Althoff G, Kothe G (1992) Dynamics of phosphate head groups in biomembranes Comprehensive analysis using phophorus-31 nuclear magnetic resonance lineshape and relaxation time measurements. Biophys. J. 61: 42–57.
217 Haberkorn RA, Herzfeld J, Griffin RG (1978) High resolution phosphorus-31 and carbon-13 nuclear magnetic resonance spectra of unsonicated model membranes. J. Am. Chem. Soc. 100: 1296–1298.
218 Bruzik KS, Salamonczyk GM, Sobon B (1990) ^{13}C CP-MAS study of the gel phases of 1,2-dipalmitoylphosphatidylcholine. Biochim. Biophys. Acta 1023: 143–146.
219 Wittebort RJ, Blume A, Huang TH, Das Gupta SK, Griffin RG (1982) Carbon-13 nuclear magnetic resonance investigations of phase transitions and phase equilibria in pure and mixed phospholipid bilayers. Biochemistry 21: 3487–3502.
220 Petersen NO, Chan SI (1977) More on the motional state of lipid bilayer membranes: interpretation of order parameters obtained from nuclear magnetic resonance experiments. Biochemistry 16: 2657–2667.
221 Weisz K, Gröbner G, Mayer C, Stohrer J, Kothe G (1992) Deuteron nuclear magnetic resonance study of the dynamic organization of phospholipid/cholesterol bilayer membranes: molecular properties and viscoelastic behavior. Biochemistry 31: 1100–1112.
222 Blume A, Rice DM, Wittebort DJ, Griffin RG (1982) Mmolecular dynamics and conformation in the gel and liquid-crystalline phases of phosphatidylethanolamine bilayers. Biochemistry 21: 6220–6230.
223 Hübner W, Blume A (1990) 2-H-NMR-studies of oriented lipid bilayers in the gel phase. J. Phys. Chem 94: 7726–7730.
224 Auger M, Carrier D, Smith ICP, Jarell HC (1990) Elucidation of motional modes in glycoglycerolipid bilayers. A ^{2}H NMR relaxation and line-shape study. J. Am. Chem. Soc. 112: 1373–1381.
225 Blume A, Griffin RG (1982) Carbon-13 and deuterium nuclear magnetic resonance study of the interaction of cholesterol with phosphatidylethanolamine. Biochemistry 21: 6230–6242.
226 Huang TH, Lee CWB, Das Gupta SK, Blume A, Griffin RG (1993) A ^{13}C and ^{2}H nuclear magnetic resonance study of phosphatidylcholine/cholesterol interactions. characterization of liquid-gel phases. Biochemistry 32: 13277–13287.
227 Blume A, Wittebort RJ, Das Grupta SK, Griffin RG (1982) Phase equilibria, molecular conformation and dynamics in phosphatidylcholine/phosphatidylethanolamine bilayers. Biochemistry 21: 6243–6253.
228 Schorn K, Marsh D (1996) Dynamic chain conformations in dimyristoyl glycerol-dimyristoyl phosphatidylcholine mixtures. ^{2}H-NMR studies. Biophys. J. 71: 3320–3329.
229 Warschawski DE, Fellmann P, Devaux PF (1996) High-resolution ^{31}P-^{1}H two-dimensional nuclear magnetic resonance spectra of unsonicated lipid mixtures spinning at the magic-angle. Eur. Biophys. J. 25: 131–137.
230 Sternin E, Bloom M, MacKay AL (1983) DePakeing of NMR spectra. J. Magn. Res. 55: 274–282.
231 Heyn MP (1989) Order and viscosity of membranes: analysis by time-resolved fluorescence depolarization. Methods Enzymol 172: 462–471.
232 Jovin TM, Vaz WLC (1989) Rotational and translational diffusion in membranes measured by fluorescence and phosphorescence methods. Methods Enzymol. 172: 471–513.
233 Vaz WLC (1996) Consequences of phase separations in membranes. In: DD Lasic, Y Barenholz (eds): *Handbook of Nonmedical Applications of Liposomes*. Vol. 2, CRC Press, Boca Raton, 51–60.
234 Blume A (1996) Properties of lipid vesicles: FT-IR-spectroscopy and fluorescent probe dtudies. Curr. Opin. Coll. Interf. Sci. 1: 64–77.
235 Jähnig F (1979) Structural order of lipids and proteins in membranes. Evolution of fluorescence anisotropy data. Proc. Natl. Acad. Sci. USA 76: 6361–6365.

236 Jähnig F, Vogel H, Best L (1982) Unifying description of the effect of membrane proteins and lipid order. verification for the melittin/dimyristoyl-phosphatidylcholine system. Biochemistry 21: 6790–6798.
237 Pebay-Peyroula E, Dufourc EJ, Szabo AG (1994) Location of diphenyl-hexatriene and trimethylammonium-diphenyl-hexatriene in dipalmitoylphosphatidylcholine bilayers by neutron diffraction. Biophys. Chem. 53: 45–56.
238 Van der Heide U, Eviatar H, Levine YK (1996) What do probe molecules monitor in lipid bilayers? In: DD Lasic, Y Barenholz (eds.): *Handbook of Nonmedical Applications of Liposomes*. Vol. 2, CRC Press, Boca Raton, 61–76.
239 Kaiser RD, London E (1998) Location of diphenylhexatriene (DPH) and its derivatives within membranes: comparison of different fluorescence quenching analyses of membrane depth. Biochemistry 37: 8180–8190.
240 Beck K (1987) Mechanical concepts of membrane dynamics: diffusion and phase deparation in two dimensions. In: J Bereiter-Hahn, OR Anderson, W-E Reif (eds): *Cytomechanics*, Springer-Verlag, Berlin. 79–99.
241 Galla HJ, Hartmann W, Theilen V, Sackmann E (1979) On two-dimensional passive randon walk in lipid bilayers and fluid pathways in biomembranes. J. Membrane Biol. 48: 215–236.
242 Sassaroli M, Vauhkonen M, Perry D, Eisinger J (1990) Lateral diffusivity of lipid analogue excimeric probes in dimyristoylphosphatidylcholine bilayers. Biophys. J. 57: 281–290.
243 Caruso F, Grieser F, Thistlethwaite PJ, Almgren M (1993) Two-dimensional diffusion of amphiphiles in phospholipid monolayers at the air-water interface. Biophys. J. 65: 2493–2503.
244 Almeida PFF, Vaz WLC, Thompson TE (1993) Percolation and diffusion in three-component lipid bilayers: effect of cholesterol on an equimolar mixture of two phosphatidylcholines. Biophys. J. 64: 399–412.
245 Bar LK, Barenholz Y, Thompson TE (1997) Effect of sphingomyelin composition on the phase structure of phosphatidylcholine-sphingomyelin bilayers. Biochemistry 36: 2507–2516.
246 Ruf H, Georgalis Y, Grell E (1989) Dynamic laser light scattering to determine size distributions of vesicles. Methods Enzymol. 172: 364–390.
247 Hui SW (1987) Ultrastructural studies of the molecular assembly in biomembranes: diversity and similarity.. In: RD Klausner, D Kempf, J van Renswonde (eds.): *Current Topics in Membranes and Transport*. Vol. 29, Academic Press, Orlando, 29–70.
248 Almgren M, Edwards K, Gustafsson J (1996) Cryotransmission electron microscopy of thin vitrified samples. Curr Opin Colloid Interface Sci 1: 270–278.
249 Gulik-Krzywicki T (1997) Freeze fracture transmission electron microscopy. Curr. Opin. Colloid Interf. Sci. 2: 137–144.
250 Zasadzinski JA (1996) Scanning force microscopy: new instrumentation and applications. Curr. Opin. Colloid Interf. Sci. 1: 264–269.
251 Birdi KS, Vu DT, Moesby L, Kristensen D, Olsen K, Andersen KB (1997) Application of scanning tunnelling microscopy (STM) and atomic force microscopy (AFM) in colloid and surface chemistry. In: KS Birdi (ed.): *Handbook of Surface and Colloid Chemistry,* CRC Press, Boca Raton, 701–741.
252 Salamon Z, Macleod HA, Tollin G (1997) Surface plasmon resonance spectroscopy as a tool for investigating the biochemical and biophysical properties of membrane protein systems. I: Theoretical principles. Biochim. Biophys. Acta 1331: 117–129.
253 Tsong TY (1974) Kinetics of the crystalline-liquid crystalline phase transition of dimyrestoyl La-Lecithin bilayers. Proc. Natl. Acad. Sci. USA 71: 2684–2688.
254 Gruenewald B, Blume A, Watanabe F (1980) Kinetic investigations on the phase transition of lecithin bilayers. Biochim. Biophys. Acta 597: 41–52.
255 Blume A, Hillmann M (1986) Dimyristoyl phosphatidic acid/cholesterol bilayers. thermodynamic properties and kinetics of the phase transition as studied by the pressure jump relaxation technique. Eur. Biophys. J. 13: 343–353.
256 Caffrey M, Magin RL, Hummel B, Zhang J (1990) Kinetics of the lamellar and hexagonal phase transitions in phosphatidylethanolamine. Biophys. J. 58: 21–29.
257 Caffrey M, Cheng A (1995) Kinetics of lipid phase changes. Curr. Opin. Struct. Biol. 5: 548–555.

258 Elamrani K, Blume A (1984) Phase transition kinetics of phosphatidic acid bilayers. A stopped-flow-study of the electrostativeally induced transition. Biochim. Biophys. Acta 769: 578–584.
259 Walter A, Siegel DP (1993) Divalent cation-induced lipid mixing between phosphatidylserine liposomes studied by stopped-flow fluorescence measurements: effects of temperature, comparison of barium and calcium, and perturbation by DPX. Biochemistry 32: 3271–3281.
260 Lawaczeck R (1979) On the permeability of water molecules across vesicular lipid bilayers. J. Membrane Biol. 51: 229–261.
261 Jansen M, Blume A (1995) A comparative study of diffusive and osmotic water permeation across bilayers composed of phospholipids with different head groups and fatty acyl chains. Biophys. J. 68: 997–1008.
262 Paula S, Volkov AG, Van Hoek AN, Haines TH, Deamer DW (1996) Permeation of protons, potassium ions, and small polar molecules through phospholipid bilayers as a function of membrane thickness. Biophys. J. 70: 339–348

Bioelectrochemistry of Membranes
ed. by D. Walz, J. Teissié and G. Milazzo†

CHAPTER 4
Electroconformational coupling

Tian Yow Tsong

Department of Biochemistry, Molecular Biology and Biophysics, University of Minnesota College of Biological Sciences, St. Paul, Minnesota, USA, and Department of Physics, National Taiwan University, and Institute of Physics, Central Research Academy, Taipei, Taiwan

1. Introduction

Electric fields are omnipresent in a cell, tissue, organ or organism. Cells, over millions of years of evolution, have adapted to the presence, and learned to take advantage of these electric fields to fuel or regulate many of the essential reactions of cells. Some examples of these reactions are the generation of neural impulses for the transmission of sensory and perceptual signals, control of ion channels and ion pumps, ATP synthesis, and regulation of biochemical redox reactions [1, 2]. The advent of molecular biology enables biochemists to study these membrane processes at the molecular level. The general strategy is to solubilize and purify a membrane enzyme or protein and study its properties in solution. Reconstitution into liposomes is also a popular approach. Other strategies include preparing membrane fragments containing the desired protein or permeabilizing a cell membrane for study. These procedures have greatly assisted us to understand membrane and cellular reactions. However, a solubilized and purified enzyme also loses its natural habitat and the properties revealed by these biochemical studies may not correspond to the

properties of the functional enzyme *in vivo*. One obvious shortfall is that these procedures are not capable of, or suitable for, studying the effect of intramembrane electric fields on the enzyme function. Voltage clamp and single channel measurement provide a badly needed technology [3, 4]. However, up to the present time, they are mainly used to study membrane channels. Rarely have these methods been employed to study ion pumps or membrane enzymes. Furthermore, the use of oscillatory electric fields in voltage clamp is uncommon. This chapter describes a different type of experiments, which allow us to study the effects of a membrane electric field on membrane transporter functions.

One class of enzymes that would be a logical choice for testing the effect of electric fields is the ATP-synthesizing enzymes. According to the chemiosmotic theory, a difference in electrochemical potential of protons, $\Delta\tilde{\mu}_H$, is the driving force for ATP synthesis [1, 5]. However, $\Delta\tilde{\mu}_H$ is composed of two terms (cf. section 2.2 in chapter 1), the electric term comprising the transmembrane potential difference, $\Delta\phi_m$, and the chemical term comprising the concentration ratio of protons, or ΔpH. In the following the short term "membrane potential" will be used for $\Delta\phi_m$ since none of the other types of membrane potentials discussed in section 2 of chapter 2 will be considered. The presence of $\Delta\phi_m$ of the order of 200 mV across the inner membranes of actively respiring mitochondria has been demonstrated, but ΔpH was found to be rather small. Conversely, experiments to measure $\Delta\phi_m$ across the energy-transducing membranes of chloroplasts, i.e. thylakoid membranes, during illumination have failed to detect any significant value of $\Delta\phi_m$, but ΔpH values of up to 3 units were found [6]. Nevertheless, the H^+/ATP synthase of thylakoids can also use a $\Delta\tilde{\mu}_H$ which consists essentially of $\Delta\phi_m$ only. Witt and coworkers exposed thylakoid membranes to dc electric pulses and could show that ATP is indeed synthesized [7]. Using this technique similar results were obtained also with submitochondrial particles prepared from rat liver and beef heart mitochondria [8, 9], as well as with *Escherichia coli* cells [10]. Moreover, it was shown that the presence of DTT greatly enhanced the ATP yield in submitochondrial particles [11], however the reason for this enhancement remains unknown.

There were many difficulties in these electric field induced ATP synthesis experiments. An energy input of approximately 50 kJ/mol is required for ATP synthesis under normal physiological conditions. If this energy is to come from the electric field alone, it will require a membrane potential of 150 mV or greater [12–14]. As mitochondria or submitochondrial particles are small in size, this will require an applied field of the order of 5 kV/cm or higher to generate such a potential [15] (see also Eqn. 8). Furthermore, as the assay solution for ATP synthesis contains certain concentrations of salts and ions, a field

of 5 kV/cm will produce considerable Joule heating, and a heat denaturation of the sample cannot be avoided. To minimize the damage due to Joule heating, the applied field was kept in the microsecond range (pulsed-electric field). The complication due to Joule heating and the use of a short duration of the electric field in these experiments greatly limited our ability and prevented us from a detailed and quantitative analysis of experimental results [8, 9].

For these reasons, most of the experiments discussed in this chapter have been done with another system, i.e. the Na^+/K^+-ATPase of human erythrocytes (red blood cells) [16–19]. Since intact erythrocytes were used, the native environment of the *in vivo* system was preserved for the Na^+/K^+-ATPase. In addition, since Na^+- and K^+-pumping in human erythrocytes does not require as much energy as the synthesis of ATP, a much weaker field, of the order of 10 to 100 V/cm, was sufficient to induce ion transport. As will be discussed below, the optimal field strength for Na^+- and K^+-transport in human erythrocytes was found to be 40 V/cm (peak-to-peak). With this field, Joule heating was relatively minor, and a continuing field exposure of an erythrocyte sample could be done with a proper cooling device.

2. Electrical activation of Na^+/K^+-ATPase

The Na^+/K^+-ATPase of human erythrocytes is responsible for maintaining the balance of Na^+ and K^+, which in turn maintains the osmotic balance of the cell. Normally the transport of the two ionic species is tightly coupled and three Na^+ ions are pumped out of the cytoplasm in exchange for two K^+ ions per ATP hydrolyzed. In other words, it is an energy transducer, which converts the chemical bond energy of the γ-phosphoanhydride bond of ATP to the electrochemical potential energy of the cations. The pump is said to be asymmetrical because the stoichiometry of Na^+ and K^+ per enzyme cycle differs. The enzyme is also said to be electrogenic because the asymmetric pumping of ions leads to a polarization of the plasma membrane [1, 2]. All these properties of the enzyme suggested to us that it would be an ideal system for the electrical stimulation experiment, and also for testing some ideas we had been formulating over years on the theory of electroconformational coupling (ECC).

The experiment was relatively straightforward to perform but the precision required for the analysis was challenging. Basically, radioactive tracers of Na^+, K^+, and Rb^+ (which is a stable isotope substitution for K^+) were used to follow the movement of ions in and out of human erythrocytes in suspension [18–21]. Most experiments were performed at 2–3 °C, under which the ATP hydrolysis activity of the enzyme was negligible. This condition greatly reduced the background

or the baseline level of ionic fluxes. Any ionic flux due to an electrical stimulation could then be measured with better precision. Erythrocytes have many transport paths, and the plasma membrane is also not completely tight to these ions. There are leaks due to purely passive movement of ions. To ensure that the ion fluxes we were measuring did not come from pump-unrelated passive movements of ions, we measured ion fluxes of four samples concurrently for each experiment. These samples are: a sample stimulated with an electric field (S), a sample not stimulated with an electric field (NS), a sample stimulated with an electric field in the presence of 0.2 mM ouabain (SO), and a sample not stimulated with an electric field in the presence of 0.2 mM ouabain (NSO). Three quantities in these measurements are of particular interest: the quantity S-NS which measures the total ionic flux arising from electric stimulation, the quantity S-SO which measures the net ionic flux due to the electric stimulation of the Na^+/K^+-ATPase, and the quantity NS-NSO which measures the basal level of the ATP-dependent transport of Na^+ and K^+. As mentioned above the basal activity (NS-NSO) was negligible at 2–3 °C, however, when we used higher temperatures to investigate other properties of the pump, it became significant. It was also found that for the three ions we have been investigating, the quantities S-SO and S-NS are similar. This finding points out that other modes of movement for these ions are not sensitive to electric stimulation.

2.1. Uphill cation transport induced by sinusoidal electric fields

The first experiment we did was to search for the frequency and amplitude with which we can obtain maximal ac-dependent transport activity. After some testing we found that for the best results the ac would have an amplitude of 20 V/cm, i.e. a strength of 40 V/cm (peak-to-peak). The optimum field strength was the same for both Rb^+ (or K^+) transport and Na^+ transport. Figure 1 shows a typical experiment, monitoring Rb^+ uptake into erythrocytes with an ac field at the optimal frequency of 1 kHz but a suboptimal amplitude of 16 V/cm [18]. It is seen that there were considerable leak fluxes, but these fluxes were not sensitive to electric fields for the intensity range being used (up to an ac amplitude of 100 V/cm). The field-sensitive fluxes were due entirely to the activity of the Na^+/K^+-ATPase because they were completely inhibited by ouabain, a specific inhibitor of the enzyme. When the amplitude was fixed at 20 V/cm and the frequency was varied, it was found that there was an optimal frequency of 1.0 kHz for Rb^+ transport, but the optimal frequency for Na^+ transport was found to be 1 MHz. This unexpected finding was confirmed by repeated experiments, and we therefore concluded that the two transport func-

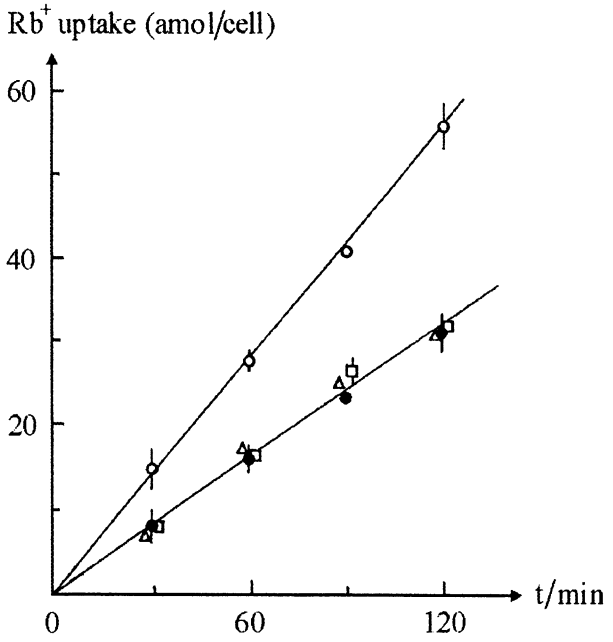

Fig. 1. Rb^+ uptake by human erythrocytes. Samples stimulated with a sinusoidal electric field with amplitude 16 kV/cm and frequency 1 kHz (S, ○) and samples not stimulated with a field (NS, ●). The corresponding samples in the presence of 0.2 mM ouabain are SO (□) and NSO (△), respectively. The slopes of the straight lines indicate the rates of Rb^+ uptake, and their difference (13 amol h^{-1}/cell) is due to the field-stimulated transport by the Na^+/K^+-ATPase. Temperature 3 °C. After Ref. 17.

tions of the enzyme can occur independently under our experimental conditions. With 1 kHz ac, K^+ but not Na^+ is actively transported, and vice versa with 1 MHz ac. Certainly the conditions under which we performed our electrical stimulation experiments are quite different from the physiological conditions. Hence, this finding does not mean that the ATP-dependent transports of Na^+ and K^+ are uncoupled *in vivo*. But it does indicate that the enzyme has different pathways for the transfer of ions; one pathway may dominate under a given experimental condition, while different pathways may become dominant under other conditions.

At 2–3 °C no ATP-dependent, ouabain-sensitive Na^+, K^+, or Rb^+ pumping could be detected. Under such conditions, the maximal net efflux of Na^+ due to ac stimulation ranged from 15 to 30 ion/s per enzyme, while the maximal net influx of K^+ ranged from 10 to 20 ion/s per enzyme. The variation in the measured values was due to a variation in the sources of the red cells. Furthermore, these ac-stimulated activities did not depend on ATP concentration in the range from 10 μM to 1 mM, i.e. ac activates only the Na^+- and K^+-transport modes

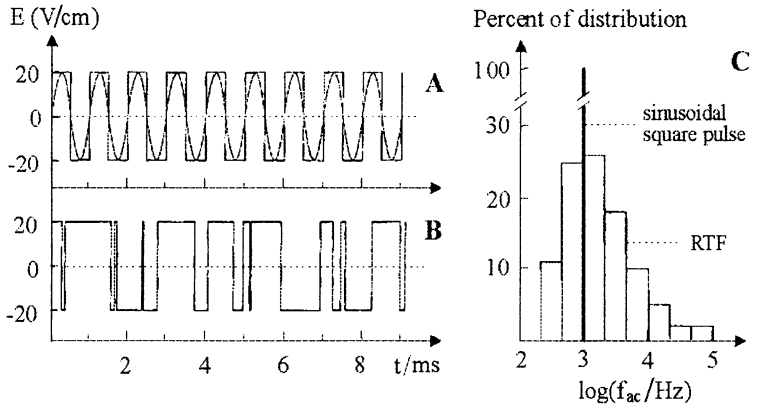

Fig. 2. Different waveforms of electric fields and their frequency distribution. A sinusoidal and a square-pulse field are shown in panel A, while a random telegraph fluctuating field (RTF) is illustrated in panel B. The corresponding frequency distributions in panel C display a single frequency value of 1 kHz for the former, but a Poisson distribution with a mean frequency of 1 kHz for the latter. After Ref. 20.

of the enzyme [17–19]. The K_m values of the ions for the ac-induced activities agreed with those for the ATP-dependent pumping. Various inhibitors of the enzyme also showed similar K_I values. These results suggest that the two different energy sources fuel the enzyme via similar catalytic mechanisms.

2.2. Uphill cation transport induced by randomly fluctuating electric fields

The above observations suggested to us that electrically induced cation transport by the Na^+/K^+-ATPase was relevant to the *in vivo* function of the enzyme. However, some questions remained. The first question concerns the magnitude of $\Delta\phi_m$ fluctuations in a cell. Is the amplitude of 24 mV, which arises from an applied ac field with 20 V/cm amplitude, a realistic value? If not, the applied field-induced membrane potential oscillations would have no relevance to the enzyme function *in vivo*. Most physiologists consider membrane electric noise to be in the range of 1 to 2 mV. But this is a spatial average over the whole cell and does not represent the $\Delta\phi_m$ fluctuation which an enzyme molecule will actually experience. What is then the actual value? Unfortunately no information is presently available to answer this question. However, in view of the magnitude of the action potentials in neural cells [2], a local potential fluctuation of ± 24 mV for the Na^+/K^+-ATPase is not a too far-fetched thought. The second question concerns

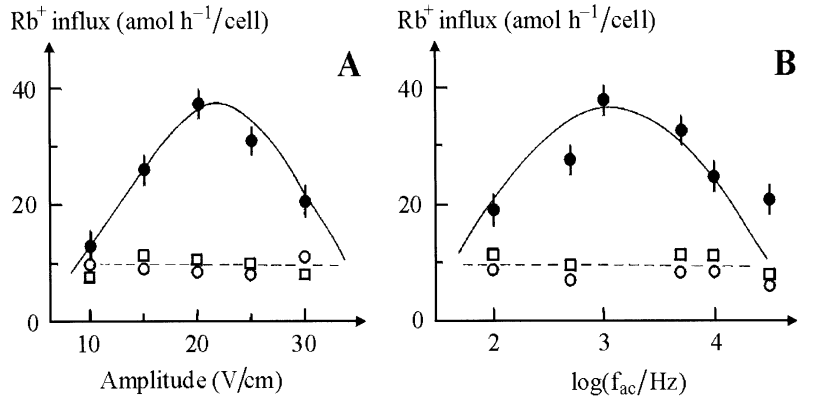

Fig. 3. Rb^+ influx into human erythrocytes stimulated by an RTF electric field. Dependence on amplitude at a fixed frequency of 1 kHz (A) and dependence on frequency at a fixed amplitude of 20 V/cm (B). Samples with (S, •) and without (NS, ○) the electric field, as well as field-stimulated samples in the presence of 0.2 mM ouabain (SO, □). After Ref. 20.

the waveform. Could a membrane potential $\Delta\phi_m$ oscillate with a regular periodic waveform with constant periodicity? This question led us to consider the next experiment, i.e. the electrical activation using a field with the waveform of a random-telegraph noise (RTF). An RTF should mimic a real-world signal much better than a sinusoidal electric field. In an RTF, the pulse width δt is expressed by the relationship

$$\delta t = -(1/\langle f \rangle) \ln \Gamma_r \qquad (1)$$

where $\langle f \rangle$ is the mean frequency, which is equal to the reciprocal of the mean lifetime $\langle \tau \rangle$, and Γ_r denotes a random number between 0 and 1 (in actual experiments, Γ_r was taken between 0.01 and 1). A computer generated a chain of RTF triggering pulses to drive a functional generator which produced square-wave electric pulses with a constant amplitude of 20 V/cm and fluctuating life-times δt distributed according to Eqn. 1 with a given value of $\langle f \rangle$. Figure 2A shows a sinusoidal and a square-pulse electric field, and Fig. 2B illustrates an RTF electric field. The frequency distributions of the three waveforms are shown in Fig. 2C. The sinusoidal and the square-pulse waveforms have a single frequency value of 1 kHz, but the RTF field displays a Poisson distribution with a mean frequency $\langle f \rangle$ of 1 kHz.

Electrical activation experiments with RTF electric fields are shown in Fig. 3. Indeed, RTF stimulated Rb^+ uphill transport in human erythrocytes with an efficiency similar to that of sinusoidal fields. Moreover, the optima for frequency and amplitude were found to be the

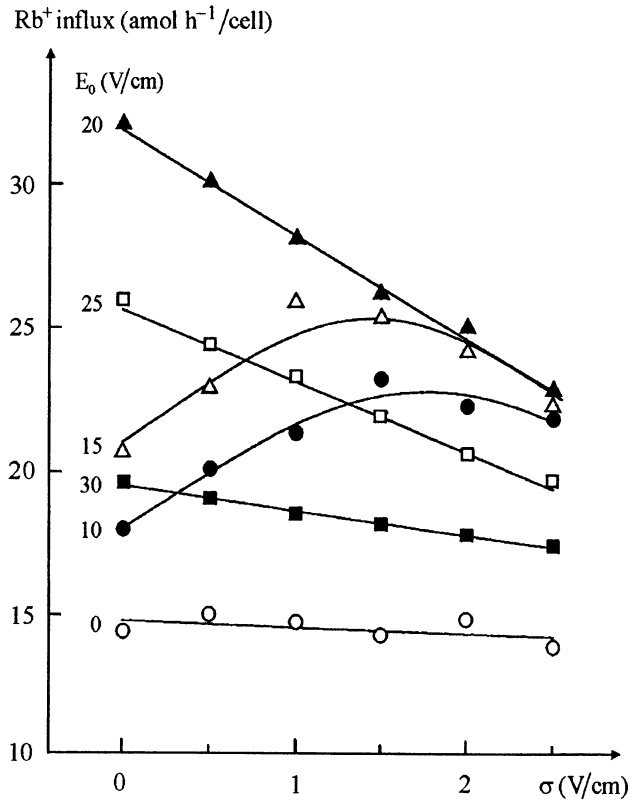

Fig. 4. Rb^+ influx into erythrocytes stimulated by an RTF electric field with variable amplitude. The mean frequency of the RTF fields was 1 kHz, and their amplitude varied according to a Gaussian distribution with a standard deviation σ. The different symbols represent experiments done with fields of different peak amplitude E_0 as indicated. After Ref. 21.

same as in the case of sinusoidal fields [20]. In further experiments RTF electric fields with amplitudes fluctuating according to a Gaussian distribution with different standard deviations σ were used (Fig. 4). In general, increasing σ causes a decrease in transport activity, except for the lower field strengths (E_0 = 10 and 15 V/cm) where stimulation is first found at low values of σ. These results clearly demonstrate that the Na^+/K^+-ATPase can also use an RTF with a fluctuating amplitude as energy source [21].

3. Electroconformational coupling (ECC)

It is known that conformational changes often occur when an enzyme performs its catalytic function. A conformational change can be

induced by many factors, the most prevalent of which is the interaction with a ligand or a substrate. Temperature, ionic strength, pH and solvent composition are other common factors. That an electric field can induce a conformational change is well known to physiologists but less familiar to biochemists. A protein is susceptible to an electric field because of the following reasons. First, the amino acid residues Arg, Asp, Glu, His and Lys, as well as the carboxyl and amino terminal of a protein are usually charged at neutral pH. Second, an electric dipole moment of 1.5 Debye is associated with each peptide bond, whose positive end points toward the NH group. In a helical protein these peptide dipoles are aligned, and the overall dipole moment of a helix is approximately equal to n × 0.75 Debye, where n is the number of peptide units in the helix. Third, cofactors of proteins are often charged. Finally, phosphorylation of a protein introduces negative charges into its structure. This point may be important for the regulation of signal-transducing proteins by electric fields.

3.1. Membrane potential and electroconformational change

Let us consider a molecule which can adopt two conformational states P_1 and P_2 with molar electric moments $\mathbf{M}_1$ and $\mathbf{M}_2$, respectively.

$$P_1 \underset{k_{2,1}}{\overset{k_{1,2}}{\rightleftharpoons}} P_2 \tag{2}$$

The rate constants $k_{1,2}$ and $k_{2,1}$ of the transition between these states are susceptible to an electric field $\mathbf{E}$ according to

$$k_{1,2} = k_{1,2}^{o} \exp [\gamma \, \Delta\mathbf{M} \cdot \mathbf{E}/(RT)] \tag{3}$$

$$k_{2,1} = k_{2,1}^{o} \exp [(\gamma - 1) \, \Delta\mathbf{M} \cdot \mathbf{E}/(RT)] \tag{4}$$

Here

$$\Delta\mathbf{M} = \mathbf{M}_2 - \mathbf{M}_1 \tag{5}$$

and $k_{1,2}^{o}$ and $k_{2,1}^{o}$ denote the rate constants in the absence of the field. R and T are the gas constant and the Kelvin temperature, respectively. The quantity γ is an apportionment factor and has a value between 0 and 1 depending on the structure of the transition state. The scalar product $\Delta\mathbf{M} \cdot \mathbf{E}$ in Eqns. 3 and 4 implies that the electric field is only effective for an appropriate orientation of the vectors $\mathbf{E}$ and $\Delta\mathbf{M}$. Hence molecules in solution are relatively insensitive to electrical perturbation because the effect is averaged out by their rapid rotation.

However, if the molecules are partially or completely obstructed in degrees of freedom, e.g. obstructed in rotational or translational motion, an electric field can induce a conformational change because the equilibrium constant K of the transition shown in Eqn. 2 is dependent on the electric field

$$K = k_{1,2}/k_{2,1} = K^{o} \exp [\Delta \mathbf{M} \cdot \mathbf{E}/(RT)] \quad (6)$$

Here $K^{o} = k_{1,2}{}^{o}/k_{2,1}{}^{o}$ denotes the equilibrium constant in the absence of the field. As a consequence, the concentration ratio of P_2 and P_1 in the presence of the field differs from that in the absence, and the equilibrium is shifted towards P_2 or P_1 if $\Delta \mathbf{M} \cdot \mathbf{E}$ is positive or negative, respectively. When **E** is an oscillating or fluctuating field K will also oscillate or fluctuate. This is the essential feature of the ECC treatment. It should be pointed out, however, that rather large electric field strengths are necessary to induce appreciable conformational changes. Thus, for a protein with a few charges, a field strength of the order of 10^6 V/cm would be required [12, 22–24].

The conditions of restricted mobility and sufficiently high electric field strengths can be easily met with membrane-bound proteins. There are different ways to investigate a protein in a membrane. A straightforward approach is to reconstitute the protein into a bilayer lipid membrane (BLM) and to apply a membrane potential $\Delta\phi_m$ across the BLM (cf. section 4 in chapter 1). Since the potential drops essentially across the membrane (see section 2.3.4 in chapter 1) the electric field strength in the membrane becomes

$$E_m = -\Delta\phi_m/d_m \quad (7)$$

The thickness of a BLM is approximately 5 nm [15, 25], and a membrane potential of some Volts then yields sufficiently large E_m values. This method is suitable only for channel proteins whose conformational states display different conductivities for ion(s), and thus give rise to different electric currents which can easily be measured. For an ion pump, however, the currents are very much smaller (about one millionth) than that for a channel, and it is practically impossible to measure a pump activity with the BLM method.

Another method is to investigate proteins in the membrane of whole cells, e.g., the Na^+/K^+-ATPase of human erythrocytes used in the experiments described in section 2. However, one then needs to have a specific inhibitor for the transporter (ouabain in the case of the Na^+/K^+-ATPase) because, without such an inhibitor, it would be difficult to separate the fluxes that are due to the transporter from those which arise from other transport pathways. Reconstitution of a purified transporter into liposomes would be a cleaner approach,

but leak fluxes and the correct orientation of the enzyme in the reconstituted proteo-liposomes could become an issue. In order to estimate the electric field strength in the membrane of cells or liposomes a rough approximation should suffice. The cells are represented by a spherical shell with a thickness d_m and a radius r, which has a much lower conductivity than that of the external and internal fluids. It then follows from Maxwell's equations that the upper limit for the membrane potential induced by an externally applied homogeneous electric field of strength E is (see section 3.1 in chapter 6)

$$\Delta\phi_m = -1.5\ r\ E \tag{8}$$

where $\Delta\phi_m = \phi_{in} - \phi_{ex}$. When an oscillating field with frequency f_{ac} is used, $\Delta\phi_m$ should also oscillate according to

$$\Delta\phi_m = \Delta\phi_{m,0}/[1 + (2\pi\ f_{ac}\ \tau_m)^2]^{1/2} \tag{9}$$

where $\Delta\phi_{m,0}$ denotes the maximal value of $\Delta\phi_m$ at the peak value of the oscillating field, and τ_m is the electrical relaxation time of the membrane. If $f_{ac}\ \tau_m \leq 0.1$ the denominator in Eqn. 9 can be approximated by 1. Since τ_m is of the order of 0.1 μs for a lipid membrane this approximation is valid if $f_{ac} \leq 1$ MHz which was true for most of the experiments described in section 2. The strength of the electric field E_m in the membrane in response to a sinusoidal external electric field is then given by

$$E_m = E_{m,0} \sin (2\pi\ f_{ac}\ t) \tag{10}$$

where $E_{m,0} = \Delta\phi_{m,0}/d_m$ (cf. Eqn. 7). Note that the field lines of E_m are perpendicular to the membrane surface.

The above analysis shows that when a protein, which can adopt different conformations with different electric moments, is obstructed in its mobility at a certain orientation and exposed to an oscillating electric field, its conformation will also oscillate. Because of the dependence of the rate constants on the electric field (see Eqns. 3 and 4) the rate of oscillation, or the periodicity, will occur with a frequency identical to that of the field. This phenomenon shall be called *enforced conformational oscillation* [13, 14].

3.2. Enforced conformational oscillation and energy transduction

The enforced conformational oscillation by itself cannot harvest electrical energy for productive use, but a coupling of the conformational

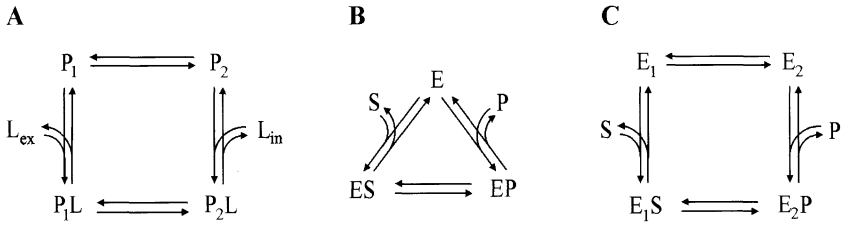

Fig. 5. Catalytic cycles of enzymes. (A) A membrane-bound enzyme which transports the ligand L from the external medium (subscript ex) into the interior space of a cell or liposome (subscript in). (B) An enzyme E catalyzing the conversion of substrate S to product P. (C) Same as (B) but for an enzyme with different conformations E_1 and E_2 which bind S and P, respectively.

oscillation to biochemical reactions is required. For a pump ligand-binding reactions have to be added which, in the simplest case, leads to the kinetic scheme shown in Fig. 5A. To keep the analysis of this scheme in clear perspective, we have assumed that the ligand L has neither charges nor permanent or inducible electric dipoles. Such a neutral ligand does not interact with an electric field, and any effect seen in the simulations necessarily reflects the effect of field interactions with the transporter protein. The simple four-state cyclic model in Fig. 5A has been analyzed in great detail [12–14, 26, 27]. It could be shown that it works as an ECC machine, providing the following asymmetries are built into the mechanism: (i) the rate of the conformational changes between P_1 and P_2, and between P_1L and P_2L must be larger than the mean frequency of the applied field; (ii) the rate of ligand binding/dissociation must be smaller than the frequency of the applied field; and (iii) the affinities of P_1 and P_2 for L must be different. These properties enable the system to function like a chemical ratchet which can harvest electrical energy to pump the ligand against its concentration gradient. The ECC system is thus a special case of the Brownian ratchet which can harvest energy from a randomly fluctuating force field [21, 28]. Section 6 briefly discusses Brownian ratchet and ECC mechanisms.

The performance of the ECC machine can be illustrated as follows. For demonstration purposes only, let us assume that the affinity of P_1 for L is much higher than that of P_2. For the system at equilibrium without an applied electric field, one then expects $[P_1] << [P_1L]$ and $[P_2] >> [P_2L]$. Moreover, the rate constants shall be chosen such that the inequalities $[P_1] < [P_2]$ and $[P_1L] > [P_2L]$ are established. When a sinusoidal electric field is now applied, the equilibrium constants of the conformational transitions will oscillate according to (cf. Eqns. 6 and 10)

$$K = K^{o} \exp [\Delta M_n E_{m,0} \sin (2\pi f_{ac} t)/(RT)] \quad (11)$$

where ΔM_n is the component of $\Delta \mathbf{M}$ with respect to the membrane normal. Again for demonstration purposes only, let us assume a value for $\Delta M_n E_{m,0}$ such that, during the first half-cycle of the sinusoidal field, P_2 and P_2L are favored over P_1 and P_1L, respectively. The field will then generate two fluxes, one from P_1 to P_2 and the other from P_1L to P_2L. However, since initially $[P_1] << [P_1L]$, the magnitude of the second flux will be much larger than that of the first one. The newly elevated concentration of P_2L will lead to its dissociation and $[P_2]$ will increase further. Conversely the decreasing concentration of P_2L will lead to a binding of L and $[P_1]$ will become even lower. Hence, during the first half-cycle, the field will induce a net counterclockwise movement in the scheme of Fig. 5A thus transferring L from ex to in. In the subsequent second half-cycle the polarity of E_m is opposite to that in the first half-cycle, which favors P_1 over P_2 and P_1L over P_2L. The applied field during this second half-cycle will likewise generate two fluxes, but now one from P_2 to P_1 and the other from P_2L to P_1L. However, since $[P_2] > [P_2L]$ because of the low affinity of P_2 for L, the first flux will be larger than the second one. The net result is again a counterclockwise movement during the second half-cycle of the sinusoidal field. Ideally the system returns close to the equilibrium state from which it started, and the next two half-cycles of the field will again cause the phenomena described before. With the asymmetries built into the model, the ac field induces only counterclockwise movements in the scheme of Fig. 5A. In other words, the system becomes a catalytic wheel, which is driven by the external field to spin unidirectionally thus pumping L from the external medium (ex) into the cell or liposome (in).

Due to the pumping L_{in} will accumulate and L_{ex} decrease with time, but this process cannot continue indefinitely. There is an upper limit for the concentration ratio $[L_{in}]/[L_{ex}]$ which can be achieved by an oscillating electric field. In the model analysis some assumptions have been made to estimate the maximal level of gradient which a four state cyclic model (Fig. 5A) can sustain at steady state, and the efficiency of energy transduction under various experimental conditions has been investigated. If the amplitude of a sinusoidal field is large enough to induce the maximal degree of conformational change, and if the inequalities $k_{conf} >> f_{ac} >> k_{bind}$ hold, the ECC transport model of Fig. 5A will achieve the maximal efficiency of 100%. However, there is an optimal field strength with which an enzyme can function most effectively. Beyond this field strength, an applied field may impair the catalytic function of the enzyme. In other words, a rate cannot be enhanced indefinitely with a field to a greater value than this limit. Beyond this limit the rate will decrease again.

3.3. ECC pumping versus electrical rectification

If the ligand is charged, the behavior of the scheme in Fig. 5A will be different, and the efficiency of energy transduction also changes. Careful examination of all plausible combinations between charges of the transporter (represented by charge number Z_P, gating charges only) and that of the ligand (charge number Z_L) shows that only six combinations are possible [29]. Among these six, the one with $Z_P = 0$ and $Z_L = 0$ does not respond to an electric field and hence need not be considered. The five other combinations of charges in the ECC model are:

1. Transporter with gating charges and neutral ligand, e.g. $Z_P = 1, Z_L = 0$. In this case, the sign of Z_P is irrelevant.
2. Transporter without gating charges and charged ligand, e.g. $Z_P = 0, Z_L = 1$. In this case, the sign of Z_L is irrelevant.
3. Transporter with gating charges which are neutralized by the ligand, e.g. $Z_P = -1, Z_L = 1$.
4. Transporter and transporter-ligand complex have charges with opposite signs, e.g. $Z_P = -1, Z_L = 2, Z_{PL} = 1$.
5. Transporter and transporter-ligand complex have charges with the same sign, e.g., $Z_P = 1, Z_L = 1, Z_{PL} = 2$.

The numerical values for Z_P and Z_L given here are for illustration only. For understanding the general behavior of a system the actual numbers are not important. What is crucial is the sign of the charges of P, L, and PL (cf. Fig. 5A), and their inter-relationships.

Some properties of the five classes of ECC models under oscillatory electric fields have been summarized. Basically, an oscillatory electric field can induce two types of fluxes, one arising from the rectification of charges and the other arising from ECC effects. It is therefore essential to distinguish fluxes induced by the two distinctly different mechanisms. Systems 1 and 5 are pure ECC systems, and their efficiency for energy transduction can reach the theoretical maximum of 100%. System 2 is a pure electric rectification system. In this system, there are no gating charges in the protein, i.e. $Z_P = 0$, and the electric field acts directly on the charged ligand. The efficiency of such an electric rectification system reaches a mere 8.7%. This is an interesting finding especially with respect to the interpretation of experimental data because electric field-induced pumping of a ligand by itself is not sufficient to prove that it occurs by the ECC mechanism. Other evidence has to be available.

One interesting feature of the electrical activation experiments and the analysis based on the ECC model is the observation that windows for field frequency, field strength, and ligand concentration exist in

which energy conversion becomes optimal. These windows had been observed even before the ECC model was developed, but the model has furnished us with new insights concerning the mechanisms of electrical activation processes, and allows us to distinguish the ECC mechanism from the rectification process. Indeed, system 4 does not exhibit a frequency window, while systems 1 and 5 do. The experimental results obtained with the Na^+/K^+-ATPase show clearly a frequency window for Rb^+- and K^+-pumping, and another for Na^+-pumping. Therefore, this enzyme is more consistent with an ECC system.

3.4. Biological effects of low level electric fields – Oscillatory Activation Barrier Model

The ECC model is applicable to electric field strengths which are much larger or comparable to the field strength in a membrane due to a physiological membrane potential (100 to 200 mV). However, it has been attempted to use the ECC concept also for the interpretation of biological effects arising from much smaller fields. It has been suggested that an ECC model can explain effects due to an electric field strength as low as 1 μV/cm, providing signal averaging is allowed. Sharks, rays, and birds are known to have a sensing ability far below 1 μV/cm. The ECC mechanism alone may not be sufficient to explain this exceedingly wide range of molecular sensing abilities of organisms. Not all of the sensual perceptions of cells or organisms require input of energy. But a sensual perception, however sensitive it may be, must be performed by cells and hence must involve reactions of biomolecules [24, 30]. Working with this premise, we have proposed a model, called the Oscillatory Activation Barrier (OAB) model, to explain biological effects of very weak electric fields [14, 30, 31]. Field strengths as low as 1 μV across the dimension of an enzyme can produce substantial effects, for example, enhancement of the rate of ATP hydrolysis.

The basic postulate of the OAB model is that the transition state of a step in enzyme catalysis is an internal oscillator with an intrinsic frequency f so that the activation energy barrier is oscillatory, and that this transition state is highly charged thus making it susceptible to electrical perturbation. If an externally applied electric field has a frequency which matches the intrinsic frequency f, a resonance will ensue, and the amplitude of the oscillation will increase (Fig. 6A). The activation energy barrier for the transition $i \rightarrow j$ amounts to (cf. Fig. 6A)

$$\Delta G^{\#} = G^{\#} - G_i \tag{12}$$

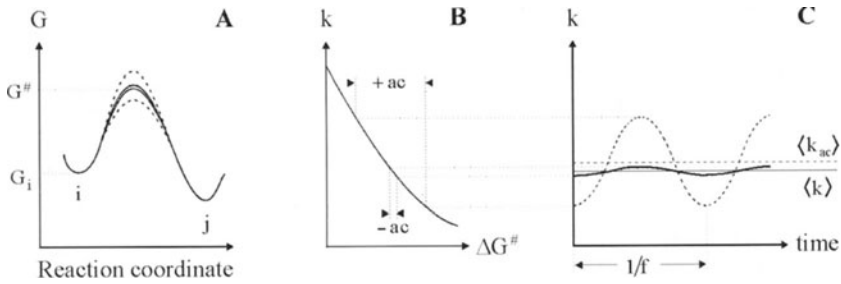

Fig. 6. Oscillatory Activation Barrier model. (A) Profile of Gibbs energy G for the transition between states i and j in an enzyme cycle. The transition state is an oscillator with an intrinsic frequency f so that the Gibbs energy $G^{\#}$ of this state varies with time, as shown by the solid lines. An externally applied ac electric field with the same frequency causes an increase in amplitude due to resonance (broken lines). (B) Dependence of rate constant k on activation barrier $\Delta G^{\#}$ (cf. Eqns. 12 and 13). The dotted lines with arrowheads indicate the ranges of $\Delta G^{\#}$ variations in the absence (– ac) and presence (+ ac) of the field. (C) Time dependence of k in the absence (solid line) and presence (broken line) of the field. The horizontal straight lines represent the corresponding average rate constants $\langle k \rangle$ and $\langle k_{ac} \rangle$. After Ref. 14.

and the pertinent rate constant k depends on $\Delta G^{\#}$ according to

$$k \propto \exp [- \Delta G^{\#}/(RT)] \tag{13}$$

with similar relations holding for the transition j → i. If the oscillation is symmetrical with respect to the magnitude of the activation energy, the increased amplitude of oscillation due to the ac electric field will increase the average rate constant, as illustrated in Figs. 6B and 6C. It should be understood that, unlike in the case of ECC, the electric field does not supply energy to the catalyzed reaction because a weak electric field does not carry sufficient energy to fuel an endergonic chemical reaction. However, it can change the rate of a spontaneous chemical reaction which runs energetically downhill. The reaction we studied, i.e. ATP hydrolysis, is a spontaneous reaction under physiological conditions. For a suitable enzyme the activation barrier of the transition state should limit the overall rate, and a weak electric field of appropriate frequency should alter the rate by enhancing the oscillation of the activation barrier. An experimental test for the OAB model was attempted. ATP hydrolysis catalyzed by Ecto-ATPase isolated from chicken oviducts was measured in the presence of an ac field, and an enhancement of the rate of ATP hydrolysis was indeed detected [31].

4. Stochastic resonance and effect of noise on ion pumping

The sinusoidal and the RTF electric fields discussed in section 2 can be considered as electric signals because they are characterized by the three elements of a signal, viz. frequency, amplitude, and waveform. Our experiments indicate that an enzyme molecule in a cell membrane can recognize an electric signal by virtue of the rate of the processes in its catalytic cycle. Other dynamic properties of a molecule can also be used to recognize an electric signal, e.g. by the OAB mechanism. This is a rather novel concept because with this concept, cells and organisms should be able to receive signals of wide ranges of strength, frequency and waveform. These oscillating or fluctuating electric fields have been called "the language of cells" [24, 30]. A signal may be masked if the ambient noise exceeds a certain power level. Does an electrical noise interfere with the ability of cells to recognize an electric signal? There are different schools of thought; some consider noise to have little effect, others think that it interferes, and still others consider it to have beneficial effects on signal transduction. This signal-enhancing effect is known as the stochastic resonance [32, 33].

We have tested these different hypotheses by investigating the effect of electrical noise on the electric field-induced ion pumping activity of the Na^+/K^+-ATPase. A white-noise generator was designed which can produce a broad power spectrum from 1 Hz to 100 kHz. Electrical stimulation was done with sinusoidal or RTF electric fields in the presence and the absence of various power levels of the electrical noise. The salient features of the experimental results [34] are as follows. At an *optimal* electric field strength (see section 2.1) noise at any power level reduces the efficiency of ion pumping. However, low level noise enhances the efficiency of ion pumping with *sub-optimal* electric field strengths. This enhancement diminishes at higher noise levels. Furthermore, noise is able to carry a *sub-threshold* electric field strength over the threshold. It was also found that noise did not change the optimal frequency of the electric field. These results are consistent with the concept of stochastic resonance. Further study is underway to understand its mechanisms. However the above experiment indicates that the RTF with $\langle f \rangle$ of 1.0 kHz is a signal, and the "white-noise" with a power spectrum cutting off at 1 MHz is a noise for the Na^+/K^+-ATPase. The former is a monochromatic noise and the latter is a polychromatic noise. We surmise that the monochromatic noise selectively channels energy to the pumping process, but that the polychromatic noise may elevate the system-wise activation energy which is equivalent to elevating the equilibrium fluctuation of the entire system. Equilibrium fluctuation does not support directional flow of energy [34, 35].

5. "Catalytic Wheel" and immobilized enzyme as energy and signal transducer

Although this chapter focuses on harvesting of energy from oscillating and fluctuating electric fields, the concept developed here has evidently broader implication to the problem of biological energy and signal transduction [12–14]. In particular, it was suggested that transduction of acoustic signals by cochlea cells can be explained by molecular responses to pressure oscillation, thus converting acoustic energy into ionic currents or ionic gradients [36]. Transduction of other types of signals and energy, such as the mechanical energy of muscle contraction and motor function, are also within the scope of the present discussion. What is interesting is that an enzyme with a catalytic mechanism of the Michaelis-Menten type can become equivalent to the kinetic scheme in Fig. 5A. Consider the simple reaction where substrate S is converted to product P, and which is catalyzed by an enzyme

$$E + S \rightleftharpoons ES \rightleftharpoons EP \rightleftharpoons E + P \tag{14}$$

Since the enzyme E is recycled in each turnover, the reactions of Eqn. 14 are more appropriately represented by the catalytic cycle shown in Fig. 5B. As was discussed in sections 3.1 and 3.2, an essential feature for a protein to harvest energy from an oscillating or fluctuating driving force is a restraint in its degrees of freedom and some asymmetries built into the catalytic cycle. Hence, if the enzyme E is immobilized, and if the conformations of E which bind S and P are distinguishable due to different properties, the scheme shown in Fig. 5C is obtained which is fully equivalent to the scheme in Fig. 5A. Moreover, if there is a difference in volume ΔV (instead of a difference in electric moment $\Delta \mathbf{M}$) between E_1 and E_2, the system shall be able to transduce an acoustic, a pressure or a mechanical signal [13, 14]. This finding will have a great ramification on our study of the action of immobilized enzymes, e.g. enzymes of the cell membrane, a supramolecular structure, a tissue, or an organ. The three mechanisms shown in the figure are "Catalytic Wheels" and they are thus amenable to perturbation by oscillating or fluctuating driving forces. The thermodynamic and kinetic quantities that characterize a catalytic wheel determine the "Natural Frequency" of the wheel [13, 14, 27].

6. Biological motors and engines, and Brownian ratchet mechanisms

As mentioned above, the ECC mechanism exhibits all the essential features of the Brownian ratchet [12, 28, 34]. A Brownian ratchet is a

microscopic device, which can harvest energy from an oscillating or fluctuating force field (in the present case an electric field) to perform chemical or mechanical work. The field provides an off-equilibrium oscillation or fluctuation of the protein conformation, and in so doing transfers energy of the electric field to the chemical potential energy of the cations. The basic construct of a Brownian ratchet is for the system to oscillate or fluctuate between two states, with different activation barriers for particle transport. Some asymmetry must be built into these barriers to produce ratchet effects [12, 22, 35].

Different types of ratchets have been discussed, and comprehensive reviews are available [28, 34–36]. For example, Huxley has considered off-equilibrium thermal noise as an energy source and a ratchet mechanism as plausible mechanism for muscle contraction [37]. The idea that ATP hydrolysis may amplify local thermal fluctuations and fuel muscle contraction through a ratchet mechanism has continued to stimulate discussion and new experimental design in myosin/actin and kinesin/microtubule interactions [28, 38, 39]. However, temperature gradients dissipate in picoseconds on a nanometer-scale structure and, unless there are elaborate mechanisms for temporarily retaining energy, a picosecond-ratchet would seem difficult to drive millisecond events. Our ECC analysis indicates that the mean frequency of monochromatic fluctuation, be it thermally or electrically induced, is determined by chemical rate constants of the catalytic wheels as shown in Fig. 5. Chemical ratchets, electrical ratchets, acoustic ratchets, etc. can occur in various time ranges and would be effective for coupling to energy requiring events [12, 34].

Oscillation or fluctuation of a pair of conjugate thermodynamic quantities, such as pressure/volume (acoustic transduction), membrane area/surface tension, concentration/chemical potential, etc. may be an effective means to convert energy from one form to another by the ratchet mechanisms if the reactions are to take place in an anisotropic medium [13, 14]. A similar analysis as done for the ECC system should also be applicable to these biological motors and engines. The efficiency of Brownian ratchets greatly depends on mechanistic detail of the ratchet. For example, the reversible ratchet of ECC can achieve an efficiency reaching 100% [27, 40], while the flushing ratchet discussed in Ref. 36 can achieve a maximal efficiency of 50%. Other ratchets may have lower efficiencies. In particular, a ratchet based on electric charge rectification can achieve a maximal efficiency of only 8.7% [29]. This property of ratchets may be used as diagnostic, but it is interesting to note that the ECC mechanism is one of the most efficient free energy transducing mechanism [29]. The ECC concept has also been studied under different contest, and ion-induced membrane potential fluctuation is used to explain stochastic resonance phenomena [41, 42]. An enzyme as a catalytic wheel made

of soft matter protein has recently been discussed in greater detail in reference to the Brownian ratchet mechanisms for the biological energy transduction [43]. Finally it should be mentioned that in other publications of the author the acronym TEC (Theory of Electroconformational Coupling) has been used for the phenomenon called ECC in this chapter.

References

1 Stryer L (1995) *Biochemistry*, 4th Edition. WH Freeman and Co., New York.
2 Nicholls JG, Martin AR, Wallace BG (1992) *From Neuron to Brain*, 3rd Edition. Sinauer Assoc. Inc., Sunderland, Massachusetts.
3 Neher E, Sakmann B (1976) Nature 260: 799–801.
4 Neher E, Sakmann B, Steinbach JH (1978) Pflügers Arch. 375: 219–228.
5 Mitchell P (1979) Science 206: 1148–1159.
6 Rottenberg H, Grunwald T, Avron M (1971) FEBS Lett. 13: 41–44.
7 Witt HT, Schlodder E, Gräber P (1976) FEBS Lett. 69: 272–276.
8 Teissié J, Knox B, Tsong TY, Wehrle J (1981) Proc. Natl. Acad. Sci. USA. 78: 7473–7477.
9 Knox BE, Tsong TY (1984) J. Biol. Chem. 259: 4757–4763.
10 Teissié J (1986) Biochemistry 25: 368–373.
11 Tsong TY, Liu D-S, Chauvin F, Gaigalas A, Astumian RD (1989) Bioelectrochem. Bioenerg. 21: 319–331.
12 Tsong TY, Astumian RD (1986) Bioelectrochem. Bioenerg. 15: 457–476.
13 Tsong TY (1990) Annu. Rev. Biophys. Biophys. Chem. 19: 83–106.
14 Tsong TY (1992) Biochim. Biophys. Acta. 1113: 53–70.
15 Tsong TY (1991) Biophys. J. 60: 297–306.
16 Teissié J, Tsong TY (1980) J. Membrane Biol. 55: 133–140.
17 Serpersu EH, Tsong TY (1983) J. Membrane Biol. 74: 191–201.
18 Serpersu EH, Tsong TY (1984) J. Biol. Chem. 259: 7155–7162.
19 Liu D-S, Astumian RD, Tsong TY (1991) J. Biol. Chem. 265: 7260–7267.
20 Xie TD, Marszalek P, Chen YD, Tsong TY (1994) Biophys. J. 67: 1247–1251.
21 Xie TD, Chen YD, Marszalek P, Tsong TY (1997) Biophys. J. 72: 2497–2502.
22 Tsong TY, Astumian RD (1987) Prog. Biophys. Molec. Biol. 50: 1–45.
23 Tsong TY, Astumian RD (1988) Annu. Rev. Physiol. 50: 273–290.
24 Tsong TY (1989) Trends Biochem. Sci. 14: 89–92.
25 Tien HT (1974) *Bilayer Lipid Membranes* (BLM). Dekker, New York.
26 Markin VS, Tsong TY (1991) Biophys. J. 59: 1308–1316.
27 Markin VS, Tsong TY, Astumian RD, Robertson B (1990) J. Chem. Phys. 93: 5062–5066.
28 Astumian RD (1997) Science 276: 917–922.
29 Markin VS, Tsong TY (1991) Bioelectrochem. Bioenerg. 26: 251–276.
30 Tsong TY (1994) Biophys. J. 67: 1367–1368.
31 Markin VS, Liu D-S, Rosenberg MD, Tsong TY (1992) Biophys. J. 61: 1045–1049.
32 Weisenfeld K, Moss F (1995) Nature 373: 33–36.
33 Bezrukov SM, Vodyanoy I (1995) Nature 378: 362–364.
34 Tsong TY, Xie TD (2002) Appl. Phys. A 75: 345–352.
35 Reimann P (2002) Phys. Rep. 361: 57–265.
36 Astumian RD, Bier M (1994) Phys. Rev. Lett. 72: 1766–1769.
37 Huxley AF (1957) Prog. Biophys. 7: 255–320.
38 Ishi Y, Esaki S, Yanagida T (2002) Appl. Phys. A 75: 325–330.
39 Oosawa F (1996) Adv. Biophys. 32: 1–15.
40 Markin VS, Tsong TY (1991) Biophys. J. 59: 1317–1324.
41 Fulinski A (1998) Chaos 8: 549–556.
42 Fulinski A, Grywna Z, Mellor I, Siwy Z, Usherwood PNR (1998) Phys. Rev. E 58: 919–924.
43 Tsong TY, Chang CH (2003) Asso. Asia Pacific Phys. Soc. Bulletin 13/2: 12–18.

Bioelectrochemistry of Membranes
ed. by D. Walz, J. Teissié and G. Milazzo†

CHAPTER 5
Lipid bilayer electropermeabilization

Yuri A. Chizmadzhev[1], Justin Teissié[2], and Dieter Walz[3]

[1]*Frumkin Institute of Electrochemistry, Russian Academy of Sciences, Moscow, Russia*
[2]*Centre National de la Recherche Scientifique, Toulouse, France*
[3]*Biozentrum, University of Basel, Basel, Switzerland*

1. Introduction

In the majority of cells, under normal physiological conditions, there exists a transmembrane potential difference of about several tens of millivolts. This means that the electric field in biomembranes is rather high, approximately 10^5 V/cm. With a further increase in the electric field, biomembranes undergo changes that lead to a drastic (by 5–7 orders of magnitude) increase in their conductance and permeability (for reviews see Refs. 1–4). If this conductance increment is accompanied by mechanical rupture of the membrane, one speaks of irreversible electrical breakdown. When such an increment is temporary, the phenomenon is called reversible electrical breakdown [5, 6]. Electropermeabilization of cell membranes has attracted significant attention because it has found many biomedical and biotechnological applications [1–4].

The data available in the literature favor the assumption that the impairment of the barrier function of biomembranes as a result of electrical breakdown is determined by processes in the lipid matrix. This enables one to study the electrical breakdown phenomenon using a very convenient model, namely, the planar bilayer lipid membrane (BLM, see section 4 in chapter 1 and section 4.2 in chapter 3). It is noteworthy that the planar membrane in contact with a meniscus differs in a number of properties from the closed membrane of a cell or a liposome. However, the general picture of electrical breakdown remains unchanged. For the physical chemistry of surface phenomena, the BLM appears to offer quite unique possibilities. In fact, by applying an electric field, which disturbs the lipid film, and by recording the current through it as a function of time, one can study the dynamics of the behavior of a film up to its rupture.

This chapter outlines the basic experimental facts concerning the electrical breakdown of BLM. For a description of this phenomenon, different types of theories based on a variety of ideas about the mechanisms of the process were put forward in the literature. We present first a critical analysis of these theoretical studies. Subsequently, we describe the theory using mainly the idea about the decisive role of local defects, i.e. lipidic pores.

2. Phenomenology of bilayer lipid membrane electropermeabilization

Figure 1 presents the general shape of the current I(t) flowing through a bilayer lipid membrane as a function of time t when a stepped voltage pulse is applied [7]. After the initial phase due to charging of the membrane, a steady state current is attained which depends on the membrane potential $\Delta\phi_m$ (the short term "membrane potential" for "transmembrane potential difference" can be used here since none of the other types of membrane potentials discussed in section 2 of chapter 2 will be considered). Then severe current fluctuations appear, followed by a drastic irreversible current increase up to its saturation. It is very simple to ascertain that in the region of current saturation the membrane has already ruptured. For this purpose, it suffices to lower $\Delta\phi_m$ and to measure the current, which turns out to be equal to that flowing through the cell in the absence of the membrane. If now a new membrane is formed and the experiment is repeated, the time dependence of the current I(t) is reproduced qualitatively although the lifetime of the membrane turns out to be different. The character of the fluctuations and the duration of this stage are also changed. Thus, the membrane lifetime is a random quantity such that its study calls for a stochastic approach.

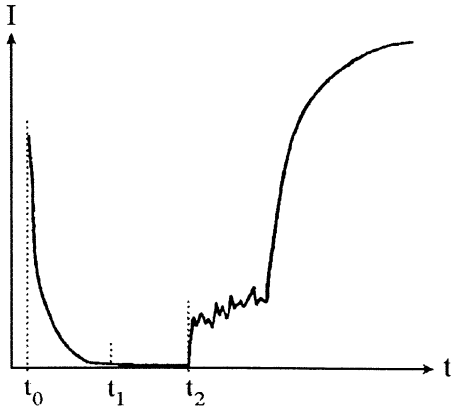

Fig. 1. General behavior of current I as a function of time t observed with a bilayer lipid membrane (BLM). At t_0 a voltage step is applied to the membrane. The initial decrease of I is due to charging of the membrane capacity. The steady state value for $t_1 < t < t_2$ reflects the membrane conductance. At t_2 a sudden increase in I with random fluctuations occurs which precedes the final rise due to membrane breakdown. The lifetime t_ℓ of the membrane is defined as $t_2 - t_0$. For BLMs formed with brain lipids and subjected to a voltage step of 400 mV the mean lifetime is about 1s, the steady state current is of the order of 5×10^{-9} A, and the current after breakdown, which is limited by the cell resistance, is approximately 5×10^{-5} A.

As is evident from Fig. 1 the membrane passes through at least two stages during its lifetime: a stage of steady-state current and a stage of pre-breakdown current fluctuations. Sometimes the membrane returns from the region of breakdown fluctuations to its initial state and, if the pulse duration is not too long, it remains intact. When a high $\Delta\phi_m$ is applied to a BLM for only a short time, the intact membrane often goes over into a peculiar long-lived (tens of minutes) "excited" state. This membrane state, which was termed a stress state, is characterized by a high conductance and considerable current fluctuations. The phenomenon of irreversible breakdown was also studied with the charge pulse technique [8]. In a first charge pulse experiment a membrane potential of 100 mV was attained, and the discharge process was very slow because the relaxation time $\tau = R\ C$ is large (Fig. 2, curve 1). In a second experiment, the membrane was charged to 400 mV. The discharge was faster and, after 300 to 400 ms, $\Delta\phi_m$ declined to zero because of an irreversible breakdown of the membrane (Fig. 2, curve 2).

2.1. Influence of various factors on membrane stability

For solving the problem of stability and elucidating possible mechanisms of breakdown it is necessary to investigate the dependence of

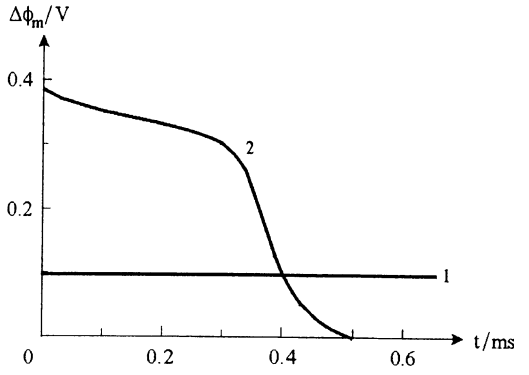

Fig. 2. Dependence of membrane potential $\Delta\phi_m$ on time t in charge pulse experiments. BLMs were formed with oxidized cholesterol dissolved in n-decane; electrolyte solution 1M KCl, temperature 17 °C. Charge pulses of 0.5 μs duration were applied with amplitudes adjusted such that different membrane potentials were attained. After Ref. 8.

membrane lifetime on various factors, primarily on the membrane potential $\Delta\phi_m$. Figure 3 shows the dependence of the mean lifetime $\langle t_\ell \rangle$ on $\Delta\phi_m$ for brain lipid BLMs [7]. It is seen that the dependence of $\log\langle t_\ell \rangle$ on $\Delta\phi_m$ is nearly linear between 100 and 500 mV, and an increase in $\Delta\phi_m$ by about 100 mV causes a tenfold decrease of $\langle t_\ell \rangle$. At higher potentials the decrease of $\langle t_\ell \rangle$ with increasing $\Delta\phi_m$ becomes less noticeable. Thus, with $\Delta\phi_m$ varying from 0.1 to 1.4 V, the lifetime changes by more than 6 orders of magnitude and drops down to about 10 μs. The physical reasons for such a strong dependence of $\langle t_\ell \rangle$ on $\Delta\phi_m$ will be discussed in section 3.1. The distribution function of the membrane lifetime t_ℓ for brain lipid membranes at $\Delta\phi_m = 400$ mV is depicted in Fig. 4. This function allows the calculation of the variance of t_ℓ. It is noteworthy that this variance decreases with increasing $\Delta\phi_m$.

The behavior of membranes of various composition has been studied [7, 9]. Examples of such compositions are brain lipids, egg lecithin, lecithin-cholesterol mixtures, asolectin, oxidized cholesterol and so on. The overall course of electrical breakdown, including mechanical rupture, is the same for all lipids studied, with the exception of oxidized cholesterol and membranes specifically modified with uranylacetate. The last two systems exhibit the so-called reversible electrical breakdown (see section 2.2). The membrane stability depends also on the nature of the organic solvent used to form the BLM. The stability of the membranes decreases as the solvent is changed from hexadecane to decane and from decane to carbon tetrachloride. However, this sequence of solvents is not universal, e.g. membranes formed with

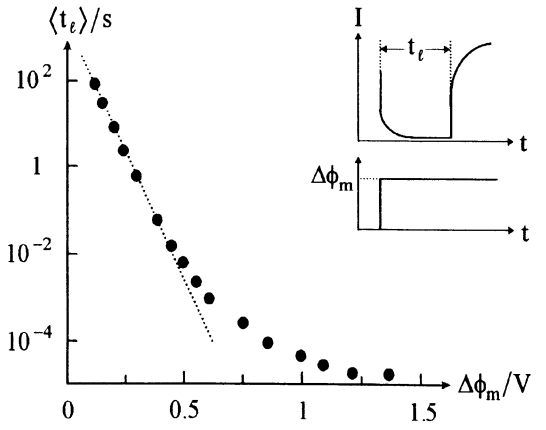

Fig. 3. Dependence of the average membrane lifetime $\langle t_\ell \rangle$ on the applied membrane potential $\Delta\phi_m$. BLMs were formed with brain lipids in n-decane, and each point was obtained by averaging over 30 to 100 measurements [7]. The dotted line represents the relation $\log[\langle t_\ell \rangle/s] \propto \Delta\phi_m/0.085$ V. The inset shows schematically the experimental protocol used to determine t_ℓ (cf. Fig. 1).

brain lipids dissolved in decane are more stable than those in hexadecane. The stability of the membranes does not correlate with the relative change in their capacitance $\Delta C_m/C_m$ due to an electric field (cf. section 3.3 in chapter 1). Specifically, $\Delta C_m/C_m$ is about 15% at $\Delta\phi_m$ = 750 mV for decane membranes, but only about 1% at $\Delta\phi_m$ = 690 mV for the less stable hexadecane membranes.

Increasing the temperature causes a significant decrease in membrane stability. For instance, the mean membrane lifetime $\langle t_\ell \rangle$ at $\Delta\phi_m$ = 600 mV is 342 μs and 224 μs at a temperature of 30 °C and 62 °C, respectively. The dependence of $\ln\langle t_\ell \rangle$ on the reciprocal absolute temperature 1/T (Arrhenius plot) enables one to estimate the activation energy of the BLM breakdown in an electric field. Such plots yield activation energies of 83, 71 and 50 kJ/mol at $\Delta\phi_m$ values of 200, 600 and 800 mV, respectively. Thus, the electrical breakdown activation energy markedly decreases with increasing $\Delta\phi_m$. It is worth mentioning that these values are close to the value of the temperature coefficient of BLM conductance, which is approximately 60 kJ/mol.

The BLM stability in an electric field is also dependent on the electrolyte composition. However, in spite of quantitative differences, the general qualitative trend of the $\langle t_\ell \rangle$ dependence on $\Delta\phi_m$ is preserved. Membrane stability in solutions containing $MgCl_2$ or $SrCl_2$ is much lower than that in NaCl or KCl solutions. It seems that some correlation exists between the stability and the charge number of cations, i.e. the higher the charge number the lower the stability. On the other hand, Ca^{2+}, La^{3+} and UO_2^{2+} manifest stabilizing effects which are con-

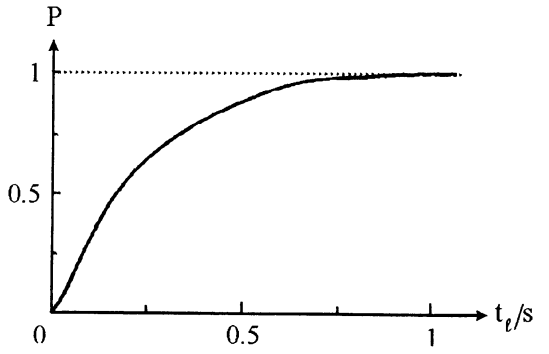

Fig. 4. Distribution function for the lifetime t_ℓ of BLMs at $\Delta\phi_m$ = 400 mV (brain lipids in n-decane). The probability that a membrane lifetime is shorter or equal to t_ℓ is $P(t_\ell)$. After Ref. 7.

nected with strong interactions of these cations with the polar head groups of the phospholipid molecules. There are indications that Ca^{2+} at low (10 mM) and high (100 mM) concentrations destabilizes a BLM. Usually the stability of a BLM increases with decreasing electrolyte concentrations. This effect is more pronounced at small values of $\Delta\phi_m$.

2.2. Reversible electrical breakdown

In 1979, Benz et al. [8], using the charge relaxation method (cf. section 4 in chapter 1), found that membranes of oxidized cholesterol, which are rapidly charged to about 1 V, show a reversible decrease in membrane resistance by nearly nine orders of magnitude. In the experiments illustrated in Fig. 5, the membrane was charged to 0.9 and 1.2 V and the rapid relaxation of $\Delta\phi_m$ after the end of the pulse is attributable to a large increase in membrane conductance (curves 1,2 in Fig. 5). After being discharged the membrane remains mechanically stable and can be recharged. Using a higher amplitude of the charge pulse yielded again a membrane potential of about 1.2 V but a faster decay of $\Delta\phi_m$ (curve 3). With even higher (supercritical) charge pulses electrical breakdown, and the decrease in resistance caused by it, already occurs during the charging process. Hence the first $\Delta\phi_m$ value, which can be recorded due to the limited time resolution of the measuring device, is lower than 1.2 V (not shown). It should be noted that a residual $\Delta\phi_m$ remains at the end of the electrical breakdown experiment (in contrast to curve 2 in Fig. 2) which is too small to cause the irreversible, i.e. mechanical, breakdown of the membrane discussed in the preceding section (cf. curve 1 in Fig. 2). Thus, reversible breakdown for planar lipid membranes could be observed for the first time.

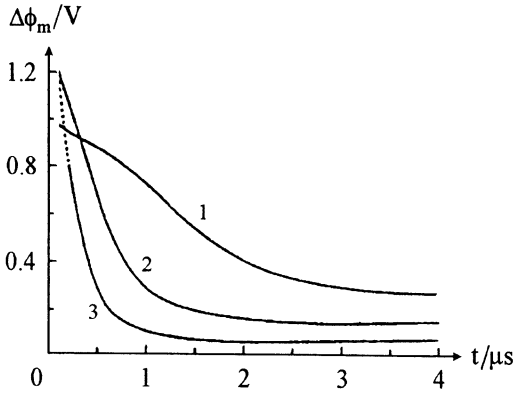

Fig. 5. Dependence of membrane potential $\Delta\phi_m$ on time t in charge pulse experiments showing reversible breakdown. BLMs were formed with oxidized cholesterol dissolved in n-decane; electrolyte solution 1M KCl, temperature 17 °C. Charge pulses of 0.5 μs duration were applied with amplitudes adjusted such that different membrane potentials were attained. After Ref. 8.

Reversible breakdown was later studied with voltage clamp techniques [4, 10]. Figure 6 presents a set of I(t) curves obtained in successive applications of voltage pulses with different amplitudes to a membrane consisting of oxidized cholesterol. Dominating at the onset of a pulse is a charging current which rapidly falls off. Simultaneously, a conduction current develops which becomes dominating just after 5 μs in the case of a pulse of 0.7 V (curve 1). At the end of this pulse the conduction current is about 5×10^{-5} A, which corresponds to a conductance value of 10^{-5} to 10^{-6} Ω^{-1}. Thus, the conductance increases against the background conductance (10^{-9} to 10^{-10} Ω^{-1}) by a factor of 10^4 to 10^5. An increase in the pulse amplitude leads to a rapid increase in the rate of current development (curves 3 to 5). If the pulse duration is not too long, the increase in conductance is reversible and the I(t) curve is fully reproducible in a repeated application of the same pulse (curve 2). A pulse with a long duration, however, will cause the increase in conductance to become irreversible. In the case of irreversible breakdown I(t) curves for repeated pulses are of random character.

2.3. The local character of electrical breakdown

To elucidate the mechanism of electrical breakdown of a BLM, one must give an answer to the following question: Do large scale processes dominate in the electrical breakdown or are the rupture and the permeabilization of the BLM in an electric field associated with the

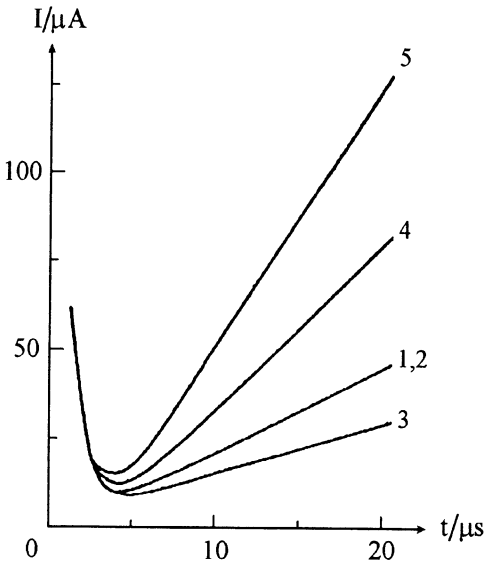

Fig. 6. Time dependence of current I through a BLM of oxidized cholesterol under voltage clamp. The voltage clamp was switched on for 20 ms and had amplitudes of 0.68 V (curve 3), 0.72 V (curve 4), and 0.73 V (curve 5). The amplitude of 0.7 V was applied twice (curves 1 and 2). The time interval between successive applications was longer than 1 min. After Ref. 16.

development of local defects? Large-scale deformations of a membrane which lead to a variation of the membrane thickness can be revealed by measuring the membrane capacitance (cf. section 3.3 in chapter 1). The influence of the membrane potential $\Delta\phi_m$ on the capacitance of a BLM has been explored thoroughly [11–13]. It has been established that applying $\Delta\phi_m$ gives rise to at least two kinds of processes that cause the membrane capacitance to change. The first process, with a time scale of more than 0.1 s, consists of a change in total BLM area, i.e. in a redistribution of the area between the meniscus and the bilayer. The second process, which is much faster, is a change of the membrane thickness as a result of electrical compression (electrostriction). The breakdown must be directly preceded by a change in the capacitance if the application of $\Delta\phi_m$ leads to an overall compression of the membrane before it ruptures.

Chernomordik and Abidor [14] showed that when relatively high membrane potentials are applied ($\Delta\phi_m$ = 800 mV and $\Delta\phi_m$ = 600 mV), the BLM capacitance rapidly attains the value corresponding to the applied $\Delta\phi_m$ and thereafter remains constant within 1% up to the moment of breakdown. In the case of smaller $\Delta\phi_m$ values, where the membrane lifetime is larger than 0.1 s, the capacitance is increased as a result of an increase in the area by 3–5% and remains practically

constant until the breakdown [11, 15]. In these experiments, the capacitance was measured with an accuracy of at least 0.5 to 1%. Hence, at least within the $\Delta\phi_m$ range covered, the processes causing the breakdown of the membrane, which are in particular reflected by the pre-breakdown current fluctuations, are not accompanied by any noticeable change in BLM capacitance. If we assume that the pre-breakdown current fluctuations indeed reflect changes in the membrane capacitance, we would obtain capacitance fluctuations with an amplitude of about 2×10^{-8} F, which is as large as the initial capacitance value.

In view of these findings large-scale BLM deformations as a possible cause of electrical break-down can be ruled out. The data obtained favor the assumption that local defects underlie the rupture of membranes in an electric field. This conclusion is supported by even more accurate measurements of the capacitance in a long-lived stress state where the capacitance was found to be constant with an accuracy of 0.5% [14]. Moreover, the capacitance of UO_2^{2+}-modified membranes, which show reversible breakdown, was measured in that phase of breakdown where the conduction current is still small compared with the capacitive current [16]. It was found that the capacitance of the membranes remains unchanged within 2%, and it was unambiguously concluded that this behavior arises from *local* defects. Based on the value of the current observed at a resistance of about 10^4 Ω the total area of the defects can be estimated as approximately 10^{-8} cm^2 which is much less than the area of the whole membrane (about 10^{-3} cm^2). The reproducibility of the currents I(t) for successive applications of the same pulses (curves 1 and 2 in Fig. 6) in the case of reversible breakdown, as well as the absence of any visible fluctuations at even relatively large currents indicate that the "law of large numbers" holds true in this system, i.e. a host of defects (or pores) in the membrane exists.

Recently new experimental data in favor of a pore model were obtained [17]. Unmodified BLM were clamped at $\Delta\phi_m$ values between 150 and 550 mV for a long period of time in order to detect single pores. Fast transitions between different conductance levels were observed which reflect opening and closing of metastable lipidic pores. Although the mean lifetime of the pores was 3 ± 0.8 ms (at 250 mV), some pores remained open for up to 1 s. The mean amplitude of the conductance fluctuations (~ 500 pS) was independent of $\Delta\phi_m$ and very similar for bilayers of different area (4×10^4 and 10 μm^2), indicating the local nature of the conductive defects. The distribution of the pore conductance was rather broad with a dispersion of about 250 pS. Based on the conductance value and its dependence on the ion size, an average pore radius of about 1 nm was estimated. Short bursts of conductance spikes (i.e. opening and closing of pores)

were often separated by periods of background conductance. Within a burst the conductance between spikes was indistinguishable from the background conductance. The mean time interval between spikes in a given burst was much smaller than that between subsequent bursts. These data indicate that opening and closing of lipidic pores proceed through some electrically invisible (silent) pre-pore state.

2.4. Theoretical description of bilayer lipid membrane stability

2.4.1. Electromechanical collapse: There are several different approaches to the description of the BLM stability in an electric field. For example, Crowley [18] suggested that electrical breakdown of the BLM can be considered as an electromechanical collapse caused by the compression of the membrane by the electric field. According to Crowley, the membrane represents an elastic capacitor filled with a dielectric with a constant permittivity ε_m. The pressure exerted on the dielectric by the electric field is

$$P_e = \varepsilon_m \Delta\phi_m^2/(2d_m^2) \tag{1}$$

where d_m is the membrane thickness. The modulus of elasticity (Young's modulus) E_Y of the membrane is considered as being independent of the deformation so that the elastic force P_m per unit area can be calculated by means of Hooke's law as

$$P_m = -E_Y \int_{d_{m,0}}^{d_m} dx/x \tag{2}$$

where $d_{m,0}$ is the membrane thickness in the absence of a field. With the equilibrium condition $P_e = P_m$ we obtain the following relation for d_m

$$E_Y \ln(d_{m,0}/d_m) = \varepsilon_m \Delta\phi_m^2/(2d_m^2) \tag{3}$$

It is easy to show that Eqn. 3 has no roots if $\Delta\phi_m > \Delta\phi_m^*$, where $\Delta\phi_m^{*2} = 0.368\, E_Y\, d_{m,0}^2/\varepsilon_m$. The quantity $\Delta\phi_m^*$ is referred to as the breakdown potential. Thus, according to Crowley, breakdown takes place only for supercritical potentials, i.e. for $\Delta\phi_m > \Delta\phi_m^*$.

It follows from Eqn. 3 that breakdown occurs if $d_m/d_{m,0}$ is about 0.61, i.e. when the thickness has changed by 39%. For such large deformations it can hardly be assumed that Hooke's law with a constant E_Y is still valid. It was also pointed out by Requena et al. [19] that the value of E_Y used by Crowley is greatly underestimated. Furthermore, an important argument against Crowley's model is the absence of a marked change in the BLM capacitance before electrical breakdown

(see section 2.3), such a capacitance increase being an inevitable consequence of a membrane thinning. The most essential discrepancy between Crowley's model and reality, however, is the dependence of membrane breakdown on $\Delta\phi_m$ predicted by this model. In contrast, the experimental data indicate that the membrane lifetime, rather than the breakdown, depends on $\Delta\phi_m$. This strong dependence of the lifetime on $\Delta\phi_m$ is very difficult to explain in the framework of Crowley's model because one can hardly expect that the time of mechanical relaxation of a membrane is so strongly dependent on $\Delta\phi_m$.

2.4.2. Electrohydrodynamic instability: Michael and O'Neil [20] considered the problem of the electrohydrodynamic instability of a flat layer of a nonconducting liquid, straddled on either side by a conducting liquid. On the whole, the system analyzed by these authors is similar to a membrane system if one neglects the fact that the motion in the membrane cannot be described by the usual hydrodynamic equations. Nevertheless, one can draw an analogy between the stability of a flat dielectric layer and the electrical breakdown of a BLM. Specifically, Michael and O'Neil analyzed the conditions for stability with respect to two types of perturbations of plane surfaces: one which is symmetric with respect to the mid-plane of the dielectric layer (the dielectric surfaces oscillate in antiphase) and one with antisymmetric waves (oscillation of surfaces in phase). In view of the fact that the membrane possesses a relatively moderate rigidity, it might be expected that symmetric waves (squeezing modes) will arise, whereas the development of antisymmetric waves (stretching modes) is impeded by the high elasticity of the membrane. Thus, the result obtained by Michael and O'Neill for symmetric waves could be applied to BLM. According to these authors, the system is unstable with respect to long-wave perturbations if

$$\varepsilon_m \Delta\phi_m^2 > \gamma_{ip} d_m \tag{4}$$

where γ_{ip} is the surface tension at the interface between the non-conducting and the conducting liquid. This implies the existence of a breakdown potential

$$\Delta\phi_m^* = (\gamma_{ip} d_m/\varepsilon_m)^{1/2} \tag{5}$$

If we attempt to apply this formula to a BLM using the parameter values $\gamma_{ip} = 5 \times 10^{-4}$ N/m (which corresponds to a membrane tension $\gamma \approx 2\gamma_{ip}$ of the order of 10^{-3} N/m), $d_m = 5$ nm, and $\varepsilon_m = 1.8 \times 10^{-11}$ F/m, we obtain $\Delta\phi_m^* = 375$ mV. Thus, the hydrodynamic approach gives a value of $\Delta\phi_m^*$ that is not too large, but this model does also not account for the above-mentioned specific features of BLM breakdown.

In order to elucidate the physical meaning of Eqn. 5 we shall derive it by means of a simple reasoning (as in Ref. 3). Because of the incompressibility of the dielectric layer its volume remains more or less constant, and a small decrease $d(d_m)$ in its thickness leads to an increase dA of its surface area such that $A\, d(d_m) + dA\, d_m = 0$. The corresponding change in free energy of the system comprises both the surface and the electrical energy term and reads

$$dF = 2(\gamma_{ip} - \varepsilon_m \Delta\phi_m^2/d_m)dA \tag{6}$$

From the instability condition $dF < 0$ it follows that breakdown occurs if

$$\Delta\phi_m > \Delta\phi_m^* = (\gamma_{ip}\, d_m/\varepsilon_m)^{1/2} \tag{7}$$

It is worth mentioning that the mechanism of instability as described by the electrohydrodynamic approach of Michael and O'Neill is essentially the same as that described by Crowley. The only difference is that Crowley attributed the increase in system energy to the elasticity of the membrane, whereas in the hydrodynamic approach it corresponds to the work of formation of new membrane surface. In both cases the development of instability ("breakdown") represents a nonlocal process that occurs simultaneously on a large area of the membrane.

2.4.3. Wave instability: The analysis of the wave instability of membranes, taking into account their viscoelastic properties, was made by Steinchen et al. [21] and Maldarelli et al. [22]. The elastic properties of the material of the film were described within the framework of the models by Kelvin and Maxwell, which also consider the compression of the film owing to Van der Waals attraction of the external solutions. For deformations of the stretching type the instability was associated with the achievement of a negative tension due to the action of Van der Waals forces. For deformations due to compression the film is always stable in the Kelvin model, but always unstable in the Maxwell model. In the latter case the results are qualitatively similar to those obtained by Dimitrov [23], i.e. the surface tension and the viscosity of the film increase its lifetime. Thus, the wave analysis in this case also leads to significantly differing results as compared with the analysis within the framework of metastability (see section 2.4.4) where the tension of the film promotes a decrease of its lifetime.

Dimitrov describes a membrane as a viscoelastic medium. The analysis of time evolution of symmetrical waves shows that the characteristic time τ of the process depends on the wavelength λ:

$$\tau = \eta_m/[-E_Y/3 + \varepsilon_m \Delta\phi_m^2/(12\lambda^2) - \gamma\, d_m^3/(24\lambda^4)] \quad (8)$$

where η_m is the effective viscosity of the membrane and γ the membrane tension. The lifetime of the membrane in an electric field was obtained from Eqn. 8 as the minimal time for the increase in surface disturbance,

$$\tau = \eta_m/[\varepsilon_m^2\, \Delta\phi_m^4/(24\gamma\, d_m^3) - E_Y/3] \quad (9)$$

The threshold potential according to Eqn. 9 is equal to

$$\Delta\phi_m^* = [24\gamma\, E_Y\, d_m^3/(3\varepsilon_m^2)]^{1/4} \quad (10)$$

An interesting variation of Crowley's idea is realized in Ref. 24, in which the phase transitions of membranes are studied by methods of statistical physics. In calculations of the energy of the membrane, the electrical term was considered only through the compression of the membrane by the field. It was shown that at sufficiently low values of $\Delta\phi_m$ (less than 250 mV) there are two stable values for the area per lipid molecule. The transition from the state with the smaller area to the one with the larger area corresponds to the solid-liquid phase transition. Values of $\Delta\phi_m$ above 280 mV lead to an unrestricted increase of the area per molecule, i.e. to the breakdown of the membrane.

2.4.4. Bilayer lipid membrane as a metastable system: The most adequate approach for the analysis of membrane stability goes back to the kinetic studies of first order phase transitions. This approach is based on the view that the plane bilayer is a metastable system. The metastable character of the membrane becomes especially clear in view of the fact that a certain work has to be done in order to form a film from lipids in solution. In other words, the tension of the membrane is essentially positive. This implies that the state with the broken membrane is characterized by a lower reserve of free energy and, therefore, the bilayer is a metastable system.

In this approach the breakdown of the film is considered as a phase transition which realizes a more stable state of the system. The basis for such a theory was laid by Gibbs who introduced the concept of the nucleus of a new phase and showed that the lifetime of the metastable phase, t_{mp}, depends exponentially on the maximal value W* of the work which is required for forming a critical nucleus,

$$t_{mp} \propto \exp[W^*/(kT)] \quad (11)$$

The kinetic theory of phase transitions was largely developed by contributions of Becker and Dering [25] and Christiansen [26] as well as

Kramers [27] and Zeldovich [28]. Interestingly, virtually all these authors treated physically different systems by means of the same mathematical technique.

To conclude this section, it should be noted that the theory of electrical breakdown makes use of two different approaches. One is based on a linear analysis of system stability, whereas the other is exclusively non-linear. The latter approach introduces some intermediate structures (defects, pores) which are not reduced to small perturbations. It is similar to the approaches used in the absolute rate theory for chemical reactions, which is based on the idea of an activated complex, or in the theory of forming a new phase, which introduces the concept of the critical nucleus of the new phase.

3. Mechanisms of electroporation

3.1. Transient aqueous pore model for irreversible breakdown

We shall consider a structural defect of the membrane, such as a narrow pore, as the new phase nucleus. We assume that the radius of the pore is so small that its conductance can be neglected. In this approximation the BLM/water interfaces are equipotential. The mechanical work W_{mech} for the formation of such a pore is calculated by taking into account the decrease in film area and the increase in area of the pore edges [29, 30]

$$W_{mech} = -\pi r^2 \gamma + 2\pi r \gamma_\ell \tag{12}$$

where r is the pore radius, γ the membrane tension, and γ_ℓ the linear tension equal to the energy per length along the circumference of the pore. In order to calculate the electrical term W_{el} for the work of pore formation, we consider the membrane and the cylindrical pore as two capacitors connected in parallel [31]. The capacitance of such a capacitor is (cf. section 2.3.1 in chapter 1)

$$C(r) = (A - \pi r^2)\, \varepsilon_m/d_m + \pi r^2\, \varepsilon_w/d_m \tag{13}$$

Here A is the area of the membrane without pore and ε_w is the permittivity of water within the pore. W_{el} is then equal to the change in electrical energy associated with the change in capacitance C(r)–C(0), i.e. (see Eqn. 19 in chapter 1)

$$W_{el} = -\Delta\phi_m^2\, [C(r) - C(0)]/2 = -\Delta\phi_m^2\, \pi\, r^2(\varepsilon_w - \varepsilon_m)/(2d_m) \tag{14}$$

The total change in free energy ΔF of the system is equal to the sum of the two work terms and thus depends on the parameters r and $\Delta\phi_m$:

$$\Delta F(r, \Delta\phi_m) = 2\pi\, r\, \gamma_\ell - \pi\, r^2\, (\gamma + \Delta C_A\, \Delta\phi_m^2/2) \tag{15}$$

where

$$\Delta C_A = (\varepsilon_w - \varepsilon_m)/d_m \tag{16}$$

is the difference in capacitance per unit area. The linear tension γ_ℓ promotes pore closing. In contrast, the membrane tension γ tends to increase the pore size, and the effect of $\Delta\phi_m$ is equivalent to increasing γ. Hence, an electric field as well as a tension leads to an increase in pore radius. The field effect can be understood as the tendency of a polar solvent to displace the hydrophobic medium from the region of high electric intensity.

According to Eqn. 15 the free energy change ΔF as a function of the pore radius r for a given value of $\Delta\phi_m$ is a parabola (see Fig. 7) with a maximal value

$$\Delta F^*(\Delta\phi_m) = \pi\, \gamma_\ell^2/(\gamma + \Delta C_A\, \Delta\phi_m^2/2) \tag{17}$$

at the point

$$r^*(\Delta\phi_m) = \gamma_\ell\, /(\gamma + \Delta C_A\, \Delta\phi_m^2/2) \tag{18}$$

The shape of the curves in Fig. 7 already indicates that the plane BLM is a metastable system. A pore whose radius is less than the critical value r* tends to close. If, however, the size of a pore exceeds the critical value r* due to thermal fluctuation, its radius begins to grow unlimitedly which eventually leads to membrane breakdown. The barrier $F^*(0)$ is rather high (curve 1 in Fig. 7) so that the membrane possesses a large lifetime. However, when a field is applied ($\Delta\phi_m \neq 0$), the height of the barrier decreases and so does the value of the critical radius (curves 2 and 3 in Fig. 7). This describes qualitatively the observed dependence of the mean lifetime on $\Delta\phi_m$ (cf. Fig. 3).

The quantitative theory [31] uses approaches developed for the description of the nucleation phenomenon, i.e., new phase nucleus formation. This formalism considers pore diffusion in the radius space in the presence of an external restoring force for $r < r^*$. If one does not strive to calculate the pre-exponential factor, which is not of paramount significance, one can obtain an expression for the mean lifetime from simple considerations based on a common approach used, e.g., in the theory of absolute reaction rates [32]. If we assume that the

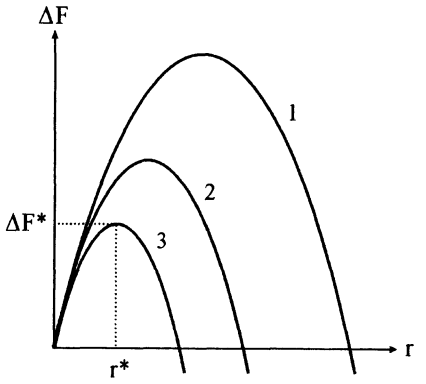

Fig. 7. Dependence of free energy change for pore formation ΔF on pore radius r at different but constant values of $\Delta\phi_m$. Curve 1, $\Delta\phi_m = 0$; curve 2, $\Delta\phi_m \neq 0$; curve 3, larger $\Delta\phi_m$ as for curve 2.

distribution of pores up to the critical size is at equilibrium we obtain according to Boltzmann's law

$$c_P(r^*)/c_{P,0} \propto \exp[-\Delta F^*/(kT)] \tag{19}$$

where $c_P(r^*)$ denotes the concentration of pores with radius r*, and $c_{P,0}$ is the total pore concentration. The mean lifetime $\langle t_\ell \rangle$ of the membrane then becomes

$$\langle t_\ell \rangle \propto \exp[-\Delta F^*/(kT)] \tag{20}$$

with ΔF* as given in Eqn. 17. The exact formula for the case of a high barrier has the form [31]

$$\langle t_\ell \rangle = \frac{(kT)^{3/2} \exp\{\pi \gamma_\ell^2/[kT(\gamma + \Delta C_A \Delta\phi_m^2/2)]\}}{4\pi c_{P,0} A D_p \gamma_\ell (\gamma + \Delta C_A \Delta\phi_m^2/2)^{1/2}} \tag{21}$$

where D_p denotes the pore diffusion coefficient in the r-space. As shown in Fig. 8 experimental results are satisfactorily represented by Eqn. 21 if the parameters γ_ℓ and D_p are properly adjusted by curve fitting. The value of γ was obtained from an independent measurement.

3.1.1. Spreading resistance: The aqueous pore model has been extended to include the conductance of the pores [33]. Ions can pass through sufficiently large pores and the corresponding current flowing through the pore not only results in a potential drop within the pore,

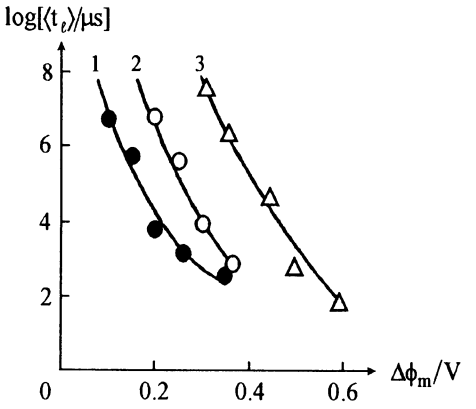

Fig. 8. Effect of membrane potential $\Delta\phi_m$ on mean lifetime $\langle t_\ell \rangle$ of BLMs with different composition. The experimental data were obtained as described in Fig. 3 and with membranes consisting of phosphatidylcholine (●), phosphatidylcholine in the presence of 0.4 mg/l lysophosphatidylcholine in the electrolyte solution (○), and phosphatidylethanolamine (△). Electrolyte solution 0.1 M KCl. The curves were calculated with Eqn. 21 using $\gamma = 2 \times 10^{-4}$ N m^{-1} and the following adjusted values for γ_ℓ and D_p: $\gamma_\ell = 3.3 \times 10^{-12}$ N, $D_p = 2.5 \times 10^{-5}$ cm^2 s^{-1} (1); $\gamma_\ell = 8.6 \times 10^{-12}$ N, $D_p = 8 \times 10^{-8}$ cm^2 s^{-1} (2); $\gamma_\ell = 1.66 \times 10^{-12}$ N, $D_p = 3.1 \times 10^{-7}$ cm^2 s^{-1} (3).

but also in the regions of electrolyte solution near the entrance of the pore. Therefore, the BLM/water interfaces are no longer equipotential, and the electrical work term W_{el} given in Eqn. 14 is no longer valid. The increment dW_{el} due to the radial displacement of the cylindrical wall of a pore by the increment dr is

$$dW_{el} = -[\pi\, r\, \varepsilon_w\, \Delta\phi_p(r)^2/d_m]\, dr \tag{22}$$

Here $\Delta\phi_p(r)$ denotes the potential drop along the wall of a pore with radius r, and terms of the order of $\varepsilon_m/\varepsilon_w$ (≈ 0.025) << 1 are neglected. The potential drop near a pore's openings can be associated with a "spreading resistance" which exists in (or spreads out to) the electrolyte solution. Assuming that the pore mouths can be modeled as equipotential discs [34] the spreading resistance R_s for both entrances to a pore becomes

$$R_s = 1/(2g_w\, r) \tag{23}$$

where g_w denotes the conductivity in the aqueous solution. The internal resistance R_p of a pore can be estimated by means of the conductivity g_p within the pore,

$$R_p = d_m/(\pi r^2\, g_p) \tag{24}$$

The two resistances R_s and R_p are in series, so that a "voltage divider" exists where

$$\Delta\phi_p(r) = \Delta\phi_m/[1 + q_R(r)] \tag{25}$$

with the abbreviation

$$q_R(r) = R_s/R_p = \pi\, r\, g_p/(2d_m\, g_w) \tag{26}$$

This means that $\Delta\phi_p(r) < \Delta\phi_m$, and $\Delta\phi_p(r) \to \Delta\phi_m$ for $r \to 0$, while $\Delta\phi_p(r) \to 0$ for $r \to \infty$. Inserting Eqn. 26 into Eqn. 22 and integrating over r yields a new expression for the electrical work term (instead of Eqn. 14)

$$W_{el} = -(\pi\, \varepsilon_w\, \Delta\phi_m^2/d_m) \int_0^r x\, dx/[1 + q_R(x)]^2 \tag{27}$$

The parameter q_R includes the conductivity g_p in the pore (cf. Eqn. 26) which itself is dependent on r because of the displacement of ions from the pores due to image forces.

3.1.2. Conduction within pores: According to the Born approximation the work W_{wm}, which is necessary to transfer an ion with radius a and charge number Z from the aqueous phase of the electrolyte solution to the hydrocarbon core of the membrane, amounts to

$$W_{wm} = [(Ze)^2/(8\pi a\, \varepsilon_0)]\,(1/\varepsilon_{r,m} - 1/\varepsilon_{r,w}) \tag{28}$$

Here ε_0 is the absolute permittivity, while $\varepsilon_{r,m}$ and $\varepsilon_{r,w}$ denote the relative permittivity (or dielectric constant) of the membrane and the aqueous bulk solution, respectively (see section 2.3.2 in chapter 1). With the parameter values a = 0.2 nm, $Z = \pm 1$, $\varepsilon_{r,m} \approx 2$, and $\varepsilon_{r,w} \approx 80$ we obtain $W_{wm} = 2.8 \times 10^{-19}$ J which is about 70 kT at room temperature (see dotted line in Figure 9A). Already this simple calculation clearly shows that the lipid bilayer forms a very high hydrophobic barrier on the way of transferring hydrophilic ions across the membrane. A more accurate calculation of this barrier, which uses the technique of "multiple reflections" on the membrane/water interfaces for calculating the image forces, accounts for the rather small thickness of the membrane [35]. Although it yields a smooth transition on the interfaces (see broken line in Fig. 9A) it differs less than 10% from the Born approximation (Eqn. 28) for the major part of the hydrophobic membrane.

In order to explain the sharp increase in membrane conductivity induced, e.g., by a short pulse of a strong electric field, a mechanism is required which causes, at least locally, a substantial decrease of the

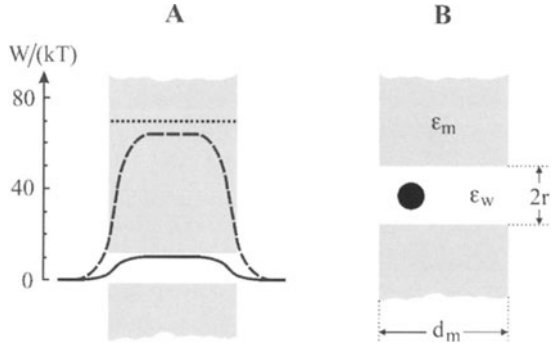

Fig. 9. (A) Profiles of work W for transferring an ion across a membrane at room temperature. Dotted line, Born approximation (Eqn. 28); broken line, W calculated with image forces using the technique of "multiple reflections" on the membrane/water interfaces [35]. Solid line, W for an aqueous pore calculated as described in the text for $Z = \pm 1$, $\varepsilon_m/\varepsilon_w = 0.025$ and $r = 0.5$ nm (cf. Eqn. 29), using the geometry and parameters shown in (B).

hydrophobic barrier. Such a mechanism is provided by the electrostatic treatment of an aqueous pore of radius r in the membrane. The work necessary to transfer an ion from the aqueous solution into this pore can be written as

$$W_{wp} = [(Ze)^2/(4\pi\varepsilon_m r)]\, f(\varepsilon_m/\varepsilon_w) \tag{29}$$

providing the permittivity of water in the pore is approximated by ε_w. The function $f(\varepsilon_m/\varepsilon_w)$ has to be calculated numerically for the geometry depicted in Fig. 9B, and taking image forces into account [36]. The resulting barrier for $\varepsilon_m/\varepsilon_w = 0.025$ and $r = 0.5$ nm is shown by the solid line in Fig. 9A. At the center of the membrane $f(\varepsilon_m/\varepsilon_w) = 0.18$, and the barrier height according to Eqn. 29 amounts to 4.1×10^{-20} J, which is about 10 kT at room temperature. A more profound analysis of this problem was performed by Jordan [37–39].

The conductivity g_p is proportional to the concentration of ions c_p in the pore (cf. section 3.2 in chapter 1) which may be estimated by the Boltzmann formula,

$$c_p = c_w \exp[-W_{wp}/(kT)] \tag{30}$$

where c_w is the corresponding ion concentration in the aqueous solution. It is then found that

$$g_p/g_w = \exp(-1/\xi) \tag{31}$$

where $\xi = r/d_m$ is a dimensionless pore radius, and from Eqn. 26

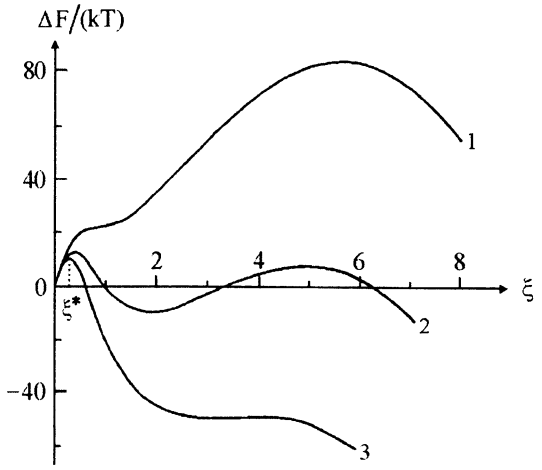

Fig. 10. Dependence of free energy change for pore formation ΔF on dimensionless pore radius $\xi = r/d_m$. The curves were calculated as described in the text for $\Delta\phi_m$ = 55 mV (1), 80 mV (2), and 100 mV (3). Other parameter values are $\gamma = 3 \times 10^{-4}$ N m^{-1}, $\gamma_\ell = 10^{-11}$ N, temperature 20 °C.

$$q_R(\xi) = (\pi\,\xi/2)\,\exp(-1/\xi) \tag{32}$$

Inserting $q_R(\xi)$ from Eqn. 32 into Eqn. 27 and performing the integration yields the electric work W_{el} and, together with W_{mech} from Eqn. 12, we obtain the change in free energy ΔF upon pore formation which is a function of the dimensionless pore radius ξ. Some examples of $\Delta F(\xi)$ are shown in Fig. 10. Note that $\Delta F(\xi)$ for $\Delta\phi_m$ = 80 mV has a minimum at $\xi \approx 2$, which corresponds to $r \approx 10$ nm for d_m = 5 nm. For such a large pore $\Delta\phi_p(r)/\Delta\phi_m \approx 0.2$, i.e. the difference between $\Delta\phi_p$ and $\Delta\phi_m$ becomes significant.

It is worth mentioning that Eqn. 15 is also applicable to vesicular systems [40], but the tension in this case is given by the Laplace equation

$$\gamma = \Delta p\, R_v/2 \tag{33}$$

where Δp denotes the pressure difference between the inner space of the vesicle and the surrounding solution, and R_v is the radius of the vesicles. The same is true for the refinements introduced by considering the spreading resistance and the conduction within a pore. However, there is an important difference between a BLM and vesicles because, in contrast to a planar structure, the surface of a sphere is not equipotential in a homogeneous electric field. As a consequence, the membrane potential $\Delta\phi_m$, the membrane lifetime before rupture and the associated permeability changes are dependent on

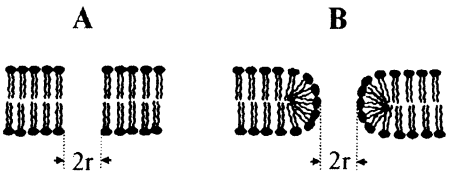

Fig. 11. Sketch of a cross section through a lipid membrane showing a hydrophobic pore (A) and a hydrophilic pore (B), both with radius r.

the polar angle θ between the field vector and the radius vector of the sphere (for details see section 3.1 in chapter 6). One could then expect a more pronounced threshold-like behavior for the permeabilization of vesicles as compared to the planar BLM. This question has recently been addressed on a theoretical level under simplifying assumptions [41–43].

3.2. Pore structure

While membrane breakdown can be well described by the formalism developed in the preceding section, reversible electroporation requires additional consideration. Up to now we did not care about the molecular organization of a pore, but this aspect has to be considered now, as will become clear from the following discussion. There are several indications that pores of relatively large size ($r > 0.5$ nm) are hydrophilic, i.e. their inner surface is covered with polar heads of phospholipids (see Fig. 11B). The most important argument is a strong dependence of the BLM lifetime in an electric field on the molecular geometry of the phospholipid molecules, a point which should be dwelt upon in more detail. In recent years, use has been frequently made of the classification of phospholipid molecules by their effective molecular geometry (see Fig. 12 and section 3 in chapter 3). Some lipids, such as phosphatidylcholine (PC), are represented by a cylinder, whereas others, such as phosphatidylethanolamine (PE) and lysophosphatidylcholine (LPC), are represented by a cone and an inverse cone, respectively. As is evident from Fig. 12 a hydrophilic pore could be most conveniently formed by molecules shaped as inverse cones (e.g., LPC). Hence, the smallest lifetime should be observed for membranes containing lysoform-lipids, providing the pores indeed have the hydrophilic edge which is formed as a result of intramembrane-directed monolayer bending. On the other hand, the largest lifetime should be a characteristic of PE membranes. This prediction is supported by the experimental data presented in Fig. 8, and makes one doubt whether the energy curves shown in Fig. 7 are cor-

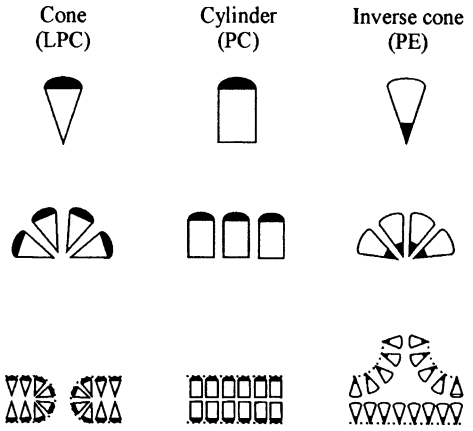

Fig. 12. Molecular geometry of lipids. The top row shows the effective molecular geometry with the polar end of the molecule marked in black. Possible arrangements of lipids due to their geometry and in a membrane are depicted in the middle and bottom row, respectively. Abbreviations: LPC, lysophosphatidylcholine; PC, phosphatidylcholine; PE phosphatidylethanolamine.

rect for small radii. In fact, these curves were obtained with the assumption that the linear tension γ_ℓ does not depend on the pore radius. However, if pore formation includes monolayer bending (i.e. the turn of phospholipid molecules at the pore edge) this bending will cause excessive energy losses for small radii where the curvature of the pore is large. Another factor to be considered is hydrational repulsion at the pore edge which is significant at distances less than 1 nm [44]. Therefore, there are good reasons to believe that the energy curve for a hydrophilic pore should have the form shown by curve 1 in Fig. 13.

Hydrophilic pores with small radii are so disadvantageous energetically that they are not realized at all. This means that some other low-energy and transient structures must exist which are capable of a transformation into hydrophilic pores. Intuitively attractive is the idea of hydrophobic pores (Fig. 11A) which are formed spontaneously by lateral thermal fluctuations of the lipid molecules. When their radius exceeds some critical value a reorientation of the lipids becomes energetically favorable. There are indeed few experimental data in the literature which support this idea. They were obtained with methods having a sufficiently high space and time resolution, such as ESR, NMR, as well as optical and electrical measurements. Effects of electric fields up to 10^5 V/cm on phosphatidylcholine multiple bilayers were investigated with ESR using cholane and stearic acid spin labels, as well as with ^{31}P-NMR [45]. The ^{31}P-NMR signal is specific for the polar head group region, and an electric field pulse caused an asym-

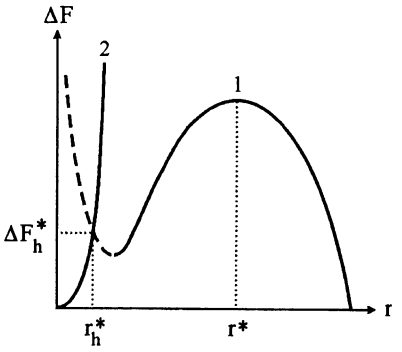

Fig. 13. Free energy change ΔF as a function of pore radius r for the formation of hydrophilic (1) and hydrophobic pores (2). The broken part of curve 1 marks the strong increase in ΔF at small radii, while curve 2 represents ΔF_h according to Eqn. 36 with $\Delta\phi_m=0$.

metric broadening and a down-field shift of the ^{31}P signal which are fully reversible and can be reproduced many times (Fig. 14). The stearic acid spin label probes the hydrocarbon part at defined depths in the membrane, while the rigid cholestane spin label is sensitive to more global structural changes. No changes in the ESR signal of these probes were observed suggesting that the number of hydrophilic pores is very low, if present at all. In fact, conductance measurements showed that transient changes in current occurred only with field pulses larger than 10^5 V/cm [45]. Although a detailed interpretation of these phenomena cannot be achieved they indicate that a reversible change in the polar headgroup orientation occurs in an electric field which affects a large part of the phospholipid population. No direct correlation was found between this change in orientation and the current fluctuations.

Structural changes were also analyzed by means of relaxation kinetics. An electric field-jump spectrometer permits to measure simultaneously field-induced changes in electric conductance and in light scattering properties of lipid vesicle suspensions in the nanosecond to millisecond time range. Square wave pulses of 10 μs duration and with amplitudes of up to 60 kV/cm were applied by means of a cable discharge device [46]. Figure 15A shows that there are up to three conductance relaxation modes. Mode I has the feature of a displacement current, while modes II and III correspond to the subsequent conductance relaxation. The shapes and the amplitudes of the relaxation curves depend on the field strength. Figure 15B reveals at most two relaxation modes for the field-induced light scattering dichroism. At all field strengths mode I has the same relaxation rate as the interfacial polarization current (i.e. mode II). The optical change thus seems to be caused and rate-limited by the buildup of the membrane poten-

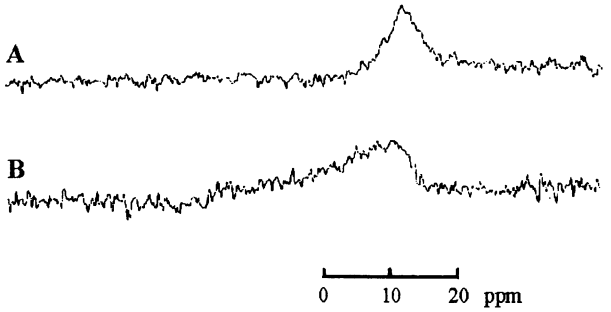

Fig. 14. ^{31}P-NMR signal of dimyristoyl phosphatidylcholine in the absence (A) and presence (B) of an electric field. Oriented lipid multilayers were spread between two silver-coated glass slides, and a field pulse of 83 kV/cm was repetitively applied. The NMR spectrometer sweeps were processed just after each pulse and averaged in order to increase the signal to noise ratio. Frequency 145.7 MHz, ppm values relative to H_3PO_4, magnetic field parallel to the bilayer surfaces. After Ref. 45.

tial. Mode II with a negative slope appears only at higher field strengths for which also mode III in the conductance relaxation is visible. These changes in light scattering dichroism are attributed to the formation of pores in the vesicle membranes, with hydrophobic pores appearing first (mode I) and hydrophilic pores being formed only at sufficiently high field strengths (mode II). The characteristic time of mode I is rather short as compared to that of mode II. This is in accord with the intuitive prediction that transforming hydrophobic pores into hydrophilic ones, which involves a reorientation of lipid molecules, should be slower than the formation of hydrophobic pores.

3.3. Formation of hydrophilic pores

The accumulation of hydrophilic pores in the membrane due to an electric field is considered to be the reason for reversible breakdown. Since hydrophilic pores most likely arise from a transformation of hydrophobic pores the formation of the latter has first to be considered. When calculating the mechanical work W_{mech} for the formation of such a pore one has to take the hydrophobic attraction of the pore edges into account [47] and then obtains (instead of Eqn. 12)

$$W_{mech} = 2\pi r d_m \gamma_h(r) \tag{34}$$

where γ_h denotes the tension at the interface between the hydrophobic lipid tails and water which depends on the pore radius r

$$\gamma_h(r) = \gamma_h(\infty)\, I_1(r/r_o)/I_0(r/r_o) \tag{35}$$

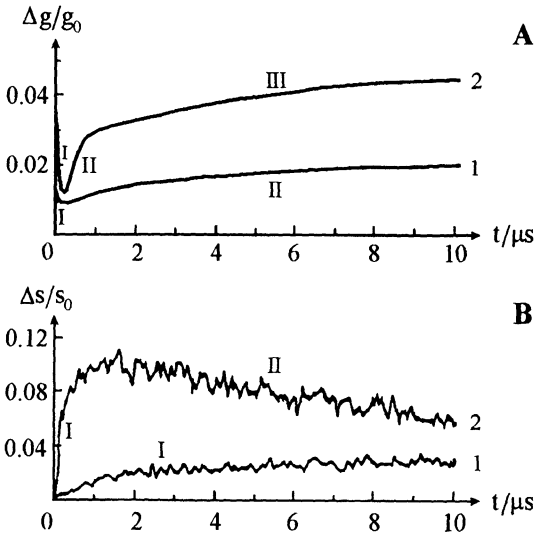

Fig. 15. Changes in conductance (A) and light scattering dichroism (B) as a function of time t, induced by electric field pulses with amplitudes of 20 (1) and 60 kV cm^{-1} (2). The signals are normalized with the corresponding values before application of the pulses. Different kinetic modes are marked with Roman numbers.

$I_n(r/r_o)$ are modified Bessel functions of n-th order, and $r_o \approx 1$ nm is a scaling length which has the meaning of an order parameter describing changes in water structure near the hydrophobic surface [48]. The electrical work W_{el} is still given by Eqn. 14, hence the change in free energy due to hydrophobic pore formation becomes

$$\Delta F_h(\Delta\phi_m,r) = 2\pi r d_m \gamma_h(r) - \Delta\phi_m^2 \pi r^2(\varepsilon_w-\varepsilon_m)/(2d_m) \qquad (36)$$

As is evident from Fig. 13 the formation of hydrophobic pores with very small radii is energetically more favorable than that of hydrophilic pores. But when their radius exceeds a critical value r_h^*, for which $\Delta F_h = \Delta F$, the hydrophilic pores become energetically favorable, and such a pore can be formed from a hydrophobic pore by a reorientation of the lipids. This process shall be called the inversion of the pore.

The hydrophobic pores are formed spontaneously due to the lateral thermal fluctuations of the lipid molecules, which is a zero order process described by the rate constant k_p. The lifetime of hydrophobic pores is of the order of the lipid fluctuations, hence they are only intermediate stages in the formation of hydrophilic pores. Providing the energy barriers for intermediate steps in the inversion of a pore are negligibly small the inversion occurs almost instantaneously once the critical radius r_h^* is reached, and k_p also describes the rate of

hydrophilic pore formation. According to the absolute rate theory k_p can be calculated as

$$k_p(\Delta\phi_m) = (\nu\, A/A_\ell)\, \exp[-\Delta F_h^*/(kT)] \tag{37}$$

where A is the area of the membrane and A_ℓ the area per lipid molecule, while $\Delta F_h^* = \Delta F_h(\Delta\phi_m, r_h^*)$. The quantity ν is a characteristic frequency of the thermal fluctuations of the lipid molecules, which comes in because the opening of a hydrophobic pore is mainly determined by lateral fluctuations of the lipids.

In order to test this model of reversible electroporation a witty experiment was designed [47]. A three-step pulse, consisting of two measuring parts with $\Delta\phi_m = \Delta\phi_M$ and one testing part with $\Delta\phi_m = \Delta\phi_T$ was applied to UO_2^{2+}-modified membranes. The difference ΔI between the current at the end of the first and at the start of the second measuring part was determined (see Fig. 16A). Providing the conductance of the hydrophilic pores does not strongly depend on the membrane potential ΔI is proportional to the number of pores $\Delta N(\Delta\phi_T)$ formed during the testing pulse $\Delta\phi_T$, which in turn is equal to the rate of pore formation times the length Δt of the testing pulse, hence

$$\Delta I/\Delta t \propto \Delta N(\Delta\phi_T)/\Delta t = k_p(\Delta\phi_T) \tag{38}$$

From Eqns. 36 and 37 with $\Delta\phi_m = \Delta\phi_T$ one can obtain the following relation for the rate constant k_p

$$\ln[k_p(\Delta\phi_T)] = \ln(\nu\, A/A_\ell) - \Delta F_h(0, r_h^*) / (kT) + \Delta\phi_T^2\, \pi\, r_h^{*2}\, (\varepsilon_w - \varepsilon_m)/(2 d_m\, kT) \tag{39}$$

Combining Eqns. 38 and 39 shows that $\ln(\Delta I/\Delta t)$ should be linearly dependent on $\Delta\phi_T^2$, as is indeed the case (Fig. 16B).

3.4. Resealing and extension of pores

The reverse transformation of a hydrophylic pore into a hydrophobic one is known as pore resealing. The kinetics of this process was studied with an experimental protocol similar to that described in the preceding section (cf. Fig. 16A). Two- and three-step pulses of different amplitudes were applied to UO_2^{2+}-modified BLMs and the relaxation of the current was recorded [2]. Three characteristic relaxation times could be detected. A first one, which is smaller than 5 μs, reflects non-ohmic properties of the membrane conductance. A second one ranging between 1 and 10 ms corresponds to the redistribution of hydro-

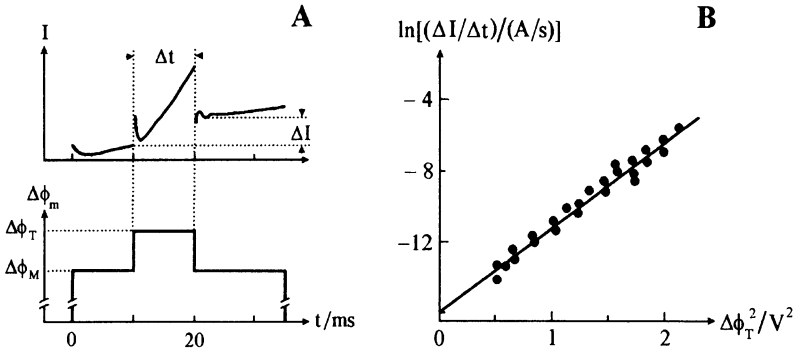

Fig. 16. Kinetics of pore formation during reversible breakdown of UO_2^{2+}-modified BLMs. (A) Experimental protocol, showing current I as a function of time t (top) in response to stepwise changes in membrane potential $\Delta\phi_m$ (bottom). (B) Dependence of $\ln(\Delta I/\Delta t)$ on $\Delta\phi_T$ for $\Delta\phi_M = 0.9$ V (cf. Eqns. 38 and 39).

philic pores in the radius space without any change in total number of pores. The third relaxation time has values between 1 and 100 s depending on the conditions of electrical treatment. It arises from the actual resealing of pores, thus indicating that this is relatively slow process. The total number of hydrophilic pores achieved at a quasi steady state was estimated to be 10^6 to 10^7 per cm^2 for a typical experimental protocol, i.e. relatively short pulses with moderate amplitudes.

The evolution of pores in time is governed by diffusion (Brownian motion) and by migration due to the driving force $-d\Delta F/dr$ (ΔF according to Eqn. 15). If $r < r^*$, where r^* is a critical radius (see Figs. 7, 10, and 13), both processes determine pore evolution. If $r > r^*$ migration dominates over diffusion, and

$$dr/dt = -[D_p/(kT)]\, d\Delta F/dr \tag{40}$$

where D_p is the diffusion coefficient in the r-space. Since most likely $q_R(r) >> 1$ for $r > r^*$ the potential drop across the pore is small (see Eqn. 25) and the electrical term in ΔF can be neglected. The solution of Eqn. 40 then reads [49]

$$r(t) = r^* \exp[2\pi\gamma D_p\, t/(kT)] \tag{41}$$

i.e. the pore size increases exponentially with a characteristic time

$$\tau = kT/(2\pi\gamma D_p) \tag{42}$$

The current $I_p(t)$ flowing through such a growing pore is (cf. Eqns. 23 and 25 with $q_R(r) >> 1$)

$$I_p(t) = \Delta\phi_p(r)/R_p \approx \Delta\phi_m/R_s = 2\Delta\phi_m g_w r(t) \quad (43)$$

Hence, one expects that the current through a membrane increases exponentially, at least during the initial stage of the process leading to mechanical rupture of the membrane. This was indeed observed in experiments and, from the characteristic time of this exponential rise, the value $D_p \approx 10^{-9}$ cm^2/s could be estimated by means of Eqn. 42 [49]. The effective diffusion coefficient D_p can also be estimated in another way. Using the assumption that the fluctuations in pore radius are associated with the influx and efflux of water molecules into and out of the pore it is found that

$$D_p = \langle v_w \rangle V_w/(8\pi d_m^2) \quad (44)$$

where V_w and $\langle v_w \rangle$ denote the volume and the average velocity of a water molecule, respectively [50]. With the parameter values $V_w = 3 \times 10^{-23}$ cm^3, $d_m = 5 \times 10^{-7}$ cm, and $\langle v_w \rangle \approx 1700$ cm/s at room temperature one obtains $D_p \approx 8 \times 10^{-9}$ cm^2/s. Thus, the agreement between the two estimates for D_p is quite good. It should be added that this description of irreversible breakdown of the membrane is valid irrespective of a membrane's ability to show reversible breakdown at moderate membrane potentials.

3.5. Electroporation of cell and lipid membranes

The results obtained from studies of electrical breakdown of BLM and cell membranes show that the basic regularities are remarkably alike. Thus, the time course of the current through the membrane of a human erythrocyte, measured by the patch-clamp technique (Fig. 17A), is similar to that for a BLM of oxidized cholesterol (Fig. 17B). In both cases the irreversible damage to the membrane is preceded by a reversible decrease of the resistance. The lifetime t_ℓ of BLMs and cell membranes in an electric field is a random quantity, and plots of $\log\langle t_\ell \rangle$ as a function of applied membrane potential (cf. Fig. 3) show linear dependencies with similar slopes [51]. Common features are also observed for the reversible breakdown of membranes, e.g. the dependence of the breakdown potential on the duration of a charging pulse is similar for the alga *Valonia* and BLMs [52]. The breakdown potential of cell membranes and BLMs depend in a similar manner on the composition of the electrolyte solution as well as on temperature. As in the case of BLMs an increase in intensity and duration of the electrical treatment leads to a simultaneous increase in both the number of pores and their mean radius [53, 54]. A sudden decrease in membrane potential causes in both systems a rapid (order of μs)

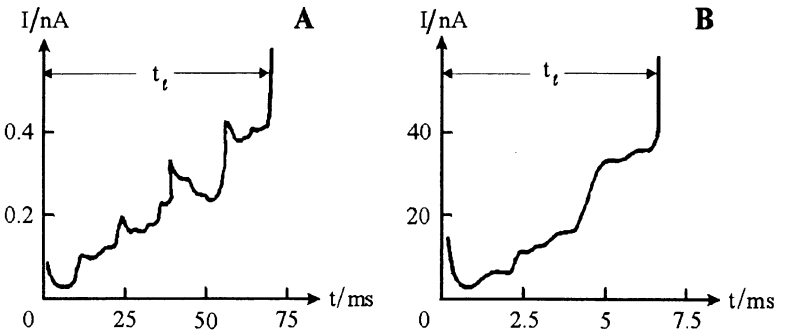

Fig. 17. Time dependence of current I trough a human erythrocyte membrane (A) and a BLM of oxidized cholesterol (B). At t = 0 a voltage step of 300 mV (A) or 200 mV (B) was applied. In both cases an initial decrease of I due to charging of the membrane capacity (cf. Fig. 1) is followed by an increase with random fluctuations, which ends in a drastic current jump due to irreversible breakdown (membrane rupture); t_t indicates the membrane lifetime. Note that the steady state for I shown in Fig. 1 is absent here.

decrease in conductance [55]. However, in cell membranes the resealing time is considerably longer (up to hours) as in BLMs where resealing occurs within seconds [47, 53, 54, 56–58]. This difference can be explained by the presence of membrane-bound proteins at the pore edges giving rise to an occlusion effect which significantly increases the pore lifetime. Moreover, secondary processes in cells, such as colloidosmotic lysis [53, 54, 59], and the low value of the cell membrane tension may cause changes of the breakdown character especially at late stages. In spite of these differences there is good evidence that pore formation in lipid domains of cell membranes can be considered as a primary effect of electrical treatment.

Acknowledgements

This work was supported by the CNRS and by a "Bourse pour chercheur de haut niveau" from the French Ministère de la Recherche.

References

1 Tsong TY (1991) Biophys. J. 60: 297–306.
2 Chernomordik LV, Chizmadzhev YA (1989) Electrical breakdown of lipid bilayer membranes. In: E Neumann, A Sowers, C Jordan (eds): *Electroporation and Electrofusion in Cell Biology*. Plenum Press, New York, 83–95.
3 Chizmadzhev YA, Pastushenko VF (1988) Electrical breakdown of bilayer lipid membranes. In: IB Ivanov (ed): *Thin Lipid Films*. Marcel Dekker Inc, New York, Basel, 1059–1126.

4 Weaver JC, Chizmadzhev YA (1996) Bioelectrochem. Bioenerg. 41: 135–160.
5 Zimmermann U, Pilwat G, Riemann F (1974) Biophys. J. 14: 881–887.
6 Zimmermann U, Pilwat G, Riemann F (1975) Biochim. Biophys. Acta 375: 201–205.
7 Abidor I, Arakelyan V, Chernomordik L, Chizmadzhev YA, Pastushenko V, Tarasevich M (1979) Bioelectrochem. Bioenerg. 6: 37–52.
8 Benz R, Beckers F, Zimmermann U (1979) J. Membr. Biol. 48: 181–204.
9 Tien HT (1974) *Bilayer Lipid Membranes (BLM)*. Marcel Dekker Inc, New York, 655.
10 Chernomordik LV, Sukharev SI, Abidor IG, Chizmadzhev YA (1983) Biochim. Biophys. Acta 736: 203–213.
11 Wobshall D (1972) J. Colloid Interf. Sci. 40: 417–421.
12 Benz R, Ianko K (1976) Biochim. Biophys. Acta 455: 721–725.
13 Babakov AV, Ermishkin LN, Libermann EA (1966) Nature 210: 953.
14 Chernomordik LV, Abidor IG (1980) Bioelectrochem. Bioenerg. 7: 617–620.
15 White SH (1970) Biophys. J. 10: 1127–1133.
16 Chernomordik LV, Sukharev SI, Abidor IG, Chizmadzhev YA (1982) Bioelectrochem. Bioenerg. 9: 149–155.
17 Melikov KC, Frolov VA, Shcherbakov AA, Samsonov AV, Chizmadzhev YA, Chernomordik LV (2001) Biophys. J. 80: 1829–1836.
18 Crowley IM (1973) Biophys. J. 13: 711–717.
19 Requena I, Haydon DA, Hladky SB (1975) Biophys. J. 15: 77–84.
20 Michael DH, O'Neill ME (1970) J. Fluid Mech. 41: 571–580.
21 Steinchen A, Gallez D, Sanfeld A (1982) J. Colloid Interf. Sci. 85: 5–12.
22 Maldarelli Ch, Jain R, Ivanov I, Ruckenstein E (1980) J. Colloid Interf. Sci. 78: 118–125.
23 Dimitrov DS (1984) J. Membr. Biol. 78: 53–60.
24 Sugar IP (1979) Biochim. Biophys. Acta 556: 72–85.
25 Becker R, Dering W (1935) Ann. Physik 24: 719–725.
26 Christiansen IA (1936) Z. Phys. Chem. 33: 145–153.
27 Kramers HA (1940) Physica 7: 284–292.
28 Zeldovich IB (1942) J. Experim. Theoret. Physics 12: 525–538 (in Russian).
29 Derjaguin BV, Gutop YV (1962) Colloid J. 24: 431–437 (in Russian).
30 Derjaguin BV, Prokhorov AV (1981) J. Colloid Interf. Sci. 81: 108–115.
31 Pastushenko VF, Chizmadzhev YA, Arakelyan VB (1979) Bioelectrochem. Bioenerg. 6: 53–62.
32 Weaver JC, Mintzer RA (1981) Phys. Lett. 86: 57–59.
33 Pastushenko VF, Chizmadzhev YA (1982) Gen. Physiol. Biophys. 1: 43–52.
34 Newman J (1966) J. Electrochem. Soc. 113: 501–502.
35 Neumcke B, Läuger P (1969) Biophys. J. 9: 1160–1169.
36 Parsegian VA (1969) Nature 221: 844–846.
37 Jordan PC (1982) Biophys. J. 39: 157–164.
38 Jordan PC (1984) Biophys. J. 45: 1101–1108.
39 Jordan PC (1984) Biophys. J. 45: 1091–1100.
40 Pastushenko V, Chizmadzhev YA (1989) Biol. Memb. 2: 1951–1972.
41 Bilska AO, DeBruin KA, Krassowska W (2000) Bioelectrochemistry 51: 133–143.
42 DeBruin KA, Krassowska W (1999) Biophys. J. 77: 1225–1233.
43 DeBruin KA, Krassowska W (1999) Biophys. J. 77: 1213–1224.
44 LeNeveu DM, Rand RP, Parsegian VA (1976) Nature 259: 601–603.
45 Stulen G (1981) Biochim. Biophys. Acta 640: 621–627.
46 Neumann E, Sprafke A, Boldt E, Wolff H (1992) Biophysical considerations of membrane electroporation. In: DC Chang, BM Chassy, JA Saunders, AE Sowers (eds): *Guide to Electroporation and Electrofusion*. Academic Press, San Diego, 77–90.
47 Glaser RW, Leikin SL, Chernomordik LV, Pastushenko VF, Sokirko AI (1988) Biochim. Biophys. Acta 940: 275–287.
48 Israelachvili JN, Pashley RM (1984) J. Colloid Interf. Sci. 98: 500–514.
49 Sukharev SI, Arakelyan VB, Abidor IG, Chernomordik LV, Pastushenko VF (1983) Biophysica 28: 756–760 (in Russian).
50 Powell K, Weaver JC (1986) Bioelectrochem. Bioenerg. 15: 211–227.
51 Chernomordik LV, Sukharev SI, Popov SV, Pastushenko VF, Sokirko AV, Abidor IG, Chizmadzhev YA (1987) Biochim. Biophys. Acta 902: 360–373.
52 Benz R, Zimmermann U (1980) Bioelectrochem. Bioenerg. 7: 723–739.
53 Kinosita K, Tsong TY (1977) Biochim. Biophys. Acta 471: 227–242.

54 Kinosita K, Tsong TY (1977) Nature 268: 438–441.
55 Benz R, Conti F (1981) Biochim. Biophys. Acta 645: 115–123.
56 Zimmermann U (1982) Biochim. Biophys. Acta 694: 227–277.
57 Dressler V, Schwister K, Haest CWM, Deuticke B (1983) Biochim. Biophys. Acta 732: 304–307.
58 Sowers AE, Lieber MR (1986) FEBS Lett. 205: 179–184.
59 Zimmermann U, Sheurich P, Pilwat G, Benz R (1981) Angew. Chem. Int. Ed. 20: 325–344.

Bioelectrochemistry of Membranes
ed. by D. Walz, J. Teissié and G. Milazzo†

CHAPTER 6
Cell membrane electropermeabilization

Justin Teissié

Centre National de la Recherche Scientifique, Toulouse, France

1. Introduction

In this chapter the description of the processes associated with cell electropulsation is presented. Although many analogies with phenomena observed in bilayer lipid membranes are found (see chapter 5), there is no experimental evidence that the processes are exactly the same. The physical perturbation is not uniform on the cell surface. The permeabilization is reversible in most cases even in the cases of pure lipid systems such as liposomes. The cell membrane cannot be described as a lipid bilayer. Proteins play a structural and an active role in the organization of the membrane. At the present stage of investigation, a molecular description of electropermeabilization remains speculative. Hence we present a phenomenological description in order to give to the reader what is needed for a good understanding of the applications. When this field induced conductance increase is accompanied by mechanical rupture, one speaks of irreversible electrical breakdown. In certain conditions this conductance increase is temporary and the membrane's initial barrier properties are restored, the phenomenon is thus reversible. The interest in these

two types of electrical perturbations is attributed to their biological significance and to a wide scope of applications. With regard to biomedical applications of reversible breakdown, we mention 1) loading cells with drugs, which makes it possible to use them as bioactive vesicles, 2) gene transfer, 3) protein insertion and 4) electrostimulated cell fusion for obtaining hybrid cells. Irreversible electrical breakdown is regarded as one of the mechanisms of impairment of the barrier function in pathology.

The cell membrane's selective permeability has the advantage to preserve the genome and the cellular machinery from the action of exogenous aggression, but at the same time is a strong limitation for the experimental manipulation of the cytoplasm. Spontaneous introduction of foreign proteins or genes is not possible and artificial methods must be found which of course should alter the membrane permeability but not affect the viability. *Electropulsation*, i.e. submitting cells to strong electric field pulses of short duration, is a new methodology which is now proved to be highly efficient to give access to the cytoplasm. The methodology is very simple. Two electrodes are connected to a voltage pulse generator. A cell suspension is brought between the electrodes. The generator is switched on for a predetermined time (pulse duration), and a field pulse is thus applied to the cell suspension. Different pulse shapes are obtained as a consequence of the nature of the voltage generator. By the use of more sophisticated technologies, cells growing spread on culture dishes or on microcarriers can be treated. *Electropermeabilization and electrotransformation* (i.e. gene transfer and expression in the pulsed cells) are very potent tools for bioengineering. The methodologies are similar whatever the cell systems. It is only the field intensity and the pulse duration which have to be adjusted. Positive results are obtained with eukaryotes as well as with prokaryotes. Very interestingly, the presence of a cell wall in bacteria and yeasts is not preventing the effect of the fields, and electrotransformation of bacteria is a routine procedure.

Electropulsation is a well controlled technological approach in cell biology where the perturbation is defined in its magnitude as well as on the definition of its onset. Two kinds of effects are triggered by the field pulse; some are present only as long as the field is present but others remain present after it. Cell viability may remain preserved. Nevertheless, one must consider that indeed very few things are known on the molecular mechanisms responsible for electropermeabilization. Very few structural data on the organization of the cell membrane, either during the pulse or after the pulse, have been published. One should take into account that studies at the single cell level on the time scale of electropulsation (i.e. less than 1 ms) need a very sophisticated instrumentation (video microscope recording on a

microsecond scale, which presently is available only in one laboratory in the world). Studies at the cell population level on the same time scale are performed by different techniques (such as measuring conductance, light scattering or fluorescence) but do not provide direct information. Post-pulse structural alterations were obtained by electronmicroscopy or by spectroscopic techniques (fluorescence, NMR). It should be emphasized that most of the experimental results have been obtained on mammalian cells but the conclusions have been shown to be fully valid for plant protoplasts and with some limitations in the case of walled microorganisms (bacteria, yeasts).

2. Physical effects of the electric field pulse

2.1. Joule effect

A very trivial effect of the field pulse on a cell suspension should not be neglected, i.e. Joule heating. In most experiments cells must be kept in a "physiological" buffer where ions must be present in order to preserve the integrity of the cell and its viability. The cell containing solution between the two electrodes where the field is created is thus a conducting medium. A current is then flowing in the cell suspension during the voltage pulse. The Joule heating can be calculated by equating the heat q, which is required to change the temperature of the sample by ΔT, to the electrical energy U_{el} of the pulse. When using square wave pulses on a sample between two flat parallel electrodes where no electrochemical reactions occur, the heat is

$$q = C_p V \Delta T \tag{1}$$

where C_p denotes the heat capacity of the cell suspension at constant pressure, which can be approximated by that of water, and V is the volume of the cell suspension between the electrodes. The electrical energy is

$$U_{el} = \Delta\phi^2 t_p/R \tag{2}$$

where $\Delta\phi$ is the potential difference applied between the two electrodes, t_p denotes the pulse duration, and R is the resistance of the sample. The latter can be expressed as

$$R = d_e/(g_s A) \tag{3}$$

Here g_s denotes the conductivity of the suspension, which is a function of the cell concentration, the membrane integrity, and the ionic con-

tent of the buffer, while A is the area of the electrodes and d_e the distance between them such that

$$V = d_e A \tag{4}$$

With $q = U_{el}$ one then obtains from Eqns. 1–4

$$\Delta T = \Delta\phi^2 t_p g_s A/(d_e^2 C_p A) = E^2 t_p g_s/C_p \tag{5}$$

where $E = -\Delta\phi/d_e$ is the electrical field strength. The temperature increase is thus proportional to the square of the field strength and to the pulse duration, and is strongly dependent on the ionic content of the buffer. If the membrane integrity is altered in such a way as to increase the conductance of the suspension, then the temperature increase is larger than computed with Eqn. 5.

If repetitive pulses are applied to the suspension and the time between the pulses is short (say less than 1 s) essentially no heat dissipation occurs, and the cumulative temperature rise is just the sum of the increments ΔT for each pulse. If the time between pulses is long enough, heat dissipation can occur, and the temperature increase becomes less than the sum of the ΔT's. Nevertheless, one point must be kept in mind. Whatever the thermostating set-up around the cell suspension, a fast temperature jump takes place during the pulse which may alter the properties of the cell if the pulse is too large. In a high salt medium such as phosphate buffered saline (PBS), an increase in temperature of 80 °C is observed by pulsing during 25 ms with 1 kV/cm, but already after 0.8 ms with 5 kV/cm. Low salt pulsing buffers must be used if long pulses with a high field strength are required, as in the case of electrotransformation of bacteria. In a 1 mM Tris buffer, the temperature increase associated with a 0.8 ms, 5 kV/cm pulse is only 2.6 °C.

If a capacitor discharge system with capacitance C is used, then (cf. Eqn.17 in chapter 1)

$$U_{el} = {}^1/_2\, C\, \Delta\phi^2 \tag{6}$$

and

$$\Delta T = C\, \Delta\phi^2/(2C_p V) \tag{7}$$

The temperature increase is no longer a function of the composition of the pulsing buffer. The geometry of the pulsing chamber plays a role in the temperature increase through V and its control of E. As an example, pulsing 0.2 ml under 2 kV with a discharge capacitor of 25 μF gives a temperature increase of 60 °C.

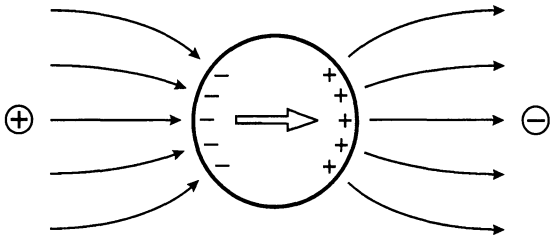

Fig. 1. A conducting particle in a poorly conducting medium showing electric field lines (arrows) and charge separation yielding an induced dipole moment (open arrow).

2.2. Dielectrophoresis

The plasma membrane of most cells carries a fixed charge. Therefore, the cells experience a force in an external constant electric field and start to move. In the steady state this force is balanced by the viscous drag and the cells migrate at a constant velocity v as given by Smolukhovsky's formula (electrophoresis, see Eqn. 46 in chapter 1). However, the field pulses are usually so short that no appreciable electrophoresis takes place, and this phenomenon can therefore be neglected.

In inhomogeneous and alternating electric fields a phenomenon known as dielectrophoresis occurs. The quantitative treatment of this phenomenon requires rather complex calculations pertaining to the distribution of electric field and potential around the cell, which can be found, e.g., in Ref. 8. In the present context it suffices to mention that the cell can be approximated as a "conducting particle in a poorly conducting medium". In this case the electric field lines concentrate at the surface of the particle, while the field inside the particle should vanish as a result of screening of the external field by the separation of mobile charges (Fig. 1). This polarization gives rise to an induced dipole moment whose orientation is parallel to the undisturbed external field lines.

The cell membrane is usually approximated as an insulator for direct current and sufficiently long pulses (although a certain intrinsic permeability for charged species does exist). But it also constitutes a capacitance (see section 2.3.4 in chapter 1) which turns it into a conductor for sufficiently short pulses. The characteristic time, which specifies the boundary between these two regions of behavior, was estimated to be about 10 μs for mammalian cell membranes. However, this time was found to be much shorter for membranes of intracellular organelles. In other words, the cell membrane is transparent only for very short pulses (~ 50 ns), while the membranes of organelles almost always behave as resistors.

2.3. Stretching deformations of cells in an electric field

The cell membrane is an elastic body and hence a cell is deformed under the action of the forces associated with an electric field. In electrostatics these forces are described by the Maxwell tension, whose analysis reveals that the force field depends on pulse duration. It is the result of electrostatic interactions between the dipole moment **p** induced in the cell (cf. Fig. 1) and the applied electric field. The magnitude of the induced dipole moment can be written as:

$$|\mathbf{p}|(t) = 4\,\pi\varepsilon_e\,\varepsilon_0 r^3\,E\,\alpha(t) \tag{8}$$

Here E is electric field strength, $\alpha(t)$ is the time-dependent polarizability of the cell, while ε_e and ε_0 denote the relative permittivity (or dielectric constant) of the external medium and the absolute permittivity, respectively. The cell is approximated as a sphere with radius r. The force is proportional to the product $E|\mathbf{p}|$, hence its time dependence is identical with that of the induced dipole which in turn is determined by the time course of α.

The polarizability of the cell is a complex function of the specific conductivities g_i and g_e of the internal cell volume and the external buffer, respectively, as well as of the cell size and of the pulse duration. Its time dependence can be summarized as follows.

- If the pulse duration is shorter than 10 ns, α can be considered as zero.
- For pulse duration between 10 ns and 5 μs,

$$\alpha(t) = (g_i - g_e)/(g_i + 2\,g_e) \tag{9}$$

  i.e., $\alpha(t)$ is positive only if $g_i > g_e$. The rise time of $\alpha(t)$ is given by:

$$\tau_\alpha = (\varepsilon_i + \varepsilon_e)/(g_i + 2\,g_e) \tag{10}$$

  where ε_i is the dielectric constant of the internal cell volume. Since values of τ_α are always in the nanosecond time range, the force reaches its maximal amplitude in this short time and is present during the whole pulse.
- For pulse duration longer than 10 μs, and if the membrane conductance is negligible (i.e. with an intact membrane),

$$\alpha(t) \approx \text{const} = -0.5 \tag{11}$$

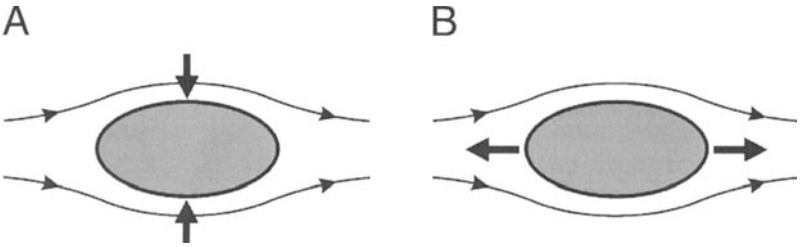

Fig. 2. The forces acting on the particle due to an external electric field for a long pulse (A) and a short pulse (B).

But if the membrane becomes conductive (which is the case with electropermeabilization) then α changes to the limiting value

$$\alpha_{lim} = (g_i - g_e) / (g_i + 2\,g_e) \tag{12}$$

In conclusion, stretching and/or compressive forces are exerted on the cell membrane whose steady state values expressed as radial force per unit membrane area yield the electrical pressure

$$p_E = (^9/_2)\ \varepsilon_e\ \varepsilon_0\ E^2 \cos^2\theta\ (g_i^2 - g_e^2) / (g_i + 2\,g_e)^2 \tag{13}$$

where θ is the angle between the direction of the field and the normal to the cell surface.

Without going into details we just mention that in the case of short pulses (less than 5 μs) in a poorly conducting buffer the forces are mainly parallel to the field lines and therefore "pull" the cell at its poles (Fig. 2) while the forces are mainly perpendicular to the field lines in a highly conducting buffer and thus "squeeze" the cell along the equator (Fig. 2A). In both cases the resulting deformation of the cell is the same, i.e. its shape changes from spherical to ellipsoidal. For long pulses, cells are first pushed at their poles, but when they are (electro)permeabilized (see below), their behaviour will become again dependent on the buffer conductivity, i.e. stretching at low g_e and squeezing at high g_e.

Cell membranes are often mechanically stabilized by elements of the cytoskeleton (cf. Fig. 1C in chapter 2) and the deformations may then be less pronounced. Nevertheless, the tension experienced by the membrane can have an effect on its performance, including its responsiveness to induction of electropermeabilization.

3. The external field alters the transmembrane potential difference of the pulsed cell

3.1. Distribution of the electrical potential around an isolated cell

Consider the distribution of the potential around a spherical cell of radius r and in its membrane upon application of a direct uniform external field E. For a medium with low conductivity the problem is reduced to the solution of the Laplace equation (cf. section 2.3.1 in chapter 1)

$$\nabla^2\phi = 0 \tag{14}$$

with the boundary conditions

$$d\phi/dx\,|_{x=r} = 0 \quad \text{and} \quad -d\phi/dx\,|_{x=\infty} = E \tag{15}$$

From a theoretical point of view, the Laplace equation predicts that the transmembrane potential difference $\Delta\phi_m = \phi_{in} - \phi_{ex}$ of a cell can be manipulated by submitting it to an external field [11]. This effect is due to the dielectric character of the membrane inducing a deformation of the lines of the electric field applied onto the cells. As described in Refs. 11–13, the field-induced transmembrane potential difference is

$$\Delta\phi_{m,E} = -\,f\,r\,E\cos\theta \tag{16}$$

where f is a parameter characteristic of the cell, r is the radius of the sphere which approximates the cell, E is the strength of the applied electric field, and θ is the angle between the direction of the field and the normal to the cell surface (see Fig. 3). Since the electric field in the membrane with thickness d_m is

$$E_m = -\,\Delta\phi_m/d_m \tag{17}$$

it follows from Eqns. 16 and 17 that the membrane acts as an electric field amplifier with a maximal gain in field strength between the intramembrane and external field of

$$E_m/E = f\,r/d_m \quad \text{at} \quad \theta = 0 \tag{18}$$

With the typical parameter values r = 5 μm and d_m = 5 nm, the amplification factor is 10^3f, i.e. an external field of 1 kV/cm will induce a membrane field of 10^6f V/cm. This is a key fact in the induction of electropermeabilization.

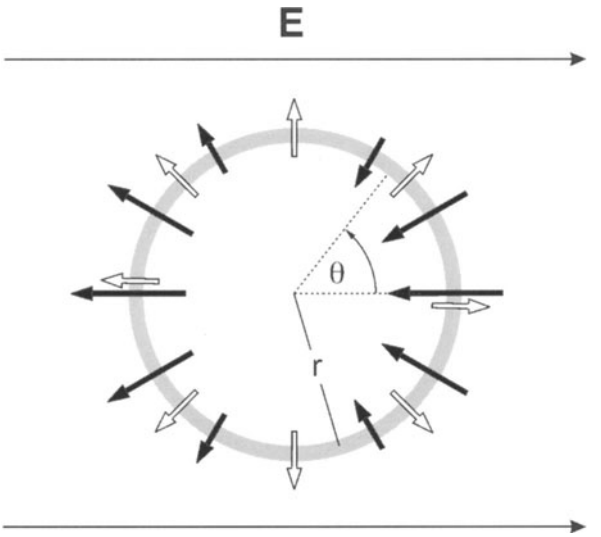

Fig. 3. Modulation of the transmembrane potential difference of a spherical cell by an external electric field. Open and closed thick arrows indicate the resting and the field-induced transmembrane potential difference $\Delta\phi_{m,r}$ and $\Delta\phi_{m,E}$, respectively. They point from negative to positive, and their lengths indicate the magnitude of the respective potentials. Thin arrows represent the electric field lines.

Most cells have a resting (or intrinsic) transmembrane potential difference $\Delta\phi_{m,r}$. Hence the total potential difference is

$$\Delta\phi_m = \Delta\phi_{m,r} + \Delta\phi_{m,E} \tag{19}$$

One hemisphere of the cell is hyperpolarized and the other depolarized with respect to $\Delta\phi_{m,r}$, while the equator is unaffected, i.e. $\Delta\phi_m$ is position dependent (Fig. 3). This theoretical approach has been confirmed experimentally by means of digitalized video microscopy [14–16].

A point often neglected when evaluating the field-induced $\Delta\phi_{m,E}$ is the role played by the parameter f in Eqn. 16. As described in Ref. 11, for the approximation of the cell as a sphere with radius r,

$$f = 3/\{(2[1 + g_m\,(2 + g_i/g_e)/(2\,g_i\,d_m/r)]\} \tag{20}$$

where g_m, g_i, and g_e denote the specific conductivities of the cell membrane, the internal cell volume, and the external buffer, respectively. As a first approximation the membrane can be considered as a pure dielectric (i.e. $g_m = 0$) which yields $f = 1.5$. Using this value for f in Eqn. 16 provides a theoretical upper limit for $\Delta\phi_{m,E}$. Similarly, an upper

limit of the maximal gain in field strength (Eqn. 18) is obtained, i.e. with r = 5 μm and d_m = 5 nm the membrane field is 1.5 MV/cm for an external field of 1 kV/cm.

In fact, the membrane is not a pure dielectric. It was indeed shown that increasing the membrane conductivity g_m induces a drop in the field-mediated $\Delta\phi_{m,E}$ [17]. In a cell membrane, many ionic leaks and pumps are present to allow the exchange of nutrients and to maintain the resting $\Delta\phi_{m,r}$. The relative density and activity of these non-dielectric sites in the cell membrane are dependent on the nature and the age of the cell. They are also a function of the physiology of the biological system.

Another unresolved problem is the approximation of the cell by a sphere with radius r. If the case of simple geometry (sphere, ellipsoid) can be approached by mathematical simulation the biological fact should take into account more sophisticated structures such as the presence of villi. A very localized definition of the electric effects is present. As a consequence, the values obtained from Eqn. 16 should be considered as a first approximation of the experimental system.

3.2. Charging time of the membrane during the field pulse

The induction of the changes in transmembrane potential difference by the electric field pulse occurs through a polarization phenomenon. This can be considered as a small perturbation which leads to exponential time courses, when the field strength is kept constant during the pulse,

$$\Delta\phi_{m,E}(t) = \Delta\phi_{m,E,max}\,[1 - \exp(-t/\tau_m)] \tag{21}$$

The relaxation time τ_m for charging the membrane is a complex function of the membrane properties, as well as of the compositions of the cytoplasm and the buffer,

$$\tau_m = r\,C_m\,(g_i + 2g_e)/[2\,g_i\,g_e + r\,g_m\,(g_i + 2g_e)] \tag{22}$$

where C_m denotes the specific membrane capacitance. In many cases the specific conductivity of the cell membrane is so small that $2\,g_i\,g_e >> r\,g_m\,(g_i + 2g_e)$, hence

$$\tau_m \approx r\,C_m\,(g_i + 2g_e)/(2\,g_i\,g_e) \quad \text{for small } g_m \tag{23}$$

The assumption of a small value of g_m is valid only as long as a few leaks are present in the membrane. This is under the control of the

physiology of the cell (more leaks are present in aged cells) or can be modified by adding chemicals such as gramicidin.

It is evident from Eqn. 22 that τ_m depends on the size of the cell or is proportional to r for small g_m (Eqn. 23). But it also depends on the composition of the pulsing buffer which determines the specific conductivity g_e. The final value of $\Delta\phi_{m,E}$ is reached after a shorter time in a high salt medium. Thus, in the case of erythrocytes, it was calculated that τ_m is increased from about 0.2 μs in 0.15 M NaCl to about 1 μs in 10 mM phosphate buffer. On the other hand, τ_m is not position-dependent, and $\Delta\phi_{m,E}$ is affected kinetically in the same relative way everywhere on the cell surface.

As will be discussed below the charging time is in fact a kinetic limiting step in the induction of cell electropermeabilization. It has to be taken into account when working with short pulses and large cells such as plant protoplasts or myeloma cells, where τ_m is as large as 10 μs. With a 5 μs square wave pulse, only a fraction (40%) of the limiting value of the field-induced $\Delta\phi_{m,E}$ is obtained at the end of the pulse. The problem is more important in the case of exponentially decaying field pulses. If the decay time is 10 μs, the field-induced $\Delta\phi_{m,E}$ will never reach more than 34% of the maximal value. When using high frequency AC fields, the induced potential difference is always much smaller than that computed from the steady state expression. With a frequency of 1 MHz, only 5% of the maximal value can be reached.

4. Methods for determining electropermeabilization

The membrane in its native state protects the cytoplasm from the outer medium by means of low or well-controlled permeabilities for all sorts of molecules. Hence, cell electropermeabilization can be easily followed by the inflow of exogenous molecules, such as dyes, or by the leakage of metabolites out of the cell.

The inflow can be monitored by the detection and quantification of the entrapped molecules; this is easy with dyes (trypan blue) or fluorescent probes (ethidium bromide, calcein, fluoresceinated dextran) by observing cells under a microscope [18–20]. This can be detected by a back effect of the penetration as in the case of Ca^{2+}. Electropermeabilization mediated Ca^{2+} penetration leads to a cytoplasmic imbalance and the cell lysis.

The outflow can be followed by the detection of the leaked molecules or ions. This is very easily done in the case of ATP by means of the luciferin-luciferase assay [21] or in the case of ions by following the increase in conductivity of the cell suspension when working

in a low ionic content pulsing buffer [22, 23]. This last approach is of great convenience for the fast kinetic resolution of the induction of permeabilization. Time resolution down to a fraction of a microsecond can be obtained. In such a case, effects kinetically associated with the field can be discriminated from those which are back-effects.

Different ways of determination of electropermeabilization in a cell population can be operated. When the net accumulation or leakage of the probe molecules can be quantitated (Method 1), it is easy to detect the occurence of permeabilization. If the flow rate of the exchange of the molecule across the pulsed cell membranes is measured, then the dependence of the permeabilization can be assayed quantitatively as a function of the field pulse parameters (strength, duration, number). But in that case, it is not possible to know the number of permeabilized cells in the population.

If the percentage of labeled cells is determined (Method 2), it is the number of cells where the amount of incorporated molecules is larger than an experimental threshold (detection limit) which is quantified. Since the time during which the reporter molecules are accumulated inside the pulsed cell is constant in a given experiment, their inflow must be larger than a critical value to detect the permeabilization. But such a detection is an all or none approach and it is not possible to determine the exact amount of molecules which is accumulated in the cells. If the permeabilization of the cell membrane is too low the accumulation is too small, and the experimental observation will be negative. Again, such an approach gives information on the dependence of electropermeabilization on the field parameters.

If the percentage of labelled cells and the level of loading in each single cell are measured simultaneously using a cell sorter technique (Method 3), all characteristics of cell permeabilization are observed [24]. One artefact of this method is that it is impossible to know if the fluorescent probe is in the cytoplasm or just inserted in the membrane or the cell wall.

Events at the cellular level can be obtained by submicrosecond imaging under a pulsed laser microscope [16, 25]. Changes in the cell shape can be observed by phase contrast observation and alterations of the membrane conductance are detected by use of specific fluorescent probes. Local post pulse accumulation of dyes (fluoresceinated dextrans, PI, ethidium bromide) can be detected at the single cell level under the microscope either by means of a photomultiplier tube or by digitized video monitoring (Method 4). In such a case, it is the new permeability at the level of the cell which is quantified, and information on the compartmentalisation inside the cell is then available.

5. The external field induces a reversible membrane permeabilization

Studies on bilayer lipid membranes (BLM) showed that a lipid membrane conductance was dramatically affected by an increase in its transmembrane potential difference $\Delta\phi_m$. In most cases, a rupture of the BLM follows, except in the case of exotic lipid mixtures (see section 2 in chapter 5). One would then predict that the application of calibrated electric field pulses on a cell or on a cell suspension would induce an increase in the cell membrane permeability. It is just needed that the external field induces a change in $\Delta\phi_m$ which exceeds a threshold $\Delta\phi_c$ above which permeabilization occurs (see section 6). This was indeed first observed in 1972 [26] as a release of catecholamines in a suspension of pulsed chromaffin granules. This leakage was only transient but nevertheless lasted much longer than the pulse duration. This observation is not specific for cells. When using lipid vesicles, an electric field pulse mediated reversible permeabilization can also be observed through the detection of the leakage of the inner content [27]. In fact, this process has been applied to many other systems, such as erythrocytes [13], plant protoplasts [3], mammalian cells [28] and bacteria [29]. In all cases, cell electropulsation was giving access to the cytoplasm in a reversible way keeping the cells viable.

A direct observation of electropermeabilization was obtained during the field pulse by video microscopy [25]. A fluorescence probe, which is sensitive to the transmembrane potential difference, was embedded in the membrane of a sea urchin egg and observed as described above in order to follow the field-induced changes in $\Delta\phi_m$. While at a low field strength the fluorescence signal complied with the dependence on position θ as predicted by Eqn. 16, a flattening of the signal appeared at high field strengths up to 200–400 V/cm in the regions of the poles (Fig. 4). This is interpreted as a sharp increase in the conductance of the membrane in the polar regions facing the electrodes, where the membrane field is maximal (θ around 0 and 180°), as a result of which the potential is shunted. The shunting phenomenon, i.e. the permeabilization process, is at least as fast as the very fast recording system used. Taking into account the delay in the induction of the potential difference change due to the charging time, the permeabilization is triggered locally on a fraction of a microsecond.

Another fast kinetic approach is to follow the conductance change in the cell suspension during the pulse by recording the intensity of the current crossing the sample. A sharp decrease is detected in less than 0.2 μs showing that permeabilization is induced on such a time scale.

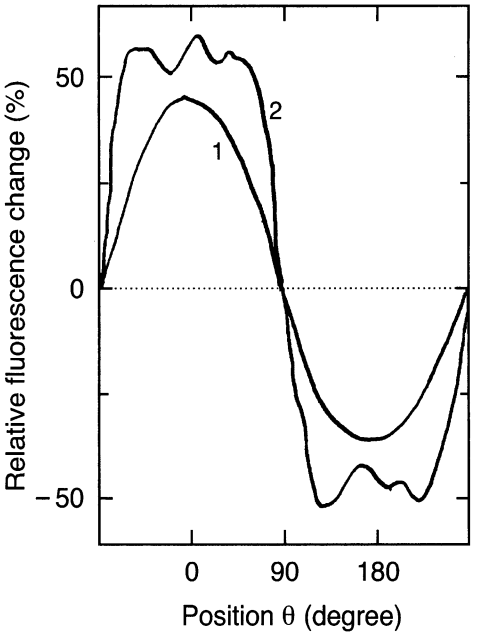

Fig. 4. Field-induced changes in the local fluorescence intensity of RH292 staining the surface of a sea urchin egg. The signal was taken 10 μs after the start of the pulse with field intensities of 125 and 400 V/cm for curves 1 and 2, respectively. The dependence on position angle θ obeys a cosine law at the low field condition (cf. Eqn. 16), but a flattening is present at the pole regions (θ around 0 and 180°) under the high field condition.

In summary, electropulsation can induce a reversible alteration of the pulsed cell membrane which brings it to a permeable state. The triggering of this process is very fast being limited by the charging relaxation time τ_m of the membrane (see Eqn. 22). Electropermeabilization abolishes the barrier function of the membrane, and cytoplasmic molecules can leak out or exogenous agents can be introduced freely in the inner volume of the pulsed cells.

6. Electric field parameters control the extent of cell permeabilization

When using square wave electric field pulses, one can control simultaneously the field strength, the pulse duration, the number of pulses and the delay between the pulses. Similar electrical pulsing conditions are obtained whatever the ionic composition of the pulsing buffer is, but Joule heating (see section 2.1) should be taken into account. Increasing the ionic content would increase the intensity of the current flowing through the sample and the energy which is dissipated

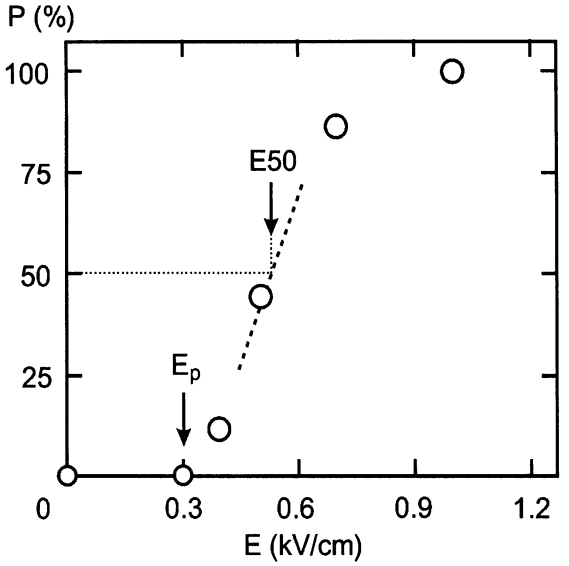

Fig. 5. Electropermeabilization is a function of the field strength E. Membrane permeabilization was assayed by the penetration of the dye trypan blue and quantified by the percentage P of stained cells. E_p and E50 denote the threshold field strength and the field strength yielding 50% permeabilization, respectively. The broken line indicates the derivative $dP/dE\,|_{E50}$. Chinese hamster ovary cells were pulsed at fixed pulse duration and number (10 square wave pulses lasting 100 μs).

during the pulse. This has to be checked to evaluate the heating contribution.

As shown in Fig. 5, at given pulse number, duration and delay, the percentage of permeabilized cells, evaluated as trypan blue stained cells (Method 2 of section 4) is a function of the field strength E. As long as the field strength is less than a threshold E_p no cell is stained, i.e. permeabilized. This critical parameter E_p is experimentally observed to be dependent on the pulse duration. With increasing field strengths the percentage of permeabilized cells increases until all cells are permeabilized at sufficiently high field strengths. This sigmoidal dependence of the percentage P of permeabilized cells on field strength can be characterized by the derivative $dP/dE\,|_{E50}$ at the field strength E50 where P = 50%. The size distribution of the cell population is controlling the shape of the plot. If the distribution is wide spread, then $dP/dE\,|_{E50}$ is smaller than if the distribution is narrow sized. A similar behavior is observed when measuring the leakage of cytoplasmic content in a cell population (Method 1 of section 4). The dependence of leakage on field strength is also sigmoidal, and $dP/dE\,|_{E50}$ is affected by the size distribution of the cell population in a similar way.

By using Method 4 for assaying cell permeabilization, one observes that leakage of cytoplasmic content following the pulse occurs across a surface which is facing the electrodes and whose area increases with increasing field strengths [19, 30, 31]. This observation is direct experimental evidence that the trigger of membrane permeabilization is not scalar. The field is acting on the cell in a position-dependent way. The effects of electric fields on cells described above is indicative that the permeabilization is due to the field induced $\Delta\phi_m$. Similar processes are obtained regardless of the cell system (different cell types, plant protoplasts, bacteria, yeasts). More interestingly, the same phenomena can also be observed on unilamellar liposomes by means of Method 2 [27]. This observation suggests that phospholipids are the target of the field effect (see also chapter 5).

Electric pulses can be generated by a capacitor discharge system where the field strength is decaying in a roughly exponential way during the discharge. The extent of cell permeabilization obeys a similar dependence on the initial value of the applied field with such a system. At a given field strength, the percentage P of permeabilized cells depends on the pulse duration and number. Increasing the pulse duration (or number) shifts the P *versus* E plot towards lower field strengths by decreasing E_p and increasing $dP/dE\,|_{E50}$. Similar effects are observed with liposomes suggesting again that phospholipids are directly involved in triggering electropermeabilization. Nevertheless, a lower limit E_c to E_p exists. This can be shown by plotting E_p as a function of the reciprocal of the cumulated pulse duration $n\,t_p$ which yields a straight line (as cartooned in Fig. 6). The intersection of this line with the ordinate then represents the threshold E_c in field strength which is required to detect electropermeabilization. It should be noted that, upon accumulation of pulses, $dP/dE\,|_{E50}$ becomes so large that the P *versus* E plot approaches a step function. Similar results are obtained when observing the leakage of cytoplasmic content at the population level.

The threshold E_c appears to be a characteristic quantity of a given cell type. It is indicative of a threshold $\Delta\phi_c$ for $\Delta\phi_m$ in the induction of membrane permeabilization. However, as is evident from Eqn. 16 and Fig. 4, this threshold is reached first in the region facing the electrodes where $\theta \approx 0$ and $\cos\theta \approx 1$. As a consequence, permeabilization appears first in this region. This is indeed observed experimentally by following the process using fluorescence microscopy [25, 30, 31]. The leakage of fluorescent molecules occurs on a larger surface at a higher field strength. Thus, electropermeabilization is affecting only a well defined part of the cell surface. A two state organization of the cell surface is present where only a topologically restricted fraction is in a highly permeant state.

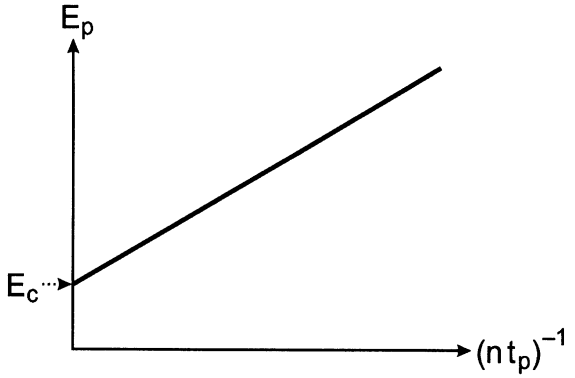

Fig. 6. The experimental critical field which triggers permeabilization is a function of the cumulated pulse duration. The threshold field strength E_p shown in Fig. 5 is a linear function of the reciprocal of the cumulated pulse duration $(n\,t_p)^{-1}$. It must be larger than a critical value E_c in order that the field can trigger membrane permeabilization. In the case of an experiment with Chinese hamster ovary cells $n\,t_p$ was varied between 0.1 and 20 ms, while the corresponding E_p values ranged between 400 to 1000 V/cm.

Since the field strength needed to induce permeabilization is dependent on many parameters (cell size, duration and number of pulses, assay method) very few reliable data on $\Delta\phi_c$ are available. Approaches using liposomes, and assuming that a lipid layer is a dielectric, gave a value of 210 mV [27]. A recent evaluation on mammalian cells brought data between 250 and 500 mV [34]. It thus appears that $\Delta\phi_c$ is roughly constant in a given cell system. However, the permeabilizing field strength depends on the cell size and thus on the cell species (cf. Eqn. 16). This explains the observation that in a cell population only a subpopulation (the larger ones) is found to be permeabilized at a given external field strength. Moreover, given that the size distribution in a cell population is usually approximately Gaussian, the sigmoidal dependence of the percentage of permeabilized cells as a function of the field strength can be explained [32]. Based on the assumption that $\Delta\phi_c$ is about the same for all mammalian cells, it should be possible to specifically permeabilize the larger ones in a mixture of different cell types. As shown in Fig. 7 this is indeed the case [32].

With increasing field strength permeabilization extends over increasingly larger areas of the cell surface. This is confirmed by direct observation of the process using fluorescence microscopy. The leakage of fluorescent molecules occurs on a larger surface for a higher field strength [19]. A more direct quantification is achieved by measuring the extent to which endogenous ATP leaks out of permeabilized cells [18]. It was found that this outflow depends linearly on the reciprocal field strength (cf. Eqn. 26 below).

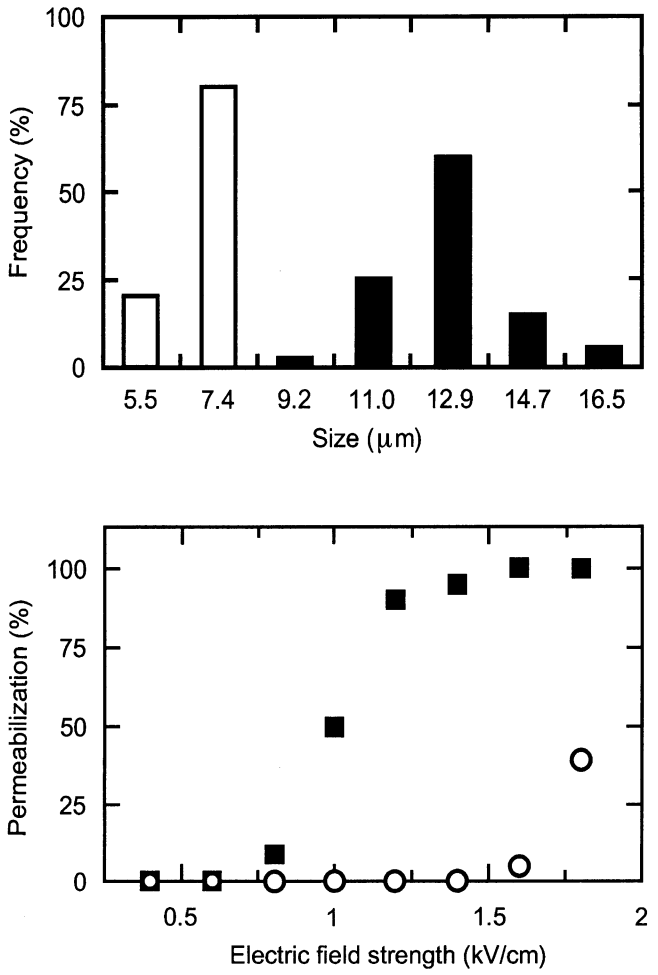

Fig. 7. Electropermeabilization is size specific. In a mixed population of Chinese hamster ovary cells (CHO, closed symbols) and erythrocytes (open symbols) with size distributions as shown in the upper panel, the larger CHO cells can be permeabilized under conditions which do not affect the integrity of the erythrocyte membranes (lower panel). Permeabilization was assessed by dye penetration for CHO cells and by hemolysis for erythrocytes.

The observed extent of electropermeabilization is dependent on the nature of the permeant species [33]. Ca^{2+} was found to penetrate more easily than trypan blue (MW 960), and even larger molecules such as FD 4000 seem to efficiently cross the membrane but only during the pulse. Macromolecules can penetrate into the cell only through a critical step mediated by the field, and for charged species an electrophoretic contribution should be taken into account present during the pulse. In the case of molecules up to 2000 Da, there is indeed an apparent molecular size limitation with respect to molecules which

are able to cross the electropermeabilized membrane. This can be explained in two different, not necessarily conflicting and maybe even complementary ways:

1) The permeability coefficient of an electropermeabilized membrane could be dependent on the nature of the permeant species.
2) The sensitivity of the cell to the penetrating molecular species used to detect electropermeabilization is dependent on the type of molecule. For example, one copy of a toxin is enough to kill a cell and this explains why electropermeabilization is experimentally proved to allow the penetration of such molecules [35]. Similarly, due to the low cytoplasmic concentration of Ca^{2+}, the toxic level of Ca^{2+} in the cell can be reached even with a small inflow of these ions.

7. Kinetics of electropermeabilization

As outlined in the preceding section, electropermeabilization is induced only when the field strength is larger than a threshold E_c which depends on cell size. But the level of the change of the membrane organization depends on many other parameters. The extent of permeabilization is dependent on the pulse duration. The kinetics of electropermeabilization can be monitored by the change in conductance of the cell suspension which reflects the permeability to small ions such as K^+ [22]. Permeabilization by the external field starts in less than 200 ns, which is actually the time limit set by the electronic detection device (Teissié and Tsong, unpublished observation). This fast step in the process is called *induction* and occurs as soon as the field strength is larger than E_p. It can be detected only when using a very sensitive and fast assay such as monitoring the conductance change. It is associated with the threshold $\Delta\phi_c$ of the transmembrane potential difference $\Delta\phi_m$. At the cell level, this means that induction is triggered as soon as $\Delta\phi_m$ of a cell is brought to a characteristic value. A delay t_d may be present which is due to the charging time of the pulsed cell membrane, and which is the kinetic limiting step in the effect of the field on the cell (see section 3.2). From Eqns. 16 and 21 with $\Delta\phi_{m,E}(t_d) = \Delta\phi_c$ it follows that

$$t_d = -\tau_m \ln[1 - \Delta\phi_c/(f\, r\, E \cos\theta)] \tag{24}$$

Since $\Delta\phi_c$ is about constant, t_d is controlled by the external field strength E, and t_d increases with decreasing E as long as $E \geq E_c$. Hence t_d should be considered as a technical delay which is not related to a step in the membrane alteration leading to the permeabilized state.

The induction step is followed by a continuous increase in conductance of the cell suspension which indicates an increasing permeability with pulse duration [22]. This can be explained by an *expansion* step which pertains to the part of the cell surface where the induction has occurred.

Very few theoretical approaches have addressed the kinetics of vesicle electropermeabilization. Using a model based on a "periodic block" description for the creation of a pore, opening and closing of pores were treated as a stochastic birth and death processes [36, 37]. A major difference between closed vesicles and the metastable BLM described in section 2.4.4 of chapter 5 is that the surface area of a cell remains constant during pore formation. The conclusion of this theoretical approach is that pore opening occurs within a narrow interval of the transmembrane potential difference, but no treatment of the pore opening kinetics was given besides the mathematical description [36, 37].

For a given field strength $E > E_p$ the electropermeabilization occurs only inside a cone in which $\Delta\phi_m > \Delta\phi_c$. The half angle θ_p of this cone is determined by the condition

$$E \cos \theta_p = E_p \tag{25}$$

The expansion step increases the permeability coefficient of the membrane cap located inside this cone and thus the exchange of molecules across the membrane. Applying several pulses at a frequency high enough to prevent any major rotation of the cell, so that the cell part which is critically affected by the field remains the same, plays a positive role for the increase in permeabilization. This is an accumulation at a local level, not an increase in the extent of the critical area. As a consequence, permeabilization depends on the number of pulses.

The expansion step is present as long as the external field is present. When the modulation drops below the critical value, a very fast *stabilisation* step occurs. This was observed indirectly by monitoring the inflow of fluorescent dextrans [19] where the diffusion rate is high only as long as the field is present (see Fig. 8). More direct evidence is obtained by measuring the change in conductance of the cell membrane electrically in a suspension [22] or directly at the single cell level by video microscopy [25]. A dramatic drop in membrane conductance occurs in the ms range following the end of the field pulse. Nevertheless, a long living permeability particularly for small molecules (molecular weight below 2000–4000) persists after the pulse. It is indeed this back-effect which is observed in most experiments due to the convenience of its detection.

The perturbed loci are not laterally mobile in mammalian cells [18, 38]. Permeability to small molecules is present only on the part of the

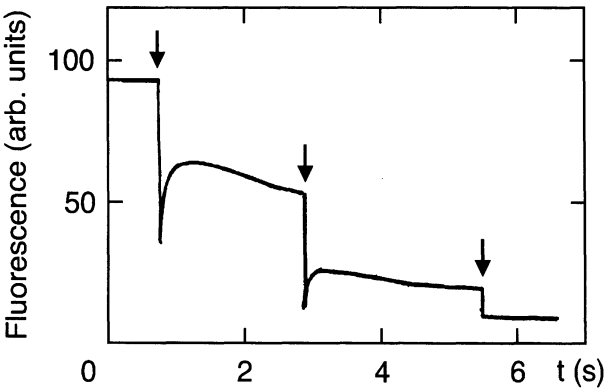

Fig. 8. Large molecules cross the membrane only during the pulse. Erythrocyte ghosts were loaded with high molecular weight fluorescent dextrans. The fluorescence emitted by each single cell decreases strongly during the pulses (arrows) or in the millisecond range following the pulses. No further decrease is observed between the pulses.

cell membrane where $\Delta\phi_m > \Delta\phi_c$. But in the case of macromolecules, such as plasmids or proteins, the transfer can be mediated only if the macromolecule is present during the pulse. No movement can be detected after the stabilization step.

In most cases permeabilization is assayed by measuring the accumulation of some reporter molecules due to their leak flow across the cell membrane after the pulse. Taking into account the above described effects of the different pulse parameters, the flow density (or flux) j_S of a species S across an electropermeabilized membrane after the pulse can be expressed as [18]

$$j_S = K P_S x(t_p,n) (1-E_c/E) \Delta c_S \quad (26)$$

Here P_S is the permeability coefficient of S for the membrane in the permeabilized state, K is a coefficient, and Δc_S is the concentration difference of S across the membrane, which is equal to the external concentration $c_{S,ext}$ when S is present only in the buffer before pulsing. Equation 26 is based on Fick's diffusion law and, as it applies to the time after the pulse, does not include electrophoretic forces (for an example see Fig. 9). The quantity $x(t_p,n)$ denotes the fraction of the membrane area which is permeabilized. It is a function of the pulse duration, t_p, and the number of pulses, n, and reflects that as soon as $\Delta\phi_m > \Delta\phi_c$ there is a time dependent transition of the membrane from a state where it is impermeable to S to a new state where P_s is present. The electric field plays a determinant role in bringing $\Delta\phi_m$ above the threshold $\Delta\phi_c$ needed for permeabilization and in determining what portion of the cell surface may be permeabilized. But in that por-

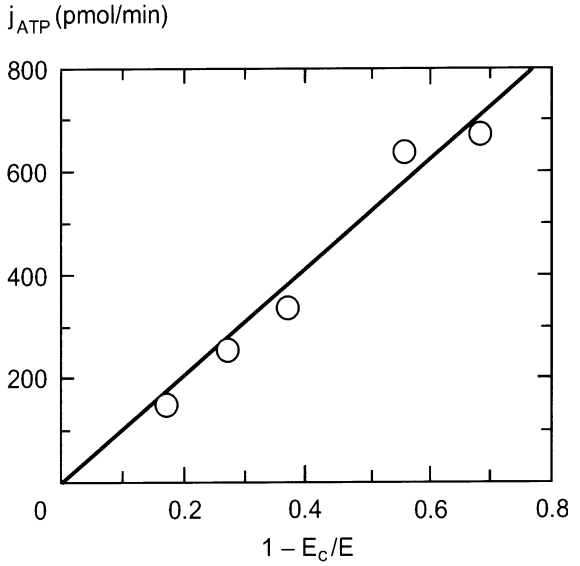

Fig. 9. Leak flow is a linear function of the reciprocal of the electric field strength E. ATP which leaked from pulsed Chinese hamster ovary cells was assayed by the luciferin-luciferase system. Mole numbers of ATP were calculated by means of a calibration curve and converted to the initial flux j_{ATP} (cf. Eqn. 26). Cumulated pulse duration n t_p = 1 ms and E_c = 700 V/cm.

tion, the extent of the structural transition of the membrane is only controlled by the cumulated pulse duration and not by the field strength. The field is just controlling the geometry of the affected part of the cell surface. These theoretical predictions are supported by online-digitized video fluorescence microscopy [56].

The observation that the local permeability coefficient is not dependent on the field strength, which created the new organization of the membrane, is indicative that the structural transition is operated at a constant $\Delta\phi_m$. This is due to the very fast induction step which affects the parameter f in Eqn. 16 in less than 1 μs. This shunt of the field effect is a direct consequence of the induction step, as was observed by video microscopy (Fig. 4).

As a practical conclusion, two approaches are giving a high level of permeabilization (i.e. a high exchange across the membrane)

1) a strong electric field of short duration, affecting a large proportion of the cell surface with a small permeability, and
2) an electric field just stronger than the threshold but with a long duration (or a large number of successive pulses) which affects a small surface area but yields a high local permeability.

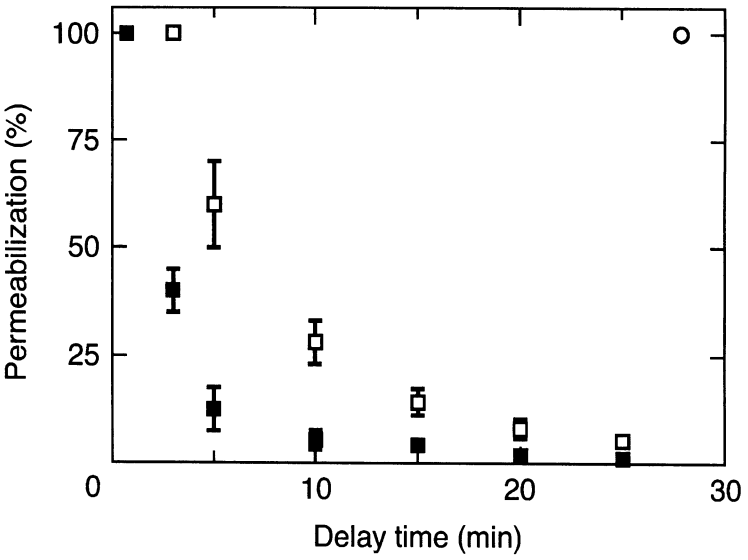

Fig. 10. Electropermeabilization is short-lived. Membrane permeabilization of pulsed Chinese hamster ovary cells was determined by adding a dye at the indicated delay times after the pulses. The permeabilization represented by the percentage of stained cells decreases with time. This process is strongly temperature dependent: ■, 37°C; □, 21°C; ○, 4°C.

Limits are linked to the viability of the pulsed cells in the sample. A high loss in viability is observed if a high level of permeabilization is triggered. Thus, the extent of local alterations of the membrane organization associated with cell electropermeabilization is controlled by the pulse duration. A higher exchange of molecules across the membrane is obtained for a given field strength when using longer pulses.

After the stabilization step, the membrane is locally permeable. This electropermeabilized state of the membrane to small molecules is reversible. The intrinsic impermeability of the membrane is recovered progresssively but spontaneously. This can be observed if pulsing the cells in a dye free medium and adding the dye at different delay times after pulsing. As shown in Fig. 10, the percentage of permeabilized cells decays back to zero with increasing delay times. It should be emphasized that reversibility of permeabilization is not always indicative of cell viability. The only true criterion for viability is the ability of the cells to grow after being subjected to pulsing in a dye free buffer.

The kinetics of the resealing shows that it is a first order process. The rate constant $k(t_p,n)$ is dependent only on the cumulated pulse reac-

tion but not on the field strength [18]. Resealing can be monitored by the inflow $j_S(t)$ of a probe S at time t after the pulse, which is given by

$$j_S(t) = f(t_p,n,E)\, P_S\, \Delta c_S \exp[-k(t_p,n)\, t] \quad (27)$$

with the abbreviation (cf. Eqn. 26)

$$f(t_p,n,E) = K\, x(t_p,n)\, (1 - E_c/E) \quad (28)$$

The process, or $k(t_p,n)$, is strongly dependent on the ambient temperature. In the case of CHO cells resealing is observed in less than 1 min at 37 °C but may last several hours if cells are kept at 4 °C (see Fig. 10). This is apparently due to the role of the cytoskeleton and membrane proteins because electropermeabilization is clearly shortlived in liposomes [27, 39]. Temperature is not playing a major role for E_c and $x(t_p,n)$, i.e. in the induction and expansion steps. It should be noted that due consideration of the field strength E is required when using Eqn. 27 for the description of the resealing process. Since $f(t_p,n,E)$ is dependent on E a cell will be considered as permeabilized during a longer time if pulsed by a stronger field at constant t_p and n.

The above description is valid in the case of small molecules whatever their hydrophilicity. In the case of macromolecules, a key event takes place as long as the field is present, whose molecular mechanism remains unclear. As a result, the pulse duration must be kept as long as possible to obtain a high level of transfer. Note that t_p acts on x and on k to increase the transfer. There is a general agreement that, for *in vitro* experiments, only long pulses bring a transfer of macromolecules across the cell membrane [63, 64]. However, the decreasing cell viability with prolonged pulse duration sets an upper limit for t_p.

The structural organization of the permeabilized state of the pulsed cell membrane is not known. By use of quick freezing technology, it was possible to detect some furtive structures in the case of erythrocyte ghosts [65]. Cracks and flaps were very transiently detected and were proposed to play a role in cell fusion. No well defined organizations were observed. In the case of intact erythrocytes, craters were imaged under hypososmolar conditions as a consequence of the induced hemolysis but are not relevant to the direct effect. Post-field effects such as an increase in the number and in the length of villi and/or a swelling to blebs are observed [61, 62]. Their lifetime is roughly the same as that of the electropermeabilized state. Another feature of the electropermeabilized membrane is that the flip-flop of phospholipids (see section 1 in chapter 3) is facilitated [23]. But because of the leakage of ATP and due to the ATPase character of the flippase, the experimental system used cannot provide direct evidence that this is indeed a feature of the electropermeabilized state of the membrane.

8. Electropermeabilization is associated with a long-lived membrane fusogenicity

Cells in close contact will fuse when electropulsed [3]. However, contact during the pulse (Contact first, CF method) is not a prerequisite. Pulsing first and then bringing into contact (PF method) induces cell fusion on a model system (erythrocyte ghosts) and on viable cells [40, 41] as well as on plant protoplasts [42]. The thermodynamic consequences of this observation is of importance in the understanding of electropermeabilization. Repulsive forces preventing a spontaneous cell fusion are weakened or abolished by the electropermeabilization associated membrane structural transitions. Some of these forces are of electrostatic origin due to the surface charges but at a very close contact between cells a much stronger repulsion is present correlated to the regular organization of interfacial water molecules, whose dipoles are oriented by the local fields arising from charges on the membrane [43]. The observation that spontaneous fusion occurs when electropermeabilized cells are brought into contact under very mild conditions is the direct indication that these repulsive "hydration" forces are not present anymore. The network of structures preventing such a close contact is not present along electropermeabilized membranes. These repulsive forces are described in native membranes as due to the structural order of the interfacial water. This local organization is due to the local electric field arising from the membrane constituents or from some dipolar effects which require a regular organization of the interface.

The last and most important implication of the spontaneous fusogenicity is that there is a new organization, presumably a more random and fluctuating one, in the membrane at the level of the interface. This is supported by ^{31}P-NMR studies which showed that the polar heads of phospholipids in multilamellar lipid vesicles were tilted during the electric field pulse [32]. This structural perturbation is long-lived in the case of electropermeabilized mammalian cells [44]. Taking advantage of the long lifetime of the electropermeabilized state in mammalian cells at a low temperature, a ^{31}P-NMR investigation of their phospholipids was possible [44]. It was observed that a major fraction of the lipids displayed a conformation of their polar heads which was different from what is present in the normal organization, but the bilayer structure is retained. Such a signal can be explained by an apparent tilt in comparison with the classical position (almost parallel to the plane of the membrane) or by the induction of short wave ripples in the membrane. This second explanation implies an increase in fluctuations in the membrane organization [45]. Enhanced fluctuations in the lipid matrix were proposed to increase the permeability of a membrane by taking into account that the energy barrier for a mol-

ecule to cross a membrane is mainly at the glycerol level rather than in the hydrocarbon chain region [46, 47]. Such fluctuations, if present, affect only a limited part of the cell surface because, as described above, electropermeabilization is topologically limited, but the majority of the phospholipids in the cap of the critical cone (cf. Eqn. 25) is affected. This observation cannot be explained by the generation of a very limited number of pores in the membrane because most of the lipids are shown to be affected by the NMR studies. One problem is nevertheless brought by confocal fluorescence microscopy on neural cells where a limited number of Ca^{2+}-channels were supporting electropermeabilization [50].

9. Interfacial consequences

The electropermeabilization associated fusogenicity shows that the energy barrier which must be overcome to trigger electropermeabilization is the same as the one needed to fuse cells. The membrane structural transition is associated with the annihilation of the molecular structures which are organizing the membrane interface, and are responsible for the so-called hydration forces when cells are brought into close contact. This conclusion implies that any modification which will facilitate such an annihilation would make electropermeabilization easier. This is indeed the case, as shown by the effects of the ionic content of the pulsing buffer [33], of molecules affecting the order of the membrane [49] or of osmotic pressure in the pulsing buffer [48]. In the last two cases, the contribution of the ondulation forces which increase the magnitude of the hydration forces in the cell repulsion was taken into account. Nevertheless, under hypoosmotic conditions, when no swelling occurs, ripples of the cell surface are prevented thus inducing a decrease in the ondulation forces. Electropermeabilization is facilitated as shown by the increase in $dP/dE\,|_{E50}$. However, it was observed that the field threshold E_c for permeabilization induction was not affected by these modifications. Since no major morphological alterations such as a change in cell size were affecting the cell, this observation proves that it is the expansion step where the membrane structure modification occurs.

Membrane electropermeabilization is triggered locally as soon as the local transmembrane potential difference $\Delta\phi_m$ reaches its critical value $\Delta\phi_c$ (between 200 and 300 mV). It is a two step process where the second step is under the control of the duration of the pulse and induces the disorganization of the interface associated to a flip of the phospholipid head groups. This transient state is present only during

the pulse and affects the structure of membrane proteins which are interacting with lipids. A fast relaxation occurs at the end of the pulse to a metastable state where the interfacial organization of the membrane remains strongly affected, as shown by the ^{31}P-NMR studies. The slow resealing process is of course much faster under conditions where permeabilization is facilitated (more order in the membrane, hypoosmolar buffer).

Another physical parameter should be considered in the description of the molecular processes associated with electropermeabilization. An increase in the membrane tension is observed to facilitate the potential induced destabilization in lipid assemblies as well as in cells [51, 52]. These effects can be explained by considering that the structural changes of the membrane are associated thermodynamically with an energy barrier. This is the energy which is required to break the organization and induce the hydration forces when cells are brought into contact. Permeabilization is facilitated if this energy barrier is lowered.

It should be emphasized that very few things are known on the molecular processes affecting the membrane organization along with electropermeabilization. Models have been proposed using simplistic descriptions of the membrane (see chapter 5). According to these models, permeabilization is due either to the electrocompression of the film [53–55] or to the increase in size of structural defects [57–59]. The expansion step can be nicely described by a percolation phenomenon [36]. Germs of permeabilized membrane patches grow in size and merge together; in this way electropermeabilization is treated as a phase transition. However, membrane proteins most likely hinder such a percolation process. A membrane is shifted from the regular impermeable organization to a more fluctuating one where molecules can cross it. The role of $\Delta\phi_m$ is to reach a critical but constant value $\Delta\phi_c$ where this transition would be permitted, but plays no other function in permeabilization. The local magnitude of the transition would then be controlled by the duration of the pulse but not by the magnitude of the applied field. One should nevertheless emphasize the primitive character of such a description. Electropermeabilization of cell membranes is triggered under conditions very analogous to what is observed in pure liposomes (after appropriate corrections for the difference in size) although the protein to lipid ratio can be high in some membrane systems (see Table 1 in chapter 3) and the membrane organization is very different from that in a lipid bilayer. Hence the relevance of such a model remains questionable. Another shortcoming of these descriptions is that the experimentally observed post-pulse fusogenicity cannot be explained.

10. Electroporation of cell and lipid membranes

The results obtained from the study of electrical breakdown of bilayer lipid membranes (BLMs) and those obtained by equivalent methods such as voltage clamp and charge relaxation for cell membranes support the notion of the lipid bilayer being the site of the electric field effect. But, as described above, the processes may be different in cells where two states of the membrane are simultaneously present in the electropermeabilized cell and where the transmembrane potential difference is not uniform over the cell surface.

The breakdown of cell membranes has specific features which distinguish it from that of planar lipid bilayers. Specifically, under certain conditions, the increase in the permeability of cell membranes during breakdown leads to secondary processes such as colloid-osmotic lysis [1, 13]. Unlike BLMs where a meniscus containing lipid molecules is present, vesicular membranes of cells and organelles are closed which may also lead to changes in the character of the breakdown especially at later stages, and the surface area of the membrane is constant during the pulse. Finally, the interesting effect of "accommodation" of membranes (or cells as a whole) to the effect of a high electric field can be observed only for some types of cell membranes. After the application of a train of equal-voltage pulses with sufficiently long intervals between them, the conductance value attained at the end of a pulse decreases with each following pulse [3, 4]. The mechanism of this phenomenon has not yet been elucidated. A striking difference between the behavior of cells and BLMs concerning their electropermeabilization is the effect of the field strength. The local permeability in the permeabilized part of the electropulsed cell membrane is a function of the pulse duration but not of the field strength. This is apparently due to the self-shunt of the field effect.

In spite of these differences, some basic regularities describing the behavior of cell and model membranes in a high electric field are remarkably alike. We primarily emphasize the similarity of oscillograms of breakdown current with that of clamping the potential across cell membranes [4, 60]. In both cases, the irreversible damage to the membrane is preceded by a reversible decrease in the resistance. The lifetime t_ℓ of lipid bilayers and cell membranes in an electric field is a random quantity. In both cases the dependence of the mean lifetime $\langle t_\ell \rangle$ on the imposed $\Delta\phi_m$ has a similar slope, i.e. increasing $\Delta\phi_m$ by about 0.1 V decreases $\langle t_\ell \rangle$ by approximately one order of magnitude (cf. Fig. 3 of chapter 5). At the reversible stage of breakdown, one can also observe common regularities. Cell membranes and lipid bilayers display qualitatively the same dependencies of reversible breakdown current on the time and amplitude of the imposed $\Delta\phi_m$. The dependence of the reversible breakdown potential on the dura-

tion of a charging pulse is similar for membranes of the algae *Valonia* and for BLMs [9]. It was established that the breakdown potentials of cell and lipid membranes depend in a similar manner on the concentration and composition of electrolyte as well as on temperature. This is not the case when pulsing cells in suspension; the ionic concentration did not affect the critical field strength which triggers the permeabilization but modulated the expansion step. Again, the major differences between clamping $\Delta\phi_m$ in BLMs and the cell electropulsation experiments should be emphasized. The transmembrane potential difference can be well controlled in BLMs and is the same at all positions of the membrane. In cells, however, changes in $\Delta\phi_m$ can be achieved only indirectly by means of external electrical fields, and these changes are position-dependent as well as modulated by the permeabilization state of the cell.

As in the case of BLMs, an increase in intensity and duration of electrical treatment leads to a simultaneous increase in the exchange processes which develop in cell membranes during reversible breakdown [1, 2]. The decrease in transmembrane potential difference across cell and model membranes, which are in the state of reversible breakdown, leads to a very rapid (within a few microseconds) decrease in conductance [5] but a slower step was described in the case of pulsed erythrocytes. Another major difference between BLMs and cell membranes pertains to the lifetime of the permeabilized state. The time of resealing in lipid bilayers turned out to be shorter than the decay time of the permeable state of biomembranes (seconds or minutes) [3, 6, 7]. In some cell membranes the time of resealing after breakdown can even be as long as tens of minutes or hours [3, 18 31, 42].

The similarity of the phenomenology of electrical breakdown of cell and lipid membranes may suggest that, if pores develop in the course of electrical breakdown of cell membranes, they arise in the lipid matrix. This localization of the early steps of cell electropermeabilization is supported by the very similar values (between 200 and 250 mV) for the triggering thresholds in cells and liposomes, although the value for cells could be obtained only with some crude assumptions on their properties. Any structural description of the processes involved in cell electropermeabilization must include the reorganization of the lipid polar head region, the long lifetime of the permeabilized state and the associated fusogenicity.

Acknowledgements

This work was supported by the CNRS. Thanks are due to Yuri Chizmadzhev for his "critical" help in the first part of this chapter, to Dieter Walz for his comments and to Lluis Mir for his "diplomatical efforts".

References

1 Kinosita K, Tsong TY (1977) Biochim. Biophys. Acta 471: 227–242.
2 Kinosita K, Tsong TY (1977) Nature 268: 438–441.
3 Zimmermann U (1982) Biochim. Biophys. Acta 694: 227–277.
4 Chernomordik LV, Sukharev SI, Popov SV, Pastushenko VF, Sokirko AV, Abidor IG, Chizmadzhev YuA (1987) Biochim. Biophys. Acta 902: 360–373.
5 Benz R, Conti F (1981) Biochim. Biophys. Acta 645: 115–123.
6 Dressler V, Schwister K, Haest CWM, Deuticke B (1983) Biochim. Biophys. Acta 732: 304–307.
7 Sowers AE, Lieber MR (1986) FEBS Lett. 205: 179–184.
8 Pohl H (1978) *Dielectrophoresis*, Cambridge University Press.
9 Margolis LB, Popov SV (1988) Bioelectrochem. Bioenerg. 20: 143–153.
10 Gass GV, Chernomordik LV, Margolis LB (1991) Biochim. Biophys. Acta 1093: 162–167.
11 Neumann E (1989) The relaxation hysteresis of membrane electroporation. In: E Neumann, AE Sowers, C Jordan (eds): *Electroporation and Electrofusion in Cell Biology*, Plenum, New York.
12 Bernhardt J, Pauly H (1973) Biophys. J. 10: 89–98.
13 Kinosita K, Tsong TY (1977) Proc. Natl. Acad. Sci. USA 74: 1923–1927.
14 Gross D, Loew LM, Webb WW (1986) Biophys. J. 51: 339–348.
15 Ehrenberg BD, Farkas DL, Fluhler EN, Lojewska Z, Loew LM (1987) Biophys. J. 51: 833–837.
16 Hibino M, Shigemori M, Itoh H, Nagayama K, Kinosita K (1991) Biophys. J. 59: 209–220.
17 Lojewska Z, Farkas D, Ehrenberg B, Loew LM (1989) Biophys. J. 56: 121–128.
18 Rols MP, Teissié J (1990) Biophys. J. 58: 1089–1098.
19 Dimitrov DS, Sowers AE (1990) Biochim. Biophys. Acta 1022: 381–382.
20 Kinosita K, Itoh H, Ishiwata S, Hirano K, Nishizata T, Hayakawa T (1991) J. Cell. Biol. 115: 67–74.
21 Teissié J, Rols MP (1988) Electropermeabilization and electrofusion of cells. In: N Latruffe, Y Gaudemer, P Vignais, A Azzi (eds): *Dynamics of membrane proteins and cellular energetics*, Springer, Berlin.
22 Kinosita K, Tsong TY (1979) Biochim. Biophys. Acta 554: 479–494.
23 Schwister K, Deuticke B (1985) Biochim. Biophys. Acta 816: 332–348.
24 Bartoletti DC, Harrison GI, Weaver J (1989) FEBS Lett. 256: 4–10.
25 Kinosita K, Hibino M, Shigemori M, Ashikawa I, Itoh H, Nagayama K, Ikegami K (1990) Submicrosecond imaging under a pulsed laser fluorescence microscope. Electroporation of cell membrane time- and space-resolved. In: S Ishizaka (ed): *Science on Form*, KTK Publishers, 97–104.
26 Neumann E, Rosenheck K (1972) J. Membr. Biol. 10: 279–290.
27 Teissié J, Tsong TY (1981) Biochemistry 20: 1548–1554.
28 Neumann E, Schaefer-Ridder E, Wang Y, Hofschneider PH (1982) EMBO J. 1: 841–845.
29 Dower WJ, Miller JF, Ragsdale CW (1988) Nucleic Acids Res. 16: 6127–6144.
30 Mehrle W, Zimmermann U, Hampp R (1985) FEBS Lett. 185: 89–94.
31 Tekle E, Astumian RD, Chock PB (1990) Biochem. Biophys. Res. Comm. 172: 282–287.
32 Sixou S, Teissié J (1990) Biochim. Biophys. Acta 1028: 154–160.
33 Rols MP, Teissié J (1989) Eur. J. Biochem. 179: 109–115.
34 Marszalek P, Liu DS, Tsong TY (1990) Biophys. J. 58: 1053–1058.
35 Orlowski S, Belehradek J, Paoletti C, Mir L (1988) Biochem. Pharmacol. 37: 4727–4734.
36 Sugar IP, Forster W, Neumann E (1987) Biophys. Chem. 26: 321–335.
37 Sugar IP (1992) Exact solutions of a stochastic model of electroporation. In: MJ Allen, SF Cleary, AE Sowers, DD Shillady (eds): *Charge and Field effects in Biosystems – 3*, Birkhäuser, Boston.
38 Sowers AE (1987) Biophys. J. 52: 1015–1020.
39 Rols MP, Teissié J (1991) Evidence of cytoskeleton implication in cell electropermeabilization and electrofusion. In: G Paillotin (ed): *The Living Cell in Four Dimensions*, A.I.P.
40 Sowers AE (1986) J. Cell. Biol. 102: 1358–1362.

41 Teissié J, Rols MP (1986) Biochem. Biophys. Res. Comm. 140: 258–266.
42 Montané MH, Dupille E, Alibert G, Teissié J (1990) Biochim. Biophys. Acta 1024: 203–207.
43 Marra J, Israelachvili J (1985) Biochemistry 24: 4608–4618.
44 Lopez A, Rols MP, Teissié J (1988) Biochemistry 27: 1222–1228.
45 Deuticke B, Schwister K (1989) Leaks induced by electrical breakdown in the erythrocyte membrane. In: E Neumann, AE Sowers, C Jordan (eds): *Electroporation and Electrofusion in Cell Biology*, Plenum, New York.
46 Nagle JF, Scott HL (1978) Biochim. Biophys. Acta 513: 236–243.
47 Miller DM (1991) Biochim. Biophys. Acta 1065: 75–81.
48 Rols MP, Teissié J (1990) Biochemistry 29: 4561–4567.
49 Rols MP, Dahhou F, Mishra KP, Teissié J (1990) Biochemistry 29: 2960–2966.
50 Teruel MN, Meyer T (1997) Biophys J. 1997 73: 1785–96.
51 Needham D, Hochmuth RM (1989) Biophys. J. 55: 1001–1009.
52 Ramos C, Teissié J (2000) FEBS Lett. 465: 141–144.
53 Crowley IM (1973) Biophys. J. 13: 711–717.
54 Zimmermann U, Pilwat G, Riemann F (1974) Biophys. J. 14: 881–899.
55 Dimitrov DS, Jain RK (1984) Biochim. Biophys. Acta 779: 437–468.
56 Gabriel B, Teissie J (1999) Biophys J. 76: 2158–65.
57 Abidor IG, Arakelyan VB, Chernomordik LV, Chizmadzhev Yu, Pastushenko VF, Tarasevich MR (1979) Bioelectrochem. Bioenerg. 6, 37–52.
58 Weaver JC, Powell KT, Mintzer RA, Ling H, Sloan SR (1984) Bioelectrochem. Bioenerg. 12, 393–412.
59 Sugar IP, Neumann E (1984) Biophys. Chem. 19: 211–225.
60 Chernomordik LV, Sukharev SI, Abidor IG, Chizmadzhev Yu (1983) Biochim. Biophys. Acta 736: 203–213.
61 Escande ML, Rols MP, Dupont MA, Gas N, Teissié J (1988) Biochim. Biophys. Acta 939: 247–259.
62 Gass, GV, Chernomordik, LV (1990) Biochim. Biophys. Acta 1023: 1–11.
63 Rols MP, Teissie J (1998) Biophys J. 75: 1415–23.
64 Kubiniec RT, Liang H, Hui SW (1990) Biotechniques 8: 16–20.
65 Stenger DA, Hui SW (1986) J. Membr. Biol. 93: 43–53.

Index